Investigation of a selective transglutaminase 2 antagonist as a novel therapeutic agent for cystic fibrosis

James Michael Gavin

Doctor of Philosophy

Aston University

December 2020

Aston University

Investigation of a selective transglutaminase 2 antagonist as a novel therapeutic agent for cystic fibrosis

James Michael Gavin

Doctor of Philosophy

2020

Thesis summary

Cystic fibrosis (CF) is a genetic disorder, characterised by the presence of a dysfunctional cystic fibrosis transmembrane conductance regulator (CFTR) protein. Currently approved therapeutic compounds all act by targeting CFTR directly. Yet, emerging evidence suggests that the proteostasis network within CF airway epithelial cells is severely disrupted, leading to fibrotic alterations of the extracellular matrix (ECM). TG2 is reported to be a key regulator of these pathogenic changes. With the advent of potent and selective inhibitors of TG2, a novel therapeutic avenue may now exist in CF.

In this study, both immortalised and primary CF human bronchial epithelial cells (HBECs) were used to investigate the role of TG2, as regards the development of fibrosis in CF airway epithelia. It was shown that the deposition of TG2 and fibronectin is elevated in the ECM of both IB3 cells and CF primary HBECs. Notably, IB3 cells were found to undergo epithelial-mesenchymal transition (EMT)-derived myofibroblast transdifferentiation, with CF primary HBECs also exhibiting varying levels of EMT progression.

Proof of concept experiments using CF primary HBECs revealed that the use of a CFTR corrector (VX-809) and TG2 specific inhibitor (1-155) in combination, could have a potentially additive therapeutic effect. A more in-depth investigation with IB3 cells, served to further validate these findings. It was demonstrated that the treatment of IB3 cells with VX-809 and 1-155, could completely reverse EMT-derived myofibroblast transdifferentiation and fully restore the barrier function of CF airway epithelium. Furthermore, the development of these pathogenic processes, was shown to be dependent on the interrelationship between extracellular TG2 and TGFβ1 signal transduction.

The mechanism of cellular TG2 export in CF was also examined. Extracellular vesicles released by IB3 cells were determined to have increased TG2 expression and activity. IB3 cells were shown to secrete elevated levels of exosomes, which were found to be reduced after combination treatment with VX-809 and 1-155. The findings within this study confirm the importance of extracellular TG2 in the pathogenesis of CF and suggest that pharmacological inhibition of its aberrant activity, represents a viable therapeutic approach.

Keywords: cystic fibrosis, transglutaminase 2, epithelial-mesenchymal transition, TG2 inhibitors, extracellular vesicles.

Dedication

For my wife, *Polina you've been through this PhD journey with me every step of the way and you are the one person who has kept me going throughout. Thank you for everything you've done. Now that it's over, I think it's about time we pack our bags and go climb Ben Nevis!*

Acknowledgements

I would first like to express my sincere gratitude to Prof Andrew Devitt, for adopting me into his lab group halfway through this PhD. Your support and guidance has been immeasurable and even in the busiest periods, you always found time to help. You've been a fantastic supervisor and real inspiration as scientist. My thanks also go to Dr Russell Collighan and Dr Jill Johnson for their help, advise and support throughout this PhD.

Special thanks to Dr Ivana Milic for her kindness when I moved lab groups and for all of her help and time spent training me in the lab, I just wish you never introduced me to the qNano. Of course, it wouldn't have been the same without all the great people that I've met along the way; Joumsi, Haris, Shaun, Carlo, Fritz, Nora, Amber, Parbs, Kiran, Lois and Limmy. Thank you for making every day in the lab enjoyable and for all the laughs.

To my parents, who have always supported me wholeheartedly in all of my endeavours. I feel very fortunate to have such a caring family behind me. Your hard-working and tenacious attitude has always been an inspiration to me. To Jason and proof of the first step in my journey towards becoming PDC champion as Dr Darts. Also, to my Russian family, Ирине, Владу, Вите, Вове and of course бабуле, thank you for always asking how I was getting on and for your continuous encouragement and support, it really made a difference.

To Dave Noonan, a fellow curious mind, a best mate and the reason behind why I chose this PhD project. This has been my small contribution to advancing the knowledge of CF and my continued hope for what will one day be a cure for the CF community. I look forward to reclaiming my social life again and meeting you for a long overdue pint. Can't wait to celebrate your wedding in the near future and getting utterly banjaxed on the big day.

Finally, to Polina, my better half and the person who made it all worthwhile. Your endless patience, devoted encouragement and unwavering support were the only reason that I overcame the many challenges of this PhD. You have made tremendous sacrifices to enable me to get to the end. Above all, we got through it together as a team and it would not have been possible without you. I only hope that I can do the same for you on your PhD journey.

Table of Contents

List of Abbreviations

3D	Three-dimensional
aa	Amino acid
ABC	ATP-binding cassette
ADP	Adenosine diphosphate
AEM	Airway epithelial medium
ALI	Air-liquid interface
ALIX	ALG-2-interacting protein X
ALK5	Activin receptor-like kinase 5
ANOVA	Analysis of variance
ATP	Adenosine triphosphate
BSA	Bovine serum albumin
Ca^{2+}	Calcium ion
$CaCl_2$	Calcium chloride
cAMP	Cyclic adenosine monophosphate
CD	Cluster of differentiation
CF	Cystic fibrosis
CFTR	Cystic fibrosis transmembrane conductance regulator
Cl^-	Chloride ion
cm	Centimetre(s)
CO_2	Carbon dioxide
COPD	Chronic obstructive pulmonary disease
CRISPR	Clustered regularly interspaced short palindromic repeats
Cryo-EM	Cryogenic-electron microscopy
DAPI	4',6-diamidino-2-phenylindole
DC	Detergent compatible
DMSO	Dimethyl sulfoxide
DNA	Deoxyribonucleic acid
DTT	Dithiothreitol
ECL	Enhanced chemiluminescent
ECM	Extracellular matrix
EDTA	Ethylenediaminetetraacetic acid
EGCG	Epigallocatechin gallate
EMT	Epithelial-mesenchymal transition
ENaC	Epithelial sodium channel

EndMT	Endothelial to mesenchymal transition
ER	Endoplasmic reticulum
ERK	Extracellular signal-regulated kinase
ESCRT	Endosomal sorting complex required for transport
EV	Extracellular vesicle
FBS	Fetal bovine serum
FITC	Fluorescein isothiocyanate
FN	Fibronectin
g	Gravity
GAPDH	Glyceraldehyde-3-phosphate dehydrogenase
GDP	Guanosine diphosphate
GTP	Guanosine triphosphate
h	Hour(s)
H_20	Water
HBEC	Human bronchial epithelial cell
HCl	Hydrochloric acid
HCO_3^-	Bicarbonate ion
HDL	High-density lipoprotein
HRP	Horseradish peroxidase
HS	Heparan sulfate
HSPG	Heparan sulfate proteoglycan
HTS	High-throughput screening
HUVECs	Human umbilical vein endothelial cells
IC_{50}	Half maximal inhibitory concentration
IPF	Idiopathic pulmonary fibrosis
JNK	c-Jun N-terminal kinase
kDa	Kilodalton
LDL	Low-density lipoprotein
M	Molar
M1-12	Membrane spanning segment 1-12
mA	Milliamp(s)
mbar	Millibar
mg	Milligram(s)
Mg^{2+}	Magnesium ion
min	Minute(s)
ml	Millilitre(s)

mm	Millimetre(s)
mM	Millimolar
mRNA	Messenger ribonucleic acid
MVB	Multivesicular body
Na_3VO_4	Sodium orthovanadate
NaCl	Sodium chloride
NaF	Sodium fluoride
NaOH	Sodium hydroxide
NBD	Nucleotide-binding domain
N-cad	N-cadherin
NF-κB	Nuclear factor kappa-light-chain-enhancer of activated B cells
ng	Nanogram(s)
NH_3	Ammonia
nm	Nanometre(s)
nM	Nanomolar
np	Not present
NP	Nanopore
ns	Not significant
^oC	Degree Celsius
OPD	o-Phenylenediamine dihydrochloride
PAGE	Polyacrylamide gel electrophoresis
PBS	Phosphate buffered saline
PCL	Periciliary layer
PDI	Protein disulfide isomerase
PIASγ	Protein inhibitor of activated STAT protein gamma
PKA	Protein kinase A
PM	Pressure module
PMSF	Phenylmethylsulfonyl fluoride
PPARγ	Peroxisome proliferator-activated receptor gamma
R domain	Regulatory domain
RGD	Arginyl-glycyl-aspartic acid peptide motif
RNA	Ribonucleic acid
ROS	Reactive oxygen species
SDS	Sodium dodecyl sulphate
SEC	Size exclusion chromatography
SEM	Standard error of the mean

siRNA	Small interfering ribonucleic acid
SNARE	Soluble N-ethylmaleimide-sensitive factor attachment protein receptor
SUMO	Small ubiquitin-like modifier
SV40	Simian virus 40
TBST	Tris-buffered saline with Tween® 20
TEER	Trans-epithelial electrical resistance
TEMED	N,N,N',N'-tetramethylethane-1,2-diamine
TG	Transglutaminase
TG2	Transglutaminase 2
TGFβ	Transforming growth factor beta
TGM2	Transglutaminase 2 gene
TMD	Transmembrane domain
Tris-HCl	Tris(hydroxymethyl)aminomethane hydrochloride
TRITC	Tetramethylrhodamine isothiocyanate
TRPS	Tunable resistive pulse sensing
TSG101	Tumour susceptibility gene 101
V	Volt(s)
VLDL	Very low-density lipoprotein
v/v	Volume per volume
VX-445	Elexacaftor
VX-661	Tezacaftor
VX-770	Ivacaftor
VX-809	Lumacaftor
w/v	Weight per volume
W1282X	Tryptophan substituted by a termination codon at position 1282 in *CFTR*
XTT	Sodium 2,3,-bis(2-methoxy-4-nitro-5-sulfophenyl)-5-[(phenylamino)-carbonyl]-2H-tetrazolium
ZO-1	Zonula occludens-1
α-SMA	Alpha-smooth muscle actin
ΔF508	Deletion of phenylalanine at position 508 in *CFTR*
µg	Microgram(s)
µl	Microlitre(s)
µm	Micrometre(s)
µM	Micromolar
Ω	Electrical resistance

List of Figures

List of Tables

Chapter 1

Introduction

CHAPTER 1: INTRODUCTION

1.1 Cystic Fibrosis

Cystic fibrosis (CF) is a monogenic autosomal recessive disease (Figure 1.1), characterised by a defective cystic fibrosis transmembrane conductance regulator (CFTR) protein. Discernment of its simple monogenic nature in 1989 (Riordan, 1989) has led to an intensive foray of investigation, elucidating the identity of approximately 2000 mutations in this single gene (Cystic Fibrosis Genetic Analysis Consortium, 2020). Such a large number of defects illustrates why this disease has a highly variable and complex clinical expression. Substantial phenotypic variability even extends to patients with the same genotype (Weiler and Drumm, 2013). Hence, it is understandable why difficulties have persisted in addressing this disease therapeutically.

CF affects approximately 70,000 - 100,000 individuals worldwide, including 10,500 from the UK alone (Kelly, 2017). There is a recognised heterogeneity in the geographical distribution of the disease, with CF found to be most prevalent within Caucasian populations (World Health Organization, 2004). The most common mutation is a deletion of phenylalanine at codon 508 (ΔF508), accounting for ~70% of all CF incidences (Davies et al., 2007). Found on the apical membrane of epithelial cells, CFTR primarily functions to transport chloride ions (Cl^-) for maintenance of cell surface hydration. A new insight by Montoro et al. (2018), indicates that a previously unknown airway epithelial hierarchy may exist, with a rare cell subtype named 'pulmonary ionocytes' being a major source of *CFTR* expression. In regard to CF, absence of a functional CFTR, alongside increased activity of the epithelial sodium channel (ENaC) results in dehydrated, hyperviscous mucus which obstructs epithelium-lined ducts. The exact relationship between CFTR and ENaC remains a subject of debate (Shei et al., 2018). To a lesser extent, CFTR transports bicarbonate ions (HCO_3^-) for regulation of: normal mucin expansion (Quinton, 2008), activation of pancreatic enzymes (Kunzelmann et al., 2017) and preservation of respiratory defences (Shah et al., 2016).

CF is often defined by its primary cause of morbidity, comprising chronic infections, inflammation and obstruction of the lungs. Yet, abnormal regulation of epithelial chloride transport results in multiple clinical manifestations, including afflictions to the intestines, liver, gallbladder, pancreas, sweat glands and reproductive system (O'Sullivan and Freedman, 2009). Ordinarily this translated to poor prognosis, but recent times have seen a dramatic increase in life expectancies; such that a child born with CF in the UK today can expect to live into the 5th decade of their life (Keogh et al., 2018), compared to that of 5 years in the early 1960's (Dodge et al., 2007). This drastic improvement can be attributed largely to the development of standardised multisystem treatments constituting: antibiotics, chest physiotherapy, supplementation of digestive enzymes and advances in transplantation surgery (Stern et al., 2014). However, a revolution in today's perspectives mean a shift away from treatment of clinical symptoms. What were once regarded as genetic nuances of CF, are now the target of precision medicine (Marson et al., 2017). Currently, there are three CFTR modulators which have been approved by the European Medicines Agency, with two of these drugs adopting the use of combination pharmacotherapy. However, at a considerable cost of around €150,000 to €250,000 per patient, per year (De Boeck, 2020); a real question mark remains over the universal accessibility of these treatments.

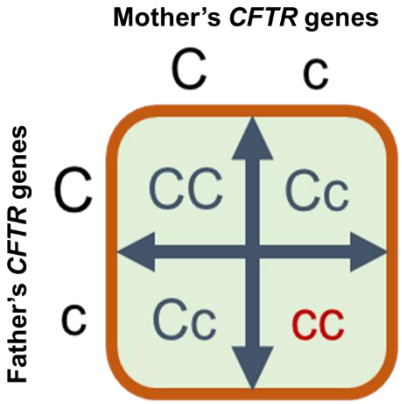

Figure 1.1. CF an inherited, recessive disorder. For CF, an individual must inherit two copies of the mutated CFTR gene. If both parents are carriers there is a 25% chance that the offspring will acquire Cystic Fibrosis. **C**: Functioning CFTR gene; **c**: CFTR gene with mutation; **CC**: Unaffected, not a CF carrier; **Cc**: Unaffected, CF carrier; **cc**: CF Affected (red).

1.1.1 CFTR: Structure and biogenesis

Considerable efforts have been made over the past 30 years to decipher the three-dimensional (3D) arrangement of CFTR. An extensive review by Callebaut et al. (2017), details how our understanding has been based primarily on the theoretical data of comparative modelling and molecular dynamics. Efforts have been restricted due to the difficulties of expressing, purifying and reconstituting high levels of full-length CFTR protein, in its active state (Hunt et al., 2013). However, a major breakthrough came in 2016 when the atomic structure of full length CFTR was resolved using single-particle cryogenic-electron microscopy (cryo-EM). This was first achieved from zebrafish (Zhang and Chen, 2016) and then from human protein (Liu et al., 2017; Zhang et al., 2018). These exciting advances offer a more complete understanding of CFTR, with a greater capacity to correlate global arrangement to function. Nevertheless, some important details are still unknown, including: conformational changes in disease mutant structures, mechanistic actions of modulator compounds and the structural specifics of CFTR gating states.

CFTR is encoded by a 230kb gene found on chromosome 7. It comprises 27 exons and exists as a 1480 amino acid polypeptide (Riordan, 1989). It is composed of two homologous halves, each consisting of a transmembrane domain (TMD) containing six membrane spanning segments (M1-12) and one nucleotide-binding domain (NBD). Both halves on the cytosolic side are interlinked via a central hydrophilic regulatory domain (R domain), which contains several phosphorylation sites (Figure 1.2).

CFTR is a member of the ATP-binding cassette (ABC) transporter gene superfamily, yet is unique from nearly all other ABC transporters. Rather than using the energy from adenosine triphosphate (ATP) hydrolysis to drive an uphill movement of substrate, CFTR instead functions as an ATP-gated ion channel (Zhang et al., 2018). Phosphorylation of the R domain is also necessary for CFTR activation and is a prerequisite for channel gating (Seibert et al., 1999). In its open state, CFTR facilitates the passive diffusion of anions down the prevailing electrochemical gradient (Bear et al., 1992).

Topology studies have shown that the M7-M8 extracellular trans-membrane loop contains two N-linked glycosylation sites that are used *in vivo* (Gregory et al., 1990). It is at the endoplasmic reticulum (ER) that a core glycosylated form of CFTR (~150kDa) is created. This immature form is then trafficked through to the Golgi apparatus and undergoes post-translational modification at its glycan moiety to produce the fully glycosylated CFTR (~170kDa) (Cheng et al., 1990). N-glycosylation enhances both productive folding of the protein (Chang et al., 2008) and its stability within the plasma membrane (Glozman et al., 2009).

In fact, the synthesis of CFTR is inefficient with only 20-50% of protein maturing beyond the ER (Lukacs et al., 1994), as at least four known molecular checkpoints tightly regulate the process of folding and trafficking (Farinha and Canato, 2017). Those that do become fully synthesised, exit in vesicles of the exocytic pathway which facilitate the insertion of CFTR into the plasma membrane (Ameen et al., 2003). Through a dynamic balance of endocytosis and recycling, a functional pool of CFTR are maintained at the cell surface (Okiyoneda and Lukacs, 2007).

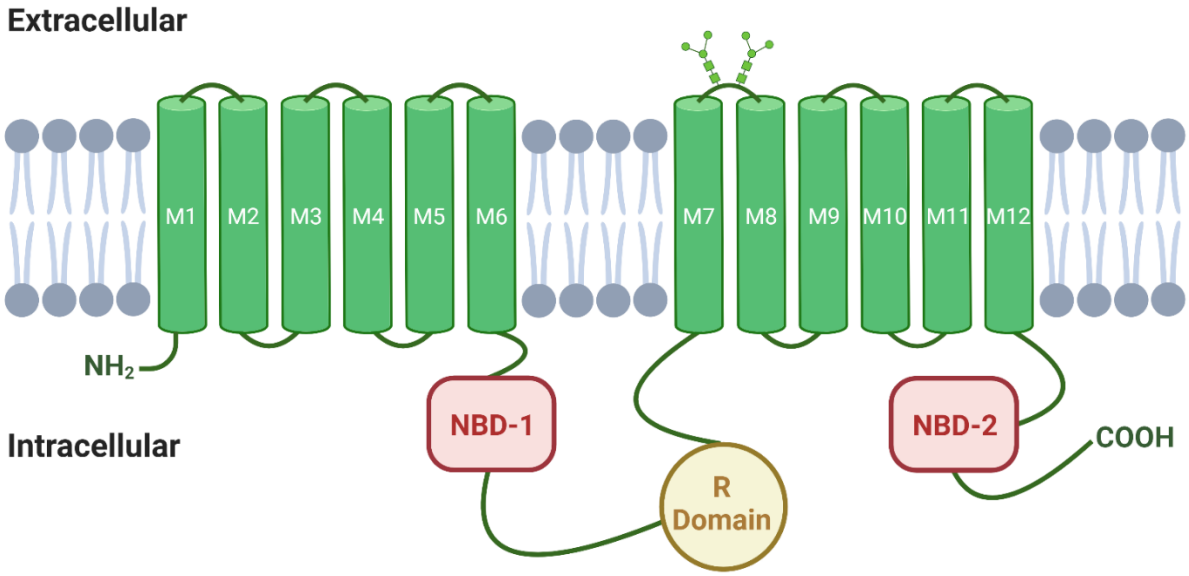

Figure 1.2. The transmembrane topology of CFTR. The protein contains two pseudo-symmetrical halves and exists as a homodimer. Each half contains a six-membrane spanning TMD segment (green), one nucleotide-binding domain (red) and is linked by an unstructured R domain (yellow), for phosphorylated activation. Two N-linked glycosylation sites are present on the M7-M8 extracellular loop.

1.1.2 CFTR: Mechanism of action

Two separate processes of phosphorylation and ATP binding control the gating of CFTR. The first is necessary for activation and the latter for regulation of conformational states. The R domain is intrinsically disordered, with bioinformatics data suggesting the domain may have evolved from a noncoding sequence in the genome, bestowing CFTR a regulatory capacity (Sebastian et al., 2013). Recent structural data suggests that in its dephosphorylated state, the R region prevents NBD dimerisation by sterically hindering physical interaction (Zhang et al., 2017), while synchronously plugging the cytoplasmic entrance of the channel (Fay et al., 2018). Central to activity are a number of phosphorylation sites, for cAMP-dependent, protein kinase A (PKA) interaction. Additionally, protein kinase C activity is fundamental to PKA phosphorylation (Chappe et al., 2004), but at present the mechanism remains less well understood. A study by Hegedus et al. (2009) determined that no one phosphorylation site is essential, rather each has an additive effect upon the activity of channel opening. Moreover, a recent paper by Chen. (2020) established that PKA phosphorylation relieves the C terminus of the R domain from an auto-inhibitory position, to potentiate CFTR gating.

Unlike classical ligand-gated ion channels, CFTR consumes ATP for channel closure. The channel opens when ATP-Mg^{2+} docks into the binding site of each NBD, with magnesium (Mg^{2+}) functioning as an important cofactor for ATP hydrolysis (Dousmanis et al., 2002). Upon interaction, the two NBDs form a head-tail dimer which occludes two molecules of ATP-Mg^{2+} along its interface (Zhang et al., 2017). Resulting conformational changes in the two TMDs, create a transmembrane pathway opening for anions. This rearrangement is akin to the flipping of TMDs from an inward to an outward facing configuration (Csanády et al., 2019). Positively charged amino acids side chains which line the cytosolic entrance between TM4 and TM6, assist in attracting chloride ions to the inner mouth of the pore (El Hiani and Linsdell, 2015). This feature extends to the inner vestibule where the pore is lined with positively charged internal residues (Zhang et al., 2017). This allows physical

interaction with anions as they traverse the channel, although CFTR remains a relatively low-grade anion selectivity filter (Hwang et al., 2018). The channel then proceeds to close upon ATP hydrolysis and the release of adenosine diphosphate (ADP)/inorganic phosphate (Gunderson and Kopito, 1995).

Aside from the primary mechanism of regulation, the influence of the CFTR C-terminus has also gained some attention. Displaying a PDZ-binding motif, the C-terminus can mediate an interaction of CFTR with the cell cytoskeleton (Moyer et al., 1999). Interestingly, the C-terminus also maintains an affinity for the R domain in its phosphorylated state (Bozoky et al., 2013). Potentially, this region may serve as a docking site for the R domain upon displacement from its inhibitory position. Although CFTR is often characterised as a simple ion channel for the passive diffusion of Cl^-, the regulation upholding this process is rather complex.

1.1.3 Pathophysiology of CF

Clinical manifestations of CF correspond to the sites in which CFTR is highly expressed. Predominantly found at the apical membrane of epithelial cells, CFTR maintains control of ion and water homeostasis in most exocrine tissues. Loss or reduction of channel activity leads to dysregulation of the osmotic gradients which drive fluid secretion into the luminal space of primarily, mucus producing organs. Mucus becomes dehydrated, with an increased concentration of polymeric mucins and aberrant biophysical properties (Ehre et al., 2014). The accumulation of viscous mucus can cause deleterious obstructions, such as plugging of the pancreatic and gallbladder ducts (Kreda et al., 2012). Indeed, pancreatic insufficiency (impaired release of proteolytic enzymes) leads to 40–50% of CF adult patients (UK) developing CF-related diabetes; the most commonly associated comorbidity of CF (Granados et al., 2019). Complications associated with liver disease (Kobelska-Dubiel et al., 2014) and gastrointestinal issues (Sabharwal, 2016), are also a feature of ductal mucus impediments. Changes related to fertility similarly demonstrate symptomatic prominence. Blockage or absence of the vas deferens underpins a significant rate of infertility in men,

reported at >98% (Yoon et al., 2019). In contrast, women do not usually exhibit anatomical abnormalities, yet dehydrated cervical secretions become a physical impediment to adequate sperm migration (Kopito et al., 1973). As a result, women are more likely to experience subfertility and seek the assistance of reproductive intervention strategies (Sueblinvong and Whittaker, 2007). Generally, less severe pathologies correspond to exocrine tissues that lack mucus secreting cells including the kidneys (Jouret and Devuyst, 2009) and sweat ducts (Quinton, 1983).

Although CF presents itself as a multi-organ disease, respiratory complications represent the major cause of morbidity and mortality in patients (Zolin et al., 2020). Research has indicated that the lungs of CF infants are predisposed to extensive bacterial colonisation, alongside diminished bacterial clearance capabilities (Stoltz et al., 2010; Muhlebach et al., 2018). It is this susceptibility to infection which contributes to a lifelong detrimental cascade of inflammation and airway remodelling. Like other organs, production of aberrant mucus is intrinsic to this process. Increasing evidence suggests that airway mucus comprises two distinct domains: the mobile layer and periciliary layer (PCL) (Button et al., 2012; Livraghi-Butrico et al., 2017). In CF, dehydration of the epithelial surface compromises periciliary liquid of the PCL. This low viscosity solution is involved in ciliary beating and acts as a lubricant for transport of mucus in the mobile layer. With viscid mucus overlying epithelial cells and a decreased periciliary height, normal clearance is prevented (Button et al., 2012). This perpetuates a cycle of destruction involving: airway mucus obstruction, disseminated bronchiectasis, persistent bacterial infections, chronic inflammation and eventual lung fibrosis (Amaral, 2015). Ultimately, irreversible lung damage precedes respiratory failure, thus leading to the imminent requirement of a lung transplant.

1.1.4 Classification of CF mutations

Recent advances in human genetics has sought to revolutionise our understanding of CF. Integral to this development has been the elucidation of cellular and molecular defects, in correlation to their *CFTR* derived mutations. With this knowledge, a contemporary

classification system has been established. Attention focuses on the applicability of specific modulators for each functional class, rather than the mutation itself. This has constituted a paradigm shift in treatment away from symptomatic management and towards a new era of precision medicine (Marson et al., 2017).

Traditionally classified into six distinct groups, mutational variants are systematised according to their adverse effect upon synthesis, function, trafficking or stability of CFTR (De Boeck, 2020). Since the conception of CFTR modulators, a seventh class has been proposed to include the abortive transcription of CFTR mRNA. Unlike the other classes, these large deletions and frameshift mutations cannot be rescued via corrective medicine (De Boeck and Amaral, 2016). Taken together, these seven functional classes are outlined in figure 1.3.

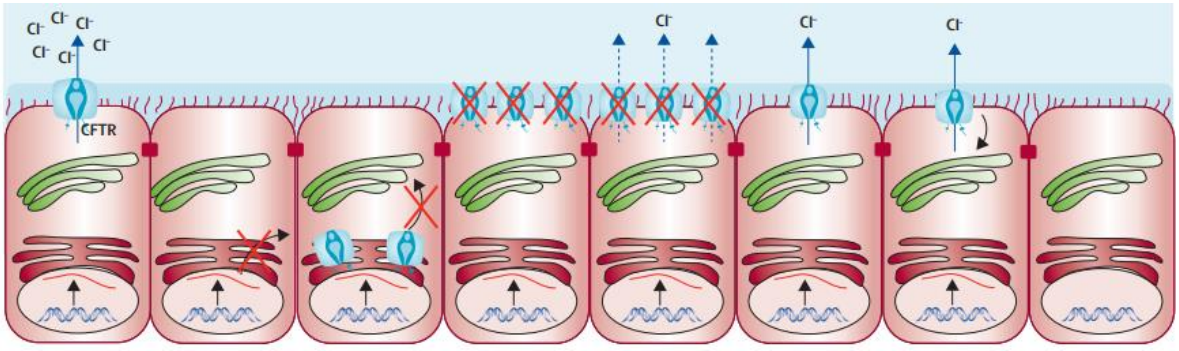

Normal	Class I	Class II	Class III	Class IV	Class V	Class VI	Class VII
CFTR Functional Defect	No function	No traffic	Impaired gating	Decreased conductance	Less protein	Less stable	No mRNA
Mutation example	W1282X	ΔF508	G551D	R117H	3272-26A→G	c.120del23	Dele2,3(21 kb)
Causative mechanism	Introduces a premature termination codon	Mutation in NBD1 prevents native folding	Imparts an insensitivity to cAMP activation	Decreases the open probability of CFTR	Antagonistic activation of a splice variant	N-truncated CFTR with decreased stability	Large deletion spanning introns 1-3
Corrective Therapy	Rescue synthesis	Rescue traffic	Restore channel activity	Restore channel activity	Correct splicing	Promote Stability	Unrescuable

Figure 1.3. Classification of *CFTR* mutations and their respective therapeutic approaches. A new strategy exists which aims to refine the myriad of *CFTR* mutations, into seven distinct functional classes. The hope is to develop modulators that are accurately targeted to a particular sub-type of CFTR defect, rather than each individual mutation. It is worth noting that most mutations can traverse the criteria of more than one class. Adapted from (De Boeck and Amaral, 2016).

Individuals with at least one class IV, V or VI mutation, typically retain residual function of the CFTR channel (Zemanick and Polineni, 2019). This generally equates to a phenotype

of attenuated severity and requires a decreased level of treatment. This is evident in the recognised clinical diagnosis of milder/later onset of symptoms, for example: lower concentration of sweat chloride, diminished presence of CF-related diabetes, reduced liver disease, less chronic *Pseudomonas aeruginosa* infections and a slower decline in lung function (McKone et al., 2003; Dewulf et al., 2015)

In reality, the classification system is likely an oversimplification, as the majority of mutations do not exclusively adhere to one definitive class (Cuyx and De Boeck, 2019). A primary example of this, is that of the most common CF mutation, ΔF508. In Europe, 80.6% of all CF patients possess at least one ΔF508 allele (Zolin et al., 2020). Deletion of the phenylalanine residue at position 508 directly affects NBD1 (Thomas et al., 1991), perturbing the thermodynamic stability of this gating domain (Protasevich et al., 2010). Resultantly, this disrupts a network of interdomain contacts, which maintain interactions between NBD1 and the TMDs (Serohijos et al., 2008). During folding, this causes an incorrect assembly in the cooperative regions of CFTR and leads to ER-associated degradation of the protein (Ward et al., 1995). This functional defect is what defines ΔF508 as a prototypical **(class II)** mutation. Compounding this issue further is the existence of a secondary level of quality control. Research has shown that any ΔF508 CFTR which successfully traffic to the cell surface, become subjected to an increased rate of degradation **(class VI)** (Okiyoneda et al., 2010). It has been estimated that only ~2% of fully glycosylated ΔF508 CFTR insert into the plasma membrane, in comparison to that of wild type protein (Van Goor et al., 2011). Ultimately, the small proportion of ΔF508 CFTR which persist at the membrane, exhibit a reduced rate of PKA-dependent activation (Wang et al., 2000) and demonstrate an instability during NBD dimerisation **(class III)** (Jih et al., 2011). In this state, the open probability of ΔF508 channel is extremely low compared to that of native CFTR (Jih et al., 2011). This exemplifies how a single *CFTR* mutation can exhibit pleiotropic functional defects across multiple classes.

Aside from the *CFTR* genotype, modifier genes and environmental factors also influence

the clinical course of this disease (Cutting, 2010). With such complexities, it is easy to understand the limitations faced when systematising *CFTR* mutations. Yet, the notion of classification is a powerful tool for pharmacologically targeting CF mutations, as it creates a provisional framework for the basis of separation and grouping (Martiniano et al., 2016).

1.1.5 A new era of precision medicine

With the advent of mutational grouping, the last decade has witnessed the emergence of CFTR modulators and heralded a new age of precision medicine for CF. The term 'precision medicine' is the idea of encompassing a wide array of individual data, to tailor treatment in personalised manner (König et al., 2017; Marson et al., 2017). Many concepts central to this strategy are already utilised in the management of CF. A primary example references the surveillance of specific respiratory pathogens in CF individuals, for precise use of particular antibiotics (Paranjape and Mogayzel, 2018). This has now advanced in a genetic capacity, with the development of CFTR modulators. These compounds act to directly target an exact class of functionally associated *CFTR* mutations.

Libraries of compounds have been tested by high-throughput screening (HTS), leading to the identification of five main groups of CFTR modulators. These include: i) potentiators that increase the open probability of CFTR channels to improve gating, ii) correctors that enhance the conformational stability of CFTR to achieve greater efficacy in protein folding and trafficking, iii) stabilisers that prolong the residence time of CFTR at the plasma membrane, iv) amplifiers that augment the expression of CFTR mRNA for increased protein abundance, v) read-through agents that supress premature termination codons by inducing a ribosomal read-through of the CFTR transcript (Lopes-Pacheco, 2020). However, of all the compounds to advance to clinical trials, at present only three drugs have been licensed for use in the UK including: Ivacaftor (Kalydeco), Lumacaftor plus Ivacaftor (Orkambi) and Tezacaftor plus ivacaftor (Symkevi).

1.1.5.1 CFTR modulator therapies

Ivacaftor (VX-770) was the first drug to be licensed, which actively targets the underlying defect of CF (Feng et al., 2018). It binds within a cleft of CFTR, situated at the interface of membrane spanning segments 4, 5 and 8 (Liu et al., 2019). This site coincides with a hinge region in M-8, which confers a conformational flexibility to CFTR during gating (Zhang et al., 2018). The interaction of Ivacaftor with this mobile segment of M-8, is thought to stabilise the open configuration of CFTR, to potentiate channel gating (Liu et al., 2019). Over the 8 years since its approval, the long-term benefits are starting to become apparent with observations of: less frequent infections with key CF pathogens (Frost et al., 2019), slower decline in lung function (Sawicki et al., 2015), reduction in sweat chloride levels (Sawicki et al., 2015), diminished number of pulmonary exacerbation episodes (McKone et al., 2014) and an overall improvement in quality of life (Quittner et al., 2016). Despite its success, the clinical benefit is predominantly restricted to individuals with at least one allele of a class III gating defect (accounting for only 3-5% of the CF population) (De Boeck et al., 2014). Nevertheless, Ivacaftor has paved the way for targeted drug development against the highly prevalent ΔF508 mutation.

The first generation of CFTR corrector to receive approval was Lumacaftor (VX-809). While the putative binding site remains contentious (Hudson et al., 2017; Loo and Clarke, 2017), it is recognised that Lumacaftor functions as a pharmacological chaperone to rescue folding, processing and trafficking of CFTR to the plasma membrane (Van Goor et al., 2011). Despite encouraging data *in vitro*, this did not translate to clinical gains for CF patients *in vivo* (Clancy et al., 2012).

As a result, a movement towards combinational pharmacotherapy was established. By co-administering Ivacaftor and Lumacaftor (a combination known as Orkambi), a modest improvement in lung function of 3% - 4% was observed, albeit for ΔF508 homozygous patients exclusively (Boyle et al., 2014). In reality, the hope for Orkambi has been affected by clinical shortcomings. Studies on Orkambi have shown that Ivacaftor abrogates the

pharmacological correction of ΔF508 CFTR; markedly increasing its turnover rate and affecting the long-term stability of the channel (Cholon et al., 2014). Furthermore, Orkambi induces the activity of hepatic drug metabolising enzyme Cytochrome P450 3A4, which results in a decrease in the plasma concentration of Ivacaftor (Schneider, 2018). On a clinical standing, Orkambi has also been reported to induce adverse events of dyspnoea and abnormal respiration (Wainwright et al., 2015).

Consequently, a second-generation corrector (based on the structure of Lumacaftor) was developed as a successor. Alongside Ivacaftor, Tezacaftor (VX-661) became the replacement compound in this progressive dual combination therapy (named Symkevi). In clinical trials, Symkevi demonstrated improved tolerability and fewer complications associated with drug-drug interactions, but therapeutic efficacy still remained comparable to that of Orkambi (Taylor-Cousar et al., 2017). In regard to viability, clinical gains extended beyond the constraints of Orkambi to benefit both ΔF508 homozygous and ΔF508 heterozygous patients with a residual function mutation (Rowe et al., 2017), approximately 50% of the CF population (De Boeck, 2020). Undoubtedly a step in the right direction, however in a therapeutic context clinical benefits remain modest and a substantial proportion of individuals heterozygous for ΔF508, lack a compatible CFTR modulator therapy.

1.1.5.2 Future treatment strategies

Symkevi has provided the backbone for the most recent advancement in CFTR modulator treatment; an endeavour to produce a triple combination therapy, through incorporation of a next-generation corrector. These next-generation correctors function via an alternative mechanism to Tezacaftor and thus seek to have an additive effect (Lopes-Pacheco, 2020). In late 2019, Kaftrio (known as Trikafta in the US), (Ivacaftor, Tezacaftor and Elexacaftor [VX-445]) became the pioneer of the triple combination therapy and was approved by the American Food and Drug Administration for patient use in the United States. Clinical trials on Kaftrio have shown a significant improvement in lung function of an 11% increase over

Symkevi for ΔF508 homozygous patients (Keating et al., 2018) and interestingly a 14.3% rise for ΔF508 heterozygous patients with a minimal function mutation, in comparison to a placebo group (Middleton et al., 2019). These data are very promising and if true, Kaftrio has the potential to provide effective treatment for ~90% of the CF population.

The development of CFTR modulators has been unquestionably transformative in the field of CF therapeutics. However, patients with rare *CFTR* mutations still present a notable challenge. Gene therapy and gene editing strategies have been proposed to treat individuals which remain unresponsive to current restorative therapies. Yet, both approaches face many barriers in regard to application, with obstacles of: safety, efficiency and vector suitability (Alton et al., 2016). Even clinically approved CFTR modulators have their limitations. A major drawback is the high cost attached to treatment; an aspect comprehensively evaluated by the Institute for Clinical and Economic Review. The report concluded that CFTR modulator therapies exceed commonly used cost-effectiveness thresholds and that lifetime reductions in the rate of CF progression, may be overly optimistic (Tice et al., 2020). This translates to a considerable burden for healthcare systems worldwide and acts to preclude citizens of low-income countries from benefiting (Cohen-Cymberknoh et al., 2016).

Strikingly, the vast majority of combination therapies have been designed to target the CFTR protein directly. In the dynamic environment of CF drug development, compounds are often fast-tracked to clinical trial at the expense of elucidating their CFTR binding sites and corresponding mechanisms of action. With an emerging trend towards the inclusion of more than two CFTR modulators, it is unknown whether antagonistic drug-drug interactions may compromise the long-term efficacy of these treatments. It may become apparent to consider strategies besides the targeting of CFTR exclusively. An alternative approach looks to address prominent changes in the proteostasis of CF cells. Appealingly, such a regulator has the capacity to be combined with any class of CFTR modulator, as proteostasis is independent of CF genotype. This concept of two-directional (direct/indirect

approach) pharmacotherapy, may be a potential avenue of exploration in order to enhance the clinical outcome of CF patients.

1.1.6 Considerations of CF model systems

When investigating aspects of CF, it is important to be mindful of the appropriate application of preclinical model systems. Animal models have served to further our understanding of disease progression and pathophysiology in CF. Murine models were engineered with an inactivated *CFTR*, soon after the discovery of the gene itself (Dorin et al., 1992; Snouwaert et al., 1992). The intrinsic advantages of cost, ease of maintenance and short reproductive cycle (facilitating efficient genetic manipulation), made the mouse an ideal candidate for studying CF *in vivo* (Guilbault et al., 2007). However, it was later discerned that inherent limitations concerning the pathophysiological relevance of CF mice exist; as observed by failure to develop spontaneous respiratory infections, progressive lung disease and pancreatic insufficiency (Durie et al., 2004; Wilke et al., 2011). This has largely been attributed to the presence of a compensatory calcium-activated Cl^- channel (Clarke et al., 1994). To this end, larger animal models for example pigs (Rogers et al., 2008) and ferrets (Sun et al., 2008) have been used to more closely recapitulate the CF pathology of humans. Nevertheless, these animals are resource intensive and intestinal obstruction is a significant caveat, impacting the postnatal survival of both animals (Semaniakou et al., 2019). Recently rabbits and rats have been added to the repertoire of CF animal models (Rosen et al., 2018a), but as of yet, their phenotypic applicability remains undefined. Ultimately, the value of CF animal models has relied upon evaluation of the accumulated data as a collective. These compiled findings have generated an insight into the pathogenesis of CF in humans. In contrast, the individual constraints of each animal model have restricted their contribution, to the development of CF pharmacotherapies (besides toxicology data) (Clancy et al., 2019).

Alternatively, immortalised epithelial cell lines have become the backbone of HTS strategies, for identification and examination of therapeutic compounds. They are generated

through implementation of heterologous expression systems by either: introducing proto-onco genes into primary CF epithelial cells or stably transfecting immortalised (transformed/cancerous) non-CF epithelial cells with mutant CFTR (Gruenert et al., 2004). Ease of culture, cost effectiveness and reliable availability have made these cells an invaluable resource. The Fischer rat thyroid cell line has been used extensively to validate preclinical modulator responsiveness, including Ivacaftor (Van Goor et al., 2009) and Lumacaftor (Van Goor et al., 2011), in addition to their application in drug label expansion studies (Han et al., 2018). However, the higher propensity for false-positive and false-negative "hits" in comparison to primary human bronchial epithelial cells (HBECs), illustrates the apparent limitations of cell line models (Mou et al., 2015).

Primary HBECs from different CF individuals constitute a more representative model of biological relevance and are considered the 'gold standard' for verifying the preclinical efficacy of potential CF therapies, prior to human trials. Cultures are established through expansion of progenitor cells isolated from biopsies, lung explants and post-mortem samples of CF patients (Randell et al., 2011). They have been used to faithfully predict the clinical outcome of pharmacological activity, for both Ivacaftor (Van Goor et al., 2009) and Lumacaftor (Van Goor et al., 2011). When cultured on a porous support at an air-liquid interface, primary HBECs differentiate to form a pseudostratified epithelium that recapitulates the mucociliary phenotype observed in native airways (de Jong et al., 1993). Despite their success, it is important to consider that the majority of CF primary HBECs are procured from lungs with end stage disease and may not genuinely reflect cell behaviour at an early disease state (Clancy et al., 2019). In addition, hindrances of expense, technical complexity, accessibility and finite lifespan have acted to constrain their application as predominant cell models.

This critical bottleneck has driven the development of increasingly sophisticated *in vitro* model systems. A recent concept by Valley et al. (2019), centres on reconditioning an established epithelial cell line (16HBE14o-) to express CFTR mutational variants, in the

native genomic context of the cell. This approach uses an adaptable CRISPR-based gene editing pipeline, to generate isogenic cell models for therapeutic testing. Akin to the individualisation observed with 'precision medicine', this research exemplifies a transition towards a personalised perspective of CF disease modelling. Alternative techniques refrain from employing cell lines completely. Novel strategies including: long term expansion of human airway organoids (Sachs et al., 2019) and differentiation of induced pluripotent stem cells (Merkert et al., 2019), seek to generate a representative library of patient-derived epithelial cells, with a sustained proliferative capacity. These innovative feats of bioengineering reveal a glimpse of what the future may hold for preclinical CF model systems. In practical terms however, the refinement, optimisation and standardisation of these contemporary protocols is essential, before their universal applicability to HTS. The question still remains, which model or combination of systems will best predict long-term clinical outcome measures of new CF drugs? For now, CF primary HBEC cultures and CF epithelial cell lines will continue to bridge the gap, acting as valuable complementary platforms of evaluation.

1.2 Transglutaminases

It has been over 60 years since Heinrich Waelsch and colleagues discovered the first mammalian transglutaminase (TG), in extracts from guinea pig livers (Sarkar et al., 1957). This pioneering study had identified an enzyme with the capacity to catalyse the incorporation of primary amines into proteins, in a calcium (Ca^{2+}) dependent manner. It would later be discerned that this protein was transglutaminase 2 (TG2) and since then, eight additional TGs have been found (Grenard et al., 2001). With the exception of erythrocyte membrane protein band 4.2 (a catalytically inactive, structural TG), all members of the mammalian TG family (TG 1-7 & factor XIII) possess identical sequence homology at their active site (Eckert et al., 2014). This highly conserved catalytic core functions to promote reactions of post-translational modification, which primarily include: deamidation,

amine incorporation and protein crosslinking (Griffin et al., 2002). It is the latter, which has become the eminent focus of research efforts in the TG field.

The mechanism of protein crosslink formation occurs via a sequential two-step process of transamidation and requires the presence of Ca^{2+} for TG activation. In the first instance, the thiol group of a cysteine residue (located in the TG active site), attacks a protein substrate at the γ-carboxamide group of a glutamine residue side chain (acyl-donor). This generates a thioester intermediate, alongside the concomitant release of ammonia (NH_3). Thereafter, the thioester bond is attacked by an ε-amine group of a peptide bound lysine residue (acyl-acceptor), resulting in the creation of an ε-(γ-glutamyl)lysine intermolecular isopeptide bond (Savoca et al., 2018) (Figure 1.4). Formation of these covalent bonds confers a resistance against proteolytic cleavage and mechanical force (Griffin et al., 2002). Ensuing supramolecular structures have a recognised pleiotropic functionality, with roles in: blood coagulation (Tahlan and Ahluwalia, 2014), skin barrier development (Hitomi et al., 2001), bone growth (Aeschlimann et al., 1996), maintenance of pregnancy and wound healing (Tahlan and Ahluwalia, 2014).

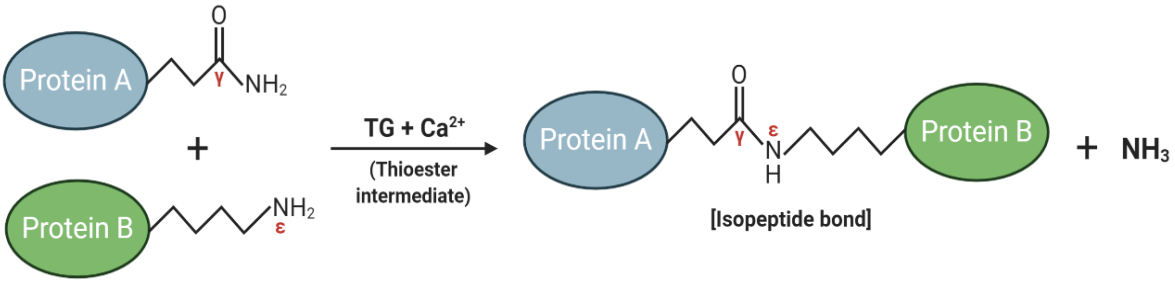

Figure 1.4. Transglutaminase mediated biocatalysis of protein crosslinking. TG subsists in an open conformation (catalytically functional), when activated by Ca^{2+}. In this state, TG can form a thioester bond with the glutamine residue side chain of a target protein substrate (blue). This intermediate product then undergoes nucleophilic attack from the lysine residue of a second protein (green). The two proteins become linked through formation of an ε-(γ-glutamyl)lysine isopeptide bond, with the generation of an ammonia by-product. The TG active site is restored and becomes available for future cycles of catalysis. Adapted from (Duarte et al., 2020)

The evolutionary significance of TGs is evidenced by their broad dissemination throughout the natural world, with their existence observed in: microorganisms, plants, invertebrates and vertebrates (Shleikin and Danilov, 2011). In relation to the mammalian system, each

TG retains a unique profile of distribution within the tissues. In humans for instance, TG2 is widely expressed by the vast majority of cell types in the body (Gundemir et al., 2012), as opposed to TG4 which is exclusively localised to the prostate (Jiang and Ablin, 2011). Overall, TGs participate in a diverse array of cellular and extracellular biological processes and as such, there resides an increased probability that TG perturbations will cause disease. Indeed, TGs are implicated in plethora of disorders including: cancer (Ablin et al., 2017), coeliac disease (Maki et al., 1997), neurodegenerative conditions (Muma, 2007) and afflictions of the skin (Huber et al., 1995); to name but a few. However, it is TG2 which has attracted substantial attention, due to its notable involvement in numerous pathological pathways and prominence as a key player in fibrotic disease.

1.2.1 TG2 Structure

The human TG2 gene is located on chromosome 20 and encodes a protein of 687 amino acids, with a molecular weight of ~78kDa (Mehta et al., 2010). To date, five crystal structures of human TG2 have been elucidated: three in a closed conformation while in complex with a specific nucleotide, GDP (Liu et al., 2002), ATP (Han et al., 2010) or GTP (Jang et al., 2014) and two in an open conformation, through association with a mimetic peptide inhibitor (Pinkas et al., 2007) or in a Ca^{2+} bound state (Jeong et al., 2020). These studies have been an invaluable resource in discerning structural and functional aspects of TG2. It is now understood that TG2 consists of four distinct domains: an N-terminal β-sandwich motif (aa 1-139), a catalytic core (aa 140-460) and two C-terminal β-barrel domains (aa 461-586 and 587-687) (Savoca et al., 2018) as illustrated in figure 1.5.

Situated within the catalytic core is an indispensable triad of residues (Cys277, His335 and Asp358), fundamental to the transamidation activity of TG2 (Liu et al., 2002). It is this nucleophilic cysteine thiol (Cys277), which attacks the glutamine residue side chain during isopeptide bond formation. Positioned in close proximity to the catalytic triad are two crucial tryptophan residues (Trp241 and Trp332). These conserved amino acids function to stabilise the transient thioester intermediate of the protein crosslinking reaction (Murthy et

al., 2002). Beyond transamidation activity, the catalytic core prevails as the primary site of Ca^{2+} binding. The long-standing absence of a Ca^{2+} bound TG2 crystal structure, has restricted our knowledge of Ca^{2+} binding motifs. Instead, structural information has depended on studies of site directed mutagenesis (Király et al., 2009) and comparative analysis (Fox et al., 1999; Ahvazi et al., 2002). With TG2 having the capacity to bind up to six Ca^{2+} ions, five putative binding sites were predicted to exist within the catalytic core domain (Király et al., 2009). However, Jeong et al. (2020) recently resolved a Ca^{2+} containing TG2 crystal, which definitively identifies two glutamate residues (Glu437 and Glu539) as Ca^{2+} binding sites. While Glu437 is situated in the catalytic core region, intriguingly Glu539 corresponds to a location within the β-barrel 1 domain. This novel data is the first to recognise a TG2 Ca^{2+} binding site, positioned outside of the catalytic core.

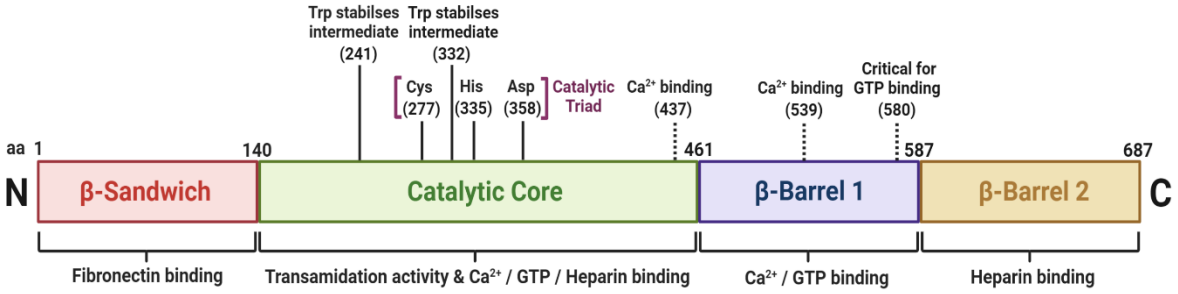

Figure 1.5. Schematic representation of the functional domains and significant binding sites of TG2. Four separate domains constitute the structural arrangement of the TG2 protein: N-terminal β-sandwich (red), catalytic core (green), β-barrel 1 (blue) and C-terminal β-barrel 2 (yellow). Each domain has specific responsibilities, which are coordinated to enable TG2 multi-functionality. Amino acid (aa) residue numbers corresponding to each functional domain and relevant binding site, are indicated above the TG2 structure. Central to transamidation activity is the catalytic triad (purple), which resides in the catalytic core domain of TG2. Adapted from (Mehta et al., 2010).

Akin to Ca^{2+}, guanosine triphosphate (GTP) is also bound by residues of both the β-barrel 1 domain and catalytic core region (Jang et al., 2014). The β-barrel 1 domain supports a critical interaction in GTP binding, whereby an Arginine residue (Arg580) forms two hydrogen bonds with a phosphate moiety of GTP (Jang et al., 2014). In fact, research has shown that a point mutation of the Arg580 residue completely abolishes the GTP binding capacity of human TG2 (Ruan et al., 2008). Alternatively, the β-barrel 2 domain is thought to be involved in the externalisation of TG2. Heparin binding sites which are integral to the

cellular export of TG2 , have been identified in both the C-terminal region (Lortat-Jacob et al., 2012) and catalytic core domain (Lortat-Jacob et al., 2012; Wang et al., 2012). The predicted binding clusters exhibit a large degree of separation in the linear sequence, yet form a single binding surface in the 3D arrangement (Lortat-Jacob et al., 2012). Consequently, for heparin binding sites to be in close spatial proximity, TG2 must subsist in a closed 'compact' configuration. In contrast, the N-terminal β-sandwich domain has been shown to bind Fibronectin, in a manner which remains independent of TG2 conformation. This interaction has been shown to play a significant role in cell: signalling (Telci et al., 2008), migration (Sergey S. Akimov and Belkin, 2001) and progression of fibrosis (Olsen et al., 2011).

1.2.2 Regulation of TG2

TG2 is predominantly characterised as a stress response protein and is dynamically regulated through different mechanisms of cellular and molecular control (Ientile et al., 2007). At a transcriptional level, the human TG2 gene (*TGM2*) associates with a plethora of factors, such as: Retinoids (Shimada et al., 2001), pro-inflammatory cytokines (Kuncio et al., 1998), interleukins (Suto et al., 1993) and steroid hormones (Fujimoto et al., 1996). These transcriptional activators target the highly receptive promoter of *TGM2*, to induce expression of TG2 (Gundemir et al., 2012). Research has shown that certain TG2 pathways even display the capacity for self-reinforcement, through formation of a positive feedback loop. For instance, both nuclear factor-kappa B (NF-*κ*B) and transforming growth factor beta (TGFβ) demonstrate a reciprocal upregulation of activity with TG2, in breast (Ai et al., 2012) and ovarian (Cao et al., 2012) cancer cells, respectively.

However, under normal physiological conditions the activity of TG2 is strictly controlled. Allosteric regulation of TG2 acts as a preventive safeguard against unrestrained crosslinking. The composition of the surrounding environment including: Ca^{2+} ions, guanine nucleotides, and redox potential, modulate conformational changes of TG2 (Eckert et al., 2014). When bound to GTP or guanosine diphosphate (GDP), TG2 adopts a closed

'compact' state. The catalytic active site of TG2 becomes physically occluded, as the two β-barrel domains are shown to be folded inwards (Liu et al., 2002). On the other hand, TG2 also has the capacity to bind up to six Ca^{2+} ions, which facilitate its dissociation from GTP/GDP (Király et al., 2009). Upon Ca^{2+} binding a large structural shift is observed, as TG2 adopts an open 'elongated' configuration. This near linear arrangement permits substrates access to the catalytic active site and eliminates the guanine nucleotide binding site. Pinkas et al. (2007) have demonstrated that the two β-barrels are displaced to a significant degree, in order to achieve this structural transition. A recent study by Jeong et al. (2020) has highlighted a further level of complexity, showing that Mg^{2+} competitively interacts at the Ca^{2+} binding sites. This novel data suggests that Mg^{2+} promotes GTP binding, to crucially control the sensitivity of TG2 to Ca^{2+}.

In a physiological context, intracellular concentrations of GDP/GTP are high and Ca^{2+} concentrations low. As a result, TG2 mainly exists in a closed conformation within the cell and transamidation activity remains broadly silent (Klöock and Khosla, 2012). Conversely, in the extracellular environment GDP/GTP levels are minimal and Ca^{2+} concentrations persist at ~2mM (Clapham, 1995). With Ca^{2+} concentrations of ~1mM required for allosteric activation of TG2, transamidation activity would be expected to prevail outside of the cell (Klöock and Khosla, 2012). However, an additional level of regulation has been evidenced in TG2, involving an intrinsic sensitivity to redox state (Siegel et al., 2008).

The principally oxidative conditions of the extracellular space renders TG2 catalytically inactive in its open form. Formation of two disulfide bonds between a triad of cysteine residues (Cys230, Cys370, and Cys371), was found to be central to this process (Stamnaes et al., 2010). It was discerned that Cys230 operates as an important redox sensor, generating a disulfide bond with Cys370, under oxidising conditions. This was shown to subsequently promote the formation of a more stable disulfide bond between Cys370 and Cys371 (Stamnaes et al., 2010). The precise mechanism by which these disulfide bonds impede the activity of TG2 remains to be elucidated. Nevertheless, it is evident that an

oxidative environment is sufficient to silence the transamidation activity of TG2, even in the presence of Ca^{2+}. Reversal of this catalytic inactivation chiefly requires the involvement of a thiol reductase, notably thioredoxin-1, a protein which selectively recognises oxidised TG2 (Plugis et al., 2017). Thioredoxin-1 is capable of reducing the disulfide bond between Cys370 and Cys371, for efficient activation of extracellular TG2 (Jin et al., 2011). An illustration summarising the allosteric regulation of TG2, is depicted in figure 1.6.

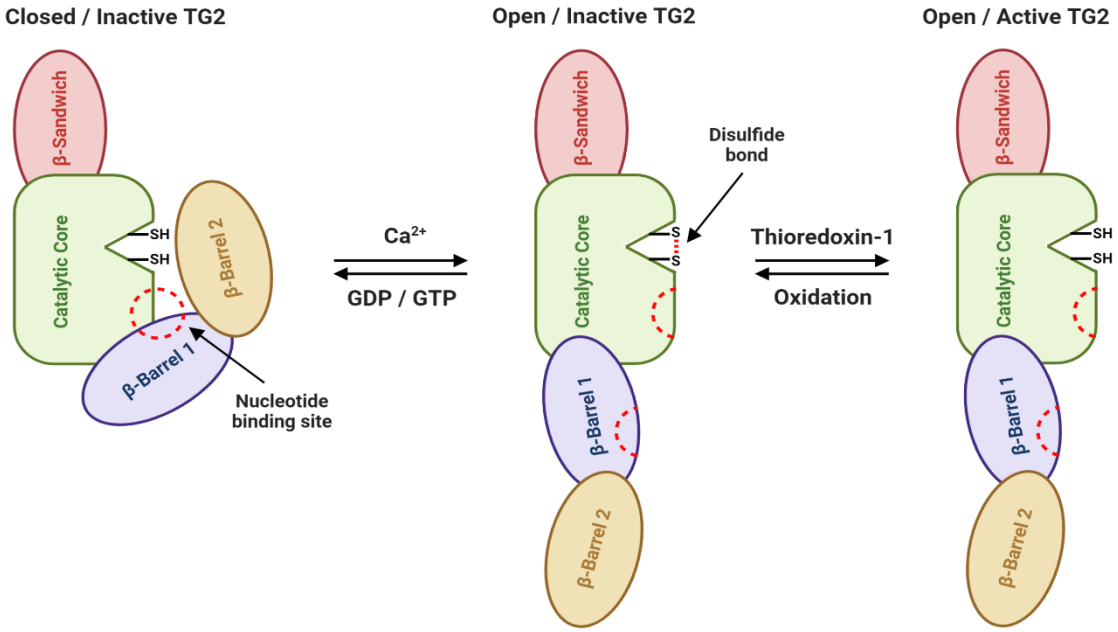

Figure 1.6. The three states of TG2 during allosteric regulation of activity. GDP/GTP binding inhibits catalytic activity by inducing a closed state conformation of TG2. Upon Ca^{2+} binding, TG2 shifts towards an open configuration, thus negating the nucleotide binding site and facilitating the dissociation of GDP/GTP. Only when thioredoxin-1 reduces a restrictive disulfide bond, can TG2 become fully active and engage its crosslinking capabilities. Adapted from (Katt et al., 2018).

Aside from changes in gene expression and allosteric control, it is thought that TG2 is also regulated by various types of post-translational modifications. Although studies addressing the subject have been limited, SUMOylation of TG2 has been evidenced as a case in point. Novel findings by Luciani et al. (2009) show that elevated levels of reactive oxygen species (ROS), mediates SUMOylation of intracellular TG2. As a result, proteasomal degradation of TG2 is prevented, thus enabling sustained activation of the enzyme. This illustrates the complexity of redox state and its influence on TG2, besides just the inhibition of its transamidation activity (Gundemir et al., 2012). Overall, control of TG2 involves the

sophisticated coordination of various regulatory mechanisms. This is vital to maintain correct TG2 functionality, but is often seen to be exploited in several pathological conditions.

1.2.3 Physiological relevance of TG2

The precise role of TG2 is intrinsically linked to the microenvironment in which it is situated (Nurminskaya and Belkin, 2012). TG2 is primarily cytosolic, but can also be found in the nucleus, extracellular matrix (ECM), and associated with the plasma membrane and mitochondria (Piacentini et al., 2014; Cardoso et al., 2015). Besides its well-known ability to crosslink proteins, TG2 displays diverse multifunctionality, combining: GTP/ATP hydrolysis, adapter/scaffolding properties, protein disulfide isomerase (PDI) activity and a kinase capacity (Nurminskaya and Belkin, 2012).

The specific function of TG2 is largely determined by its responsiveness to stimuli of the surrounding microenvironment and direct protein-protein interactions. For instance, under normal physiological conditions cytoplasmic levels of Ca^{2+} are submicromolar, while nucleotide concentrations are high. As a result, cytosolic TG2 exhibits latency in transamidation activity and instead engages in GTPase activated signal transduction (Nakaoka et al., 1994). Alternatively, mitochondrial associated TG2 predominantly operates as a PDI (Mastroberardino et al., 2006). In the presence of a key substrate known as adenine nucleotide translocator 1, mitochondrial TG2 uses its PDI activity to modulate correct assembly of the protein and thus functions as a vital regulator of energy metabolism (Malorni et al., 2009).

In an attempt to define the phenotypic significance of TG2, two groups established a mouse model with a homozygous deletion of the *TGM2* gene (De Laurenzi and Melino, 2001; Nanda et al., 2001). Surprisingly, TG2 knockout mice were found to be viable, grow to a normal weight and size and exhibit no serious abnormalities in relation to development. Considering the multifunctional nature of TG2, the absence of any discernible pathologies is a real conundrum. The general consensus is that other TGs can compensate for the loss

of TG2, therefore rescuing the phenotype of *TGM2*$^{-/-}$ mice (Nurminskaya and Belkin, 2012). However, it must also be acknowledged that other TGs lack the capacity to bind GDP/GTP (Fesus and Piacentini, 2002). This could reflect the notion that GDP/GTP related functions of TG2, show a level of redundancy in mammalian physiology. Alternatively, TG2 in general may participate as more of an auxiliary regulator, as opposed to functioning as an indispensable component of cellular physiology.

Yet, a further consideration is that *TGM2*$^{-/-}$ mice may only highlight the physiological relevance of TG2, in the presence of specific chemical or physical stressors. In actuality, TG2 knockout mice display wound healing deficiencies, as a consequence of decreased fibroblast adhesion with the ECM (Nanda et al., 2001). Sustained research efforts over the past two decades now confirm a prominent role for TG2 in processes of tissue repair and fibrosis; thus emphasising why TG2 is classified as a stress response protein (Ientile et al., 2007; Benn et al., 2019).

1.2.4 The role of TG2 in fibrosis

Acute wound repair is a fundamental biological process, which facilitates tissue regeneration after injury (Wynn, 2007). A study by Upchurch et al. (1991), proposed a pivotal role for TG2 in the regulation of the wound healing response. It was revealed that endogenous TG2 persisted in the surrounding ECM of a wound site, following puncture wounding of a human fibroblast monolayer. Haroon et al. (1999) later confirmed this observation *in vivo*, demonstrating an increase in TG2 expression and activity, up to 3 days after performing punch biopsy wounds in rats.

However, problems arise when there is no resolution of the inflammatory response. This can result if an insult persists or termination of the wound healing process becomes impaired (Verderio et al., 2004). Dysregulation leads to unrestrained remodelling of the ECM and permanent scarring. The destruction of normal tissue architecture eventually

undermines the functional capacity of the affected organ. This abnormal form of wound healing is what defines the pathogenesis of fibrotic diseases (Verderio et al., 2004).

Fibrosis is characterised by the accumulation of myofibroblasts and enhanced deposition of ECM components (Olsen et al., 2011). These pathological features are typically conserved between tissues, irrespective of the initial pro-fibrotic stimuli that drive its induction (Johnson et al., 2007). The mechanisms underlying these changes, have long been the focus of intensive research efforts. In recent times, TG2 has emerged as a common denominator. The enzyme has been implicated in the progressive scar formation of a number of major organs, including those of the lungs (Olsen et al., 2011), liver (Qiu et al., 2007), kidneys (Johnson et al., 2007) and heart (Shinde et al., 2018). Proof of concept studies which either inhibit (Wang et al., 2018), restrict externalisation (Scarpellini et al., 2014) or silence the expression of TG2 (Olsen et al., 2011), have all been shown to reduce fibrosis *in vivo*. However, caution must be taken when interpreting results, as a number of studies which state an inhibition of TG2, do so in a non-specific manner (Johnson et al., 2007; Qiu et al., 2007; Olsen et al., 2014). As such, the inhibitors used are not selective for TG2 and results may be influenced by inhibition of other TGs. It must also be noted that in one particular study, the extent and pattern of liver fibrosis in TG2 knockout mice was found to be comparable to levels measured in wild type mice (Popov et al., 2011). This may indicate that in certain tissues, TG2 is a dispensable mediator of fibrosis. Yet, these findings are more likely a reflection of the method used to induce fibrosis and/or a circumstance of the experimental model itself. Overall, research substantiates the role of TG2 as a key effector protein for the development and progression of fibrosis.

TG2 promotes fibrotic disease through its enzymatic capacity to crosslink proteins. This was demonstrated in a study by Johnson et al. (2003), which analysed 136 human biopsies from a variety of chronic renal diseases. It was established that the level of TG2 and ε(γ-glutamyl) lysine crosslinking, strongly correlated to the severity of renal scarring and that changes remained independent of the original aetiology. The transamidation activity of extracellular

TG2 has now been linked with two crucial pro-fibrotic roles. Firstly, TG2 effectively crosslinks fibrils of the ECM, principally collagen and fibronectin (Benn et al., 2019). As previously stated, these qualitative modifications create a stiffened matrix, which confers protection against proteolytic degradation. Indeed, Gross et al. (2003) measured a reduced rate of matrix turnover, in response to increased levels of TG2. The formation of a rigid ECM also supports the second role of TG2; the recruitment and activation of TGFβ1.

Initially, TG2 establishes a large reservoir of latent TGFβ1 in the ECM, by crosslinking an inactive complex of TGFβ1 to fibronectin and fibrillin (Klingberg et al., 2018). Storage is further enhanced via the multimerization of latent TGFβ1, which depends on TG2 crosslinking for stabilisation (Troilo et al., 2016). Matrix bound TGFβ1 is then activated through either proteolysis or mechanical force (Biernacka et al., 2011). Mechanical activation relies upon the contractile force of cells, which is seen to be especially efficient in a stress resistant environment (Wipff et al., 2007). This is the case in a TG2-crosslinked matrix, whereby prestress (internal tension) sensitises TGFβ1 for activation (Klingberg et al., 2014). Once active, TGFβ1 is a particularly effective mediator of fibrosis. Significantly, TGFβ1 drives myofibroblast transdifferentiation from various cellular progenitors including: fibroblasts (Masur et al., 1996), pericytes (Chang et al., 2012), endothelial cells (endothelial mesenchymal transition, EndMT) (Piera-Velazquez et al., 2011) and epithelial cells (epithelial-mesenchymal transition) (Nyabam et al., 2016).

In essence, myofibroblasts serve as the linchpin of tissue fibrogenesis. They are responsible for the excess production of fibrous ECM components and express alpha-smooth muscle actin (α-SMA), a contractile stress fibre which incorporates tensile strength into the matrix (Hinz et al., 2012). During the normal process of acute wound repair, the existence of myofibroblasts is transient and their function is both spatially and temporally constrained (Van De Water et al., 2013). However, in the presence of an unremitting inflammatory response, as seen in tissue fibrosis, a vicious self-reinforcing feedback loop between TG2 and TGFβ1 is established (Benn et al., 2019). This profound change in protein

homeostasis promotes the continuous survival of myofibroblasts (Van De Water et al., 2013). As a result, myofibroblast activity persists, which perpetuates the pathological scarring observed in fibrotic disorders. Recent findings now indicate that TG2 acts to implement such changes in CF (Nyabam et al., 2016).

1.2.5 TG2: A key player in CF

Despite the etymology of CF, research has generally focused on the genetics of the disease, rather than the pathogenesis of fibrosis itself. Lung fibrosis has remained a key hallmark of CF, yet attempts to investigate the underlying molecular changes has only recently begun. In accordance with other fibrotic diseases, expression and activity of TG2 is found to be significantly upregulated in CF. Intriguingly, this has been shown to occur both intracellularly (Maiuri et al., 2008) and within the extracellular environment (Nyabam et al., 2016). As stated previously, allosteric control mechanisms typically prevent the activation of TG2 within the cell (Katt et al., 2018). However, CF epithelial cells exhibit a dysregulation of the proteostasis network, in response to a defective CFTR (Esposito et al., 2016). This enables high levels of intracellularly active TG2, which creates an inherent pro-inflammatory profile in CF airways (Maiuri et al., 2008). Alternatively, extracellular TG2 embraces its common role as a pro-fibrotic mediator (Nyabam et al., 2016).

1.2.5.1 The pathogenic significance of intracellular TG2 in CF

Increasing evidence suggests that CF airways display a pro-inflammatory phenotype, prior to bacterial infection (Perez et al., 2007; Rosen et al., 2018b; Verhaeghe et al., 2007). This was initially linked to the defective CFTR protein (Perez et al., 2007), yet the mechanism underpinning this pathogenic trait had previously remained elusive. However, it has now become apparent that TG2 operates as a crucial mediator of this response (Luciani et al., 2011). Research has shown that misfolding of ΔF508 CFTR, induces significant stress in the ER (Bartoszewski et al., 2008). This causes increased levels of ROS and an elevation of Ca^{2+} concentration within the intracellular environment (Maiuri et al., 2008). The

overproduction of ROS facilitates PIASγ (protein inhibitor of activated STAT protein gamma) dependent, SUMOylation of TG2 (Luciani et al., 2009). It has been demonstrated with other proteins, that SUMOylation of lysine side chains is incompatible with ubiquitination of these residues (Desterro et al., 1998; Buschmann et al., 2000). Thus, impediment to the ubiquitination of TG2 prevents its targeting for proteasomal degradation and leads to an increase in its expression (Luciani et al., 2009). In conjunction, the permissive rise in cytosolic Ca^{2+}, enables TG2 to catalyse transamidation reactions within the cell (Maiuri et al., 2008). As such, intracellular proteins are crosslinked, thereby disrupting the proteostasis of CF airway epithelial cells.

Ultimately, TG2 modulates inflammation through sequestration of peroxisome proliferator-activated receptor gamma (PPARγ), a negative regulator of inflammatory gene expression. Research shows that TG2-mediated crosslinking of PPARγ can induce its formation into aggresomes, therefore enhancing classical parameters of inflammation (Maiuri et al., 2008). Normally, autophagy would respond as a cytoprotective mechanism, for the removal of these deleterious protein aggregates. However, Luciani et al. (2011) demonstrated that TG2 also triggers an inhibition of autophagy. By crosslinking Beclin 1 (a central regulator of autophagosome formation), the autophagic pathway becomes defective and damaged/misfolded proteins accumulate, (e.g. PPARγ). A destructive cycle of increased ROS and TG2 ensues, thereby contributing to the intrinsic pro-inflammatory profile seen in CF airways. Besides protein crosslinking, cytosolic TG2 also uses its PDI activity to regulate cellular proteostasis and the stress response (Rossin et al., 2018). Evidently, TG2 involvement is multifaceted regarding this CF inflammatory cascade.

1.2.5.2 The pathogenic significance of extracellular TG2 in CF

In parallel to its intracellular role, TG2 can also effectuate changes in the extracellular environment. Upon externalisation, TG2 functions as expected adopting its conventional role as a pro-fibrotic regulator. A recent study by Nyabam et al. (2016) is the first to demonstrate extracellular TG2-mediated crosslinking in CF. Akin to other fibrotic diseases,

TG2 was found to increase the expression and matrix deposition of Fibronectin. Furthermore, TG2 was shown to elevate TGFβ1 levels, which could be reduced through use of a selective TG2 inhibitor. Beyond its pro-fibrotic properties, TGFβ1 can adversely impact the function and morphology of CF epithelial cells. A study by Snodgrass et al. (2013), revealed that TGFβ1 can inhibit CFTR biogenesis and restrict the functional rescue of ΔF508 CFTR. Additional findings by Nyabam et al. (2016) show that TGFβ1 is also capable of inducing EMT in CF epithelial cells, possibly via a canonical Smad2/3 signalling pathway.

Considering the quantity of research examining the intracellular role of TG2 in CF, the literature remains comparatively limited regarding its extracellular capacity. At present, our understanding is primarily based on a single study (Nyabam et al., 2016). Clearly a positive development, yet there persists a need to validate and enhance these findings further; especially given the predominant use of cell lines in this investigation. As previously stated, CF model cell lines may be limited in their physiological relevance. Cell immortalisation has the potential to render the morphology and cellular dynamics disparate from their tissue of origin (Pan et al., 2009). For this reason, future research must substantiate these results in a more reliable model system, such as CF patient primary cells.

This work also generates some intriguing questions in relation to the specifics of TGFβ1 signalling in CF. Activation of the non-canonical (non-Smad2/3) pathways by TGFβ1, are becoming increasingly recognised as critical processes in the pathogenesis of fibrosis (Finnson et al., 2020). Is it then possible that in addition to the Smad2/3 signalling already observed (Nyabam et al., 2016), signal transduction via non-canonical pathways are also implicated in CF? Furthermore, this study demonstrates the interconnection between TG2, TGFβ1 and EMT in a CF epithelial cell line (Nyabam et al., 2016). As previously mentioned, myofibroblasts are critical components of fibrosis, which can emerge from epithelial precursors. In subsequent studies it may be pertinent to evaluate whether the development of EMT, is in reality the process of myofibroblast transdifferentiation.

As reported with CF, the externalisation of TG2 is found to be a common feature of fibrotic conditions. However, the precise mechanism by which this occurs continues to remain the focus of intense scrutiny. Recent insights have proposed an unconventional route for TG2 secretion, but further research is required for confirmation of these findings.

1.3 Externalisation of TG2

Despite the well-established link between extracellular TG2 and fibrosis, the process of TG2 secretion is still to be fully elucidated. In contrast to the majority of exported proteins, TG2 lacks a signal peptide (Chou et al., 2011). These peptide sequences are N-terminal extensions, which target proteins for externalisation using the conventional secretory pathway (via the ER, Golgi apparatus, plasma membrane and ultimately to the extracellular environment) (Owji et al., 2018). Significant findings have identified heparan sulfate proteoglycans (HSPGs), specifically syndecan-4, as essential binding partners of TG2 in a range of diseases (Furini and Verderio, 2019). It is now thought that syndecan-4 is responsible for trafficking TG2 to the ECM, via a non-classical pathway (Furini et al., 2020).

HSPGs are glycoproteins characterised by the presence of one or more covalently linked heparan sulfate (HS) chains. The HS chains are strongly negative and sulfate modifications are highly dynamic, allowing HSPGs to interact with a plethora of ligands (Sarrazin et al., 2011). One such ligand is TG2, first shown to promote a novel RGD-independent cell adhesion pathway by directly binding HS chains of HSPGs (Verderio et al., 2003). Central to this process is the specific interaction between TG2 and syndecan-4 (a membrane bound HSPG with diverse functionality) (Telci et al., 2008), Crucially, a study by Scarpellini et al. (2009) sought to further examine the relevance of this interaction, using syndecan-4 knockout fibroblasts. It was discovered that these cells displayed an ineffective capacity to externalise TG2, resulting in the concurrent accumulation of TG2 in the cytosol. This finding was a major development, establishing the first link between syndecan-4 and its role in trafficking TG2 to the ECM.

It has since been revealed, that TG2 contains a heparin binding site for direct association with HS and heparin (a heavily sulfated analogue of HS). However, no definitive consensus has been reached over its precise location within the TG2 sequence. A study by Wang et al. (2012) proposed a putative binding region of 21 amino acids (aa 202 – 222), located in the catalytic core domain. Site-directed mutagenesis of key basic residues (Lys205 and Arg209), were found to be crucial for heparin binding. In contrast, independent analysis of two mutated Lysine residues (Lys202 and Lys205) positioned within this suggested binding site, found no reduction in TG2 affinity for heparin (Lortat-Jacob et al., 2012). Instead, two isolated clusters of basic residues (aa 262 – 265 and 598 – 602) were identified as a credible alternative. Such lack of coherence may feasibly be attributed to the two separate approaches used to quantify the heparin binding properties of TG2; with one group using a heparin-sepharose affinity isolation column (Wang et al., 2012) and the other using surface plasmon resonance spectroscopy (Lortat-Jacob et al., 2012). Although the explicit placement of the heparin binding site is yet to be determined, both studies do confirm that TG2 binding of heparin/HS is conformation dependent. Only in a closed configuration does TG2 exhibit a high affinity for heparin/HS, while a significant reduction in binding is evidenced in its open form (Lortat-Jacob et al., 2012; Wang et al., 2012).

It has now been established that syndecan-4 is a key pro-fibrotic partner of TG2, integral to the cellular export of the enzyme. This was illustrated by the protective impact of syndecan-4 knockout, in two mouse models of tubulointerstitial fibrosis (Scarpellini et al., 2014). Remarkably, the absence of syndecan-4 resulted in reduced levels of extracellular TG2, a decrease in TGFβ1 activation and an amelioration of kidney fibrosis in both models. Nevertheless, the mechanism by which TG2 achieves cellular release has remained enigmatic. One leading theory which incorporates syndecan-4 involvement has recently emerged. Novel research by Furini et al. (2018) suggests that extracellular vesicles (EVs), specifically exosomes, are responsible for trafficking TG2 to the cell surface, in a syndecan-4 dependent manner.

1.3.1 Extracellular vesicles: A brief overview

EVs are a heterogenous population of lipid bilayer enclosed structures, revealed to be an important facet of intercellular communication (Van Niel et al., 2018). Initially thought to function as a process for eliminating unwanted proteins, EVs are now understood to package and transport various forms of cargo, including: lipids, nucleic acids, proteins and organelles (Doyle and Wang, 2019). Research has indicated that the overall composition of EVs is largely dependent upon cell type and its corresponding physiological state. As an example, cellular stress has been found to alter both the protein and RNA content of endothelial cell derived EVs (de Jong et al., 2012). Indeed, it is the unique composition of EVs, which defines their purpose and function. In a similar context, EVs also differ greatly in size, ranging from approximately 50–5,000 nm (Mathieu et al., 2019). The overall heterogeneity of biophysical properties has previously created difficulties in distinguishing the exact role of EVs. Therefore, a crucial breakthrough has been the recognition of EV subtypes. EVs are now broadly classified into three main subgroups, defined as: exosomes, microvesicles and apoptotic bodies. The principal features of each subtype are summarised below in Table 1.1.

Table 1.1. The main characteristics of the most widely studied and recognised EV subtypes.

EV Subtype	Exosome	Microvesicles	Apoptotic Bodies
Origin	Endosomal system	Plasma membrane	Plasma membrane
Size	~50–150 nm	~100–1,000 nm	~100–5,000 nm
Function	Intercellular communication and pathogenesis	Intercellular communication and pathogenesis	Facilitate efferocytosis
Cargo	lipids, nucleic acids and proteins	lipids, nucleic acids and proteins	Nuclear fractions, cell organelles

1.3.1.1 Exosomes

Exosomes are typically the smallest type of EV at around 50–150 nm in diameter (Mathieu et al., 2019). They form through the inward budding of early endosomes, an intermediary of

mature multivesicular bodies (MVBs). Ultimately, mature MVBs (and their contents) are either targeted for lysosomal degradation or fuse with the cell's plasma membrane for release of exosomes into the extracellular environment (Raposo et al., 1996). It is still unknown whether distinct subpopulations of MVBs exist (Buschow et al., 2009), or cells instead maintain a finely tuned balance between secretion and degradation (Villarroya-Beltri et al., 2016), or possibly a combination of both? Irrespective of the mechanism, control of the process appears to be largely influenced by the endosomal sorting complex required for transport (ESCRT) machinery, a vital regulator of cargo sorting and exosome biogenesis.

The ESCRT machinery is a family of proteins which assemble into 4 sequential protein complexes (ESCRT-0, -I, -II and -III), in conjunction with its associated accessory proteins (Schmidt and Teis, 2012). Both ESCRT-0 and ESCRT-I function to cluster ubiquitylated cargo proteins into membrane microdomains, followed by recruitment of ESCRT-II and ESCRT-III which accomplish membrane budding and scission (Van Niel et al., 2018). Intriguingly, syndecans have been found to intersect the ESCRT machinery through formation of a tripartite complex with syntenin and ALG-2-interacting Protein X (ALIX) (Baietti et al., 2012). This syndecan assembly was shown to not only support the biogenesis of exosomes, but to also influence the selective loading of these vesicles with specific cargo.

Alternatively, exosomes can form in the absence of ESCRT machinery, although the mechanism is less well defined (Stuffers et al., 2009). Proteins of the tetraspanin family appear to be instrumental in this process, particularly CD63 (van Niel et al., 2011). Moreover, ESCRT-independent exosomes are seen to be enriched in ceramide, a cone shaped lipid which induces negative curvature (intraluminal budding) of the endosomal membrane (Trajkovic et al., 2008). Taken together, the formation of exosomes involves different sorting machineries, which influence the preferential selection of vesicle cargo. By regulating the composition of exosomes, sorting machineries act as the main determinants of their functional roles.

The final step of exosome secretion involves MVB fusion with the plasma membrane. The process is not entirely understood, but is thought to involve soluble N-ethylmaleimide-sensitive factor attachment protein receptor (SNARE) complexes (Wei et al., 2017) and require Ca^{2+} (Savina et al., 2005). Once released, exosomes engage in various physiological events, yet their involvement in disease states is becoming increasingly evident. Research has now revealed that exosomes are implicated in: cancer (Hoshino et al., 2015), neurodegenerative disorders (Marie et al., 2015), cardiovascular conditions (Yu et al., 2012), viral infections (Arenaccio et al., 2014), and more recently tissue fibrosis (Furini et al., 2018).

1.3.1.2 Microvesicles and apoptotic bodies

In contrast, microvesicles and apoptotic bodies are predominantly larger than exosomes. Both EV subtypes originate from the plasma membrane, with microvesicles budding directly from the surface of healthy cells and apoptotic bodies generated through the outward membrane blebbing of dying cells (Doyle and Wang, 2019). The mechanism of microvesicle formation is still to be fully elucidated, yet the process is seen to involve changes in Ca^{2+} concentration, lipid distribution, enzymatic activity (crucially translocases and scramblases) and a rearrangement of the cytoskeletal structure (Van Niel et al., 2018). Alternatively, apoptotic bodies result from an increase in cytosolic-hydrostatic pressure following cell contraction (Charras et al., 2005). Functionally, microvesicles operate in a similar context as exosomes, mediating intercellular communication via cargo transportation. The role of apoptotic bodies remains less well defined, although they most likely promote the efficient clearance of apoptotic cells through ‘find me’ and ‘eat me’ signals (Grant et al., 2019).

Despite separate routes of biogenesis, the characterisation of EV subtypes continues to be problematic. The potential for overlapping sizes and shared vesicle composition, increases the likelihood of co-isolation when sorting EV populations (Van Niel et al., 2018). In an attempt to differentiate EV subtypes, research by Kowal et al. (2016) used quantitative proteomic analysis to compare isolated fractions of EVs. The study identified a subset of

tetraspanins (CD9, CD63 and CD81) enriched in the fractions of exosomal sized EVs. However, these proteins were also present in the fractions of large EVs, thus precluding their relevance as exosome-specific markers. Components of the ESCRT machinery have also been considered as markers of distinction, yet co-expression across EV subtypes is again an issue (Nabhan et al., 2012). Due to the large degree of commonality displayed between vesicles and the current limitations of isolation techniques, accurately distinguishing EV subtypes will be a major goal of future research. (Furini et al., 2018).

1.3.1.3 The role of extracellular vesicles in TG2 secretion

As previously stated, TG2 does not possess the necessary signal peptide required for externalisation via the classical secretory pathway. However, almost a decade ago the first insights into TG2 export began to emerge. Significantly, TG2 was identified in EVs derived from cancer cells (Antonyak et al., 2011) and its secretion was shown to be associated with the endosomal system (Santhanam et al., 2011; Zemskov et al., 2011). Thereafter, the presence of TG2 was reported in EVs derived from other cell systems (Van Den Akker et al., 2012; Piacentini et al., 2014); although the size of EVs found to be involved varied substantially between these studies.

Subsequently, research by Diaz-Hidalgo et al. (2016) sought to specifically investigate the role of smaller EVs (exosomes) in TG2 trafficking. The study confirmed that TG2 was present in secreted exosomes, but only upon induced impairment of proteostasis. Under this enforced state of cellular stress, TG2 was shown to interact with two major components of the ESCRT sorting machinery: tumour susceptibility gene 101 (TSG101) and ALIX. Surprisingly, even TG2 itself was found to be implicated in exosome biogenesis, engaging in the active recruitment of vesicular cargo (Diaz-Hidalgo et al., 2016). Crucially, these findings were the first to demonstrate that exosomes can mediate the selective release of TG2, as a response to pathophysiological conditions. On the other hand, details of syndecan-4 involvement and the extent to which large EVs contribute to this process, still remained unresolved.

To clarify this mechanism further, a recent study examined the TG2 interactome in membranes of wild type/fibrotic mouse kidneys, using co-immunoprecipitation and quantitative proteomics (Furini et al., 2018). By using a protein database to identify the functional properties of binding partners, TG2 was shown to strongly associate with exosomal proteins (including syndecan-4), especially under fibrotic conditions. Moreover, comparison of EV fractions isolated from NRK52E cells (rat renal epithelial cell line), revealed a high level of TG2 in exosomes and only weak expression in microvesicles (Furini et al., 2018). Similarly, TG2 was detected in exosomes purified from pooled urine samples of chronic kidney disease patients, while its presence was absent from microvesicle fractions (Furini et al., 2018). Predictably, TG2 was also found to co-precipitate with syndecan-4 in exosomes produced by NRK52E cells and subsequent knockout of this HSPG, led to a major reduction of TG2 in exosomes (Furini et al., 2018). In support of these findings, the inhibition of membrane fusion events (a specific requirement for exosome secretion), also acts to restrict TG2 release (Furini et al., 2020). In summary, this evidence indicates that TG2 is recruited to exosomes via its interaction with syndecan-4 and is accordingly externalised through the exosomal pathway during kidney fibrosis. A representation of this potential mechanism of TG2 secretion is depicted in figure 1.7.

Novel research has now demonstrated a functional relationship between tumour-derived exosomes and the development of metastasis (Shinde et al., 2020). Results show that exosomes released from metastatic breast cancer cells contain aberrant levels TG2, which drives the formation of a metastatic niche. Upon exosomal secretion, TG2 acts to crosslink fibronectin and transform the native matrix into a more tumour-permissive microenvironment (Shinde et al., 2020). This study highlights the importance of exosomes in TG2-mediated alterations of the ECM. In addition, TGF-β1 treatment of NRK52E cells was found to increase the expression of TG2 in exosomes (Furini et al., 2018). Overall, this indicates the dynamic interplay between release of exosomal TG2, matrix crosslinking, TGF-β1 activation and its possible stimulation of TG2 enriched exosomes.

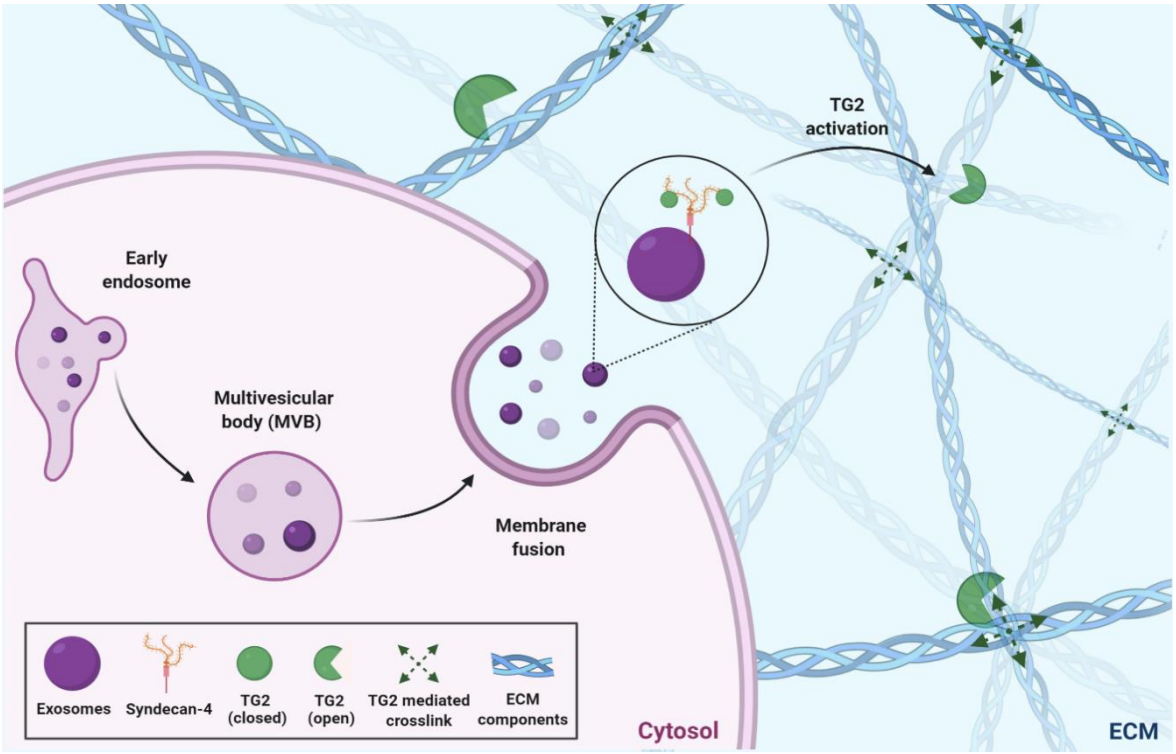

Figure 1.7. Externalisation of TG2 via a syndecan-4 dependent non-classical pathway. A proposed mechanism for TG2 secretion to the extracellular environment. Exosomes originating from early endosomes incorporate syndecan-4, allowing TG2 to directly interact with this HSPG using its heparin sulfate binding site. Exosomes contained within mature MVBs are then targeted for fusion with the plasma membrane. These intraluminal vesicles are then released to the ECM, whereby inactive TG2 is exposed to high Ca^{2+} and low GTP concentrations. This conceivably lowers the HS binding affinity of TG2 and induces a conformational change towards its linear (open) state. Once active, TG2 can crosslink protein fibres of the ECM (e.g. fibronectin and collagen) into a fibrotic matrix. Adapted from (Furini et al., 2018).

Despite recent advances in our understanding of the TG2 secretory pathway, its involvement in fibrotic conditions still remains relatively unsubstantiated. To establish whether the association between EVs and TG2 is a common feature of fibrosis, its validation in other fibrotic systems is essential. Further research is also required to determine the mechanism by which exosomes increase extracellular levels of TG2. In essence, are exosomes enriched with TG2 as suggested (Furini et al., 2018) or do cells actually produce a higher concentration of exosomes, or a combination of both? Considering that TG2 is an attractive therapeutic target, there is now a growing need to evaluate the effect of TG2 inhibition on EV secretion.

1.4 TG2 inhibitors and their therapeutic potential in fibrosis

Given the importance of TG2 in various pathological conditions, particularly fibrosis, TG2 inhibitors have been developed as both an investigative tool and as a prospective therapeutic strategy. The vast majority of inhibitors have been designed to suppress TG2 activity, although preventing TG2 externalisation has also been reported as an alternative approach (Wang et al., 2012). Depending on the mechanism of action, these inhibitors are broadly categorised into three main types: competitive amines, reversible and irreversible inhibitors (Keillor et al., 2015).

The earliest form of TG inhibitors were competitive amines. These primary amines act by competing with biogenic amine substrates, to restrain the formation of native isopeptide bonds (Keillor et al., 2015). However, lack of specificity regarding the exclusive inhibition of TG2, has led to the creation of more targeted inhibitors. Unlike amines, reversible inhibitors work in a more standard fashion. They are not directly involved in the reaction, but instead bind TG2 to impede its catalytic activity (Keillor and Apperley, 2016). The application of such inhibitors may be pharmacologically safer for clinical studies, yet poor solubility and low efficiency limits their therapeutic value (Szondy et al., 2017).

A further consideration is off-target implications. A primary example is GK921, a small molecule inhibitor which binds the N-terminus of TG2 at an allosteric binding site. Although GK921 binds outside of the catalytic core, its interaction induces a conformational change which causes polymerisation and inactivation of TG2 (Kim et al., 2018). Crucially, its site of contact overlaps with a p53 binding region, a protein supressed by TG2 (Kang et al., 2016). Thus, GK921 and p53 compete for the same binding site, which promotes the stabilisation of p53 and enables its increased activity (Kim et al., 2018). Evidently, inhibitors not directed towards the active site have a larger potential for non-specific effects.

For such reasons, many of the TG2 inhibitors developed are irreversible. Generally, these inhibitors are designed as analogs of a TG2 substrate (acyl-donor) and target the cysteine

residue of the active site (Szondy et al., 2017). They commonly incorporate a peptidomimetic scaffold, which enables an electrophilic functional group (warhead) to be positioned next to the nucleophilic thiol group of Cys277 (Keillor and Apperley, 2016). Following much research, 'warheads' have been refined for their stability and reactivity, making these compounds particularly effective inhibitors (Keillor et al., 2015). The beneficial impact of such compounds has been revealed, when applied to fibrotic model systems. Studies have demonstrated their capacity to ameliorate pathophysiological features of kidney (Badarau et al., 2015), lung (Nyabam et al., 2016) and cardiac fibrosis (Shinde et al., 2018). Indeed, the first irreversible TG2 inhibitor (ZED1227) has already entered advanced clinical trials for the potential treatment of individuals with coeliac disease (Ventura et al., 2018).

With TG2 playing a central role in the development of CF, inhibition of its aberrant activity is now a focus of therapeutic intervention. The endogenous competitive amine, cysteamine, was the first TG inhibitor to be evaluated in the context of CF. In a small scale clinical investigation, cysteamine was administered to 10 (ΔF508 homozygous) CF patients, alongside epigallocatechin gallate (EGCG), a green-tea flavonoid (De Stefano et al., 2014). Analysis of nasal epithelial cells collected from patients after treatment showed restoration of CFTR function and reduced levels of pro-inflammatory cytokines (De Stefano et al., 2014). This pilot study was followed by an open-label phase II clinical trial, which claimed to observe similar effects (Tosco et al., 2016). However, in complete contradiction to these findings, an independent study reported an absence of response for cysteamine treatment, either alone or together with EGCG (Awatade et al., 2019). Clearly, further scrutiny of cysteamine is required and issues concerning the application of a non-robust, pan TG inhibitor still need to be addressed.

In contrast, specific, irreversible peptidomimetic inhibitors of TG2 have been developed at Aston University, which target the Ca^{2+} activated configuration of the enzyme in the intracellular and/or extracellular space (Badarau et al., 2015). The cell permeable inhibitor,

1-155, has been shown to be a potent and highly selective inhibitor of TG2 (Badarau et al., 2015). Its addition to an established CF epithelial cell line was found to restore CFTR at the plasma membrane, with CFTR levels shown to increase beyond that of cysteamine treated cells (Nyabam et al., 2016). Furthermore, 1-155 was also seen to reduce the presence of TGFβ1 in the matrix and partially reverse the expression of EMT markers. These preliminary results are certainly encouraging and provide a basis for exploring the capacity of 1-155 further. CF has long been considered a channelopathy, which is only reparable by targeting the CFTR defect directly. Application of a highly specific TG2 inhibitor presents an alternative therapeutic approach, which can conveniently be combined with approved CFTR modulators.

1.5 Aims and objectives

The aim of this study is to further assess the role of extracellular TG2 in regulating CF progression and to then evaluate its importance as a therapeutic target. This study will also attempt to gain an insight into the relevance of EVs, for the externalisation of TG2 in CF. To achieve these aims, the following objectives were set:

(1) Examine the role of extracellular TG2 in CF progression, specifically its induction of EMT and EMT-derived myofibroblast transdifferentiation, using both immortalised and primary CF bronchial epithelial cells.

(2) Evaluate the therapeutic potential of two-directional (direct/indirect approach) pharmacotherapy, using a TG2 specific inhibitor and an approved CFTR corrector, in a CF cell model system.

(3) Confirm the importance of TG2-mediated TGFβ1 activation in CF and investigate the engagement of downstream signalling pathways (canonical and non-canonical).

(4) Determine the involvement of EVs in trafficking TG2 to the ECM in CF and define the impact of combination treatment on this process.

Chapter 2

Materials and Methods

CHAPTER 2: MATERIALS AND METHODS

2.1 Materials

2.1.1 Chemicals

All general laboratory chemicals and reagents used during this study were purchased from Sigma-Aldrich (UK), unless stated otherwise.

2.1.2 Equipment

- Epithelial Voltohmmeter (Worldwide Precision Instruments, USA)
- EVOS™ FL Digital Inverted Microscope (Invitrogen, UK)
- G:BOX Gel Documentation System (Syngene, UK)
- Mini-PROTEAN® Tetra Cell Gel Electrophoresis System and Mini Trans-Blot® Wet Transfer System (Bio-Rad, UK)
- Multiskan™ GO Microplate Spectrophotometer (Fisher Scientific, UK)
- qNano - Tunable Resistive Pulse Sensing (IZON Science, New Zealand)
- SpectraFluor Microplate Reader (BMG LABTECH, UK)
- Leica DMI4000 B Inverted Fluorescence Microscope (Leica Microsystems, UK)

2.1.3 Antibodies

Table 2.1. List of primary antibodies used for Western blotting and immunofluorescence staining

Primary Antibody	Biological Source	Manufacturer
α-SMA (A2547)	Mouse - monoclonal	Sigma-Aldrich, UK
E-cadherin (sc-7870)	Rabbit - polyclonal	Santa Cruz Biotechnology, USA
Fibronectin (F3648)	Rabbit - polyclonal	Sigma-Aldrich, UK
GAPDH (ab8245)	Mouse - monoclonal	Abcam, UK
N-cadherin (sc-59987)	Mouse - monoclonal	Santa Cruz Biotechnology, USA
p-Smad3 (ab52903)	Rabbit - monoclonal	Abcam, UK
Smad3 (ab40854)	Rabbit - monoclonal	Abcam, UK
TG2 (ab2386)	Mouse - monoclonal	Abcam, UK
TGFβ1 (sc-130348, HRP)	Mouse - monoclonal	Santa Cruz Biotechnology, USA
TSG101 (ab83)	Mouse - monoclonal	Abcam, UK
ZO-1 (sc-10804)	Rabbit - polyclonal	Santa Cruz Biotechnology, USA

Table 2.2. List of secondary antibodies used for Western blotting or immunofluorescence staining

Secondary Antibody	Biological Source	Manufacturer
Goat anti-mouse HRP-conjugated (ab97040)	Goat - polyclonal	Abcam, UK
Swine anti-rabbit HRP-conjugated (P0217)	Swine - polyclonal	Dako, Denmark
Goat anti-mouse FITC-conjugated (F0257)	Goat - polyclonal	Sigma-Aldrich, UK
Donkey anti-rabbit TRITC-conjugated (A16028)	Donkey - polyclonal	Thermo Fisher Scientific, UK

2.2 Methods

2.2.1 Cells

The CF model cell line IB3-1 is a human bronchial epithelial cell, with loss of CFTR channel function. It is derived from a CF patient containing a heterozygous mutation of W1282X (class I)/ΔF508 (class II) and is immortalised using a adeno-12-SV40 hybrid virus (Zeitlin et al., 1991). C38 is an isogenic IB3-1 derived cell line, corrected with an adeno-associated viral vector containing a shortened version of wild-type *CFTR*. The expressed CFTR protein is truncated at the amino-terminal, but functions with elevated Cl^- efflux (Flotte et al., 1993). Both IB3-1 and C38 cell lines were given as a kind gift by Portland VA Medical Center (USA).

Primary HBECs isolated from surface epithelium (human bronchi) of a healthy individual, were purchased from Promocell (UK). Primary HBECs isolated from surface epithelium (human bronchi) of three individuals (030, 032 & 037) all expressing a ΔF508 homozygous mutation for CF, were given as a kind gift from the Cystic Fibrosis Foundation (USA).

2.2.2 *Cell culture*

2.2.2.1 Cell culture in submerged medium

C38, IB3, HBEC and primary CF cells were all cultured in airway epithelial medium (AEM), supplemented with: Bovine Pituitary Extract (0.004 ml/ml), Epidermal Growth Factor (recombinant human) (10 ng/ml), Insulin (recombinant human) (5 µg/ml), Hydrocortisone

(0.5 µg/ml), Epinephrine (0.5 µg/ml), Triiodo-L-thyronine (6.7 ng/ml), Transferrin (recombinant human) (10 µg/ml) and Retinoic Acid (0.1 ng/ml), stated at final concentrations after addition to the medium (Promocell, UK). Cells were maintained in a humidified atmosphere at 37ºC in 5% CO_2.

2.2.2.2 Cell culture at air-liquid interface

To stimulate differentiation and recapitulate the polarity of respiratory epithelium observed *in vivo*, a biphasic chamber system was used to culture epithelial cells at air-liquid interface (ALI), as first described by Whitcutt et al. (1988). Using sterile forceps, Transwell® inserts (Corning, UK) with a pore size of 0.4 µm and an area of either 0.33 cm^2 were inserted into 24-well companion plates (Corning, UK). The membranes of each Transwell® were coated with 50 µl of 100 µg/ml solution of collagen IV (Sigma-Aldrich, UK) in 3% (v/v) acetic acid, after the acidity of the solution was neutralised to pH 7.4 with 1 M NaOH. Collagen IV was left to coat the membranes overnight at room temperature, under sterile conditions. The following day excess collagen IV was removed and AEM was used to rinse the Transwells® twice, before the plate was pre-warmed at 37ºC for 2 h. Thereafter, Transwells® were seeded at a cell density of 3 x 10^4 cells/well in 200 µl AEM, with 600 µl AEM added to the basal wells of the companion plate. The plates were then incubated at 37ºC in 5% CO_2 to allow cell attachment and treatments were added in fresh AEM after 2 h if applicable. AEM and treatments were changed every 24 h, up to the point of ALI establishment. After 4 days in submerged conditions, AEM was carefully removed from the Transwells® and the apical layer of cells exposed to air to establish ALI. AEM in the basal wells was replaced with PneumaCult™-ALI medium (STEMCELL Technologies, UK) and the cells were cultured for a further 14 days, with basal ALI medium and treatments changed every 2 days.

2.2.2.3 Cell passaging

Cells were passaged once reaching approximately 90% confluency, with all primary cells used up to a maximum passage of 5. For cell passaging, the AEM was removed from each

flask and the cells washed once with PBS (Sigma-Aldrich, UK) for the removal of dead cells, cell debris and residual medium. Cells were then treated with 0.25% trypsin-EDTA solution (Sigma-Aldrich, UK) for 5 min at 37ºC, to detach adherent cells. After cell detachment was confirmed using an inverted microscope, AEM was added to neutralise the trypsin. The cell suspension was then centrifuged at 300 x *g* for 5 min. The supernatant was discarded and the cell pellet resuspended in fresh AEM. For routine passaging, cells were seeded at an appropriate cell density in a tissue culture flask and cultured in a humidified incubator at 37°C in 5% CO_2. For experiments, cells were counted using a haemocytometer to calculate the desired cell density and then used as required.

2.2.2.4 Cell cryopreservation and storage

The initial steps of cell cryopreservation followed the same methodology as described for cell passaging (**section 2.2.2.3**), until the point of centrifugation. After discarding the supernatant, the cell pellet was resuspended in freezing mixture composed of 10% (v/v) cell culture grade DMSO (Sigma-Aldrich, UK) in fetal bovine serum (FBS) (Gibco, UK). Thereafter, 1 ml of the cell suspension (containing approximately 1 x 10^6 cells) was aliquoted per cryovial, before labelling each vial with cell type, date and passage number. The cryovials were then individually wrapped in paper towel to facilitate gradual freezing and immediately transferred to a -20°C freezer for 1 h. Cryovials were subsequently stored at -80°C for a minimum of 24 h, before being relocated to vapour phase liquid nitrogen tanks for long term storage.

2.2.2.5 Cell culture from frozen stocks

The cryovial was removed from liquid nitrogen storage and promptly placed into a 37ºC water bath, whilst avoiding immersion. Once the cells had completely thawed, the cell suspension was immediately transferred to a sterile tube and pre-warmed AEM added in a dropwise manner. The cell suspension was then transferred to a tissue culture flask and placed in a humidified incubator at 37°C in 5% CO_2. Upon cell attachment, any residual

DMSO was removed by discarding the existing medium and replacing with fresh AEM.

2.2.3 Cell viability count using Trypan Blue exclusion

To enumerate the number of live cells within a cell suspension, a Trypan Blue solution of 0.4% (w/v) (Gibco, UK) was used. This charged diazo dye is excluded from cells with an intact membrane, while non-viable cells are stained blue. In an Eppendorf tube, 50 µl of 0.4% (w/v) Trypan Blue was added to 50 µl of cell suspension and then mixed through gentle pipetting. After incubating the mixture for 2 min at room temperature, 10 µl was loaded on to each side of a haemocytometer. Using an inverted microscope, unstained cells were counted in two quadrants on both sides of the haemocytometer. An average was then calculated, multiplied by (10^4) and corrected for the dilution factor to give the number of 'viable cells/ml' in the original cell suspension. Stained cells were also counted to ensure cell viability was above 95% for the total cell population.

2.2.4 Cell toxicity assay

To quantify the cytotoxicity of compounds, a colorimetric XTT assay (ATCC, UK) was used as first described by Scudiero et al. (1988). The principle is based on the reduction of a cell impermeable yellow tetrazolium salt (XTT), a reaction facilitated by metabolically active cells only. Upon XTT reduction, a bright orange soluble formazan salt is formed. Cells were seeded in flat-bottomed 96 well plates at of density of 8 x 10^3 cells/well and incubated at 37^{o}C in 5% CO_2, for 2 h. Thereafter, the medium was replaced with fresh AEM and compounds added at set concentrations, before the plate was returned to the incubator. AEM and treatments were then changed every 24 h, for a period of 72 h. To prepare the activated-XTT solution, 20 µl of the activation reagent was mixed with 1 ml of the XTT reagent. The AEM was then removed from the wells, before an aliquot of 50µl of the activated-XTT solution was added to each well and the plate incubated at 37^{o}C for 4 h. Following the incubation period, the plate was gently shaken to evenly distribute the orange formazan derivative and the absorbance measured at a wavelength of 490 nm and 630 nm

using a SpectraFluor microplate reader. The absorbance value at 630 nm (used to assess non-specific readings) was subtracted from the absorbance value at 490 nm for each well.

2.2.5 *Cell protein analysis*

2.2.5.1 Lysis of cells in submerged culture

For the collection of whole cell lysates, AEM was removed from cells seeded in 60 mm cell culture dishes (VWR, UK) and each cell monolayer washed twice with ice-cold PBS. After removing the PBS, ice-cold lysis buffer was added (50 mM Tris-HCl, pH 7.4, 1% (v/v) Nonidet P-40, 0.5% (w/v) sodium deoxycholate, 0.1% (w/v) SDS, 2 mM EDTA, 1 mM NaF, 1 mM Na_3VO_4, 0.1 mM PMSF in methanol and 1% (v/v) Halt™ protease inhibitor cocktail (Thermo Fisher Scientific, UK)) and the adherent cells detached using pre-cooled cell scrapers. The cell lysates were then transferred to pre-cooled Eppendorf tubes and kept on ice for 30 min, with occasional agitation throughout. After this time, the cell lysates were centrifuged at 300 x *g* for 10 min at 4^{o}C to remove unwanted cell debris and the supernatants collected in fresh pre-cooled Eppendorf tubes. If not used immediately, cell lysates were stored at -80^{o}C.

2.2.5.2 Protein concentration assay

The protein concentration of cell lysates was determined using a commercially available DC™ Protein Assay kit (Bio-Rad, UK), based on the well documented Lowry assay (Lowry et al., 1951). Bovine serum albumin (BSA) standards were prepared at concentrations ranging from 0.1-1 mg/ml, as per the manufacturer's instructions. An aliquot of 5 µl per standard and sample (cell lysates were diluted in distilled water to fit within the standard curve if necessary), were pipetted into a 96 well plate in triplicate. Following this, 25 µl of reagent A was added to each well, followed by 200 µl of reagent B and the plate gently shaken. The plate was incubated at room temperature for between 15-45 min and then read at a wavelength of 750 nm using a SpectraFluor microplate reader. A linear standard curve was created by plotting absorbance values against BSA concentrations, which was

subsequently used to determine the protein concentration of cell lysates. Protein concentrations were corrected for dilution factor if applicable.

2.2.5.3 Collection of the extracellular matrix

For isolation and investigation of ECM fractions, cells were seeded into 35 mm cell culture dishes (VWR, UK) in AEM and placed in a humidified incubator at 37°C, in 5% CO_2. After 2 h, the AEM was removed and treatments were added in fresh AEM. Subsequent changes of AEM and treatments occurred every 24 h, for a period of 72 h. Thereafter, AEM was removed and each cell monolayer washed twice with PBS, before 1 ml of 2mM EDTA in PBS was added. The cell culture dishes were then incubated at 37°C for 5-10 min, at which point gentle pipetting of the solution was used to detach the cells. After three washes with PBS, an inverted microscope was used to confirm the complete removal of cells, before adding 35 µl of 2X Laemmli buffer (0.125 M Tris, pH 6.8, 4% SDS, 20% glycerol, 10% 2-mercaptoethanol, 0.004% bromophenol blue). The ECM was detached using a cell scraper and each sample transferred into an Eppendorf tube. The samples were then placed in a heat block at 95°C for 5 min, to ensure proteins were denatured. Each sample was loaded onto an SDS polyacrylamide gel in equal volume.

2.2.5.4 SDS-Polyacrylamide Gel Electrophoresis

The protein concentration of cell lysates was quantified using the DC™ Protein Assay kit, as described in **section 2.2.5.2**. Using these values, proteins were separated at equal concentrations using SDS-Polyacrylamide Gel Electrophoresis (SDS-PAGE). The SDS-PAGE gels consisted of two layers, a small-pore resolving gel (Table 2.3), with a large-pore stacking gel on top (Table 2.4). The percentage polyacrylamide of the resolving gel was chosen in accordance with the molecular weight of the target protein, for optimal separation. After preparing and pipetting the resolving solution between two glass plates (1.5 mm), propan-2-ol was overlaid to ensure an even gel surface layer. The resolving solution was then left to polymerise for 1 h at room temperature, before propan-2-ol was discarded and

the gel surface rinsed twice with distilled water. Thereafter, the stacking solution was gently pipetted above the resolving gel and a 1.5 mm comb inserted to form the wells. The stacking solution was left to polymerise for 1 h at room temperature, before the comb was carefully removed and the wells rinsed with SDS-PAGE running buffer (25 mM Tris, 192 mM Glycine and 0.1% (w/v) SDS, pH 8.3). After casting the gel, cell lysates were diluted in a 1:1 ratio with 2X Laemmli buffer and placed in a heat block at 95^{o}C for 5 min. The samples were then cooled on ice for 5 min before loading. A Kaleidoscope™ Prestained Protein Standard (Bio-Rad, UK) was loaded into an outer well, as a reference marker for protein molecular weight. The Mini-PROTEAN® Tetra Cell gel electrophoresis system was then assembled and filled with running buffer. Electrophoresis was performed at 90 V for 15 min and increased to 120 V until the bromophenol blue dye reached the bottom of the resolving gel.

Table 2.3. SDS-PAGE resolving gel composition

Resolving Gel Solutions	**% (v/v) Acrylamide Concentration**	
	10	**12**
30% Acrylamide/0.8% bisacrylamide	5 ml	6 ml
4X 1.5 M Tris-HCl/0.4% (w/v) SDS pH 8.8	3.75 ml	3.75 ml
Distilled H_20	6.25 ml	5.25 ml
10% (w/v) Ammonium persulphate	0.05 ml	0.05 ml
TEMED	0.01 ml	0.01 ml

Table 2.4. SDS-PAGE stacking gel composition

Stacking Gel Solutions	**Volume**
30% Acrylamide/0.8% bisacrylamide	0.65 ml
4X 0.5 M Tris-HCl/0.4% (w/v) SDS pH 6.8	1.25 ml
Distilled H_20	3.05 ml
10% (w/v) Ammonium persulphate	0.025 ml
TEMED	0.005 ml

2.2.5.5 Western blotting

Proteins separated by SDS-PAGE (**section 2.2.5.4**), were transferred on to nitrocellulose membrane (VWR, UK) using a Mini Trans-Blot® wet transfer system. Nitrocellulose

membrane, fibre pads and filter paper were pre-soaked in ice-cold transfer buffer (48.8 mM Tris, 39 mM Glycine and 20% (v/v) methanol, pH 8.3) for 5 min, prior to the transfer. The SDS-PAGE gel was carefully retrieved from the glass plates and positioned on a sheet of pre-soaked filter paper. Pre-soaked nitrocellulose membrane was laid on top of the gel, followed by pre-soaked filter paper and a roller used to remove any air bubbles. The transfer cassette was then assembled and placed inside an electrode module within a buffer tank. A frozen ice pack was placed adjacent to the electrode module and the tank filled with ice-cold transfer buffer. The tank was then surrounded with ice and the transfer carried out at 300 mA for 75 min. Following protein transfer, the cassette was disassembled and the membrane briefly washed with TBST (20 mM Tris base, 150 mM NaCl and 0.1% (v/v) Tween® 20, pH 7.6). The membrane was then incubated in blocking buffer (5% (w/v) skimmed milk in TBST) for 1 h at room temperature; or alternatively (5% (w/v) BSA in TBST) when targeting phosphorylated proteins. Thereafter, the membrane was immunoprobed with a protein-specific primary antibody (Table 2.1), diluted as per the manufacturer's instructions in the appropriate blocking buffer. This was left on a rocking platform overnight at 4°C or for 2 h at room temperature. After three 15 min washes with TBST, the membrane was incubated with an applicable HRP-conjugated secondary antibody (Table 2.2) diluted in the appropriate blocking buffer and left on a rocking platform for 2 h at room temperature. Following three 15 min washes with TBST, the chemiluminescent signal was developed using Amersham™ ECL™ western blotting detection reagents (G.E Healthcare Life Sciences, UK) and the signal captured using a G:BOX F3 gel documentation system.

2.2.5.6 Ponceau S staining

Ponceau S staining was used to validate the correct transfer of proteins from SDS-PAGE gel to nitrocellulose membrane and as a loading control (a suitable alternative when use of a 'housekeeping protein' was not applicable). Following protein transfer (**section 2.2.5.5**) the membrane was immersed in Ponceau S Staining Solution (Sigma-Aldrich, UK) and left to stain for 5 min at room temperature, on a rocking platform. The membrane was then

rinsed with distilled water until the background was clear, before an image of the stained proteins was captured. Thereafter, the membrane was completely destained via repeat washes with distilled water on a rocking platform, until the Ponceau S stain was no longer visible. Immunological detection was then performed as normal, continuing from the point of membrane blocking (**section 2.2.5.5**).

2.2.5.7 Stripping and reprobing of the membrane

To investigate more than one protein of interest or ensure equal loading through detection of a 'housekeeping protein', bound primary and secondary antibodies were stripped from the nitrocellulose membrane and the blot reprobed. The membrane was immersed in stripping buffer (62.5 mM Tris-HCl, 2% (w/v) SDS, 100 mM 2-mercaptoethanol (added fresh before use), pH 6.7) and incubated at 50^{o}C for 30 min, with occasional agitation throughout. After discarding the stripping buffer, the membrane was washed four times with TBST for 15 min per wash. The membrane was then incubated in blocking buffer and the western blot method followed through to immunological detection, as described in **section 2.2.5.5**.

2.2.5.8 Immunofluorescence staining

Immunofluorescence staining was performed to visualise the expression and localisation of target proteins. Cells were seeded in Nunc™ Lab-Tek™ 8-well chamber slides (Thermo Fisher Scientific, UK) at 3 x 10^4 cells/well and allowed to grow for 16 h (primary cells) or 24 h (cell lines). After this time, AEM was removed and the cells washed twice with PBS. Cells were then fixed with 3.7% (v/v) paraformaldehyde (Sigma-Aldrich, UK) in PBS for 15 min, at room temperature. Following three washes with PBS, the cells were incubated in blocking buffer (3% (w/v) BSA in PBS) for 30 min at 37^{o}C, to prevent non-specific staining. The blocking buffer was then discarded and the cells incubated with an antigen-specific primary antibody (Table 2.1) in blocking buffer (1:100 dilution) for 2 h at 37^{o}C. When examining the co-distribution of two target proteins, both primary antibodies (from different species) were added simultaneously. After three washes with PBS, the cells were incubated with

Fluorescein isothiocyanate (FITC, green) and/or Tetramethylrhodamine isothiocyanate (TRITC, red) conjugated secondary antibodies (Table 2.2) in blocking buffer (1:100 dilution), for 2 h at 37ºC. Following three washes with PBS, the rubber gasket of the chamber slide was detached, excess liquid was removed and the coverslip mounted with a drop of 4',6-diamidino-2-phenylindole (DAPI, blue) VECTASHIELD® mounting medium (Vector Laboratories, UK). Fluorescent images were captured using a Leica® DMI4000 B inverted fluorescence microscope, via widefield microscopy. Images were then analysed using ImageJ® software and relative fluorescence calculated as, [integrated density – (area of selected fluorescence x mean fluorescence of background readings)].

2.2.5.9 Transglutaminase activity assay

Transglutaminase activity was measured using a biotin-cadaverine incorporation assay, based on the method first described by Slaughter et al. (1992). The wells of a flat-bottomed 96 well plate were coated with 50 µl of 10 mg/ml N,N-dimethylcasein (Sigma-Aldrich, UK) in 50 mM Tris-HCl, pH 8.0 and left overnight at 4ºC. The following day, wells were washed three times with TBST, before the addition of recombinant human TG2 (Zedira, Germany) (IC_{50} assay) or EV sample, with 0.1 mM biotin-cadaverine, 10 mM $CaCl_2$, 1 mM DTT, stated at final concentrations in 50 mM Tris-HCl, pH 7.4. In separate wells, replacement of $CaCl_2$ with 10 mM EDTA was used as a negative control and the addition of 400 ng of recombinant human TG2 was used as a positive control. Each sample and control were prepared in triplicate and the plate incubated at 37ºC for 2h. The wells were then washed three times with TBST, before adding blocking buffer (3% (w/v) BSA in 50 mM Tris-HCl, pH 7.4) to each well and incubating for 30 min at 37ºC. After discarding the blocking buffer, incorporation of biotin-cadaverine into N,N-dimethylcasein was detected by incubating wells with ExtrAvidin®−Peroxidase (Sigma-Aldrich, UK) diluted in blocking buffer (1:1000), for 1 h at 37ºC. Following a further three washes with TBST, the reaction was developed using a SIGMAFAST™ OPD (o-Phenylenediamine dihydrochloride) substrate solution (Sigma-Aldrich, UK). One OPD tablet and one urea hydrogen peroxide buffer tablet were dissolved

in 20 ml of distilled water and 100 µl added to each well. The colour development was ended by the addition of 50 µl of 3 M HCl and the absorbance read at 490 nm using a Multiskan™ GO Microplate Spectrophotometer.

2.2.6 *Phenotypic evaluation of epithelial cells*

2.2.6.1 *In vitro* scratch assay

To evaluate epithelial cell migration *in vitro*, cells were seeded in a 24 well plate at 1 x 10^5 cells/well and incubated at 37ºC in 5% CO_2 until confluent (approximately 24 h). The AEM was then removed and a p200 pipet tip was used to scrape the cell monolayer in a straight line to create a scratch. The wells were gently washed once with PBS to remove cell debris and three reference points were made along the scratch (using an ultra-fine tip marker), on the outside bottom of each well. Treatments in fresh AEM or the secretome of treated cells were then added, before capturing images of each scratch at the three reference points/well using an EVOS™ FL digital inverted microscope (10X objective). The plate was then placed in a humidified incubator at 37°C, in 5% CO_2 and the cells left to migrate for 4 h. Following the incubation period, images were taken of each scratch at the same three reference points/well to ensure continuity. The plate was then returned to the humidified incubator and the process repeated at 16 h post wounding. The images acquired for each sample were analysed using ImageJ® software and wound closure measured as the percentage reduction in wound area, relative to the original area of the wound at 0 h time point.

2.2.6.2 Trans-epithelial electrical resistance (TEER)

An epithelial voltohmmeter was used to assess the electrical resistance (Ω) of epithelial cells grown at ALI, as a quantitative measure of cellular barrier integrity. After establishing ALI as described in **section 2.2.2.2**, an aliquot of 200 µl of PneumaCult™-ALI medium was added apically to each Transwell® insert (0.33 cm^2). Before use of the epithelial voltohmmeter, the STX2 electrode was sterilised in 70% ethanol and then pre-conditioned in ALI medium for 3 min. Thereafter, the longer arm of the STX2 electrode was extended

into the basal well of the companion plate and the shorter arm inserted into the Transwell®, whilst avoiding physical contact with the cell layer. To obtain reproducible measurements, the depth of immersion and angle of the electrode was kept consistent throughout. The electrical resistance of the cells in each Transwell® was then measured in triplicate. The apical medium was then carefully removed from the Transwells® to reinstate ALI. To determine background resistance, 200 µl of ALI medium was added apically to a collagen coated Transwell® in the absence of cells and measurement taken in triplicate. The process was then repeated at specified time points, over a period of 14 days (post ALI). The average resistance of each Transwell® was then calculated from each triplicate and the average background resistance subtracted from each of these values. Final values were expressed as unit area resistance ($\Omega.cm^2$), calculated by multiplying each background corrected sample resistance by the effective area of the membrane (0.33 cm^2).

2.2.6.3 Paracellular permeability assay

To determine the functional integrity of tight junctions in an epithelial cell layer, the paracellular permeability of horseradish peroxidase (HRP) was measured. After culturing epithelial cells at ALI for 14 days (**section 2.2.2.2**), the basal PneumaCult™-ALI medium was discarded and the basal wells washed once with PBS. Following the removal of any residual liquid, 800 µl of PBS was added to each basal well and 200 µl of HRP (~44 kDa) (Sigma-Aldrich, UK) in PBS was gently pipetted into each Transwell®, at a final concentration of 0.5 µM. A collagen coated Transwell® in the absence of cells, was used as a positive control. The plate was then incubated at 37°C for 5 min, to allow the paracellular diffusion of HRP from the apical surface to the basal compartment. Immediately following incubation, Transwell® inserts were carefully removed from the companion plate, before 50 µl aliquots were taken from each basal well in triplicate and transferred to a 96 well plate. The reaction was developed using a SIGMAFAST™ OPD substrate solution, whereby one OPD tablet and one urea hydrogen peroxide buffer tablet were dissolved in 20 ml of distilled water and 50 µl added to each well. The colour development was

terminated with the addition of 50 µl of 3 M HCl and the absorbance read at 490 nm using a Multiskan™ GO Microplate Spectrophotometer.

2.2.7 *Isolation and characterisation of EVs and extracellular soluble protein*

2.2.7.1 Size exclusion chromatography

To purify and separate EVs and extracellular soluble protein from the cell secretome, size exclusion chromatography (SEC) was used. Cells were seeded in 175 cm^2 tissue culture flasks at 5 x 10^6 cells/flask. Treatments were added if applicable and the cells incubated at 37ºC in 5% CO_2. After 72 h, AEM containing the cell secretome was removed from each flask and transferred to pre-cooled 50 ml centrifuge tubes. The samples were then centrifuged at 2000 x *g* for 20 min at 4ºC, to remove any cells and large particles. The supernatants were recovered and transferred to pre-cooled Amicon® ultra-15 ml centrifugal filter units (10 kDa molecular weight cut- off) (Merck Millipore, UK), before being centrifuged at 3200 x *g* at 4ºC (until the total sample volume was concentrated to approximately 1 ml). Thereafter, a qEVoriginal/70 nm SEC column (IZON Science, New Zealand) was fixed on a stand and equilibrated from 4ºC to room temperature. The column was flushed with 10 ml of PBS, before the first sample was loaded onto the column loading frit. The void volume was immediately collected (3 ml) and the loading frit continually topped up with PBS, once all the sample had entered the column. EVs were then collected (3.5 ml) directly after the void volume, in a pre-cooled 15 ml tube. Following the recovery of EVs, a gap of 0.5 ml was eluted from the column and discarded to avoid cross-contamination between the EV and extracellular soluble protein elution zones. Extracellular soluble protein was collected (8 ml) immediately after the gap in a pre-cooled 15 ml tube. Alternatively, the entire sample was collected in 1 ml aliquots in pre-cooled Eppendorf tubes, for the determination of elution profiles. The column was flushed with 20 ml PBS after each sample and the column re-used up to a maximum of 5 times.

2.2.7.2 Preparation of EVs and extracellular soluble protein for protein analysis

Following the purification and separation of EVs and extracellular soluble protein (**section 2.2.7.1**), samples were transferred to pre-cooled Amicon® ultra-0.5 ml centrifugal filter units (10 kDa molecular weight cut- off) (Merck Millipore, UK) and centrifuged at 14000 x *g* at 4^{o}C (until the total sample volume was concentrated to approximately 50 µl). The concentrated samples were then used for further analysis.

2.2.7.3 Tunable resistive pulse sensing

The concentration and size distribution of a population of EVs was quantified using tunable resistive pulse sensing (TRPS), via the qNano platform (IZON Science, New Zealand). The nanopore (NP), lower fluid cell and upper fluid cell were first cleaned with 70% ethanol to remove all contaminants. Either an NP100 (EV detectable size range of ~50 - 330 nm) or NP150 (EV detectable size range of ~70 - 420 nm) (IZON Science, New Zealand) were used for measurements and attached to the holding arms of the qNano. Digital callipers were used to calibrate the applied nanopore stretch (ranging between 45 – 47 mm for all experiments). An aliquot of 78 µl of PBS was applied to the lower fluid cell, with caution taken to prevent air bubbles. The upper fluid cell was then attached and the Faraday cage placed over the top to reduce background noise. Polystyrene calibration particles (IZON Science, New Zealand) complementary to the selected nanopore were vortexed and diluted in PBS to the required target particle concentration (particles/ml), before 35 µl was loaded on to the upper fluid cell. The PM2 nozzle was then connected and a constant pressure of 7 mbar applied. Using the IZON control suite software a constant voltage was applied across the fluid cell. Runs were recorded for 500 particles or 10 min, whichever came first. Following calibration, the upper fluid cell was washed twice with PBS and any residual liquid removed. EV samples purified through SEC (**section 2.2.7.1**) were then measured via the same process. Calibration particles and samples were measured under identical parameters of nanopore stretch, pressure, voltage and electrolyte solution (PBS), for each

independent experiment. Data analysis for EV concentration and size distribution was performed using the IZON control suite software.

2.2.8 Statistical analysis

All data are expressed as mean values ± standard error of the mean (SEM) taken from three independent experiments, unless stated otherwise. Statistical analysis was performed using GraphPad Prism 5 software (GraphPad, La Jolla, CA, USA). Statistical significance between data sets was calculated using a Student's t-test or analysis of variance (ANOVA) followed by an appropriate post-hoc test, as detailed in the figure legends. A p-value <0.05 was considered significant.

Chapter 3

Characterisation of TG2-mediated changes in immortalised and primary CF bronchial epithelial cell model systems

CHAPTER 3: RESULTS

3.1 Introduction

TG2 is a multifunctional protein, which is widely expressed in nearly all mammalian tissues. Although predominantly a cytosolic protein, TG2 is also found to be distributed throughout the cell and extracellular environment (Gundemir et al., 2012). To understand its physiological relevance *in vivo*, two TG2 knockout mouse models were generated via separate approaches (De Laurenzi and Melino, 2001; Nanda et al., 2001). Surprisingly, both *TGM2*$^{-/-}$ mouse models developed normally, without any overt abnormalities. It was only upon further investigation, that TG2 knockout mice were shown to have an impaired wound healing response (Merans et al., 2002; Nardacci et al., 2003). It is now understood that TG2 plays a critical role in tissue repair.

Following tissue injury, TG2 is upregulated and then externalised into the ECM (Verderio et al., 2004). Its ability to crosslink proteins is vital to processes of tissue repair, including stabilisation and remodelling of the ECM (Aeschlimann and Thomazy, 2000). However, issues occur if an insult continues or termination of the wound healing response becomes disrupted. As a result, TG2 accumulates within the extracellular environment, leading to excessive deposition of ECM fibrils (e.g. fibronectin and collagen) and increased activation of TGFβ1 (Nunes et al., 1997; Telci et al., 2009).

TGFβ1 is now recognised as an effective pro-fibrotic cytokine, which drives myofibroblast transdifferentiation from multiple cellular progenitors (Hinz et al., 2007); although the existence of EMT-derived myofibroblast formation is still hotly debated (Hill et al., 2019). During tissue repair, myofibroblasts function as the main effector cells. They secrete fibrous components of the ECM and also express α-SMA positive stress fibres, which facilitate wound contraction (Bochaton-Piallat et al., 2016). Following wound closure, myofibroblasts are normally removed via apoptosis (Desmouliere et al., 1995). However, in fibrosis a positive feedback loop exists between TG2 and TGFβ1, resulting in the persistence of

myofibroblasts (Wang et al., 2018). Ultimately, their sustained activity causes increased ECM rigidity and a progressive decline in the functional compliance of the tissue.

Research has now shown TG2 to be implicated in a number of fibrotic diseases, including CF. A study by Maiuri et al. (2008) was the first to highlight an increased expression of TG2, within CF airway epithelial cells. It was demonstrated that intracellular TG2-mediated crosslinking, induces the functional sequestration of the anti-inflammatory PPARγ protein. A further derangement of the proteostasis network was then revealed, after TG2 was seen to disable autophagy in ΔF508 CF bronchial epithelial cell lines and the lungs of ΔF508 homozygous mice (Luciani et al., 2010).

Thereafter, TG2 was found to have an additional pathological role, relating to fibrotic changes in the ECM of CF airway epithelia (Nyabam et al., 2016). This novel investigation identified a link between elevated levels of cell surface TG2, increased extracellular TGFβ1 protein expression and the subsequent induction of EMT. However, these findings are representative of a single study, with the sole use of immortalised CF epithelial cells as a model system. Validation of results and further research is therefore an important next step. Overall, given the importance of TG2 in CF, targeted inhibition of its aberrant activity represents a viable opportunity for therapeutic intervention.

3.2 Aims and Objectives

This chapter uses immortalised and primary CF bronchial epithelial cell model systems to:

(1) Examine the importance of extracellular TG2 and matrix deposition of fibronectin in CF progression.

(2) Investigate EMT-derived myofibroblast transdifferentiation in CF airway epithelial cells.

(3) Identify differences in the protein levels of TG2, fibronectin and EMT induction for CF primary HBECs, isolated from three separate (ΔF508 homozygous) CF patients.

(4) Perform proof of concept experiments using CF primary HBECs, to test the efficacy of combination treatment (an approved CFTR corrector with a TG2 specific inhibitor).

3.3 Results

3.3.1 Characterisation of TG2 protein levels in C38 and IB3 cells

As previously discussed, TG2 plays a pivotal role in the progression of a number of fibrotic conditions. In CF airway epithelial cells, TG2-mediated crosslinking has been linked to defective autophagy (Luciani et al., 2011) and the induction of EMT (Nyabam et al., 2016). This is thought to result from a constitutive upregulation of TG2 within these cells (Luciani et al., 2009). To further validate this finding, TG2 expression was measured in 'CF diseased state' IB3 cells, in comparison to 'CFTR corrected' C38 cells.

C38 and IB3 cells were cultured for 72 h, before whole cell lysates were collected and TG2 protein levels were measured via western blot analysis. As shown in Figure 3.1, TG2 protein expression was significantly higher in IB3 cells compared to C38 cells, with an observed increase of ~6.2-fold ($p<0.001$).

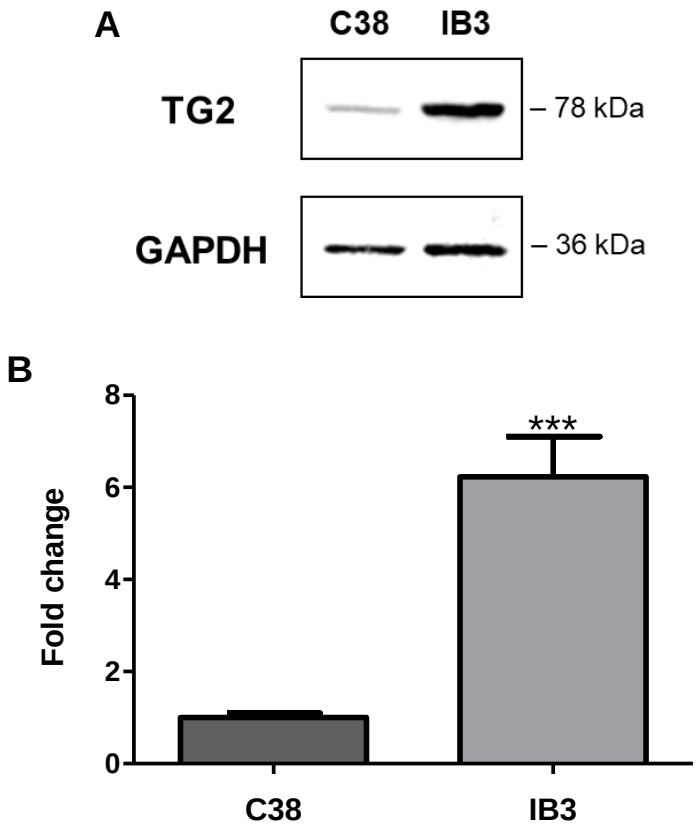

Figure 3.1. Measurement of TG2 protein expression in C38 and IB3 cells. C38 and IB3 cells were grown for 72 h, before whole cell lysates were collected and proteins separated using SDS-PAGE. Following protein transfer, western blot analysis was performed for detection of TG2. Membranes were stripped and reprobed for the loading control GAPDH. **(A)** Representative western blot of TG2 protein expression. **(B)** Densitometry of TG2 protein levels, measured using ImageJ software. Data normalised to GAPDH and expressed as the mean fold change ± SEM, in comparison to C38 cells. Statistical analysis of three independent experiments (N=3) using an unpaired, two-tailed t-test; ****P*<0.001.

3.3.2 Investigating EMT-derived myofibroblast transdifferentiation of IB3 cells

A recent study by Nyabam et al. (2016), reported that TG2 overexpression can drive EMT progression in IB3 cells. Intriguingly, EMT has also been observed in idiopathic pulmonary fibrosis (IPF), with alveolar epithelial cells functioning as the cellular progenitors of myofibroblasts (Kim et al., 2006). However, the process of epithelial to myofibroblast transdifferentiation, is yet to be examined in CF. The protein expression of α-SMA is considered the most reliable hallmark of mature myofibroblasts (Hinz et al., 2007). As such, protein levels of α-SMA and two mesenchymal-specific markers (fibronectin and N-cadherin) were measured in IB3 cells, in comparison to 'CFTR corrected' C38 cells.

C38 and IB3 cells were cultured for 72 h, before whole cell lysates were collected and samples analysed using western blot analysis. The protein expression of fibronectin, N-cadherin and α-SMA was found to be significantly higher in IB3 cells compared to C38 cells, with an increase of >2-fold ($p<0.01$) measured for all three proteins (Figure 3.2).

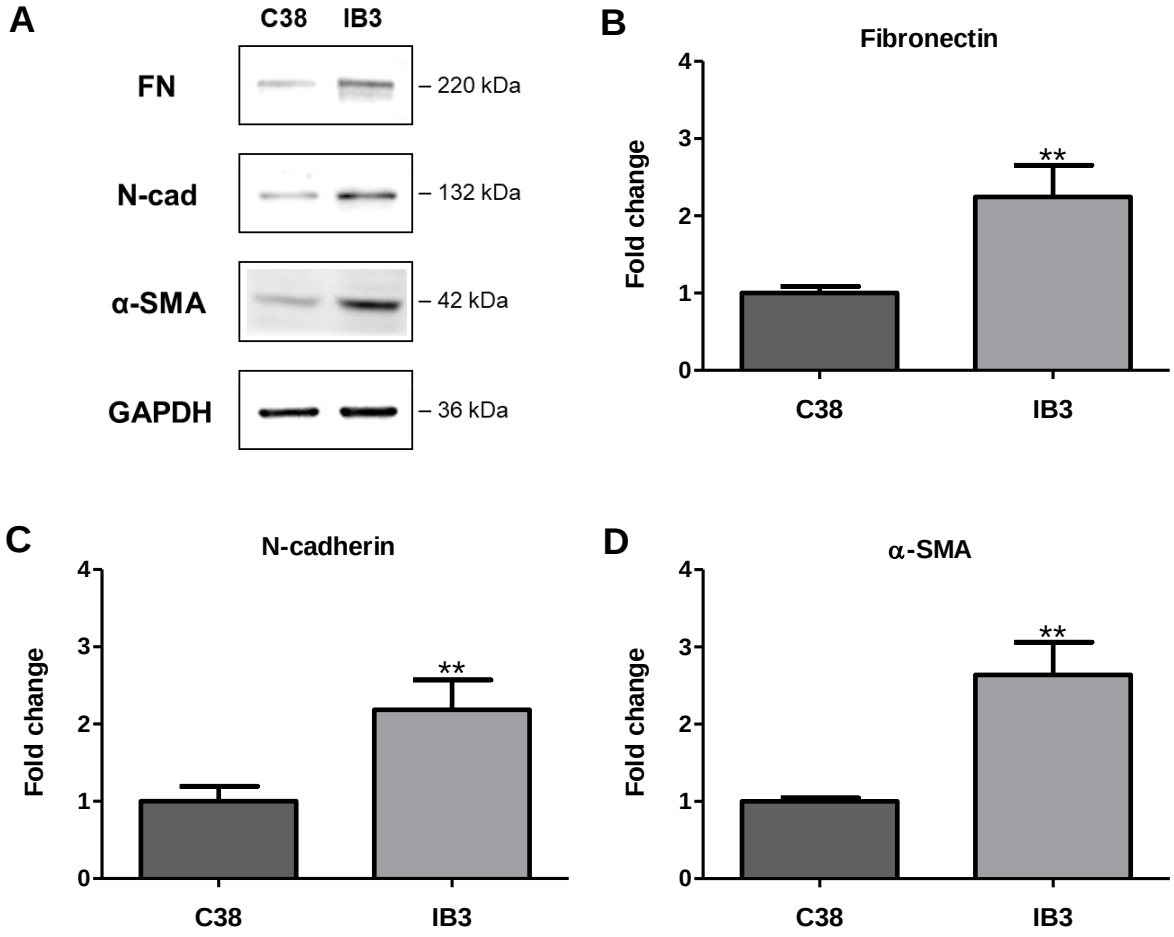

Figure 3.2. Measurement of fibronectin, N-cadherin and α-SMA protein expression in C38 and IB3 cells. C38 and IB3 cells were grown for 72 h, before whole cell lysates were collected and proteins separated using SDS-PAGE. Following protein transfer, western blot analysis was performed for detection of fibronectin, N-cadherin and α-SMA. Membranes were stripped and reprobed for the loading control GAPDH. **(A)** Representative western blots of fibronectin, N-cadherin and α-SMA protein expression. Densitometry of **(B)** fibronectin **(C)** N-cadherin and **(D)** α-SMA protein levels, measured using ImageJ software. Data normalised to GAPDH and expressed as the mean fold change ± SEM, in comparison to C38 cells. Statistical analysis of three independent experiments (N=3) using an unpaired, two-tailed t-test; ***P*<0.01.

3.3.3 Characterisation of TG2 and fibronectin deposition levels in the ECM of C38 and IB3 cells

As demonstrated in Figure 3.1, IB3 cells express intrinsically high levels of TG2. This enzyme is an important regulator of ECM stability and increased externalisation of TG2 serves as a prominent feature of fibrosis (Furini et al., 2020). Elevated levels of extracellular TG2 cause excessive deposition of fibronectin into the ECM, which is a major contributing factor in the shift from normal tissue repair to fibrogenesis (To and Midwood, 2011). Although this process has been established in other fibrotic diseases, research has so far been limited in CF. Therefore, TG2 and fibronectin protein expression was measured in the ECM of IB3 cells, in comparison to the ECM of C38 cells.

C38 and IB3 cells were cultured for 72 h, before cells were detached and the ECM collected. Samples were analysed using western blot analysis. As illustrated in Figure 3.3, TG2 and fibronectin deposition was significantly higher in the ECM of IB3 cells compared to the ECM of C38 cells, with an increase of >6-fold ($p<0.001$) measured for both proteins.

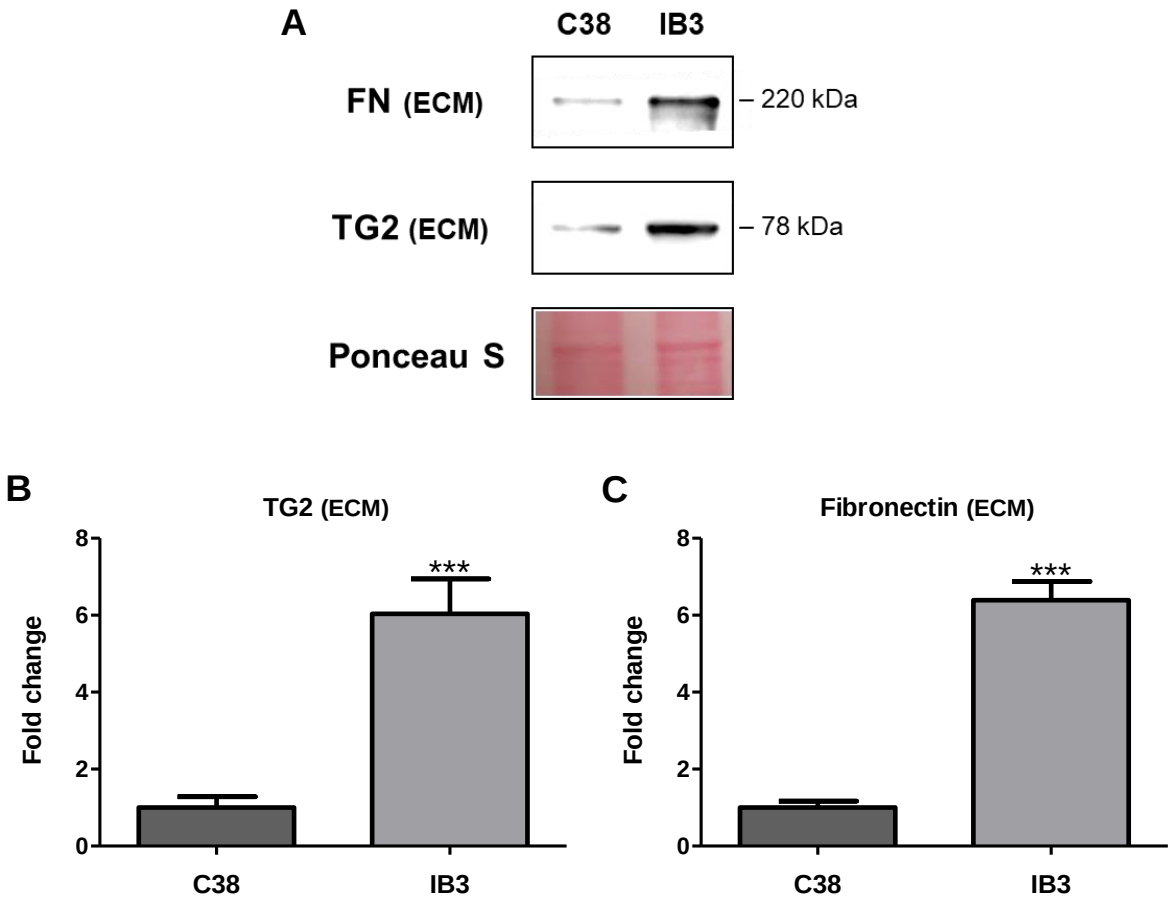

Figure 3.3. Measurement of TG2 and fibronectin protein expression in the ECM of C38 and IB3 cells. C38 and IB3 cells were grown for 72 h, before the cells were detached using 2mM EDTA. The ECM fractions were collected and proteins separated using SDS-PAGE. Following protein transfer, western blot analysis was performed for the detection of TG2 and fibronectin in the ECM. Ponceau S staining was used as a loading control. **(A)** Representative western blots of TG2 and fibronectin protein expression in the ECM. Densitometry of **(B)** TG2 (ECM) and **(C)** fibronectin (ECM) protein levels, measured using ImageJ software. Data normalised to Ponceau S staining and expressed as the mean fold change ± SEM, in comparison to C38 cells. Statistical analysis of three independent experiments (N=3) using an unpaired, two-tailed t-test; ****P*<0.001.

3.3.4 Assessing the co-localisation of TG2 and fibronectin in the ECM of C38 and IB3 cells

TG2 can promote tissue fibrosis via its direct interaction with exogenous fibronectin. Research has shown that externalised TG2 increases the matrix deposition of fibronectin through enzymatic crosslinking (Philp et al., 2018) and by acting as a coreceptor for the assembly of fibronectin-integrin complexes (Akimov et al., 2000). An increased presence of TG2 and fibronectin was found in the ECM of IB3 cells, in comparison to the ECM of C38 cells (Figure 3.3). However, the level of association between TG2 and fibronectin in the matrix, cannot be validated by this data alone. As such, both proteins were assessed for their localisation within the extracellular environment of C38 and IB3 cells, by using two-colour immunofluorescence staining.

C38 and IB3 cells were seeded in 8-well chamber slides and grown for 24 h. Extracellular TG2 and fibronectin protein expression was then visualised via indirect immunofluorescence staining, with FITC (green) and TRITC (red) labelled antibodies, respectively. As shown in Figures 3.4 B and C, TG2 and fibronectin protein levels were significantly increased in the ECM of IB3 cells ($p<0.05$), compared to the ECM of C38 cells. In addition, co-localisation of TG2 and fibronectin was detected in the ECM of both C38 and IB3 cells, as identified by the spatial overlap of the two fluorescent markers (Figure 3.4 A).

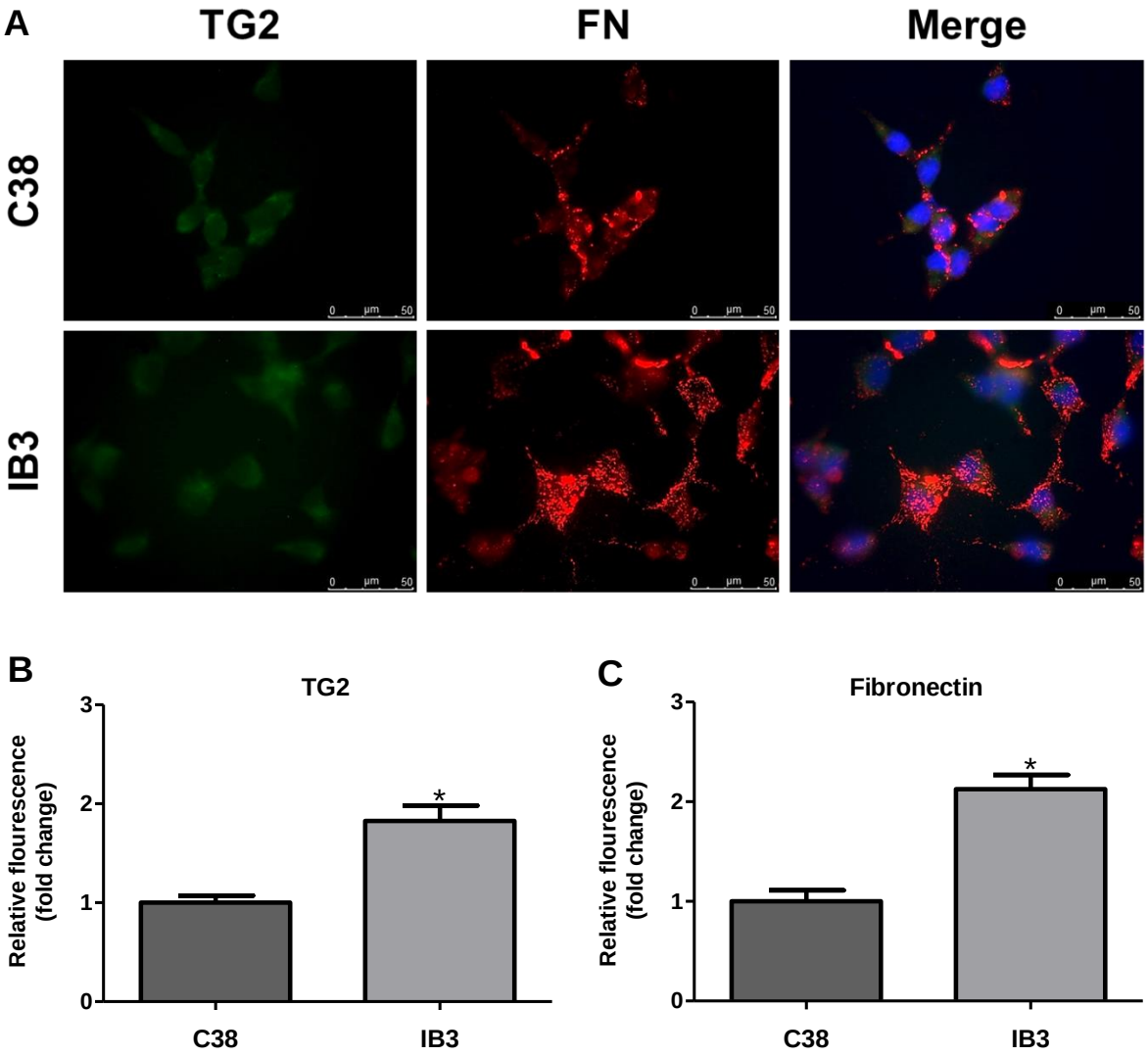

Figure 3.4. Immunofluorescence staining of TG2 and fibronectin in the ECM of C38 and IB3 cells. C38 and IB3 cells were seeded in 8-well chamber slides and grown for 24 h. Cells were then fixed and two-colour immunofluorescence staining used for the detection of TG2 and fibronectin matrix protein levels. DAPI (blue) was used as a nuclear counterstain to label cells. Images were captured using a Leica® DMI4000 B inverted fluorescence microscope, at 40X objective. **(A)** Representative images of TG2 (green) and fibronectin (red) protein expression in the ECM. Images were analysed using ImageJ software and the relative fluorescence of **(B)** TG2 (ECM) and **(C)** fibronectin (ECM) quantified. Data expressed as the mean fold change ± SEM, in comparison to C38 cells. Statistical analysis of two independent experiments (N=2) using an unpaired, two-tailed t-test; *P<0.05.

3.3.5 Evaluating the integrity of tight junctions in C38 and IB3 cells

Pulmonary epithelium serves as a structured barrier, to preclude harmful luminal contents from contacting the subepithelial tissue (Brune et al., 2015). In contrast, IB3 cells appear to undergo EMT-derived myofibroblast transdifferentiation (Figure 3.2). This would indicate a loss of apical-basal cell polarity, with CF airway epithelium possessing a diminished capacity to function as a robust cellular barrier. As a result, TEER was used to assess the electrical resistance of C38 and IB3 cell monolayers at ALI. TEER quantitatively measures the ionic conductance of the paracellular pathway, so is therefore a strong indicator of cellular tight junction integrity.

C38 and IB3 cells were cultured at ALI for 14 days. TEER values were measured using an epithelial voltohmmeter, with readings taken at stated time points between 0–14 days post ALI. C38 cells were found to have increased TEER values across all time points measured, in comparison to IB3 cells (Figure 3.5). Yet, only at day 14 was the increase in TEER seen to be statistically significant ($p<0.01$).

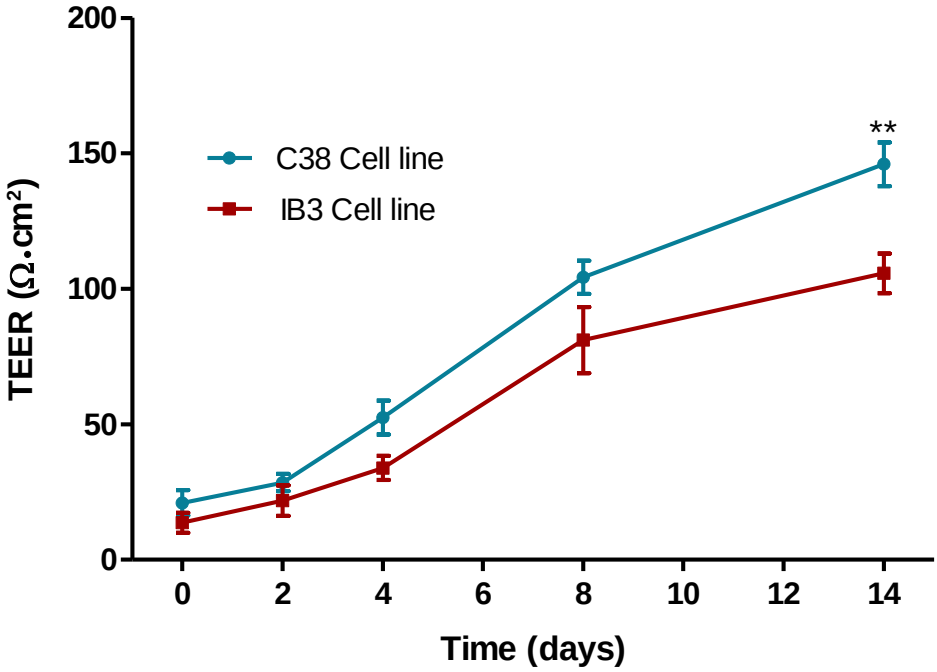

Figure 3.5. TEER measurements of C38 and IB3 cells. C38 and IB3 cells were cultured in Transwell® inserts for 14 days at ALI. The electrical resistance (Ω) of each Transwell® was measured using an epithelial voltohmmeter and recorded at time points of 0, 2, 4, 8 and 14 days post ALI. Measurements were taken in triplicate and the electrical resistance of a collagen coated Transwell® in the absence of cells, subtracted from experimental groups. Final TEER values presented as Ω.cm^2. Data expressed as the mean ± SEM of three independent experiments (N=3). Statistical analysis performed using a two-way ANOVA, with a post-hoc Bonferroni multiple comparison test; ***P*<0.01.

3.3.6 Characterisation of TG2 and fibronectin deposition levels in the ECM of HBECs and CF primary cells

Novel data shown in Figures 3.3 and 3.4, has revealed that TG2 and fibronectin deposition is upregulated in the ECM of IB3 cells. Yet, these findings are limited by the use of immortalised epithelial cell lines (C38 and IB3 cells), which have undergone extensive adaptation and selection processes. Such measures can result in genetic changes, which cause some of the original parental cell features to be altered or lost (Awatade et al., 2018). For this reason, it is important to use a more physiologically relevant model system, to substantiate results obtained from immortalised cell studies. Therefore, TG2 and fibronectin protein levels were measured in the ECM of CF primary HBECs (isolated from three ΔF508 homozygous CF patients, identified as 030, 032 & 037), in comparison to the ECM of normal primary HBECs.

HBECs and CF primary cells (030, 032 and 037) were cultured for 72 h, before cells were detached and the ECM collected. Samples were analysed using western blot analysis. As demonstrated in Figure 3.6, protein levels of TG2 and fibronectin were found to be significantly higher in the ECM of all three CF primary cells, compared to the ECM of normal HBECs. Overall, the increase in matrix deposition of TG2 and fibronectin was measured to be >3-fold, for all three CF primary cells. Interestingly, differences in protein expression were also observed between CF primary cells, with 032 cells ($p<0.05$) exhibiting significantly higher levels of fibronectin matrix deposition, in comparison to 030 cells.

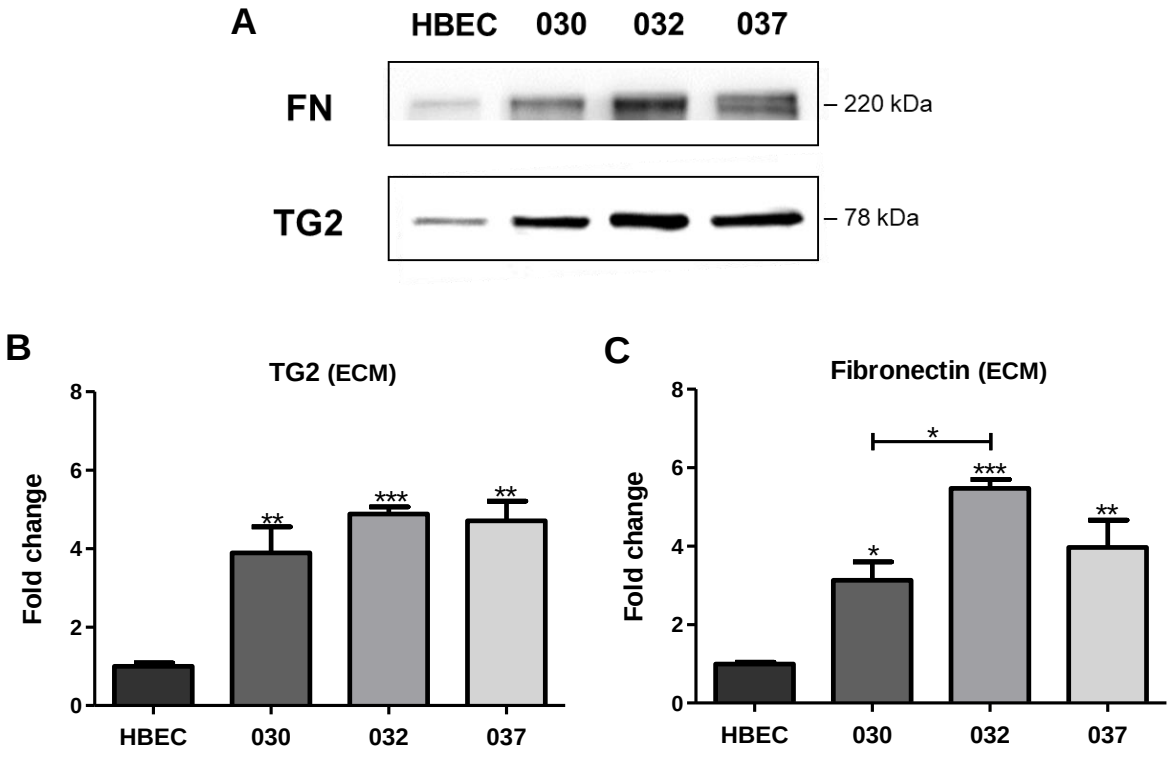

Figure 3.6. Measurement of TG2 and fibronectin protein expression in the ECM of HBECs and CF primary cells. HBECs and CF primary cells (030, 032 and 037) were grown for 72 h, before the cells were detached using 2mM EDTA. The ECM fractions were collected and proteins separated using SDS-PAGE. Following protein transfer, western blot analysis was performed for the detection of TG2 and fibronectin in the ECM. **(A)** Representative western blots of TG2 and fibronectin protein expression in the ECM. Densitometry of **(B)** TG2 (ECM) and **(C)** fibronectin (ECM) protein levels, measured using ImageJ software. Data expressed as the mean fold change ± SEM, in comparison to HBECs. Statistical analysis of three independent experiments (N=3) using a one-way ANOVA, with a post-hoc Tukey test; **P*<0.05, ***P*<0.01, ****P*<0.001.

3.3.7 Assessing the co-localisation of TG2 and fibronectin in the ECM of HBECs and CF primary cells

Data shown in Figure 3.4, evidences the co-localised overexpression of TG2 and fibronectin in the ECM of IB3 cells. In support of these findings, both proteins were found to have increased deposition in the ECM of CF primary cells (030, 032 and 037), compared to the ECM of HBECs (Figure 3.6). On the other hand, the capacity for TG2 and fibronectin to associate in the ECM of CF primary cells, has never been investigated. As such, the localisation of both proteins was assessed within the extracellular environment of CF primary cells, by using two-colour immunofluorescence staining. Normal HBECs were used for comparison as a healthy control.

HBECs and CF primary cells (030 and 032) were seeded in 8-well chamber slides and grown for 16 h. Extracellular TG2 and fibronectin protein expression was then visualised via indirect immunofluorescence staining, with FITC (green) and TRITC (red) labelled antibodies, respectively. As shown in Figure 3.7 B, TG2 protein expression was significantly increased in the ECM of 030 and 032 cells by ~3-fold ($p<0.05$) and ~4.7-fold ($p<0.001$) respectively, in comparison to the ECM of HBECs. Further to this, 032 cells ($p<0.05$) demonstrated significantly higher levels of matrix TG2, compared to 030 cells. Similarly, fibronectin protein levels were found to be increased in the ECM of 030 and 032 cells, in comparison to the ECM of HBECs (Figure 3.7 C). However, changes in protein expression failed to reach statistical significance. Interestingly, co-localisation of TG2 and fibronectin was detected in the ECM of both 030 and 032 cells, as identified by the appearance of a yellow colour after images of TG2 and fibronectin were superimposed (Figure 3.7 A).

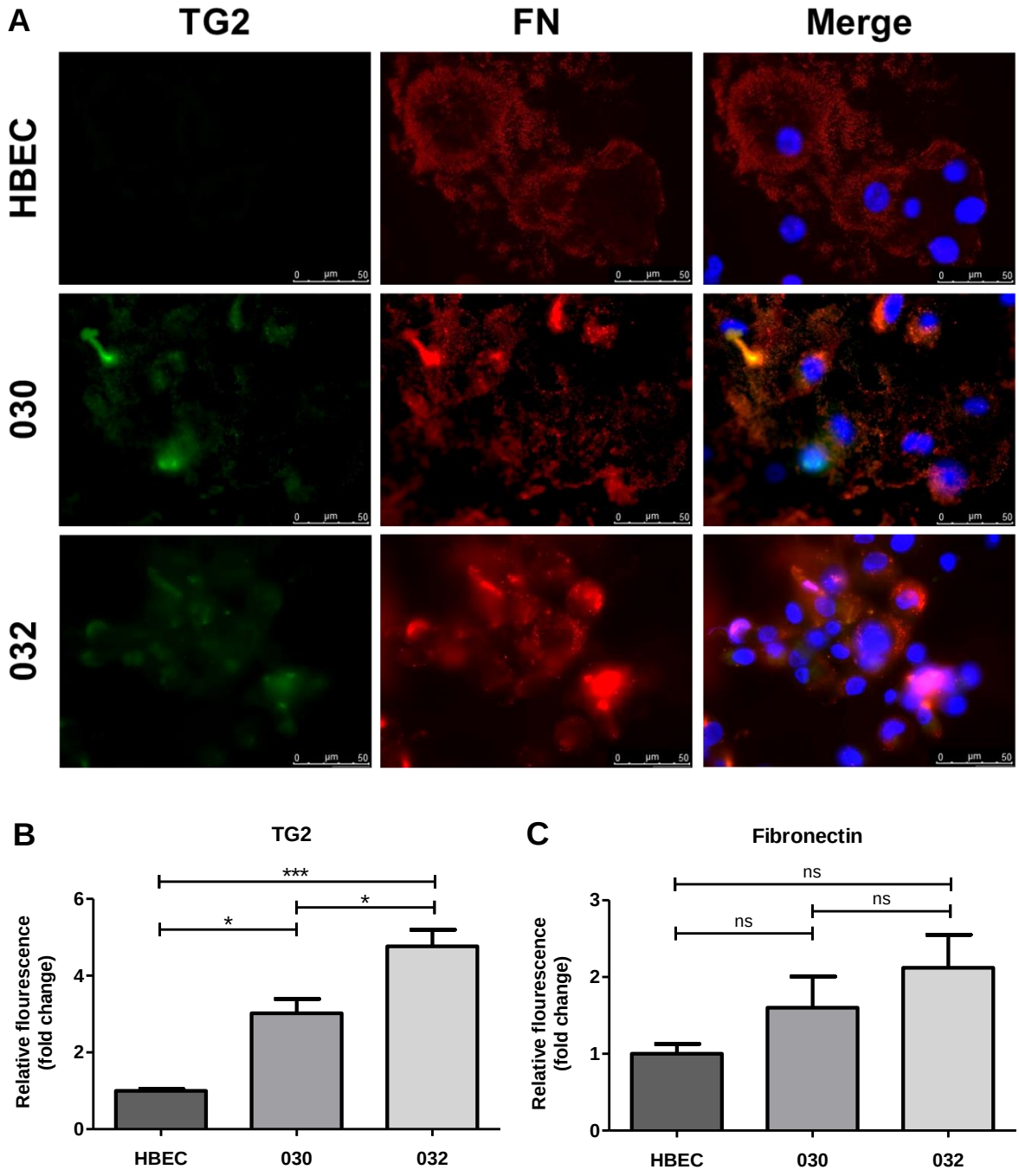

Figure 3.7. Immunofluorescence staining of TG2 and fibronectin in the ECM of HBECs and CF primary cells. HBECs and CF primary cells (030, 032) were seeded in 8-well chamber slides and grown for 16 h. Cells were then fixed and two-colour immunofluorescence staining used for the detection of TG2 and fibronectin matrix protein levels. DAPI (blue) was used as a nuclear counterstain to label cells. Images were captured using a Leica® DMI4000 B inverted fluorescence microscope, at 40X objective. **(A)** Representative images of TG2 (green) and fibronectin (red) protein expression in the ECM. Images were analysed using ImageJ software and the relative fluorescence of **(B)** TG2 (ECM) and **(C)** fibronectin (ECM) quantified. Data expressed as the mean fold change ± SEM, in comparison to HBECs. Statistical analysis of three independent experiments (N=3) using a one-way ANOVA, with a post-hoc Tukey test; ns, not significant, **P*<0.05, ****P*<0.001.

3.3.8 Examining the existence of EMT in CF primary cells

Previous research from the literature (Nyabam et al., 2016) and this study (Figure 3.2), has revealed that IB3 cells undergo EMT. Nevertheless, the existence of EMT is yet to be examined in the model system of CF primary HBECs. At present, it is unknown whether EMT is an artefact of the IB3 cell line or is indeed a common feature of CF airway epithelium. For this reason, protein levels of E-cadherin (epithelial cell marker) and N-cadherin (mesenchymal cell marker) were measured on the surface of CF primary cells, by using immunofluorescence staining. Normal HBECs were used for comparison as a healthy control.

HBECs and CF primary cells (030, 032 and 037) were seeded in 8-well chamber slides and grown for 16 h. Cell surface E-cadherin and N-cadherin protein expression was then visualised via indirect immunofluorescence staining, with TRITC (red) and FITC (green) labelled antibodies, respectively. These data show that E-cadherin protein levels were significantly decreased on the surface of all CF primary cells ($p<0.05$), in comparison to HBECs (Figures 3.8 A and B). In contrast, N-cadherin protein levels were significantly increased on the surface of all CF primary cells, in comparison to HBECs (Figures 3.8 A and C). Moreover, 032 cells ($p<0.05$) showed significantly higher surface protein levels of N-cadherin, compared to 030 and 037 cells.

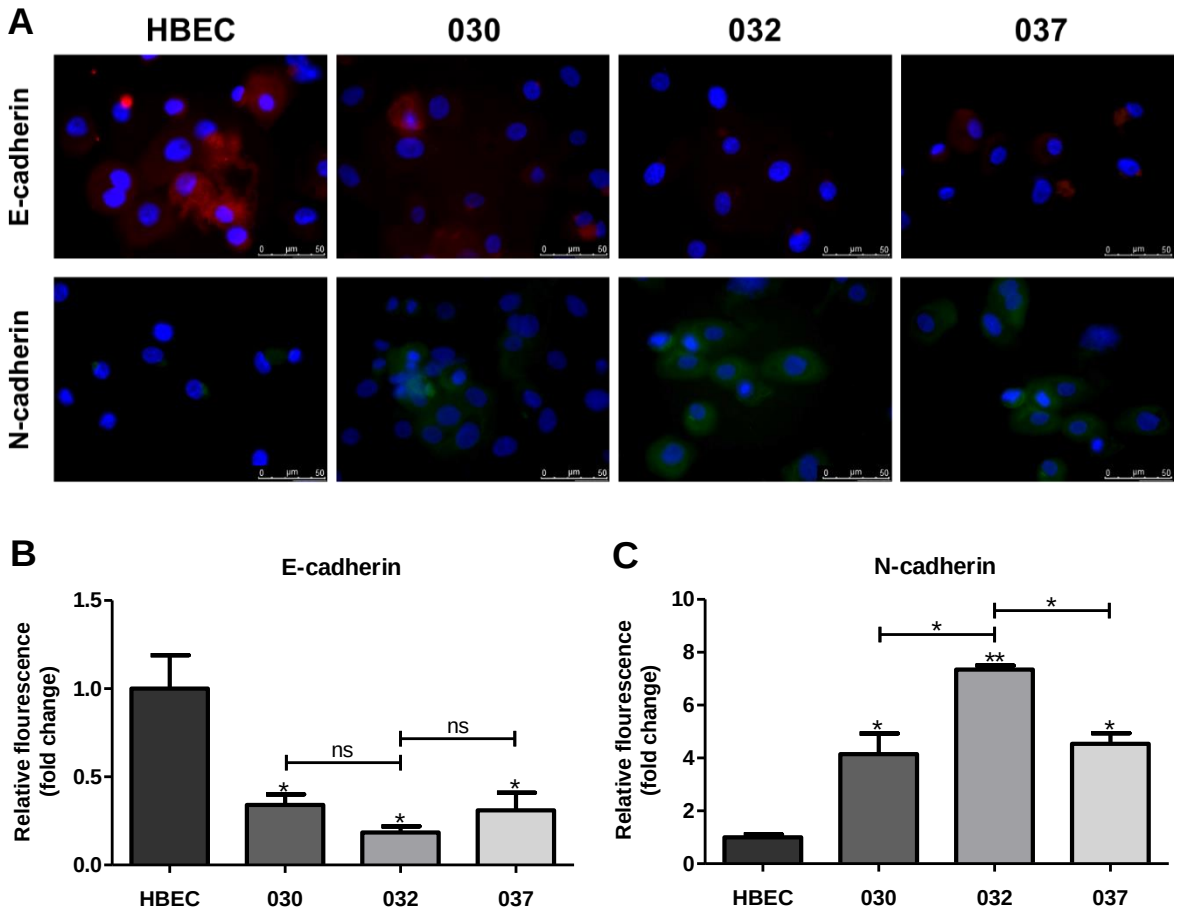

Figure 3.8. Immunofluorescence staining of E-cadherin and N-cadherin on the cell surface of HBECs and CF primary cells. HBECs and CF primary cells (030, 032 and 037) were seeded in 8-well chamber slides and grown for 16 h. Cells were then fixed and immunofluorescence staining used to independently detect E-cadherin and N-cadherin cell surface protein levels. DAPI (blue) was used as a nuclear counterstain to label cells. Images were captured using a Leica® DMI4000 B inverted fluorescence microscope, at 40X objective. **(A)** Representative images of E-cadherin (red) and N-cadherin (green) protein expression on the cell surface. Images were analysed using ImageJ software and the relative fluorescence of **(B)** E-cadherin and **(C)** N-cadherin quantified. Data expressed as the mean fold change ± SEM, in comparison to HBECs. Statistical analysis of two independent experiments (N=2) using a one-way ANOVA, with a post-hoc Tukey test; ns, not significant, **P*<0.05, ***P*<0.01.

3.3.9 Evaluating the integrity of tight junctions in HBECs and CF primary cells

C38 and IB3 cells cultured at ALI, exhibit large differences in TEER values (Figure 3.5). After 14 days, IB3 cell monolayers were found to have significantly reduced levels of electrical resistance, in comparison to C38 cell monolayers. This data suggests that the integrity of tight junctions in the epithelial cell barrier is likely compromised in CF airways. However, immortalised airway epithelial cells often experience incomplete mucociliary differentiation, when cultured at ALI (Luengen et al., 2020). By contrast, primary airway epithelial cells cultured at ALI are the considered the gold standard for obtaining a pseudostratified mucociliary phenotype *in vitro* (Srinivasan et al., 2015). Therefore, TEER was measured for HBECs and CF primary cells, to confirm the accuracy of the findings in Figure 3.5.

HBECs and CF primary cells (030, 032 and 037) were cultured at ALI for 14 days. TEER values were measured using an epithelial voltohmmeter, with readings taken at stated time points between 0–14 days post ALI. HBECs were found to have increased TEER values across all time points measured, in comparison to all three CF primary cells (Figure 3.9). Notably, HBECs showed significant increases in TEER at day 4 ($p<0.01$) and day 14 ($p<0.001$), compared to all three CF primary cells. Further differences in TEER values were also observed between CF primary cells. 030 cells demonstrated significant increases in TEER at day 8 ($p<0.01$) and day 14 ($p<0.001$), compared to 032 cells. Similarly, 037 cells were seen to have a significantly higher TEER value at day 14 ($p<0.01$), in comparison to 032 cells.

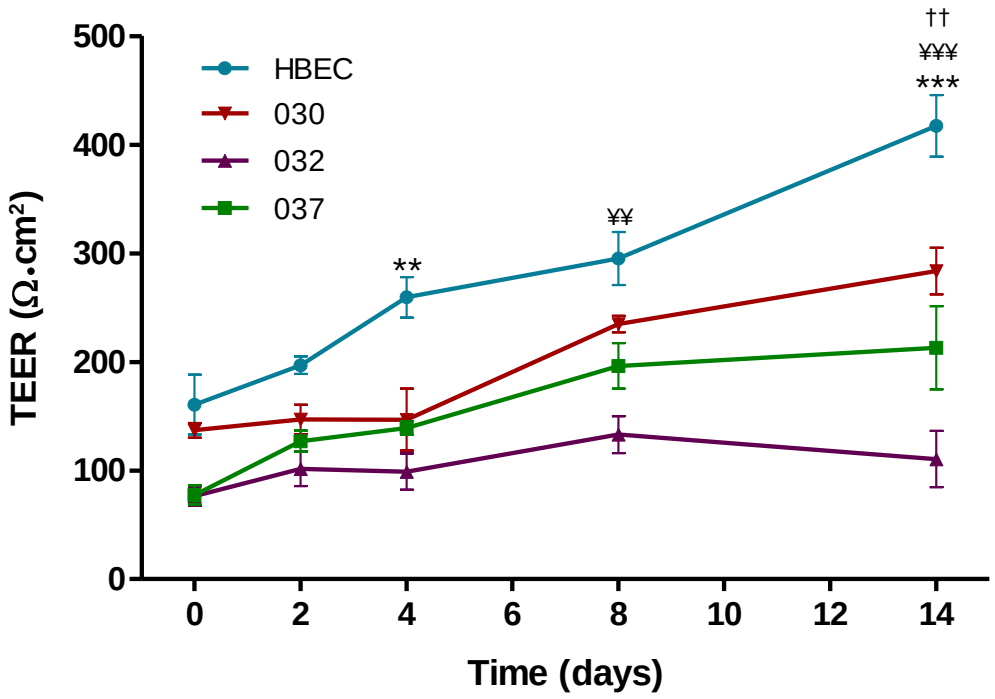

Figure 3.9. TEER measurements of HBECs and CF primary cells. HBECs and CF primary cells (030, 032 and 037) were cultured in Transwell® inserts for 14 days at ALI. The electrical resistance (Ω) of each Transwell® was measured using an epithelial voltohmmeter and recorded at time points of 0, 2, 4, 8 and 14 days post ALI. Measurements were taken in triplicate and the electrical resistance of a collagen coated Transwell® in the absence of cells, subtracted from experimental groups. Final TEER values presented as Ω.cm^2. Data expressed as the mean ± SEM of three independent experiments (N=3). Statistical analysis performed using a two-way ANOVA, with a post-hoc Bonferroni multiple comparison test; ***P*<0.01, ****P*<0.001, the minimum level of significance reached by HEBCs, in comparison to all CF primary cells; ¥¥*P*<0.01, ¥¥¥*P*<0.001 significant difference between 030 and 032 cells; ††*P*<0.01, significant difference between 032 and 037 cells.

3.3.10 Evaluating the cell migration levels of HBECs in comparison to CF primary cells

CF primary cells (030, 032 and 037) have been shown to exhibit the hallmark of EMT, with an upregulation of N-cadherin protein expression in conjunction with a downregulation of E-cadherin protein expression (Figure 3.8). CF primary cells (030, 032 and 037) were also found to have reduced TEER values in comparison to HBECs (Figure 3.9). It is now well understood that a central feature of EMT, is the loss of cell-cell adhesion and the acquisition of cell motility (Loh et al., 2019). Therefore, the cell migration levels of CF primary cells were measured in comparison to HBECs, to further validate the existence of EMT progression in CF bronchial epithelial cells.

An *in vitro* scratch assay was performed to quantify the cell migration levels of HBECs and CF primary cells (030, 032 and 037), over 16 hours. All three CF primary cells exhibited a level of increased percentage wound closure, in comparison to HBECs (Figure 3.10). Intriguingly, percentage wound closure also differed between CF primary cells, with 030 cells demonstrating the lowest percentage wound closure (63%) and 037 cells the highest (100%).

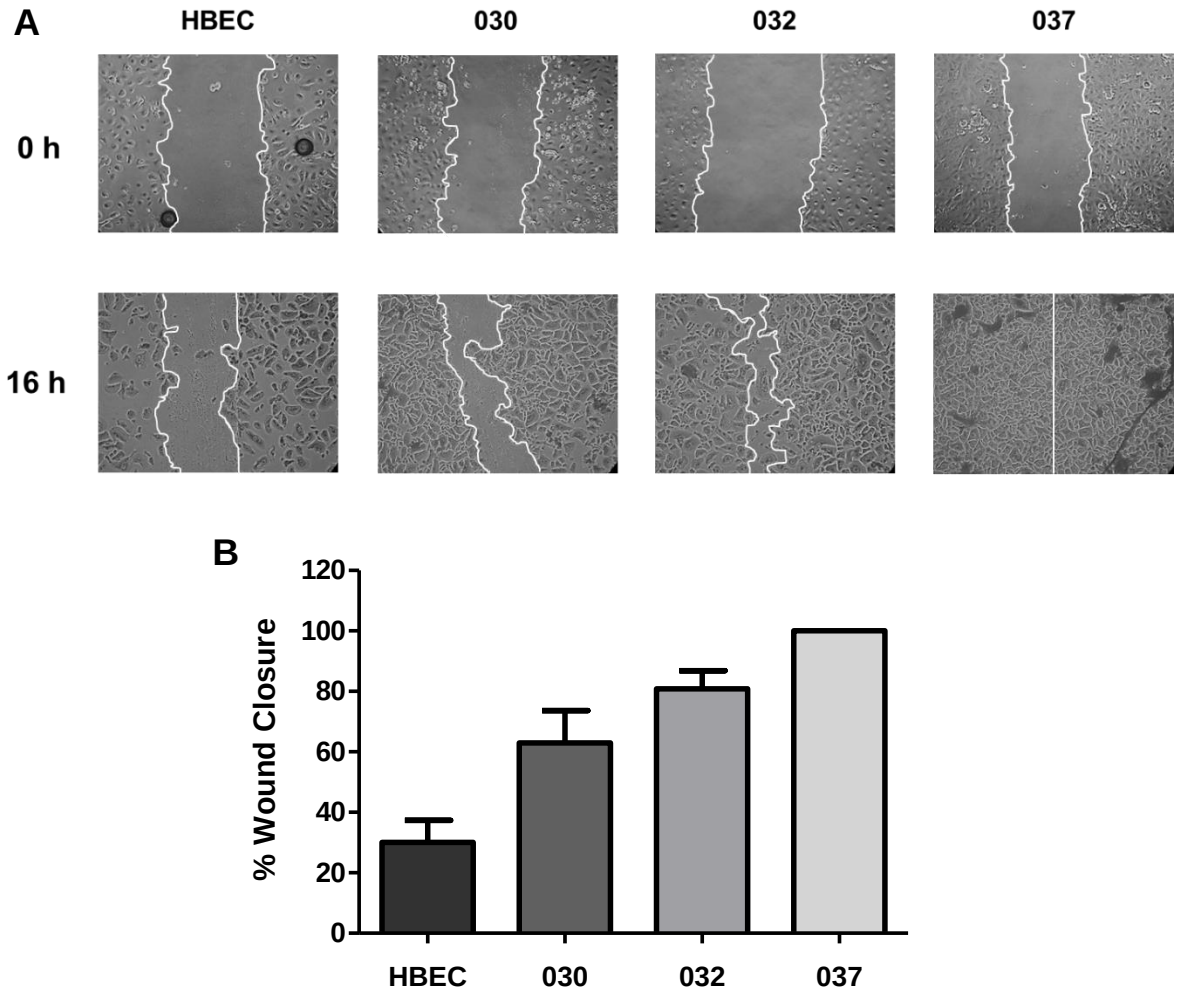

Figure 3.10. Measurement of percentage wound closure for HBECs and CF primary cells. HBECs and CF primary cells (030, 032 and 037) were seeded in a 24 well plate and grown until confluent, before a scratch was made in each cell monolayer. Images were acquired in triplicate at 0 h and 16 h post-wounding. **(A)** Representative images of each scratch, captured at the specified time points. Images were analysed using ImageJ software and **(B)** cell migration calculated as the percentage wound closure, relative to the original area of the wound at 0 h. Data expressed as the mean ± SEM of an independent experiment (N=1), performed in triplicate

3.3.11 The combined effect of a CFTR corrector and TG2 inhibitor on TG2 protein expression in CF primary cells

Emerging evidence suggests, that a complex derangement of the proteostasis network takes place within ΔF508 CF bronchial epithelial cells (Bodas and Vij, 2019). Previous research from the literature (Maiuri et al., 2008; Luciani et al., 2009, 2010; Nyabam et al., 2016) has demonstrated that TG2 is a key regulator of these changes. With the advent of potent and selective TG2 inhibitors (Badarau et al., 2015), a novel therapeutic avenue now exists. Using a two-directional (direct/indirect) approach, TG2 inhibitors could potentially be used to complement existing drugs, which currently all target CFTR directly. Thus, a proof of concept experiment was designed, to test the efficacy of this multi-pronged treatment. An approved CFTR corrector (VX-809) was used in combination with a selective TG2 inhibitor (1-155) and the effect on TG2 expression in CF primary cells was measured.

CF primary cells (030, 032 and 037) were treated with either VX-809 (2.5 µM), 1-155 (2.5 µM) or VX-809 (2.5 µM) and 1-155 (2.5 µM) combined. Following treatment for 72 h, whole cell lysates were collected and TG2 protein expression was measured via western blotting. The results from each independent experiment (involving the use of separate CF patient primary cells, i.e. 030, 032 and 037), were combined for statistical analysis. These data show a decrease in TG2 expression across all treatment conditions (Figure 3.11). Both 1-155 alone and VX-809 in combination with 1-155 were able to significantly reduce TG2 protein levels by 53% ($p<0.05$) and 67% ($p<0.01$) respectively, in comparison to untreated CF primary cells.

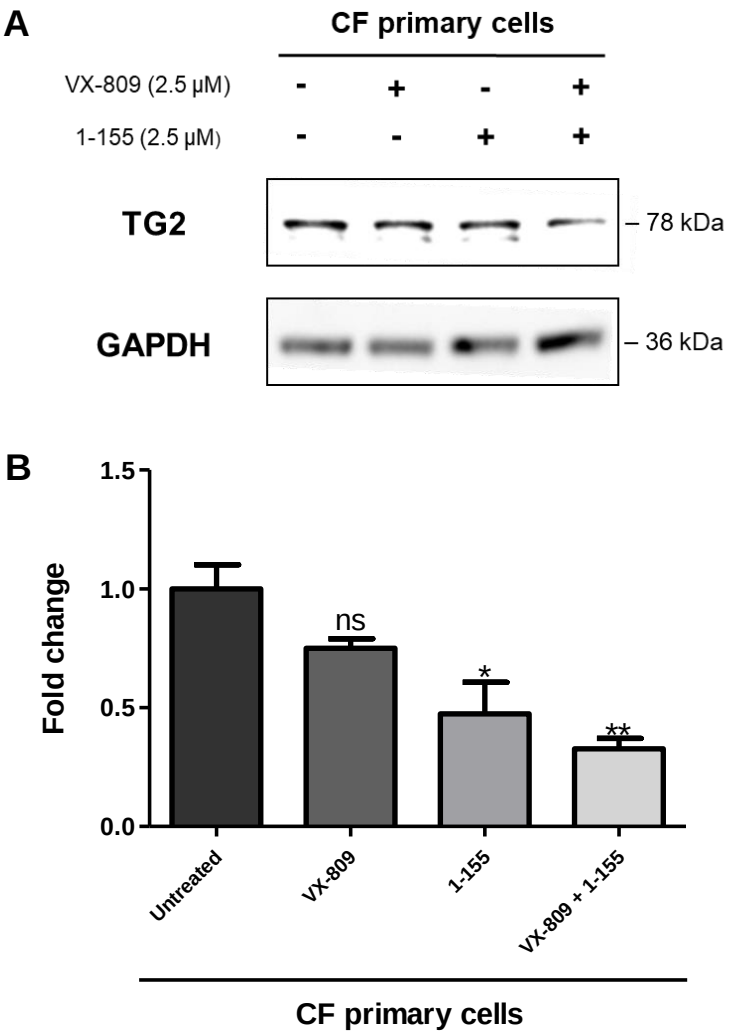

Figure 3.11. Measurement of TG2 protein expression in CF primary cells following treatment with VX-809 and 1-155 alone or in combination. CF primary cells (030, 032 and 037) were treated with VX-809 (2.5 µM), 1-155 (2.5 µM) or VX-809 (2.5 µM) and 1-155 (2.5 µM) for 72 h, with treatments changed every 24 h. Whole cell lysates were collected and proteins separated using SDS-PAGE. Following protein transfer, western blot analysis was performed for detection of TG2. Membranes were stripped and reprobed for the loading control GAPDH. **(A)** Representative western blot of TG2 protein expression. **(B)** Densitometry of TG2 protein levels, measured using ImageJ software. Data normalised to GAPDH and expressed as the mean fold change ± SEM, in comparison to untreated CF primary cells. Three independent experiments, each using separate CF patient primary cells (N=3), were statistically analysed using a one-way ANOVA, with a post-hoc Tukey test; ns, not significant, *P<0.05, **P<0.01.

3.3.12 Evaluating the integrity of tight junctions in 030 cells following treatment with a CFTR corrector and TG2 inhibitor in combination

As revealed in Figure 3.11, two-directional combination treatment (VX-809 and 1-155) significantly reduced the protein expression of TG2, in CF primary HBECs isolated from three different individuals (030, 032 and 037). Remarkably, combination treatment was also seen to decrease TG2 protein levels to a greater extent than the use of either compound alone, with a close to additive effect observed. Although the results from this initial investigation are promising, only a single protein marker (TG2) was used for analysis. Thus, an examination of epithelial cell barrier function was performed, to further assess the efficacy of two-directional pharmacotherapy. As previously revealed, the structural integrity of airway epithelium is attenuated in CF (Figures 3.5 and 3.9). Therefore, TEER was used to determine whether tight junction complexes could be restored in CF primary HBECs, following combination treatment with VX-809 and 1-155.

030 cells were cultured at ALI for 14 days and treated with either VX-809 (2.5 µM), 1-155 (2.5 µM) or VX-809 (2.5 µM) and 1-155 (2.5 µM) in combination, with treatments changed every 24 h prior to ALI and every 48 h thereafter. Normal HBECs were used for comparison as a healthy control. TEER values were measured using an epithelial voltohmmeter, with readings taken at stated time points between 0 - 14 days post ALI. At day 8, a significant increase in TEER values was observed for HBECs ($p<0.01$) and 030 cells treated with VX-809 and 1-155 ($p<0.05$), compared to untreated 030 cells (Figure 3.12). Even greater differences in TEER values were seen at day 14, with significant increases measured for HBECs ($p<0.001$) and 030 cells treated with either 1-155 ($p<0.01$) or VX-809 and 1-155 ($p<0.001$), in comparison to untreated 030 cells.

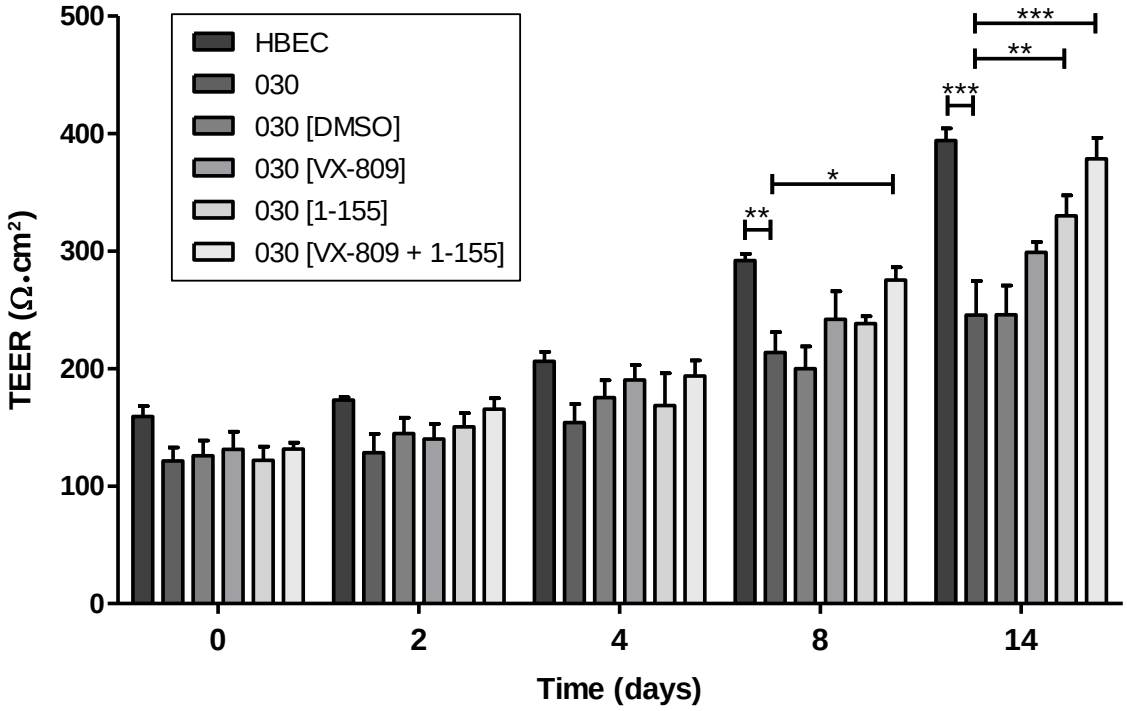

Figure 3.12. TEER measurements of 030 cells following treatment with VX-809 and 1-155 alone or in combination. HBECs and 030 cells were cultured in Transwell® inserts for 14 days at ALI. 030 cells were treated with VX-809 (2.5 µM), 1-155 (2.5 µM) or VX-809 (2.5 µM) and 1-155 (2.5 µM), with treatments changed every 24 h prior to ALI and every 48 h thereafter. DMSO was used as a vehicle control. The electrical resistance (Ω) of each Transwell® was measured using an epithelial voltohmmeter and recorded at time points of 0, 2, 4, 8 and 14 days post ALI. Measurements were taken in triplicate and the electrical resistance of a collagen coated Transwell® in the absence of cells, subtracted from experimental groups. Final TEER values presented as Ω.cm^2. Data expressed as the mean ± SEM of three independent experiments (N=3). Statistical analysis performed using a two-way ANOVA, with a post-hoc Bonferroni multiple comparison test; **P*<0.05, ***P*<0.01, ****P*<0.001.

3.4 Discussion

It is now established that TG2 plays a pivotal intracellular role, as regards to derangement of the proteostasis network in CF airway epithelia (Maiuri et al., 2008; Luciani et al., 2009, 2010; Tosco et al., 2016). However, a study has recently emerged which suggests that TG2 is also responsible for pathological changes in the extracellular environment of these cells (Nyabam et al., 2016). This chapter looks to expand upon the initial observations of that research, to further understand the interrelationship between TG2, EMT and the development of fibrosis in CF. To begin with, a comparative analysis of TG2 protein expression was performed using the 'CF diseased state' IB3 cell line and the 'CFTR corrected' C38 cell line. As expected, TG2 protein levels were significantly elevated in IB3 cells compared to C38 cells, thus reinforcing the extensively reported link between CF and TG2 overexpression in airway epithelial cells.

It is becoming increasingly clear that EMT is involved in the pathogenesis of progressive fibrosis. Induction of EMT has now been evidenced in fibrotic diseases of the kidney (Iwano et al., 2002) lung (Kim et al., 2006), liver (Rygiel et al., 2008), and heart (Zhou et al., 2010). Nevertheless, the capacity for EMT to contribute towards the myofibroblast population, still remains controversial (Hill et al., 2019). Interestingly, the upregulation of TG2 in CF airway epithelia, has been found to be associated with the acquisition of a mesenchymal phenotype (Nyabam et al., 2016). Data within this chapter confirms the elevation of mesenchymal protein expression in IB3 cells and demonstrates for the first time, an increased presence of the myofibroblast marker, α-SMA. Taken together, this indicates that CF bronchial epithelial cells undergo EMT-derived myofibroblast transdifferentiation. Yet, it must also be considered that cells are extremely sensitive to changes in their biophysical microenvironment (Tschumperlin et al., 2013). Matrix stiffness is now recognised as a crucial regulator of myofibroblast formation (Liu et al., 2010). It would seem logical that TG2-mediated ECM crosslinking, is acting as a key driver of this process. However, research suggests that the use of plasticware for *in vitro* cell culture, may also provide a rigid

substrate for the mechanoactivation of myofibroblasts (Hinz et al., 2007; Chadli et al., 2019). As such, the contribution of each element to the myofibroblast transdifferentiation of IB3 cells is unclear.

As stated above, TG2 can promote fibrotic remodelling of the ECM. Studies using separate disease models, have continued to demonstrate a strong correlation between higher levels of extracellular TG2 and the increased synthesis / deposition of fibrous ECM proteins (Telci et al., 2009; Espitia Pinzón et al., 2017; Philp et al., 2018; Shinde et al., 2020). This study is the first to confirm such changes in the context of CF. Data from this chapter identifies the co-localised overexpression of TG2 and fibronectin, in the ECM of IB3 cells. Firstly, this suggests that the cellular export of TG2 is increased by CF airway epithelia, agreeing with the work by Nyabam et al. (2016), which measured high levels of TG2 on the cell surface of IB3 cells. Furthermore, the spatial overlap of the two fluorescent markers may indicate an association between TG2 and fibronectin in the extracellular environment of CF airway epithelial cells. Nevertheless, further investigation would be required to validate the presence of such a protein-protein interaction.

EMT has now been shown to have an underlying role in various fibrotic lung diseases including: asthma (Johnson et al., 2013), IPF (Jonsdottir et al., 2015) and chronic obstructive pulmonary disease (COPD) (Milara et al., 2013). It is understood that one of the earliest cellular events of EMT is the disassembly of epithelial – epithelial cell contacts (e.g. tight junctions) and the loss of apical-basal cell polarity (Lamouille et al., 2014). In fact, an intrinsic disruption of the tight junctions has been evidenced in the airway epithelium of all the diseases mentioned prior (Heijink et al., 2014; Ohta et al., 2012; Xiao et al., 2011). Research now suggests that the barrier function of CF airway epithelium may also be compromised. Two studies have previously found that CFBE41o$^-$ (ΔF508 homozygous) cell monolayers exhibit a lower TEER, in comparison to normal 16HBE14o$^-$ cell monolayers (Weiser et al., 2011; Castellani et al., 2012). Data within this chapter supports these findings, in which TEER values were measured using a separate CF epithelial cell line. It

was shown that after 14 days at ALI, IB3 cell monolayers had significantly decreased TEER, compared to C38 cell monolayers. Taken together with the previous studies, it seems likely that tight junction integrity is diminished in CF airway epithelium. Furthermore, considering that IB3 cells undergo EMT-derived myofibroblast transdifferentiation, the loss of barrier function may well be a feature of this phenotypic change.

Although CF bronchial epithelial cell lines have proven to be of considerable value to CF research, there are inherent limitations that exist with the use of immortalised cells. The process of transformation is accompanied by karyotypic instability, which can lead to alterations in cell morphology, as well as cell function (Gruenert et al., 2004). As a result, cell lines may express dissimilar phenotypic characteristics, relative to the cell type of origin. For example, cigarette smoke exposure has been shown to have markedly different effects on CF immortalised cells, in comparison to CF primary cells (Williams et al., 2016). This research serves to highlight the importance of using primary cells, to substantiate experimental findings derived from the use of cell lines.

Therefore, primary HBECs isolated from three ΔF508 homozygous individuals were characterised, so as to confirm the results obtained with IB3 cells. Crucially, all primary cells were used up to a maximum passage of 5, to minimise the phenotypic changes associated with prolonged primary cell culture, e.g. cellular senescence. It was found that TG2 and fibronectin protein levels were significantly higher in the ECM of CF primary HBECs, compared to ECM of normal HBECs. By using two-colour immunofluorescence staining, TG2 and fibronectin were also shown to co-localise in the ECM of CF primary HBECs. These data provide further evidence that there is an increased cellular export of TG2 by CF airway epithelia, which is associated with enhanced matrix deposition of fibronectin.

As indicated previously, IB3 cells exhibit EMT induction and impaired tight junction integrity. However, the detection of functional EMT changes in CF airway epithelia, has only ever been established using the IB3 cell line (Nyabam et al., 2016). A recent literature review highlights the absence of CF primary cell studies (Amaral et al., 2020). To date, only a single

study has noted the existence of EMT in CF primary cells; a profiling transcriptome meta-analysis, which identified an EMT signature in CF patient nasal samples (Clarke et al., 2015). For that reason, CF primary HBECs were examined for functional indicators of EMT. It was revealed that CF primary HBECs show increased N-cadherin protein expression, decreased E-cadherin protein expression, reduced TEER and higher levels of cell migration, in comparison to normal HBECs. Unfortunately, due to unforeseen circumstances, CF primary HBECs could no longer be used after the first year of research. As such, it was not possible to measure α-SMA protein levels in CF primary HBECs. Furthermore, the lack of CF primary HBECs, prevented the obtainment of additional biological replicates for some experiments. Nevertheless, these findings demonstrate for the first time that CF airway epithelial cells undergo EMT, although the potential influence of *in vitro* cell culture must also be recognised.

Interestingly, differences between CF primary HBECs were also observed. In general, 032 cells exhibited the most severe phenotype, in terms of disease state. Compared to the other CF primary HBEC isolates, 032 cells showed the greatest matrix deposition of TG2 and fibronectin, the largest change in EMT protein expression and the lowest TEER. It must be noted however, that 037 cells demonstrated the highest cell migration levels. Yet, this discrepancy may possibly be explained by the fact that the result is representative of a single experiment. As a whole, these findings highlight the intersubject variability found between CF patients, even those which possess identical *CFTR* mutations. Still, it remains unclear whether these results reflect genuine biological differences, or instead denote inconsistencies in the method / circumstances of isolating cells. Moreover, CF primary HBECs are typically isolated from lung explants and post-mortem samples (Randell et al., 2011). With this tissue having progressed to an end of disease stage, it raises the question as to whether CF primary HBEC isolates ever reflect cell phenotype at an earlier disease state? (Clancy et al., 2019).

As outlined previously, CF animal models have been constrained by their inability to recapitulate organ abnormalities seen in humans with CF (Semaniakou et al., 2019). As such, CF primary cells have acted as critical bridge in terms of a relevant pathophysiological model system, which can be used to complement immortalised cell studies. Within this chapter, both types of cell model system have been used to demonstrate the importance of TG2, in CF airway epithelia. Previous research has shown that the selective inhibition of TG2, functions to have a therapeutic effect on IB3 cells (Nyabam et al., 2016). However, modulators directed at non-CFTR targets have recently failed in clinical trials (e.g. Ataluren and Cavosonstat), having lacked the relevant primary cell data (Clancy et al., 2019; Konstan et al., 2020). Hence, CF primary HBECs were used for proof of concept experiments, to test the use of TG2 specific inhibitor (1-155) with an approved CFTR corrector (VX-809).

It was revealed that VX-809 and 1-155 could reduce TG2 protein expression in CF primary HBECs, to a greater extent than the use of either compound alone. Furthermore, 030 cells treated with VX-809 and 1-155 showed significantly increased TEER after 14 days at ALI, with TEER reaching almost comparable levels as were measured for HBECs. Importantly, these data support previous findings, which employed the use of immortalised cell lines for testing (Nyabam et al., 2016). This suggests that IB3 cells will provide a reliable cell system for further investigation of combination treatment and that TG2 inhibitors could potentially be used as therapeutic agents in the treatment of CF.

In conclusion, this chapter has shown that the protein expression / matrix deposition of TG2 and fibronectin, is elevated in both IB3 cells and CF primary HBECs. In addition, IB3 cells were demonstrated to undergo EMT-derived myofibroblast transdifferentiation, with CF primary HBECs also found to exhibit increased EMT. Moreover, intersubject variability was observed between different CF (ΔF508 homozygous) primary HBEC isolates, as regards to the level of fibrotic changes within cells and the surrounding ECM. Finally, combination treatment with VX-809 and 1-155 was determined to have a potentially additive therapeutic effect on CF primary HBECs, which will be examined further in the following chapter.

Chapter 4

The combined application of a CFTR corrector and TG2 inhibitor as a potential therapy for CF

CHAPTER 4: RESULTS

4.1 Introduction

CF is a multisystem disease, that results in range of clinical manifestations. Nevertheless, the major cause of morbidity and mortality in CF patients, relates to progressive lung disease and its eventual outcome of respiratory failure (Zolin et al., 2020). Traditionally, treatment has relied upon symptomatic management including: pancreatic enzyme replacement therapy, mucolytics, physiotherapy and antibiotics (Stern et al., 2014). In addition to early diagnosis, these therapeutic regimens have substantially improved the life expectancy of CF patients, rising from early childhood in the 1960's to around 30 years in the 1990's (Dodge et al., 2007). Yet despite these advances, there remained a clear gap between the median survival of CF patients and that of the normal population. Further to this, individuals continued to suffer considerable clinical and economic burdens, which limited their quality of life (Lopes-Pacheco, 2020).

However, just over 30 years ago the discovery of the *CFTR* gene sparked a revolution in the treatment of CF (Riordan, 1989). Since then, more than 2000 variants of *CFTR* have been identified, which are now classified into seven distinct functional classes (De Boeck and Amaral, 2016). This notion of mutational grouping has laid the foundations for a pharmacological approach, in which compounds target a specific class of CFTR defect. Indeed, the first CFTR modulator (Ivacaftor) was approved in 2012, albeit this potentiator held little benefit for individuals with the most common *CFTR* mutation, ΔF508 (Flume et al., 2012). This led to the development of CFTR correctors (e.g. Lumacaftor), compounds designed to facilitate the folding and trafficking of ΔF508 CFTR to the plasma membrane. Thereafter, CFTR modulators were combined to improve drug efficacy, resulting in the most recent advancement of a triple combination therapy (Kaftrio). Clinical trials have indicated that Kaftrio may provide a significant clinical benefit to CF patients with at least one copy of the ΔF508 variant (Heijerman et al., 2019). Conversely, this means that 10% of the CF

population are still left without a treatment (Cuevas-Ocaña et al., 2020). Furthermore, the long-term effects of CFTR- directed modulator combinations are yet unknown.

Research from the literature now challenges the classical belief, that CF is simply a channelopathy (Bodas and Vij, 2019). As mentioned in the previous chapter, the proteostasis network within CF airway epithelia is deranged, meaning that correction of CFTR alone may be limited in its therapeutic capacity. In fact, TG2 activity has been found to play a crucial role in the regulation of CFTR maturation and stability (Nyabam et al., 2016; Tosco et al., 2016). Moreover, its pathological influence extends beyond CFTR, with TG2 seen to promote fibrotic changes in both CF airway epithelial cells and the surrounding ECM (Nyabam et al., 2016).

As such, selective and potent inhibitors of TG2 open up a new therapeutic avenue in CF and one which can be combined with currently approved CFTR modulators. By targeting the underlying proteostasis dysfunction in CF airway epithelia, therapeutic benefits might be gained, in addition to the already impressive results reported for Kaftrio (Griese et al., 2021). Further to this, TG2 inhibitors have the advantage of acting independently of any *CFTR* mutation and are therefore applicable to all CF patients. Although the preliminary data has been encouraging (Nyabam, 2015), this innovative approach of two-directional (direct/indirect) pharmacotherapy now requires further investigation.

4.2 Aims and Objectives

This chapter aims to evaluate the effectiveness of two-directional combination treatment by:

(1) Investigating the effect of using an approved CFTR corrector (VX-809) with a TG2 specific inhibitor (1-155) on IB3 cells, compared to use of either compound alone.

(2) Using a cell-impermeable TG2 inhibitor to understand the role of extracellular TG2 in the pathogenesis of CF.

(3) Examining the significance of TG2-mediated TGFβ1 activation in CF and to determine the involvement of canonical and non-canonical downstream signalling pathways.

4.3 Results

4.3.1 Determination of half-maximal inhibitory concentration (IC_{50}) for the cell-permeable TG2 inhibitor 1-155

Data from chapter 3 establishes a possible link between TG2 and CF progression. Hence, TG2 may be a potential therapeutic target for the treatment of CF. Specific, irreversible peptidomimetic inhibitors have been developed at Aston University, which target TG2 in its Ca^{2+} activated form. The cell-permeable compound 1-155, has been shown to be a potent and highly selective inhibitor of TG2, which was originally determined to have IC_{50} value of ~6 nM (Badarau et al., 2015). However, published data evaluating the inhibitory effect of 1-115 on TG2 activity has been limited. Thus, it is vital to validate the efficacy of 1-155 as a TG2 inhibitor, before investigating its therapeutic potential.

To confirm the IC_{50} value of 1-155, a transglutaminase activity assay was performed. Ten concentrations of 1-155 ranging from 1 nM – 50 µM were tested and decreases in TG2 activity measured as a percentage, relative to the TG2 activity of a DMSO control. From the dose-response curve, the IC_{50} value of 1-155 was determined to be 18.47 nM (Figure 4.1).

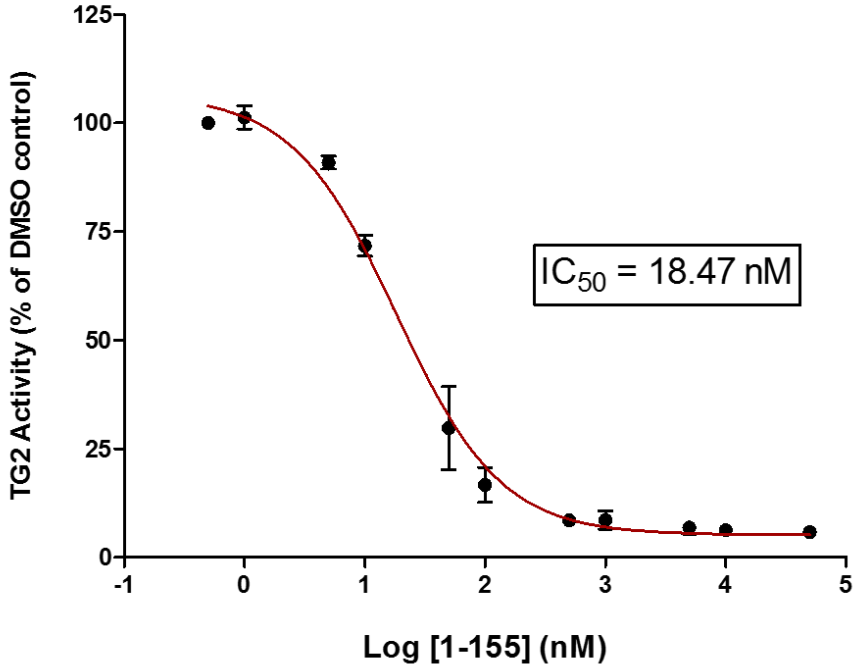

Figure 4.1. Quantification of the IC_{50} value for TG2 inhibitor 1-155 using a transglutaminase activity assay. Biotin-cadaverine incorporation into N,N-dimethylcasein was used as a quantitative measure of TG2 activity. Cell-permeable TG2 inhibitor 1-155 was added to wells at concentrations ranging from 1 nM – 50 µM. A DMSO control was used as a reference of total TG2 activity. A does-response curve was generated and the inhibitory effect of 1-155 measured as the percentage reduction in total TG2 activity. The relative IC_{50} was determined as the half-maximal inhibitory concentration. Data expressed as the mean ± SEM of three independent experiments (N=3), each performed in triplicate.

4.3.2 The effect of a CFTR corrector on TG2 and fibronectin protein expression in IB3 cells

Corrector compounds form the backbone of currently approved CFTR modulator therapies (De Boeck, 2020). Numerous studies have demonstrated that correctors rescue the folding, processing and trafficking of CFTR mutants to the plasma membrane, for increased Cl^- transport (Lopes-Pacheco, 2020). However, recent data indicates that CF is more complicated than just a simple imbalance in Cl^- movement. Loss of CFTR leads to a major dysregulation of the proteostasis network in CF airway epithelial cells (Maiuri et al., 2008; Luciani et al., 2009, 2011), with TG2 overexpression leading to adverse alterations of the ECM (Nyabam et al., 2016). Despite the fact that correctors have been proven to rescue CFTR, it is yet to be investigated whether this also translates to the reversal of fibrotic changes.

To determine the effect of CFTR correction on fibrotic progression in CF, IB3 cells were treated with the established CFTR corrector, VX-809. Following an extensive review of the literature, VX-809 was found to be predominantly used at concentrations ranging from 1–5 μM. These data show a reduction in the protein expression of TG2 and fibronectin, in response to all three concentrations of VX-809 (Figure 4.2). The use of VX-809 at 2.5 μM caused the largest decrease in TG2 and fibronectin protein levels. However, changes were not seen to be statistically significant across the range of VX-809 concentrations tested.

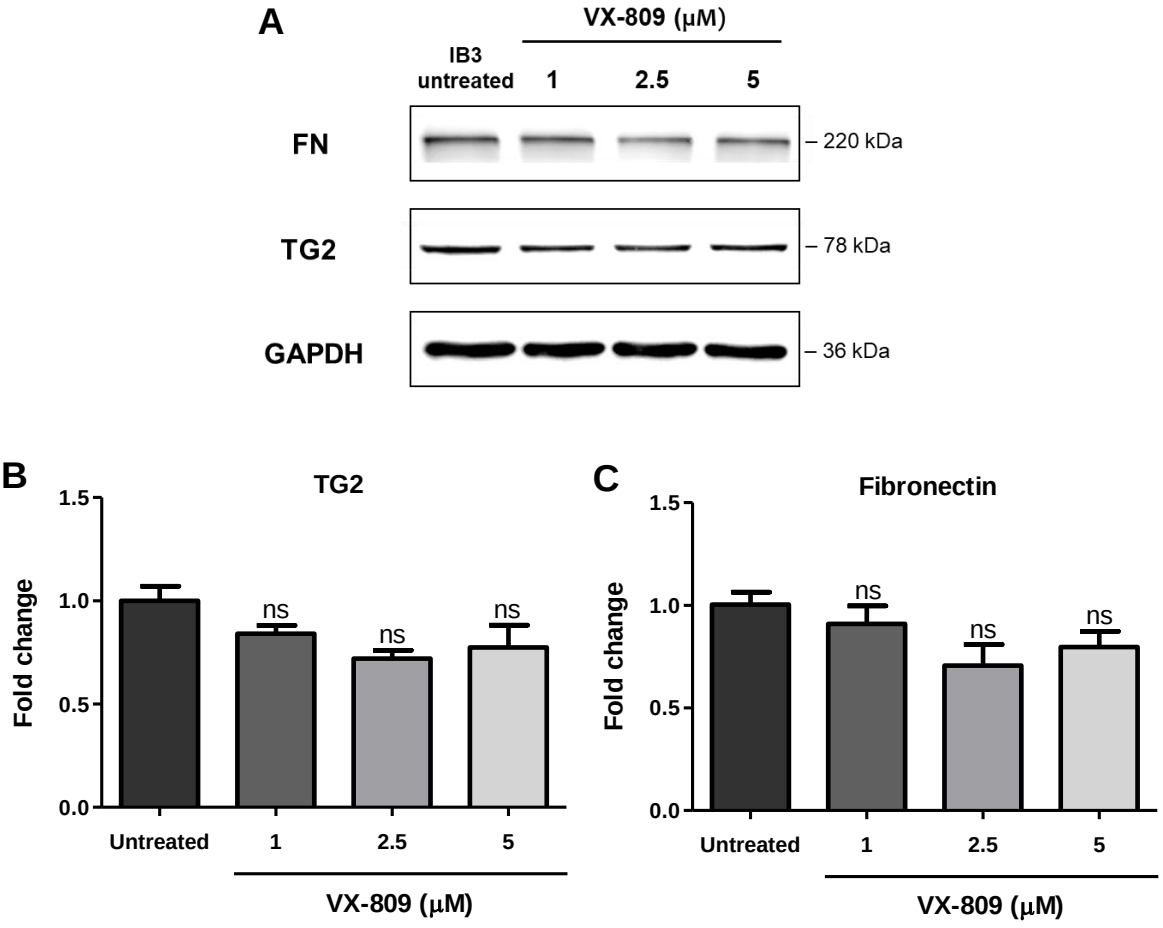

Figure 4.2. Measurement of TG2 and fibronectin protein expression in IB3 cells in response to different concentrations of CFTR corrector VX-809. IB3 cells were treated with three different concentrations of VX-809 (1, 2.5 and 5 μM) for 72 h, with treatments changed every 24 h. Whole cell lysates were collected and proteins separated using SDS-PAGE. Following protein transfer, western blot analysis was performed for detection of TG2 and fibronectin. Membranes were stripped and reprobed for the loading control GAPDH. **(A)** Representative western blots of TG2 and fibronectin protein expression. Densitometry of **(B)** TG2 and **(C)** fibronectin protein levels, measured using ImageJ software. Data normalised to GAPDH and expressed as the mean fold change ± SEM in comparison to untreated IB3 cells. Statistical analysis of three independent experiments (N=3) using a one-way ANOVA, with a post-hoc Tukey test; ns, not significant.

4.3.3 Evaluating the cytotoxicity of compounds VX-809 and 1-155 on C38 and IB3 cells

Compounds 1-155 and VX-809 have been shown to reduce both the activity (Figure 4.1) and protein expression (Figure 4.2) of TG2, respectively. It has not previously been determined whether use of a TG2 inhibitor with a CFTR corrector, can decrease aberrant levels of TG2 in an additive or synergistic manner. Before testing VX-809 and 1-155 in combination, a preliminary assessment of compound cytotoxicity was conducted. This was performed to eliminate cell death as a factor of influence when interpreting the results of further investigations. Based on the data from Figure 4.2, VX-809 was tested at its most effective concentration of 2.5 μM. TG2 inhibitor 1-155 was also tested at 2.5 μM, a known concentration for efficacy of the compound.

An XTT assay was used to assess the cytotoxicity of VX-809 and 1-155, either alone or in combination. C38 and IB3 cells were treated for 72 h, with both compounds used at a concentration of 2.5 μM. These data show no significant difference in cell viability across all treatment conditions, for either C38 cells (Figure 4.3 A) or IB3 cells (Figure 4.3 B).

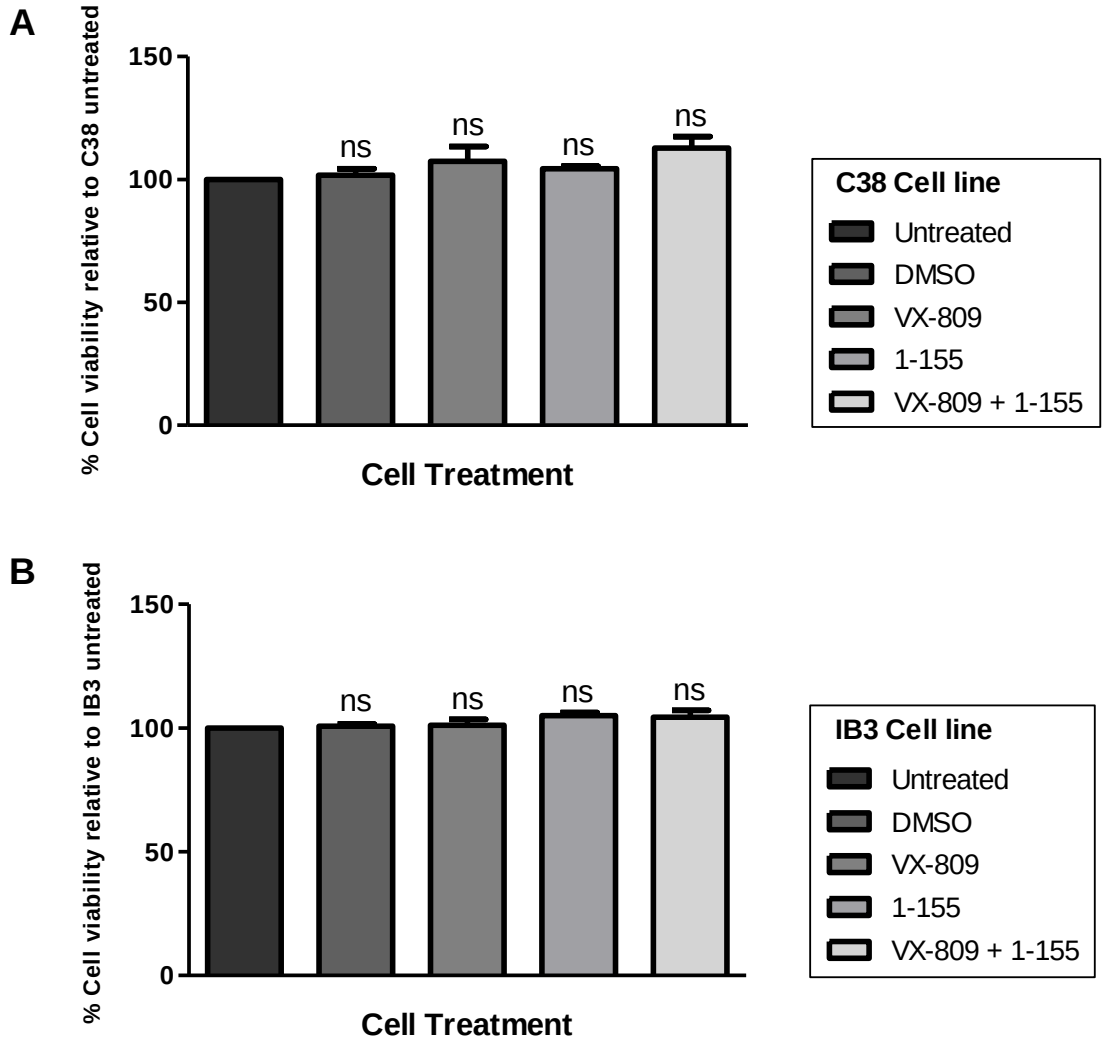

Figure 4.3. The cytotoxicity of VX-809 and 1-155 used alone or in combination on C38 and IB3 cells. C38 and IB3 cells were treated with VX-809 (2.5 µM), 1-155 (2.5 µM) or VX-809 (2.5 µM) and 1-155 (2.5 µM) for 72 h, with treatments changed every 24 h. DMSO was used as a vehicle control. An XTT assay was performed and the absorbance read at a wavelength of 490 nm and 630 nm. The background absorbance (630 nm) was subtracted from the sample absorbance (490 nm) for each well. The percentage cell viability of **(A)** C38 and **(B)** IB3 cells following treatment with VX-809 and 1-155 used alone or in combination, relative to untreated C38 or IB3 cells. Data expressed as the mean ± SEM of three independent experiments (N=3). Statistical analysis performed using a one-way ANOVA, with a post-hoc Tukey test; ns, not significant.

4.3.4 The combined effect of a CFTR corrector and TG2 inhibitor on TG2 protein expression in IB3 cells

The TG2 inhibitor 1-155 has previously been shown to reduce the protein expression of TG2 in IB3 cells (Nyabam et al., 2016). However, the relevance of this data is limited, as the investigation lacks the inclusion of a 'CFTR corrected' control cell line. As such, the extent to which 1-155 decreases TG2 protein expression, relative to native levels of TG2 in non-CF airway epithelial cells, is yet to be determined. Data within this report has demonstrated that VX-809 can also reduce the presence of TG2 in IB3 whole cell lysates (Figure 4.2). As a result, IB3 cells were treated with VX-809 and 1-155 either alone or in combination, to establish whether 1-155 can completely abrogate the increased expression of TG2 or rather VX-809 can be used together with 1-155 to have an additive or synergistic effect.

IB3 cells were treated with either VX-809 (2.5 µM), 1-155 (2.5 µM) or VX-809 (2.5 µM) and 1-155 (2.5 µM) combined. Following treatment for 72 h, whole cell lysates were collected and TG2 protein expression was measured via western blot analysis. C38 cells were used to determine normal protein levels of TG2. These data show a decrease in TG2 expression across all treatment conditions (Figure 4.4). Both 1-155 alone and VX-809 with 1-155 were able to significantly reduce TG2 protein levels by 47% ($p<0.05$) and 65% ($p<0.01$) respectively, in comparison to untreated IB3 cells. Interestingly, the combined decrease in TG2 expression for use of 1-155 (47%) and VX-809 (19%) alone totalled 66%, thus matching the reduction observed for treatment with VX-809 and 1-155 in combination (65%).

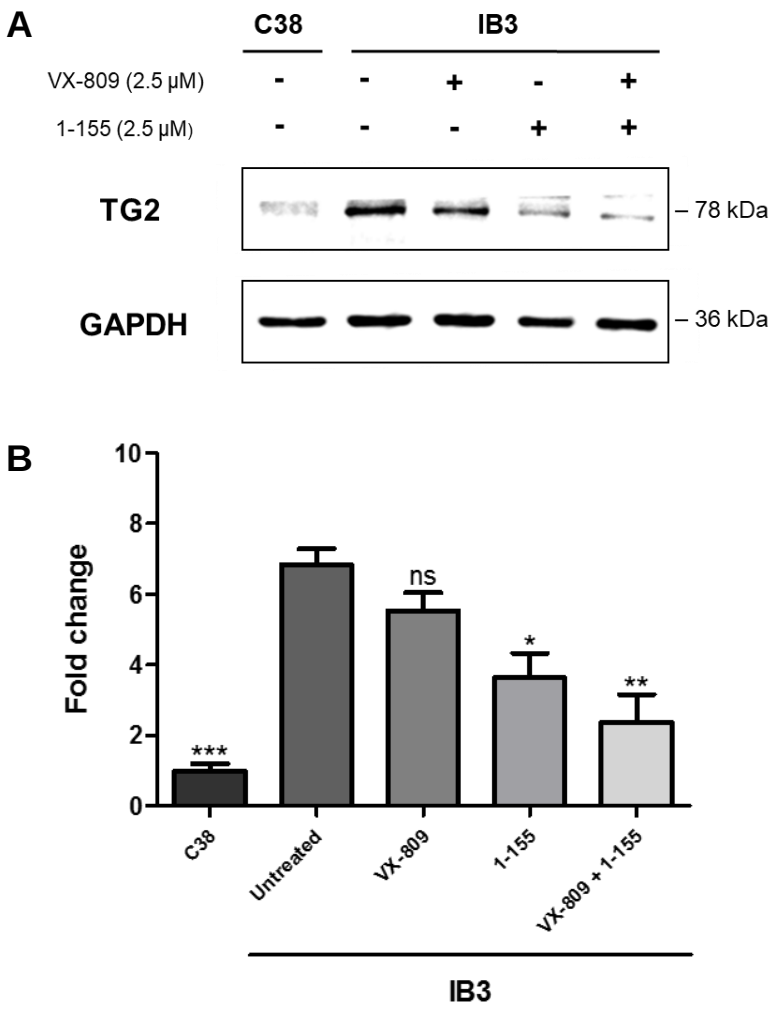

Figure 4.4. Measurement of TG2 protein expression in IB3 cells following treatment with VX-809 and 1-155 alone or in combination. IB3 cells were treated with VX-809 (2.5 µM), 1-155 (2.5 µM) or VX-809 (2.5 µM) and 1-155 (2.5 µM) for 72 h, with treatments changed every 24 h. C38 cells were used as a CFTR corrected control. Whole cell lysates were collected and proteins separated using SDS-PAGE. Following protein transfer, western blot analysis was performed for detection of TG2. Membranes were stripped and reprobed for the loading control GAPDH. **(A)** Representative western blot of TG2 protein expression. **(B)** Densitometry of TG2 protein levels, measured using ImageJ software. Data normalised to GAPDH and expressed as the mean fold change ± SEM, in comparison to untreated IB3 cells. Statistical analysis of three independent experiments (N=3) using a one-way ANOVA, with a post-hoc Tukey test; ns, not significant, **P*<0.05, ***P*<0.01, ****P*<0.001.

4.3.5 The combined effect of a CFTR corrector and TG2 inhibitor on EMT-derived myofibroblast transdifferentiation of IB3 cells

Data within this report has revealed that TG2 protein levels are inherently increased in IB3 cells (Figure 3.1), alongside enhanced expression / deposition of fibronectin (Figures 3.2 and 3.3) and the induction of EMT-derived myofibroblast transdifferentiation (Figure 3.2). As shown in Figure 4.4, both VX-809 and 1-155 were able to independently reduce protein levels of TG2 in IB3 whole cell lysates, with a further decrease measured in response to combination treatment. To further understand the relationship between TG2 and the presence of fibronectin / myofibroblasts, IB3 cells were again treated with VX-809 and 1-155 alone or in combination. The effect on fibronectin, N-cadherin and α-SMA protein expression was then measured, to test whether a corresponding downregulation of the three pro-fibrotic markers would be observed

IB3 cells were treated with either VX-809 (2.5 µM), 1-155 (2.5 µM) or VX-809 (2.5 µM) and 1-155 (2.5 µM) for 72 h, before whole cell lysates were collected and samples analysed using western blot analysis. A C38 control was used for comparison of normal protein expression. These data show a decrease in protein levels of fibronectin, N-cadherin and α-SMA across all treatment conditions, in comparison to untreated IB3 cells (Figure 4.5). Both 1-155 alone and VX-809 with 1-155 were able to significantly reduce protein levels by ≥28% ($p<0.05$) and ≥67% ($p<0.001$) for all three proteins respectively, in comparison to untreated IB3 cells. Remarkably, combination treatment caused a greater decrease in protein expression, than the total decrease measured when combining the effect of VX-809 and 1-155 used alone, for all three proteins analysed.

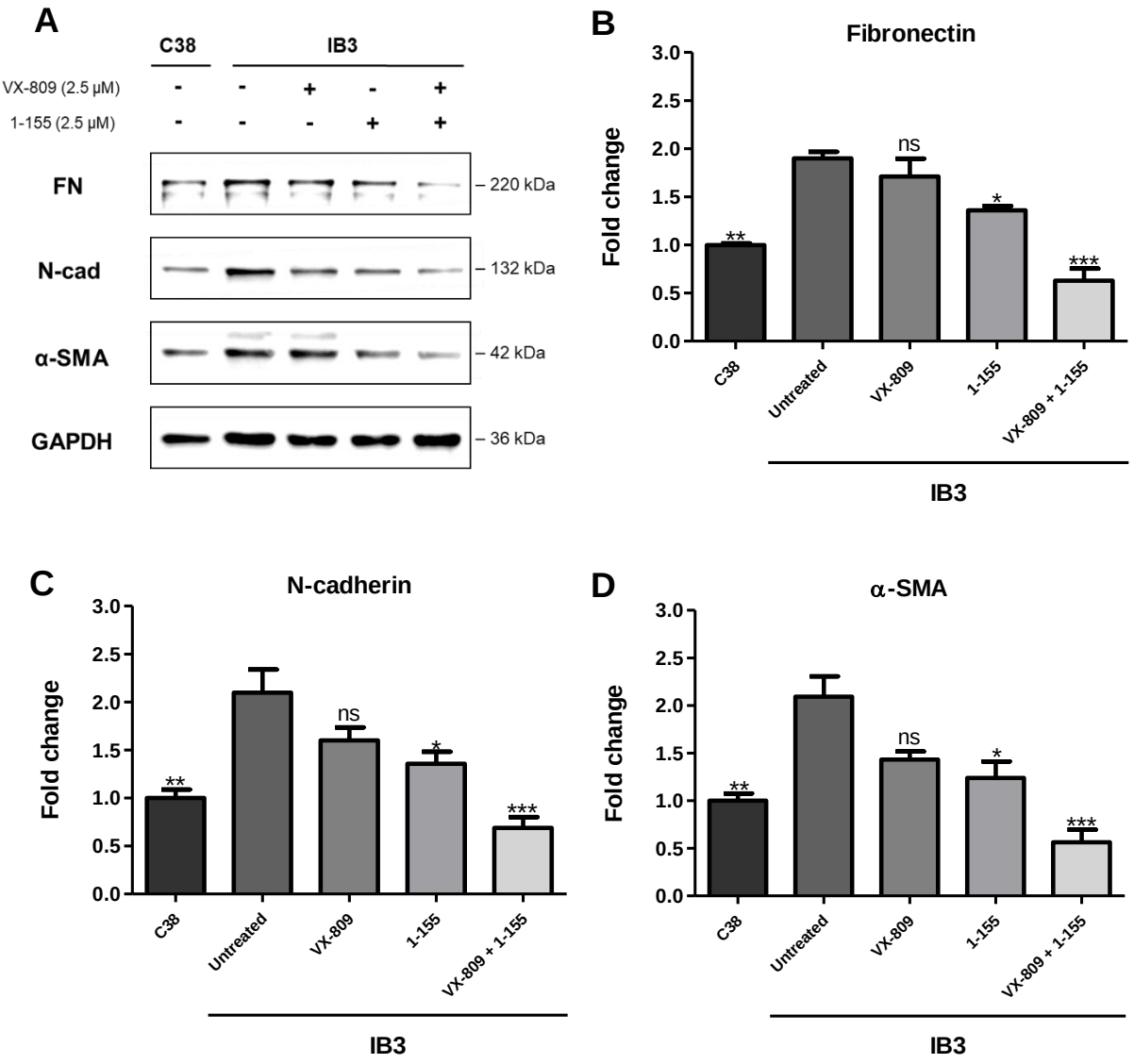

Figure 4.5. Measurement of fibronectin, N-cadherin and α-SMA protein expression in IB3 cells following treatment with VX-809 and 1-155 alone or in combination. IB3 cells were treated with VX-809 (2.5 μM), 1-155 (2.5 μM) or VX-809 (2.5 μM) and 1-155 (2.5 μM) for 72 h, with treatments changed every 24 h. C38 cells were used as a CFTR corrected control. Whole cell lysates were collected and proteins separated using SDS-PAGE. Following protein transfer, western blot analysis was performed for detection of fibronectin, N-cadherin and α-SMA. Membranes were stripped and reprobed for the loading control GAPDH. **(A)** Representative western blots of fibronectin, N-cadherin and α-SMA protein expression. Densitometry of **(B)** fibronectin **(C)** N-cadherin and **(D)** α-SMA protein levels, measured using ImageJ software. Data normalised to GAPDH and expressed as the mean fold change ± SEM in comparison to untreated IB3 cells. Statistical analysis of three independent experiments (N=3) using a one-way ANOVA, with a post-hoc Tukey test; ns, not significant, **P*<0.05, ***P*<0.01, ****P*<0.001.

4.3.6 Determination of half-maximal inhibitory concentration (IC_{50}) for the cell-impermeable TG2 inhibitor R281

As demonstrated in Figures 4.4 and 4.5, 1-155 can decrease the aberrant expression of TG2 and pro-fibrotic markers in IB3 whole cell lysates. However, 1-155 is a cell-permeable compound, capable of inhibiting TG2 both inside and outside of the cell (Badarau et al., 2015). As such, it is unknown whether 1-155 effectuates these changes by inhibiting intracellular or extracellular TG2, or possibly a combination of both. To specifically determine the role of externalised TG2, a membrane-impermeable TG2 inhibitor known as R281 was used to treat IB3 cells. Originally shown to have an IC_{50} value of ~10 µM (Griffin et al., 2008), this compound has been used extensively to investigate the role of extracellular TG2 in various cellular processes (Nadella et al., 2015; Feriotto et al., 2017; Zonca et al., 2017). With inhibitory capacity varying between each synthesis of the compound, an initial measurement IC_{50} was performed to validate the efficacy of R281.

The IC_{50} value of R281 was quantified using a transglutaminase activity assay. Ten concentrations of R281 ranging from 0.5 µM – 10 mM were tested and decreases in TG2 activity measured as a percentage, relative to the TG2 activity of a DMSO control. From the dose-response curve the IC_{50} value of R281 was determined to be 39.14 µM (Figure 4.6).

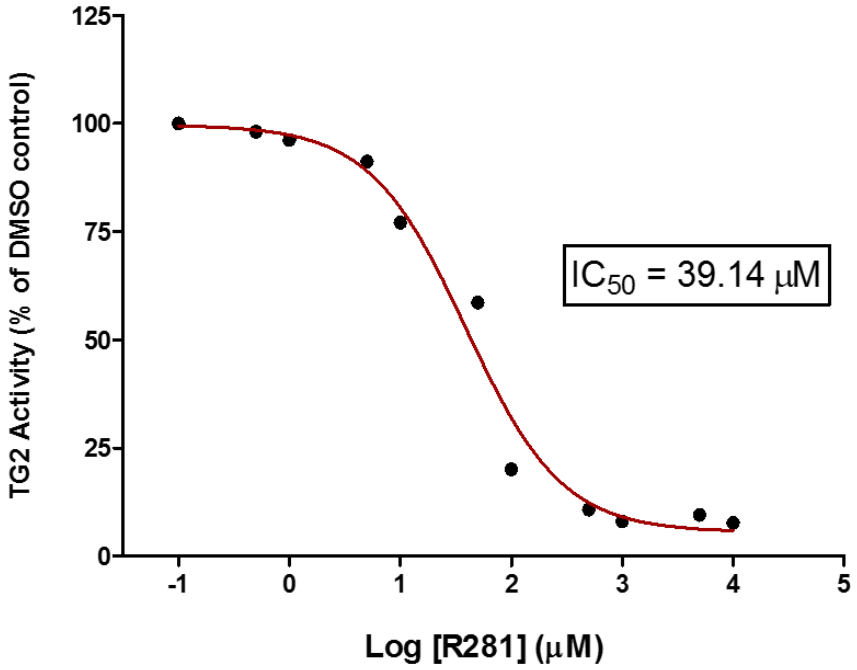

Figure 4.6. Quantification of the IC_{50} value for TG2 inhibitor R281 using a transglutaminase activity assay. Biotin-cadaverine incorporation into N,N-dimethylcasein was used as a quantitative measure of TG2 activity. Cell-impermeable TG2 inhibitor R281 was added to wells at concentrations ranging from 0.5 µM – 10 mM. A DMSO control was used as a reference of total TG2 activity. A does-response curve was generated and the inhibitory effect of R281 measured as the percentage reduction in total TG2 activity. The relative IC_{50} was determined as the half-maximal inhibitory concentration. Data expressed as the mean of one independent experiment (N=1), performed in triplicate.

4.3.7 The combined effect of a CFTR corrector and cell-impermeable TG2 inhibitor on TG2 protein expression in IB3 cells

Previous research has identified deleterious effects associated with the overexpression of TG2, both inside (Maiuri et al., 2008; Luciani et al., 2009, 2011; Rossin et al., 2018) and outside (Nyabam et al., 2016) of CF airway epithelial cells. As shown in Figure 4.4, the use of 1-155 to inhibit TG2 activity within the intracellular and extracellular environment of IB3 cells, led to a significant reduction in TG2 protein levels. Moreover, a further decrease was measured when using 1-155 in combination with VX-809. Although this is promising from a therapeutic standpoint, mechanistically it is unknown whether complete or localised inhibition of TG2 is required to promote this response. To determine the importance of extracellular TG2, the cell-impermeable compound R281 was used to inhibit externalised TG2 exclusively.

IB3 cells were treated with either VX-809 (2.5 µM), R281 (500 µM) or both in combination for 72 h. A C38 control was used for comparison of normal protein expression. Whole cell lysates were collected and TG2 protein expression was measured via western blotting. Use of R281 or VX-809 and R281 significantly decreased TG2 protein levels by 60% ($p<0.001$) and 76% ($p<0.001$) respectively, in comparison to untreated IB3 cells (Figure 4.7). Treatment with VX-809 (21%) or R281 (60%) alone, jointly reduced TG2 expression by 81%. This was comparable to the decrease seen with VX-809 and R281 combined (76%).

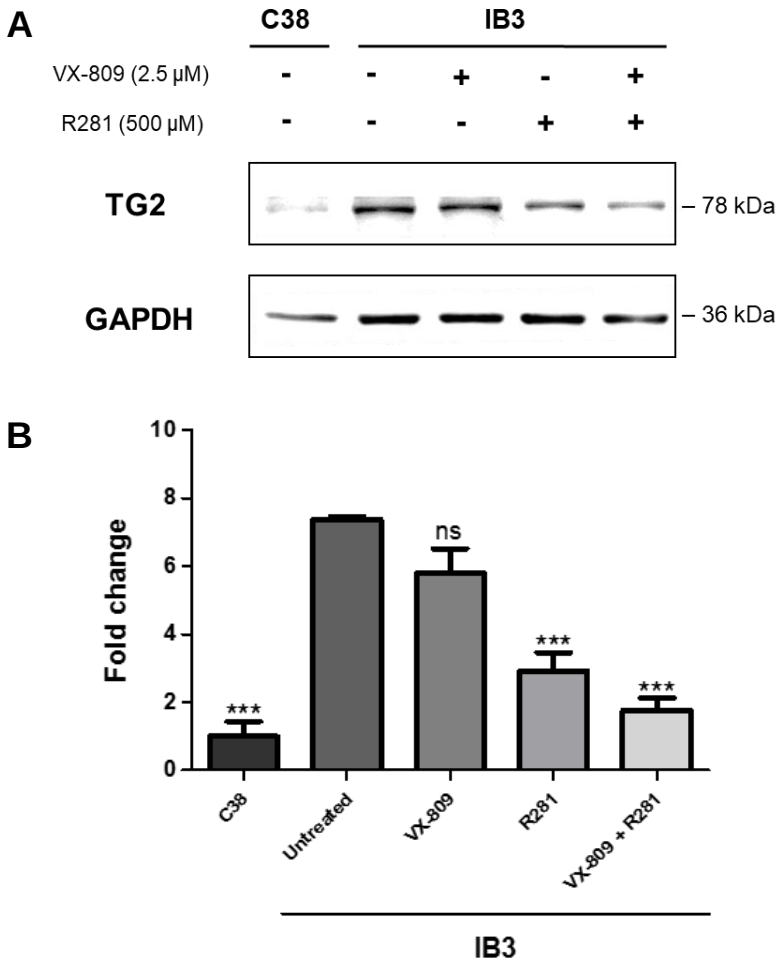

Figure 4.7. Measurement of TG2 protein expression in IB3 cells following treatment with VX-809 and R281 alone or in combination. IB3 cells were treated with VX-809 (2.5 µM), R281 (500 µM) or VX-809 (2.5 µM) and R281 (500 µM) for 72 h, with treatments changed every 24 h. C38 cells were used as a CFTR corrected control. Whole cell lysates were collected and proteins separated using SDS-PAGE. Following protein transfer, western blot analysis was performed for detection of TG2. Membranes were stripped and reprobed for the loading control GAPDH. **(A)** Representative western blot of TG2 protein expression. **(B)** Densitometry of TG2 protein levels, measured using ImageJ software. Data normalised to GAPDH and expressed as the mean fold change ± SEM in comparison to untreated IB3 cells. Statistical analysis of three independent experiments (N=3) using a one-way ANOVA, with a post-hoc Tukey test; ns, not significant, ****P*<0.001.

4.3.8 The combined effect of a CFTR corrector and cell-impermeable TG2 inhibitor on EMT-derived myofibroblast transdifferentiation of IB3 cells

As demonstrated in Figure 4.5, TG2 inhibitor 1-155 partially decreased fibronectin, N-cadherin and α-SMA protein expression in IB3 whole cell lysates. Moreover, a complete reduction in the protein levels of all three pro-fibrotic markers, was seen in response to combination treatment (VX-809 and 1-155). The subsequent replacement of 1-155 with a cell-impermeable TG2 inhibitor (R281), found R281 capable of reducing TG2 protein expression (Figure 4.7) to a similar level as measured with 1-155 (Figure 4.4). As a result, the effect of R281 on fibronectin, N-cadherin and α-SMA protein expression was assessed, to further evaluate extracellular TG2 inhibition in comparison to total TG2 inhibition.

IB3 cells were treated with either VX-809 (2.5 µM), R281 (500 µM) or VX-809 (2.5 µM) and R281 (500 µM) for 72 h, before whole cell lysates were collected and samples analysed using western blot analysis. A C38 control was used for comparison of normal protein expression. As shown in Figure 4.8, the protein expression of fibronectin, N-cadherin and α-SMA was reduced across all treatment conditions, in comparison to untreated IB3 cells. Treatment with R281 alone decreased protein levels by ≥30% for all three proteins compared to untreated IB3 cells, although the change in N-cadherin expression was not found to be significant. Furthermore, combination treatment with VX-809 and R281 significantly reduced protein levels by ≥57% ($p<0.001$) for all three proteins, in comparison to untreated IB3 cells. Overall, combination treatment reduced protein expression to a greater extent than the sum effect of VX-809 and R281 used independently, for all three proteins analysed.

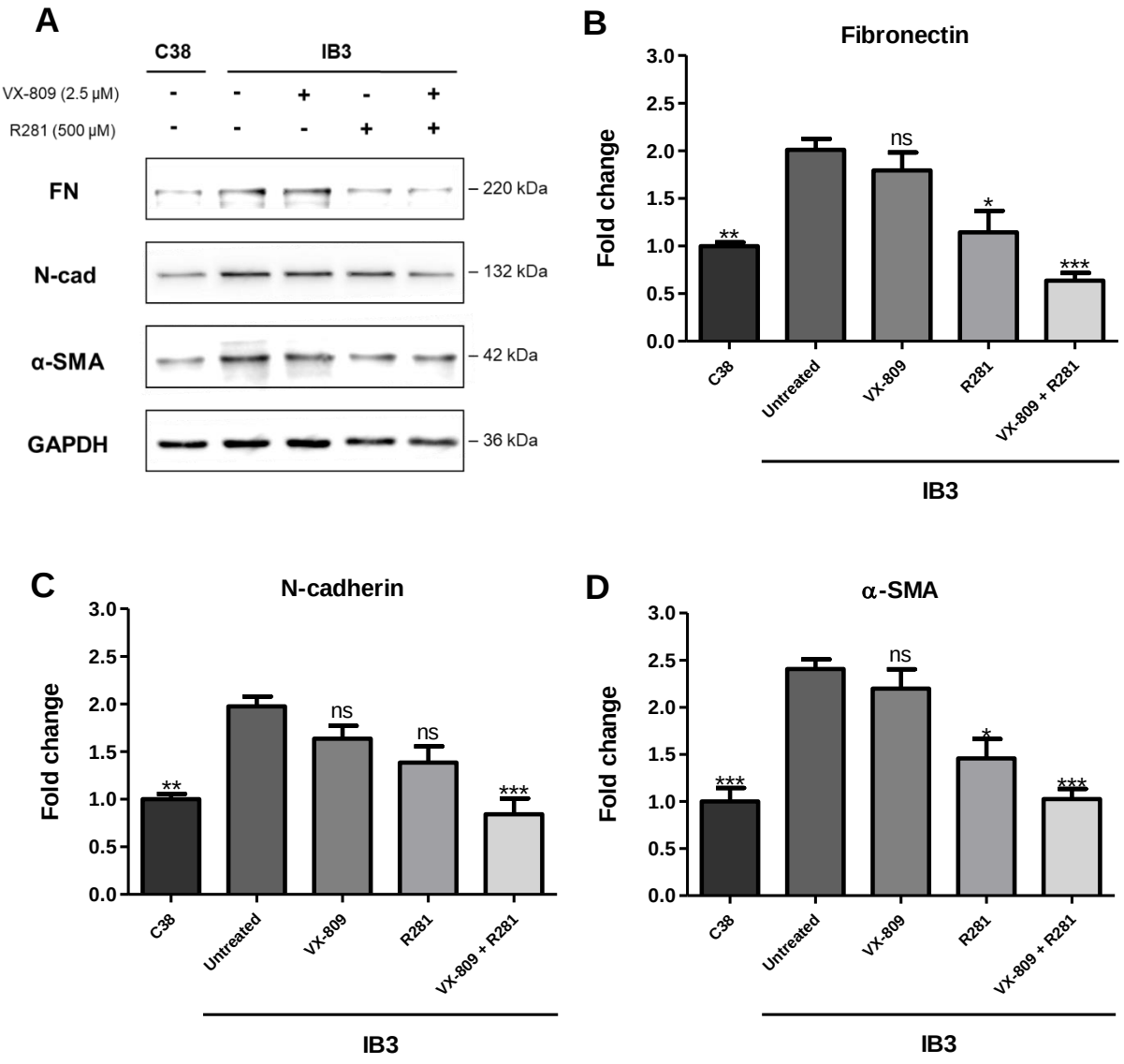

Figure 4.8. Measurement of fibronectin, N-cadherin and α-SMA protein expression in IB3 cells following treatment with VX-809 and R281 alone or in combination. IB3 cells were treated with VX-809 (2.5 μM), R281 (500 μM) or VX-809 (2.5 μM) and R281 (500 μM) for 72 h, with treatments changed every 24 h. C38 cells were used as a CFTR corrected control. Whole cell lysates were collected and proteins separated using SDS-PAGE. Following protein transfer, western blot analysis was performed for detection of fibronectin, N-cadherin and α-SMA. Membranes were stripped and reprobed for the loading control GAPDH. **(A)** Representative western blots of fibronectin, N-cadherin and α-SMA protein expression. Densitometry of **(B)** fibronectin **(C)** N-cadherin and **(D)** α-SMA protein levels, measured using ImageJ software. Data normalised to GAPDH and expressed as the mean fold change ± SEM in comparison to untreated IB3 cells. Statistical analysis of three independent experiments (N=3) using a one-way ANOVA, with a post-hoc Tukey test; ns, not significant, **P*<0.05, ***P*<0.01, ****P*<0.001.

4.3.9 The effect of TGFβ receptor I inhibition on TG2 protein expression in IB3 cells

It has long been established that TG2 facilitates the activation of TGFβ1, a key mediator of fibrosis capable of upregulating TG2 and promoting myofibroblast formation (Benn et al., 2019). As demonstrated in Figures 3.1 and 3.2, both TG2 and α-SMA are highly expressed in IB3 whole cell lysates, compared to C38 whole cell lysates. These data suggest a central pro-fibrotic role for TGFβ1 in CF. This was investigated by treating IB3 cells with a TGFβ receptor I (ALK5) inhibitor. TG2 protein expression was measured to establish whether restriction of TGFβ1 signal transduction, would generate a similar response as inhibition of extracellular TG2 (Figure 4.7). In addition, recombinant human TGFβ1 was used alone to examine its influence on TG2 protein levels or in combination with ALK5 inhibitor to ensure efficacy of the compound.

IB3 cells were treated with ALK5 inhibitor (10 µM), TGFβ1 (1 ng/ml), or ALK5 inhibitor (10 µM) combined with either VX-809 (2.5 µM) or TGFβ1 (1 ng/ml) for 72 h, before whole cell lysates were collected and samples analysed using western blot analysis. Treatment with TGFβ1 resulted in a >7-fold increase ($p<0.001$) in TG2 protein expression, compared to untreated IB3 cells (Figure 4.9). Conversely, the use of TGFβ1 in the presence of an ALK5 inhibitor ($p<0.05$) saw a significant reduction (31%) in TG2 protein levels, in comparison to untreated IB3 cells. Both ALK5 inhibitor alone and ALK5 inhibitor with VX-809 were able to decrease TG2 protein levels further by 71% ($p<0.001$) and 86% ($p<0.001$) respectively, in comparison untreated IB3 cells.

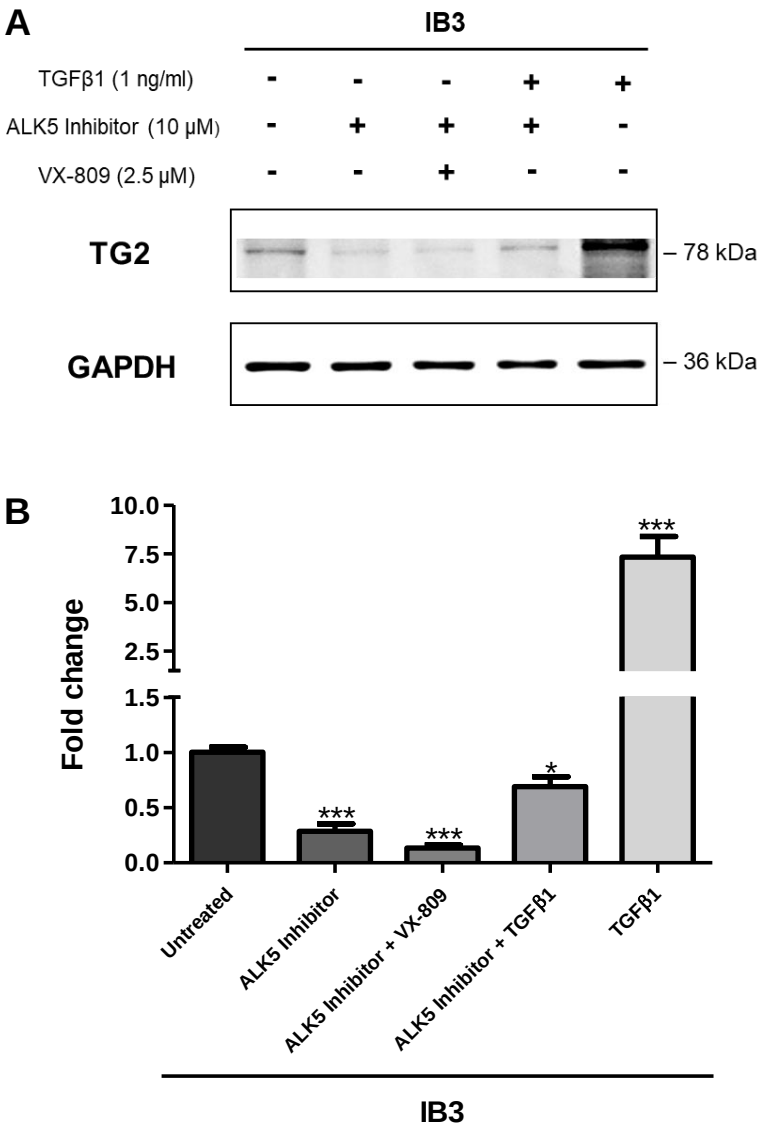

Figure 4.9. The effect of ALK5 inhibitor treatment alone or in combination with VX-809 on TG2 protein expression in IB3 cells. IB3 cells were treated with TGFβ (1 ng/ml) or an ALK5 inhibitor (10 μM) either alone or in combination with VX-809 (2.5 μM) or TGFβ (1 ng/ml) for a period of 72 h, with treatments changed every 24 h. Whole cell lysates were collected and proteins separated using SDS-PAGE. Following protein transfer, western blot analysis was performed for detection of TG2. Membranes were stripped and reprobed for the loading control GAPDH. **(A)** Representative western blot of TG2 protein expression. **(B)** Densitometry of TG2 protein levels, measured using ImageJ software. Data normalised to GAPDH and expressed as the mean fold change ± SEM in comparison to untreated IB3 cells. Statistical analysis of three independent experiments (N=3) using a one-way ANOVA, with a post-hoc Bonferroni multiple comparison test; **P*<0.05, ****P*<0.001.

4.3.10 The effect of TGFβ receptor I inhibition on EMT-derived myofibroblast transdifferentiation of IB3 cells

The importance of TGFβ1 signalling in CF airway epithelial cells, has been demonstrated in Figure 4.9. Inhibition of the ALK5 receptor significantly reduced TG2 protein levels in IB3 whole cell lysates, with a further decrease measured in response to VX-809 and ALK5 inhibitor combined. These findings correspond to the effect seen with R281 treatment (Figure 4.7), indicating a mechanistic link between extracellular TG2 activity and TGFβ1 signal transduction. Inhibition of extracellular TG2 has also been shown to reduce the expression of fibronectin, N-cadherin and α-SMA (Figure 4.8). Thus, IB3 cells were again treated with ALK5 inhibitor alone or in combination with VX-809, to determine whether a similar downregulation of pro-fibrotic markers would be observed.

IB3 cells were treated with ALK5 inhibitor (10 µM), TGFβ1 (1 ng/ml), or ALK5 inhibitor (10 µM) combined with either VX-809 (2.5 µM) or TGFβ1 (1 ng/ml). Following treatment for 72 h, whole cell lysates were collected and samples analysed using western blot analysis. As shown in Figure 4.10, treatment with TGFβ1 induced a significant >1.5-fold increase in protein expression for all three proteins, in comparison to untreated IB3 cells. Alternatively, TGFβ1 treatment in the presence of ALK5 inhibitor was found to reduce the levels of all three proteins, compared to untreated IB3 cells. Both ALK5 inhibitor alone and ALK5 inhibitor with VX-809 significantly decreased the expression of all three pro-fibrotic markers by ≥31% and ≥50% respectively, in comparison to untreated IB3 cells.

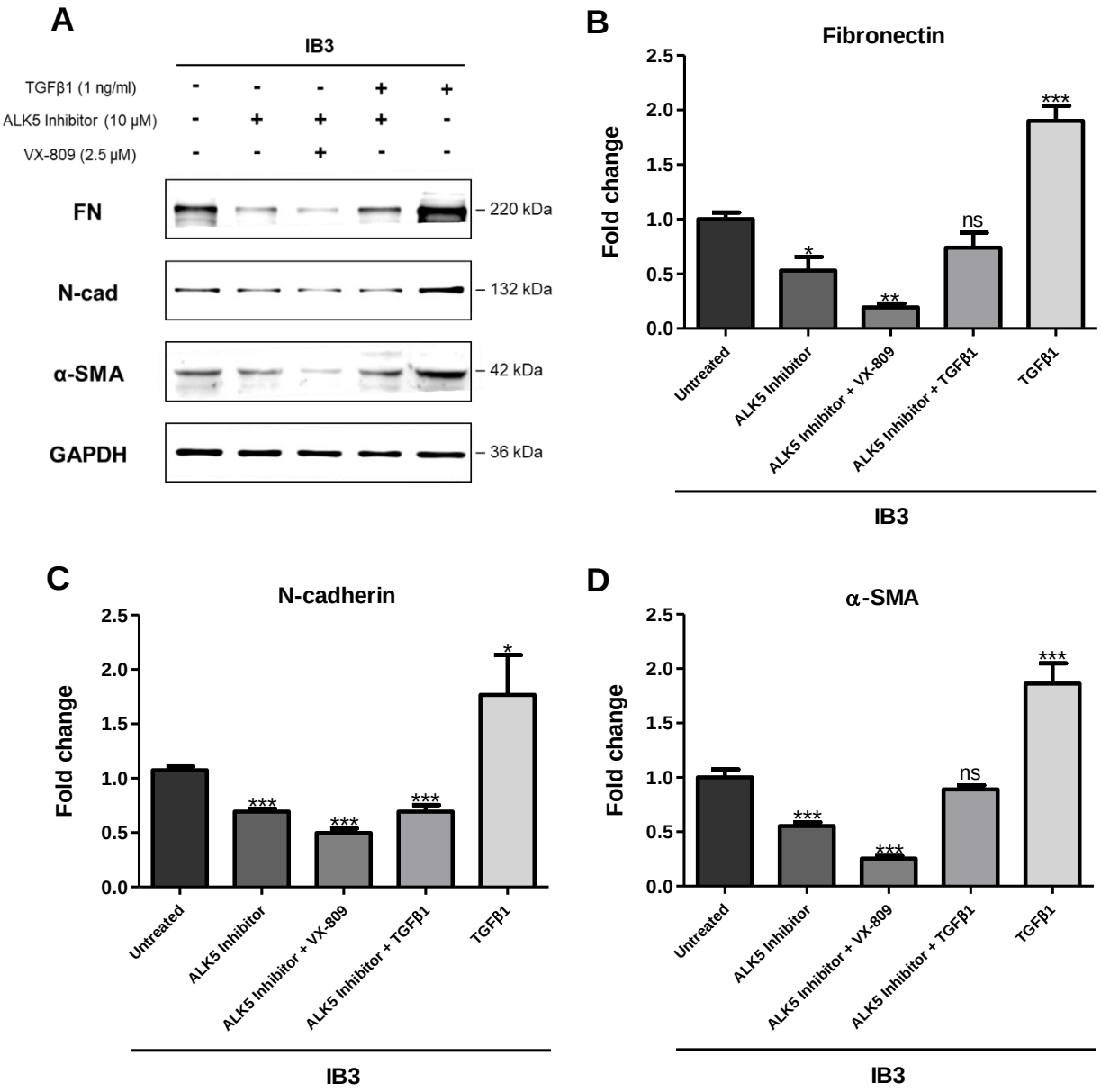

Figure 4.10. The effect of ALK5 inhibitor treatment alone or in combination with VX-809 on fibronectin, N-cadherin and α-SMA protein expression in IB3 cells. IB3 cells were treated with TGFβ (1 ng/ml) or an ALK5 inhibitor (10 μM) either alone or in combination with VX-809 (2.5 μM) or TGFβ (1 ng/ml) for a period of 72 h, with treatments changed every 24 h. Whole cell lysates were collected and proteins separated using SDS-PAGE. Following protein transfer, western blot analysis was performed for detection of fibronectin, N-cadherin and α-SMA. Membranes were stripped and reprobed for the loading control GAPDH. **(A)** Representative western blots of fibronectin, N-cadherin and α-SMA protein expression. Densitometry of **(B)** fibronectin **(C)** N-cadherin and **(D)** α-SMA protein levels, measured using ImageJ software. Data normalised to GAPDH and expressed as the mean fold change ± SEM in comparison to untreated IB3 cells. Statistical analysis of three independent experiments (N=3) using a one-way ANOVA, with a post-hoc Bonferroni multiple comparison test; ns, not significant, **P*<0.05, ***P*<0.01, ****P*<0.001.

4.3.11 The impact of combination treatment on reducing activation of the canonical TGFβ signalling pathway in IB3 cells

TGFβ1 activation of the cell surface ALK5 receptor, leads to the propagation of intracellular signalling via two separate routes: the Smad dependent canonical pathway or the Smad independent non-canonical pathways (Akhurst and Hata, 2012). Previous research has suggested the possible involvement of the Smad 2/3 signalling pathway in IB3 cell fibrosis (Nyabam et al., 2016). As such, the canonical TGFβ1 signalling pathway was investigated. Activation of the canonical Smad2/3 pathway was assessed by measuring levels of phosphorylated Smad3 (p-Smad3), a requisite of Smad dependent signal transduction. Total Smad3 (t-Smad3) was measured to ensure normalisation of p-Smad3 levels. IB3 cells were treated with VX-809 and 1-155 either alone or in combination, to determine their effect upon canonical TGFβ1 signal transduction in CF.

IB3 cells were treated with either VX-809 (2.5 µM), 1-155 (2.5 µM) or VX-809 (2.5 µM) and 1-155 (2.5 µM) for 72 h, before whole cell lysates were collected and samples analysed using western blot analysis. This data shows that p-Smad3 levels are inherently lower in C38 cells ($p<0.001$), compared to IB3 cells (Figure 4.11). Treatment with either VX-809 or 1-155 alone significantly decreased levels of p-Smad3 by 39% ($p<0.05$) and 61% ($p<0.001$) respectively, in comparison to untreated IB3 cells. Further to this, treatment with VX-809 and 1-155 in combination reduced p-Smad3 levels by 73% ($p<0.001$), which was found to be roughly equivalent to the expression of p-Smad3 measured in C38 whole cell lysates.

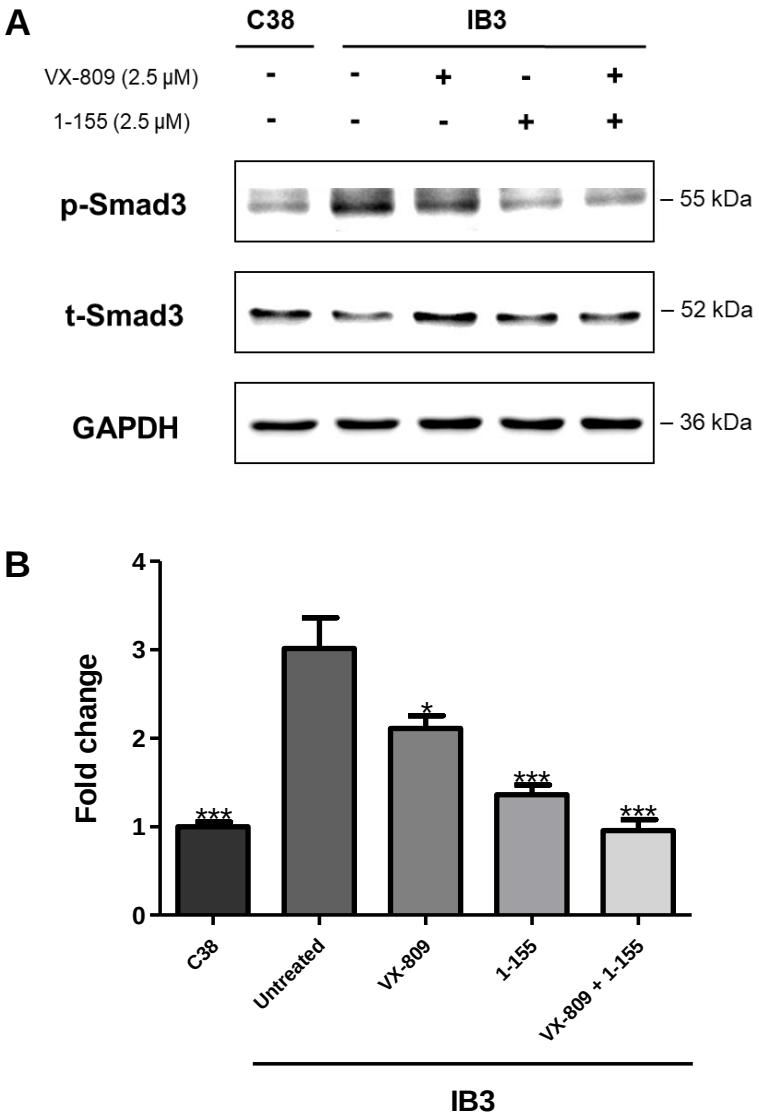

Figure 4.11. The relative levels of phosphorylated Smad3 in IB3 cells following treatment with VX-809 and 1-155 alone or in combination. IB3 cells were treated with VX-809 (2.5 µM), 1-155 (2.5 µM) or VX-809 (2.5 µM) and 1-155 (2.5 µM) for 72 h, with treatments changed every 24 h. C38 cells were used as a CFTR corrected control. Whole cell lysates were collected and proteins separated using SDS-PAGE. Following protein transfer, western blot analysis was performed for detection of p-Smad3 and t-Smad3. Membranes were stripped and reprobed for the loading control GAPDH. **(A)** Representative western blot of p-Smad3 and t-Smad3 protein expression. **(B)** Densitometry of p-Smad3 protein levels, measured using ImageJ software. Data normalised to t-Smad3 and GAPDH, then expressed as the mean fold change ± SEM in comparison to untreated IB3 cells. Statistical analysis of three independent experiments (N=3) using a one-way ANOVA, with a post-hoc Tukey test; **P*<0.05, ****P*<0.001.

4.3.12 Influence of the non-canonical extracellular signal-regulated kinase (ERK) signalling pathway on TG2 and fibronectin protein expression in IB3 cells

As shown in Figure 4.11, IB3 cells exhibit increased activation of the TGFβ1 Smad dependent canonical pathway. However, growing evidence now implicates several of the Smad independent non-canonical pathways in the pathogenesis of fibrosis (Finnson et al., 2020). In particular, the ERK signalling pathway has been found to be activated in a variety of fibrotic conditions including: kidney (Cheng et al., 2013), liver (Foglia et al., 2019), cardiac (De Boer et al., 2004) and pulmonary (Madala et al., 2012) fibrosis. Nonetheless, the ERK signalling pathway is yet to be investigated with regard to fibrotic development in CF. As a result, the protein expression of TG2 and fibronectin was measured in IB3 cells, in response to ERK inhibitor treatment.

IB3 cells were treated with ERK inhibitor (10 µM), TGFβ1 (1 ng/ml) or ERK inhibitor (10 µM) combined with either VX-809 (2.5 µM) or TGFβ1 (1 ng/ml). Following treatment for 72 h, whole cell lysates were collected and samples analysed using western blot analysis. Treatment with ERK inhibitor alone did not significantly affect TG2 and fibronectin protein levels (Figure 4.12). Conversely, the use of VX-809 and ERK inhibitor in combination ($p<0.05$) led to a significant reduction in the expression of TG2 (42%) and fibronectin (54%), in comparison to untreated IB3 cells. Interestingly, ERK inhibition did not prevent TGFβ1 induced increases of TG2 (>1.5-fold) and fibronectin (>3-fold) protein levels.

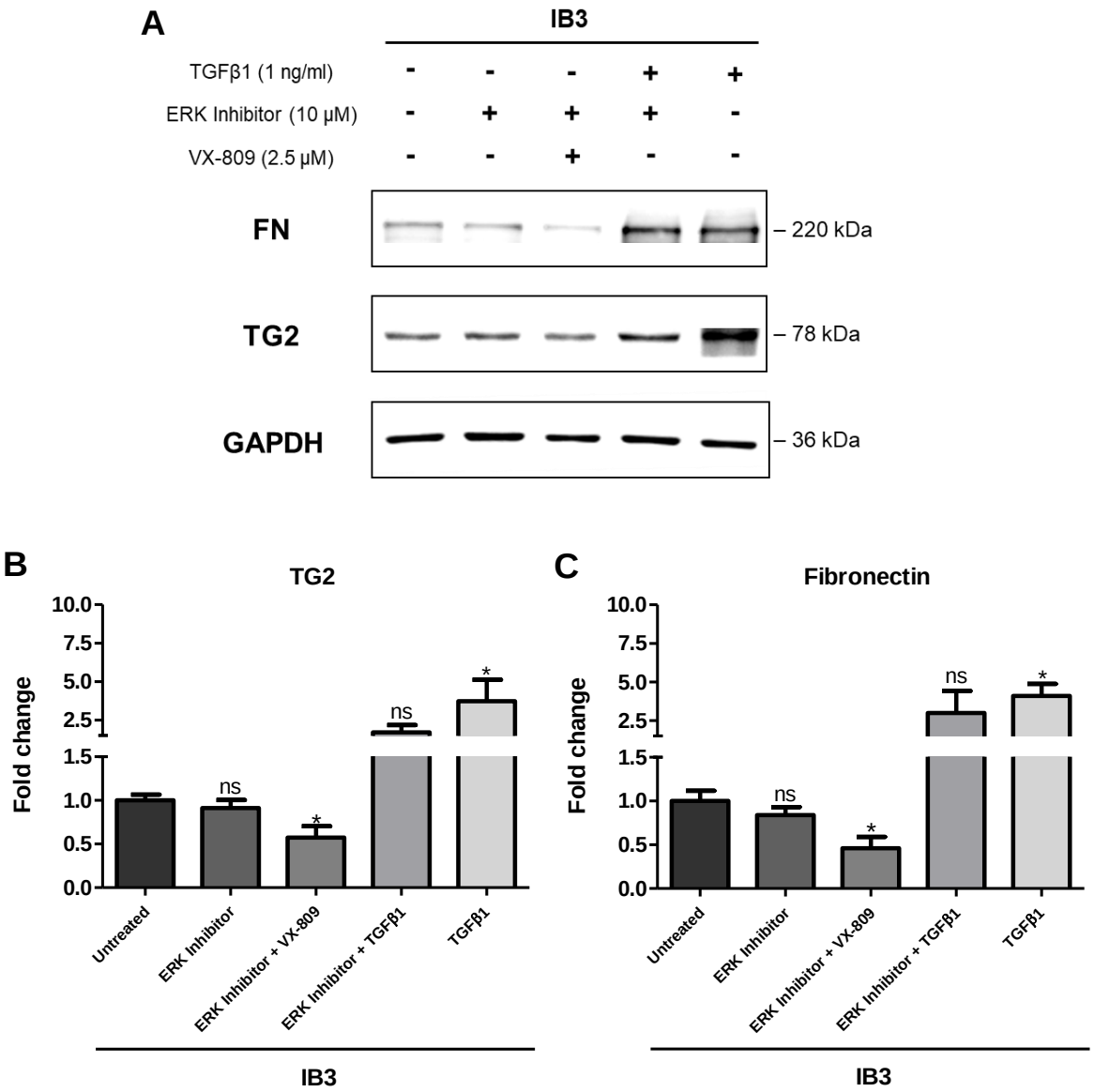

Figure 4.12. The effect of ERK inhibitor treatment alone or in combination with VX-809 on TG2 and fibronectin protein expression in IB3 cells. IB3 cells were treated with TGFβ (1 ng/ml) or an ERK inhibitor (10 μM) either alone or in combination with VX-809 (2.5 μM) or TGFβ (1 ng/ml) for 72 h, with treatments changed every 24 h. Whole cell lysates were collected and proteins separated using SDS-PAGE. Following protein transfer, western blot analysis was performed for detection of TG2 and fibronectin. Membranes were stripped and reprobed for the loading control GAPDH. **(A)** Representative western blots of TG2 and fibronectin protein expression. Densitometry of **(B)** TG2 and **(C)** fibronectin protein levels, measured using ImageJ software. Data normalised to GAPDH and expressed as the mean fold change ± SEM, in comparison to untreated IB3 cells. Statistical analysis of three independent experiments (N=3) using a one-way ANOVA, with a post-hoc Bonferroni multiple comparison test; ns, not significant, **P*<0.05.

4.3.13 The combined effect of a CFTR corrector and TG2 inhibitor on restoring the presence of tight junction protein Zonula occludens-1 (ZO-1) in IB3 cells

Previous research in the literature has focused on the upregulation of mesenchymal markers in CF airway epithelia cells (Nyabam et al., 2016). Data from this study has revealed this to be a consequence of cells undergoing EMT-derived myofibroblast transdifferentiation (Figure 3.2). Combination treatment has been shown to reverse increases in the protein expression of fibronectin, N-cadherin and α-SMA, in IB3 whole cell lysates (Figures 4.5 and 4.8). However, a critical aspect of EMT is the loss of cell polarity and disassembly of cell adhesion systems, allowing epithelial cells to transition towards a more motile mesenchymal phenotype (Willis et al., 2006). As such, it is crucial to assess indicators of epithelial cell phenotype, to fully validate the extent of EMT reversal following treatment. The tight junction protein ZO-1 was selected as an appropriate marker, due to its native expression in normal epithelial cells (Stevenson et al., 1986) and recognised downregulation in CF epithelial cells (Castellani et al., 2012; Carbone et al., 2014; Ruan et al., 2014).

IB3 cells were treated with either VX-809 (2.5 µM), 1-155 (2.5 µM) or VX-809 (2.5 µM) and 1-155 (2.5 µM) in combination. Following treatment for 72 h, whole cell lysates were collected and ZO-1 protein expression was measured via western blot analysis. C38 cells were used to determine normal protein levels of ZO-1. As illustrated in Figure 4.13, the protein expression of ZO-1 increased across all treatment conditions, in comparison to untreated IB3 cells. Notably, treatment with VX-809 and 1-155 in combination significantly increased ZO-1 protein levels by ~3-fold ($p<0.001$), compared to untreated IB3 cells. This was seen to be largely comparable to the ~3.5-fold ($p<0.001$) change in ZO-1 protein expression, observed between untreated C38 and IB3 cells.

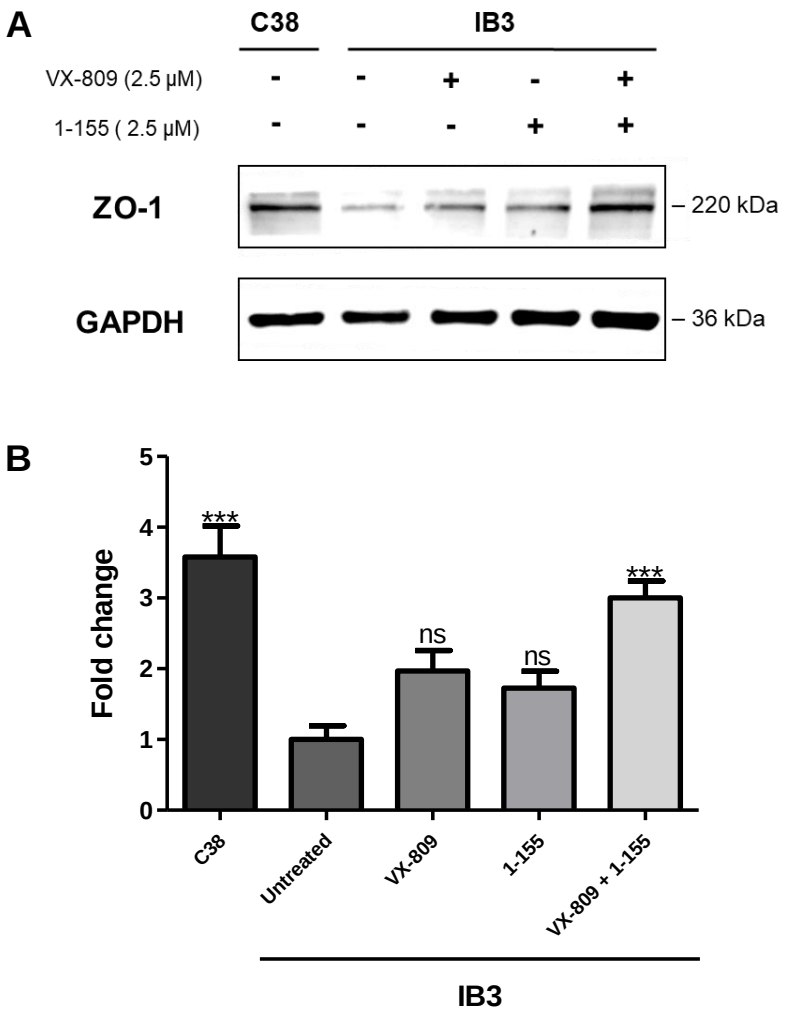

Figure 4.13. Measurement of ZO-1 protein expression in IB3 cells following treatment with VX-809 and 1-155 alone or in combination. IB3 cells were treated with VX-809 (2.5 µM), 1-155 (2.5 µM) or VX-809 (2.5 µM) and 1-155 (2.5 µM) for 72 h, with treatments changed every 24 h. C38 cells were used as a CFTR corrected control. Whole cell lysates were collected and proteins separated using SDS-PAGE. Following protein transfer, western blot analysis was performed for detection of ZO-1. Membranes were stripped and reprobed for the loading control GAPDH. **(A)** Representative western blot of ZO-1 protein expression. **(B)** Densitometry of ZO-1 protein levels, measured using ImageJ software. Data normalised to GAPDH and expressed as the mean fold change ± SEM in comparison to untreated IB3 cells. Statistical analysis of three independent experiments (N=3) using a one-way ANOVA, with a post-hoc Tukey test; ns, not significant, ***P<0.001.

4.3.14 The effect of TGFβ receptor I inhibition on restoring the presence of tight junction protein ZO-1 in IB3 cells

Inhibition of ALK5 reduces the protein expression of TG2 and pro-fibrotic markers in IB3 whole cell lysates (Figures 4.9 and 4.10), in the same manner as treatment with TG2 inhibitors 1-155 (Figures 4.4 and 4.5) and R281 (Figures 4.7 and 4.8). Further to this, ZO-1 protein expression was found to be largely restored in IB3 whole cell lysates, following combination treatment with VX-809 and 1-155 (Figure 4.13). Consequently, IB3 cells were treated with ALK5 inhibitor either alone or in combination with VX-809, to determine whether a similar restoration of ZO-1 protein expression would be observed.

IB3 cells were treated with ALK5 inhibitor (10 μM), TGFβ1 (1 ng/ml) or ALK5 inhibitor (10 μM) combined with either VX-809 (2.5 μM) or TGFβ1 (1 ng/ml). Following treatment for 72 h, whole cell lysates were collected and ZO-1 protein expression was measured via western blot analysis. As shown in Figure 4.14, treatment with ALK5 inhibitor alone and in the presence of TGFβ1 increased ZO-1 protein levels by ~3-fold compared to untreated IB3 cells, although changes did not reach statistical significance. Moreover, combination treatment with VX-809 and ALK5 inhibitor significantly increased ZO-1 protein levels by >5-fold ($p<0.05$), in comparison to untreated IB3 cells. TGFβ1 did not have a significant effect on ZO-1 protein expression, compared to untreated IB3 cells.

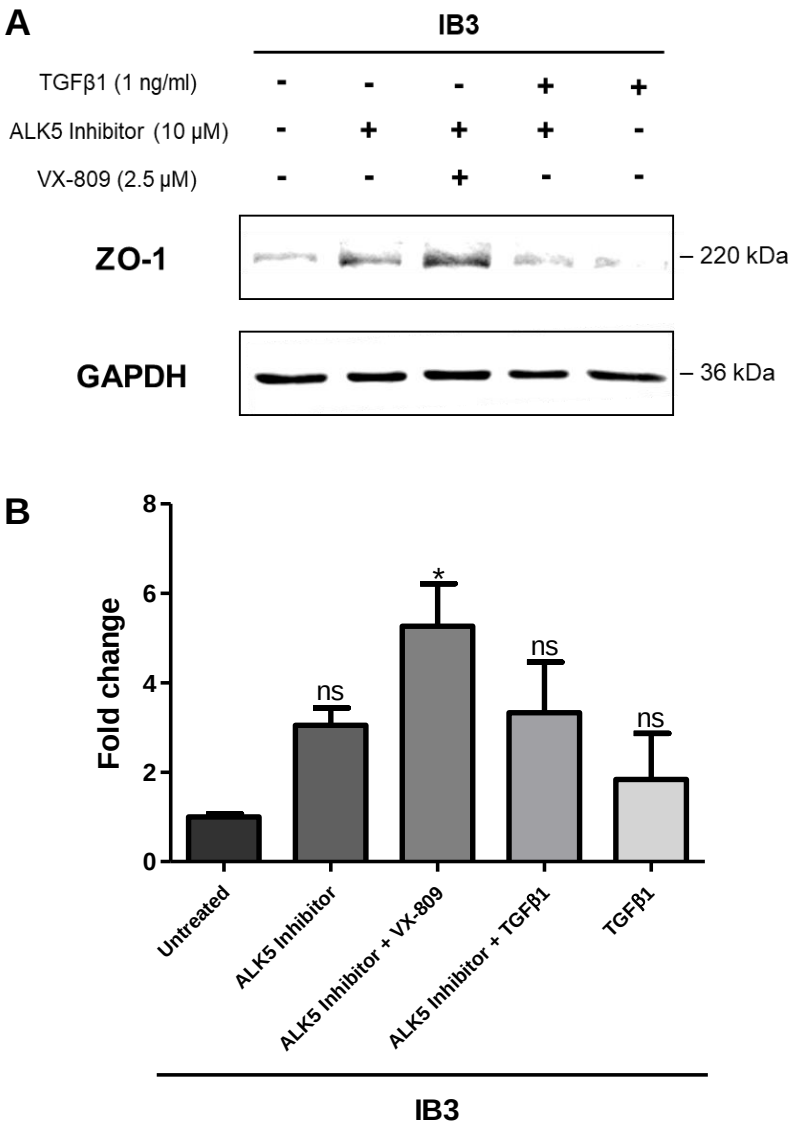

Figure 4.14. The effect of ALK5 inhibitor treatment alone or in combination with VX-809 on ZO-1 protein expression in IB3 cells. IB3 cells were treated with TGFβ (1 ng/ml) or an ALK5 inhibitor (10 μM) either alone or in combination with VX-809 (2.5 μM) or TGFβ (1 ng/ml) for a period of 72 h, with treatments changed every 24 h. Whole cell lysates were collected and proteins separated using SDS-PAGE. Following protein transfer, western blot analysis was performed for detection of ZO-1. Membranes were stripped and reprobed for the loading control GAPDH. **(A)** Representative western blot of ZO-1 protein expression. **(B)** Densitometry of ZO-1 protein levels, measured using ImageJ software. Data normalised to GAPDH and expressed as the mean fold change ± SEM in comparison to untreated IB3 cells. Statistical analysis of three independent experiments (N=3) using a one-way ANOVA, with a post-hoc Tukey test; ns, not significant, **P*<0.05.

4.3.15 Evaluating the integrity of tight junctions in IB3 cells following treatment with a CFTR corrector and TG2 inhibitor in combination

As shown in Figure 4.13, expression of the epithelial tight junction protein ZO-1 is found to be diminished in IB3 cells, compared to CFTR corrected C38 cells. However, protein levels of ZO-1 can be largely restored via combination treatment with VX-809 and 1-155. This data suggests that the development of EMT in CF airway epithelial cells can be therapeutically reversed. Nevertheless, further research was needed for confirmation of EMT reversal, specifically an investigation into the effect of treatment in a physiological context. As such, IB3 cells were grown at ALI and treated with VX-809 and 1-155 alone or in combination. The ohmic resistance of each cell monolayer was then measured, as a direct assessment of tight junction integrity.

IB3 cells were cultured at ALI for 14 days and treated with either VX-809 (2.5 µM), 1-155 (2.5 µM) or VX-809 (2.5 µM) and 1-155 (2.5 µM) in combination, with treatments changed every 24 h prior to ALI and every 48 h thereafter. TEER values were measured using an epithelial voltohmmeter, with readings taken at stated time points between 0 - 14 days post ALI. At day 14, a significant increase in TEER values was observed for C38 cells ($p<0.05$) and IB3 cells treated with either 1-155 ($p<0.05$) or VX-809 and 1-155 ($p<0.01$), in comparison to untreated IB3 cells (Figure 4.15). Furthermore, the TEER values for C38 (145.31 $\Omega.cm^2$) and IB3 cells treated with VX-809 and 1-155 (148.50 $\Omega.cm^2$) reached comparable levels, at 14 days ALI.

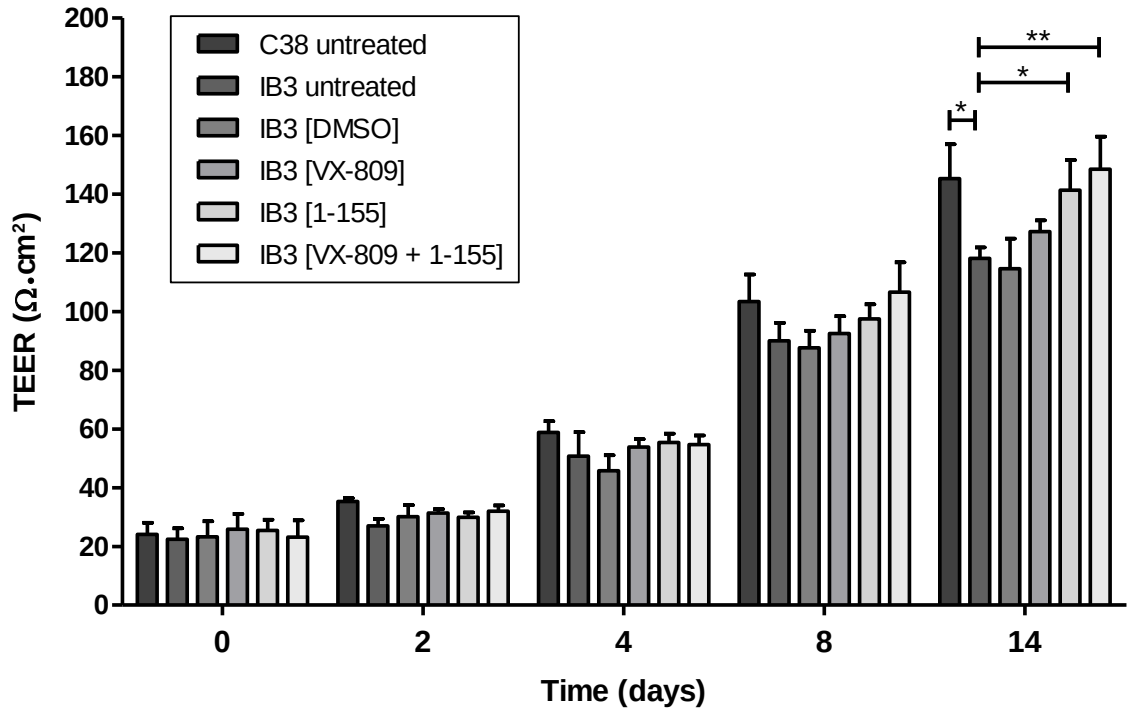

Figure 4.15. TEER measurements of IB3 cells following treatment with VX-809 and 1-155 alone or in combination. C38 and IB3 cells were cultured in Transwell® inserts for 14 days at ALI. C38 cells were used as a CFTR corrected control. IB3 cells were treated with VX-809 (2.5 µM), 1-155 (2.5 µM) or VX-809 (2.5 µM) and 1-155 (2.5 µM), with treatments changed every 24 h prior to ALI and every 48 h thereafter. DMSO was used as a vehicle control. The electrical resistance (Ω) of each Transwell® was measured using an epithelial voltohmmeter and recorded at time points of 0, 2, 4, 8 and 14 days post ALI. Measurements were taken in triplicate and the electrical resistance of a collagen coated Transwell® in the absence of cells, subtracted from experimental groups. Final TEER values presented as Ω.cm^2. Data expressed as the mean ± SEM of three independent experiments (N=3). Statistical analysis performed using a two-way ANOVA, with a post-hoc Bonferroni multiple comparison test; *P<0.05, **P<0.01.

4.3.16 Assessing the barrier function of IB3 cells in response to treatment with a CFTR corrector and TG2 inhibitor in combination

TEER values measured in Figure 4.15, indicate that the physical integrity of tight junctions is compromised in CF airway epithelial cells, which can be rescued via combination treatment with VX-809 and 1-155. However, TEER only reflects the ionic conductance of the paracellular pathway and does not assess the actual barrier function of an epithelial cell monolayer. Therefore, enzymatic markers such as HRP can be used, to study the physical diffusion of macromolecules across the paracellular pathway. As such, IB3 cells were treated with VX-809 and 1-155 alone or in combination and HRP diffusion used as a measure of paracellular permeability.

IB3 cells were cultured at ALI for 14 days and treated with either VX-809 (2.5 µM), 1-155 (2.5 µM) or VX-809 (2.5 µM) and 1-155 (2.5 µM) in combination, with treatments changed every 24 h prior to ALI and every 48 h thereafter. After this time, HRP (~44 kDa) was added to each Transwell® and the paracellular diffusion of HRP from the apical surface to the basal compartment was measured. These data show a decrease in the paracellular flux of HRP across all treatment conditions (Figure 4.16). Notably, IB3 cells treated with either 1-155 alone or VX-809 and 1-155 significantly reduced HRP paracellular flux by 38% ($p<0.05$) and 49% ($p<0.01$) respectively, in comparison to untreated IB3 cells. Interestingly, decreases in HRP paracellular flux for combination treatment (49%) and C38 cells (52%), closely matched.

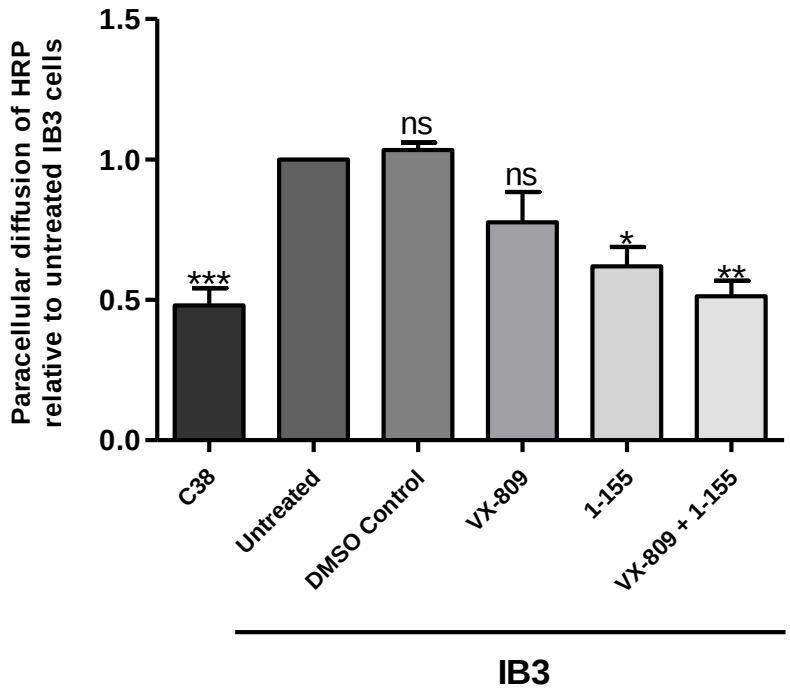

Figure 4.16. The paracellular permeability of IB3 cells grown at ALI following treatment with VX-809 and 1-155 alone or in combination. Cells were cultured in Transwell® inserts for 14 days at ALI. C38 cells were used as a CFTR corrected control. IB3 cells were treated with VX-809 (2.5 µM), 1-155 (2.5 µM) or VX-809 (2.5 µM) and 1-155 (2.5 µM), with treatments changed every 24 h prior to ALI and every 48 h thereafter. DMSO was used as a vehicle control. HRP (0.5 µM) was added apically to each Transwell®. Paracellular diffusion of HRP was measured after 5 min via detection of peroxidase activity, using an OPD substrate solution. Absorbance was read at a wavelength of 490 nm. Measurements of HRP paracellular diffusion were taken in triplicate for each sample. Data expressed as the mean ± SEM of three independent experiments (N=3), in comparison to untreated IB3 cells. Statistical analysis performed using a one-way ANOVA, with a post-hoc Tukey test; ns, not significant, **P*<0.05, ***P*<0.01, ****P*<0.001.

4.3.17 Evaluating the cell migration levels of IB3 cells in response to treatment with a CFTR corrector and TG2 inhibitor in combination

Data shown throughout this study has illustrated that CF airway epithelia cells lose their inherently structured phenotype and subsequently acquire mesenchymal characteristics. This results in the conversion of adherent epithelial cells into myofibroblasts, via the process of EMT (Figures 3.2). Fundamentally, EMT confers a migratory capacity to epithelial derived myofibroblasts, which require motility to move to the site of injury (Stone et al., 2016). Combination treatment with VX-809 and 1-155 has been shown to consistently reverse the development of EMT in IB3 cells, measured through changes in protein expression (Figures 4.5 and 4.13), TEER (Figure 4.15) and paracellular permeability (Figure 4.16). However, as increased cell motility is a central outcome of EMT and a major feature of myofibroblasts, it was essential to confirm the effect of treatment on IB3 cell migration levels.

An *in vitro* scratch assay was performed to quantify cell migration levels over 16 h. A 16 h time course was set as the limit, due to non-proliferative rates of C38 and IB3 cells measured to be within 16 h (Nyabam, 2015). Immediately after wounding, IB3 cells were treated with either VX-809 (2.5 µM), 1-155 (2.5 µM) or VX-809 (2.5 µM) and 1-155 (2.5 µM) in combination. As shown in Figure 4.17, all treatment conditions significantly decreased percentage wound closure compared to untreated IB3 cells, at 4 h and 16 h time points. Moreover, treatment of IB3 cells with VX-809 and 1-155 ($p<0.001$) significantly reduced percentage wound closure at 4 h post-wounding, compared to the use of either VX-809 or 1-155 alone. However, the same effect was not found to be statistically significant at 16 h. Interestingly, the percentage wound closure for C38 cells and IB3 cells treated with VX-809 and 1-155 was seen to be largely equivalent (4 h and 16h).

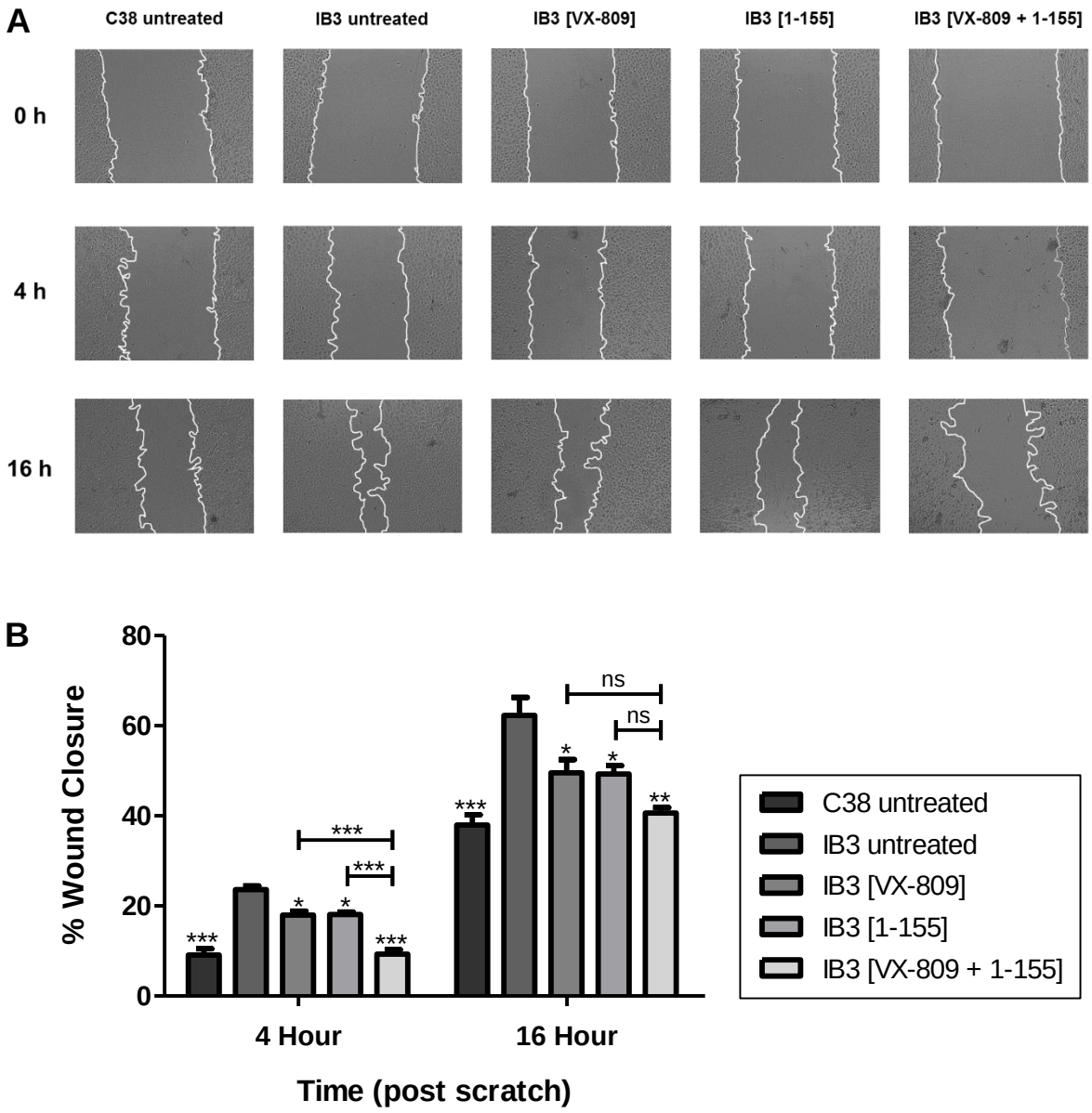

Figure 4.17. Measurement of percentage wound closure for IB3 cells following treatment with VX-809 and 1-155 alone or in combination. Cells were seeded in a 24 well plate and grown until confluent, before a scratch was made in each cell monolayer. IB3 cells were treated with VX-809 (2.5 µM), 1-155 (2.5 µM) or VX-809 (2.5 µM) and 1-155 (2.5 µM) post-wounding. C38 cells were used as a CFTR corrected control. Images were acquired in triplicate at 0, 4 and 16 h post-wounding. **(A)** Representative images of each scratch, captured at the specified time points. Images were analysed using ImageJ software and **(B)** cell migration calculated as the percentage wound closure, relative to the original area of the wound at 0 h. Data expressed as the mean ± SEM of three independent experiments (N=3), in comparison to untreated IB3 cells. Statistical analysis performed using a one-way ANOVA, with a post-hoc Tukey test; ns, not significant, **P*<0.05, ***P*<0.01, ****P*<0.001.

4.4 Discussion

Current treatment strategies for CF have become largely centred around the development of CFTR-directed drugs. However, it is now recognised that a defect in the CFTR protein has broader implications, than the mere absence of its chloride transport. Emerging evidence suggests that the proteostasis network within CF airway epithelial cells is severely perturbed (Maiuri et al., 2008; Luciani et al., 2009, 2010; Nyabam et al., 2016). In chapter 3, it was confirmed that the overexpression of TG2 is strongly associated with these pathogenic changes. Indeed, the inhibition of TG2 activity in CF primary HBECs, greatly decreased TG2 protein levels and partially restored tight junction integrity. Moreover, when used in combination with a CFTR corrector (VX-809), the TG2 inhibitor (1-155) was found to have a roughly additive therapeutic effect. Although these results are promising, the experiments have limited scope and serve mainly as a proof of concept. As such, this chapter focuses on a more in-depth investigation of two-directional pharmacotherapy and its effect on CF airway epithelia, through use of the established IB3 cell line.

The notion of inhibiting TG2 activity as a therapeutic strategy for CF, has previously been explored using the compound cysteamine (Tosco et al., 2016). However, cysteamine is a non-robust pan transglutaminase inhibitor, which is known to have multiple off-target interactions, besides its inhibition of transglutaminases (Bodas and Vij, 2017; Paul and Snyder, 2019). Conflicting data in the literature now questions whether cysteamine in fact elicits any response in CF airway epithelial cells (Awatade et al., 2019). Alternatively, this study uses a potent and selective inhibitor of TG2, known as 1-155. Furthermore, both cell-permeable (1-155) and cell-impermeable (R281) compounds were used, so as to investigate the effect of inhibiting total TG2 activity and extracellular TG2 activity, respectively. Initially, the relative IC_{50} of both TG2 inhibitors was measured using a transglutaminase activity assay. This was undertaken to validate the efficacy of 1-155 and R281, before their use in further experiments. It was found that 1-155 had a relative IC_{50} value of 18.47 nM and R281 a relative IC_{50} value of 39.14 µM. These IC_{50} values are largely

comparable to measurements reported in the literature, which have been stated at ~6 nM and ~10 µM for 1-155 and R281, respectively (Griffin et al., 2008; Badarau et al., 2015). By contrast, cysteamine has previously been determined to have an IC_{50} value of ~178–232 µM (Jeon et al., 2004), thus highlighting differences in the potency of these compounds in terms of TG2 inhibition.

Although a substantial body of research has been produced assessing the efficacy of CFTR correctors, their capacity to reinstate the proteostasis network in CF airway epithelial cells, is yet to be investigated. Thus, IB3 cells were treated with VX-809 and its effect on TG2 / fibronectin protein expression was measured. Following an extensive review of the literature, VX-809 was deemed to be used at concentrations between 1–5 µM for cell based studies (Awatade et al., 2015; Pranke et al., 2017; Garbuzenko et al., 2019). Accordingly, three concentrations of VX-809 (1, 2.5 and 5 µM) were tested within this range. Interestingly, CFTR correction was found to impact the proteostasis network of IB3 cells. All three concentrations of VX-809 were shown to decrease TG2 and fibronectin protein levels, albeit without reaching statistical significance. This implies that CFTR correction may only partially restore the proteostasis network in CF airway epithelia, which questions the therapeutic strategy of correcting CFTR alone. With VX-809 (2.5 µM) proving the most effective, this concentration was used for all subsequent experiments.

Considering the involvement of TG2 in cellular processes, it is not known whether TG2 inhibition can negatively impact the cell viability of airway epithelia. Data from the current literature has shown that 1-155 is non-toxic up to at least 100 µM in HUVECS, over a period of 72 h (Badarau et al., 2015). Furthermore, no obvious signs of toxicity were observed in mice following treatment with 1-155 over 14 days (Badarau et al., 2015). However, the use of 1-155 in combination with VX-809 has also never been evaluated and the presence of detrimental interactions are undetermined. It was demonstrated that the use of VX-809 and 1-155 alone or in combination, had no effect on C38 and IB3 cell viability. These findings suggest that the compounds are safe to use together at the tested working concentrations.

Yet, it must also be acknowledged that immortalised cells may not reflect the response of primary cells or mammalian systems, and thus warrants further testing.

With preliminary testing complete, an investigation of combination treatment (VX-809 and 1-155) was conducted. As demonstrated in chapter 3, IB3 cells show increased TG2 protein expression and undergo EMT-derived myofibroblast transdifferentiation. Within this chapter it was revealed that the treatment of IB3 cells with 1-155, can cause a partial reduction of TG2, fibronectin, N-cadherin and α-SMA protein levels. This suggests that TG2 inhibition can somewhat reverse the intrinsic pro-fibrotic profile of CF airway epithelia. These findings also support data from a recent study, which reported that EndMT-derived myofibroblast transdifferentiation in cardiac fibrosis can be attenuated via the application of 1-155 (Wang et al., 2018). Moreover, this is the first study to show that use of VX-809 in combination with 1-155 can have an approximately additive therapeutic effect. Mechanistically it is very unlikely that VX-809 and 1-155 act on the same target in terms of an increased dose response, as VX-809 (5 μM) was previously found to have no additional effect over VX-809 (2.5 μM). These results may instead indicate that both VX-809 and 1-155 are acting independently of one another, although it is quite possible that the two compounds have a direct / indirect effect on the same pathway.

To understand the role of extracellular TG2 in these pro-fibrotic changes, the 1-155 cell-permeable TG2 inhibitor was replaced with a cell-impermeable compound (R281). Previous research has examined this in the context of a chronic renal fibrosis rat model (Johnson et al., 2007). It was revealed that the cell-impermeable TG2 inhibitor was equally as effective in reducing fibrosis, as the cell-permeable TG2 inhibitor. Intriguingly, the same outcome was also demonstrated in this study. The treatment of IB3 cells with R281 was found to decrease TG2, fibronectin, N-cadherin and α-SMA protein levels, to the same extent as shown with 1-155. In addition, R218 was also seen to generate a roughly additive effect when used in combination with VX-809. Intracellular TG2 activity has previously been linked with pro-inflammatory changes in CF airways (Maiuri et al., 2008). However, these data

suggest that the pathogenic significance of TG2 regarding fibrotic alterations of the CF lungs, centres around its function in an extracellular capacity.

The current literature is of the consensus that TG2 mediates fibrosis through activation of TGFβ1. Research has shown that the transamidation activity of extracellular TG2 creates a large reservoir of latent TGFβ1 in the ECM, which becomes mechanically activated by a stiffened matrix (Nunes et al., 1997; Klingberg et al., 2014). Indeed, an interrelationship between TG2, TGFβ1 and EMT has previously been identified in CF (Nyabam et al., 2016). Data within this chapter confirms the importance of TGFβ1 signalling in CF airway epithelial cells, using an ALK5 (TGFβ type I receptor) inhibitor and recombinant human TGFβ1. ALK5 inhibition was shown to have much the same effect as TG2 inhibition, albeit with a stronger reduction of TG2 protein levels. By contrast, the application of recombinant human TGFβ1 acted to significantly increase TG2, fibronectin, N-cadherin and α-SMA protein expression in IB3 cells. These data indicate the potential existence of positive feedback loop between TGFβ1 and TG2, whilst also highlighting the importance of TGFβ1 as a main driver of EMT-derived myofibroblast transdifferentiation in CF airway epithelia. Interestingly, a therapeutic limit was not reached with the inhibition of ALK5, as its use in combination with VX-809 had an additional effect. This suggests that the inherent pro-fibrotic phenotype of CF airway epithelia, cannot be fully alleviated via inhibition of TGFβ signalling alone.

TGFβ signalling has now been shown to operate through the canonical Smad2/3 dependent pathway in various fibrotic lung diseases including: asthma (Wnuk et al., 2020), IPF (Kolosova et al., 2011) and COPD (Mahmood et al., 2017). Data within this chapter supports these findings, suggesting that this also occurs in CF (Nyabam et al., 2016). It was demonstrated that IB3 cells have enhanced levels of p-Smad3, in comparison to C38 cells. Moreover, the relationship between TG2 and TGFβ was further confirmed, as treatment with 1-155 led to reduced levels of p-Smad3. Intriguingly, the use of VX-809 also decreased p-Smad3 levels, indicating that CFTR correction can somehow influence TGFβ signal transduction in CF airway epithelial cells.

Emerging evidence now suggests that non-canonical TGFβ pathways may also be involved in the pathogenesis of fibrosis, specifically ERK signalling (Finnson et al., 2020). For example, the aberrant activation of both ERK and Smad signalling pathways have been found to be implicated in kidney fibrosis (Cheng et al., 2013). Thus, ERK signalling was investigated in IB3 cells using an ERK inhibitor. It was demonstrated that ERK inhibition did not significantly affect TG2 and fibronectin protein expression. This was expected as TGFβ signal transduction can still propagate via alternative pathways, despite the inhibition of ERK. Yet, when used in combination with VX-809, both TG2 and fibronectin protein levels were significantly decreased. This is important, as the use of VX-809 alone was previously determined to lack the capacity to induce significant decreases in TG2 and fibronectin. As such, these data highlight the effect of ERK inhibition and elucidates a role for ERK signalling in fibrotic processes of CF. This is the first study to propose that TGFβ signal transduction operates via both canonical and non-canonical pathways in CF bronchial epithelial cells. However, the notion that ERK signal transduction may also or independently occur via direct growth factor binding to receptor tyrosine kinases, cannot be ruled out. Thus, the mechanism of ERK activation in CF warrants further investigation, alongside research into the involvement of other non-canonical pathways.

Finally, the capability of combination treatment (VX-809 and 1-155) to restore an epithelial phenotype to CF airway epithelial cells was examined. Notably, only the combined use of 1-155 or ALK5 inhibitor with VX-809, could significantly rescue ZO-1 protein expression. It has previously been discerned that CFTR interacts with ZO-1 to regulate tight junction assembly (Ruan et al., 2014) and this could explain why CFTR correction is vital to the restoration of ZO-1. Moreover, the treatment of IB3 cells with VX-809 and 1-155 was shown to ameliorate functional indicators of EMT (TEER, paracellular permeability and cell migration), reaching comparable levels as were measured for C38 cells. This indicates that combination treatment acts to reverse EMT and ultimately recover the structured barrier function of CF airway epithelium. Taken together, these findings demonstrate that the

combined use of a CFTR corrector with a TG2 inhibitor, may provide an effective treatment for individuals with CF.

In conclusion, these data reinforce the results obtained in the proof of concept experiments with CF primary HBECs. It was demonstrated that a TG2–TGFβ1 axis exists in CF bronchial epithelial cells, with signal transduction occurring via canonical and potentially non-canonical pathways. Treatment of IB3 cells with VX-809 and 1-155 was shown to diminish TG2 overexpression and fully reverse EMT-derived myofibroblast transdifferentiation. In addition, combination treatment acted to restore the native phenotypic characteristics of CF airway epithelial cells, including: tight junction integrity, barrier function and low cell motility. Strikingly, it was found that the pathogenic significance of TG2 in fibrotic processes of CF airway epithelial cells, relates to its activity within the extracellular environment. In the next chapter, the mechanism facilitating TG2 externalisation to the ECM will be investigated.

Chapter 5

A study of the TG2 secretory pathway in CF

CHAPTER 5: RESULTS

5.1 Introduction

The importance of extracellular TG2 activity in fibrosis is now well-established. Indeed, the increased cellular export of TG2 has been linked to fibrotic conditions of the lungs (Olsen et al., 2011), kidneys (Burhan et al., 2016), liver (Tatsukawa et al., 2017) and heart (Wang et al., 2018). However, unlike most externalised proteins, TG2 lacks a signal peptide and is therefore not exported via the classical secretory pathway (Chou et al., 2011). As a result, TG2 must be trafficked to the cell surface via an unconventional secretory pathway. Over the past decade, there has been an extensive research effort to try and uncover the mechanism responsible.

In the search for ligands that could influence TG2 export, a prominent role for syndecan-4 was identified. It had previously been shown that TG2 could bind directly to syndecan-4 via its HS chains (Telci et al., 2008). Subsequent research by Scarpellini et al. (2009) revealed that syndecan-4-null fibroblasts lacked the capacity to externalise TG2, resulting in its intracellular retention. It was later discerned that TG2 only had a high binding affinity for heparin/HS, when in its closed conformation (Lortat-Jacob et al., 2012; Wang et al., 2012). Significantly, these studies had indicated that the externalisation of TG2 was dependent on its interaction with syndecan-4, whilst in a closed configuration. Nevertheless, the actual mechanism of TG2 secretion, still remained elusive.

Initially, a hypothesis centred around non-vesicular transport was proposed, which predicted the direct translocation of TG2 through the plasma membrane (Verderio et al., 2009). However, this theory has since been largely dismissed and replaced by one involving a vesicular-related mechanism. In fact, a breakthrough came in 2011, when TG2 was found to be incorporated in cancer cell-derived EVs (Antonyak et al., 2011) and its cellular secretion associated with the endosomal system (Santhanam et al., 2011). Thereafter, the presence of TG2 was detected in EVs derived from other cell types (Van Den Akker et al.,

2012; Piacentini et al., 2014). Despite these advances, the findings were largely observational and the mechanistic details remained relatively undefined.

Thus, research by Diaz-Hidalgo et al. (2016) sought to gain further insight by focusing on a particular EV subtype, namely exosomes. It was demonstrated that TG2 plays a vital role in the biogenesis of exosomes, specifically under stressful cellular conditions. Moreover, upon induction of proteostasis impairment, TG2 was seen to be selectively recruited to exosomes and released into the extracellular environment. Crucially, these findings had shown that TG2 export was facilitated by exosomes, as a response to pathophysiological conditions. However, the contribution of larger EVs had yet to be investigated.

In an attempt to determine the importance of both exosomes and microvesicles in TG2 secretion, a global proteomic study was conducted (Furini et al., 2018). Binding partners of TG2 were identified in a kidney fibrosis animal model, which highlighted clusters of exosomal proteins and syndecan-4 in the interactome. In contrast, TG2 was seen to be only weakly expressed in microvesicles. Furthermore, knockout of syndecan-4 led to a large reduction in exosomal TG2. Overall, these data indicated a potential pathway for TG2 export in fibrosis, which involves the targeted recruitment of TG2 to exosomes via syndecan-4. Further research is now needed to understand the dynamic changes in EV populations during fibrosis and the effect of TG2 inhibition on exosome secretion.

5.2 Aims and Objectives

This chapter aims to investigate the TG2 secretory pathway in CF by:

(1) Measuring the protein expression of TG2, fibronectin and TGFβ1 in the ECM of IB3 cells, in response to the inhibition of extracellular TG2.

(2) Comparing the size distribution profiles of C38 and IB3 cell derived EV populations.

(3) Determining the involvement of EVs in the externalisation of TG2 from IB3 cells.

(4) Examining the impact of combination treatment (VX-809 and 1-155) on the dynamics of IB3 cell derived EV populations.

5.3 Results

5.3.1 The combined effect of a CFTR corrector and TG2 inhibitor on matrix deposition of TG2 and fibronectin

As demonstrated in Figures 4.4 and 4.5, combination treatment (VX-809 and 1-155) can reverse the overall expression of TG2 and fibronectin in IB3 whole cell lysates. Yet from these data alone, it remains unclear the extent to which TG2 and fibronectin are reduced in the ECM specifically. As outlined previously, it is predominantly alterations of the ECM which act as the main driver of progressive fibrosis (Benn et al., 2019). One such feature is the aberrant overexpression of extracellular TG2, which leads to increased crosslinking of ECM fibrils (Collighan and Griffin, 2009). For this reason, IB3 cells were treated with VX-809 and 1-155 alone or in combination and changes measured in the ECM exclusively.

IB3 cells were treated with either VX-809 (2.5 µM), 1-155 (2.5 µM) or VX-809 (2.5 µM) and 1-155 (2.5 µM) for 72 h, before cells were detached and the ECM collected. Samples were analysed using western blot analysis. A C38 control was used for comparison of normal ECM protein expression. These data show a decrease in matrix protein levels of TG2 and fibronectin across all treatment conditions, in comparison to untreated IB3 cells (Figure 5.1). Notably, the use of 1-155 alone significantly reduced matrix protein levels of TG2 and fibronectin by 48% ($p<0.05$) and 53% ($p<0.01$) respectively, compared to untreated IB3 cells. A further decrease in matrix protein levels was measured in response to combination treatment with VX-809 and 1-155, whereby TG2 and fibronectin protein expression was reduced by 67% ($p<0.01$) and 65% ($p<0.001$) respectively, compared to untreated IB3 cells.

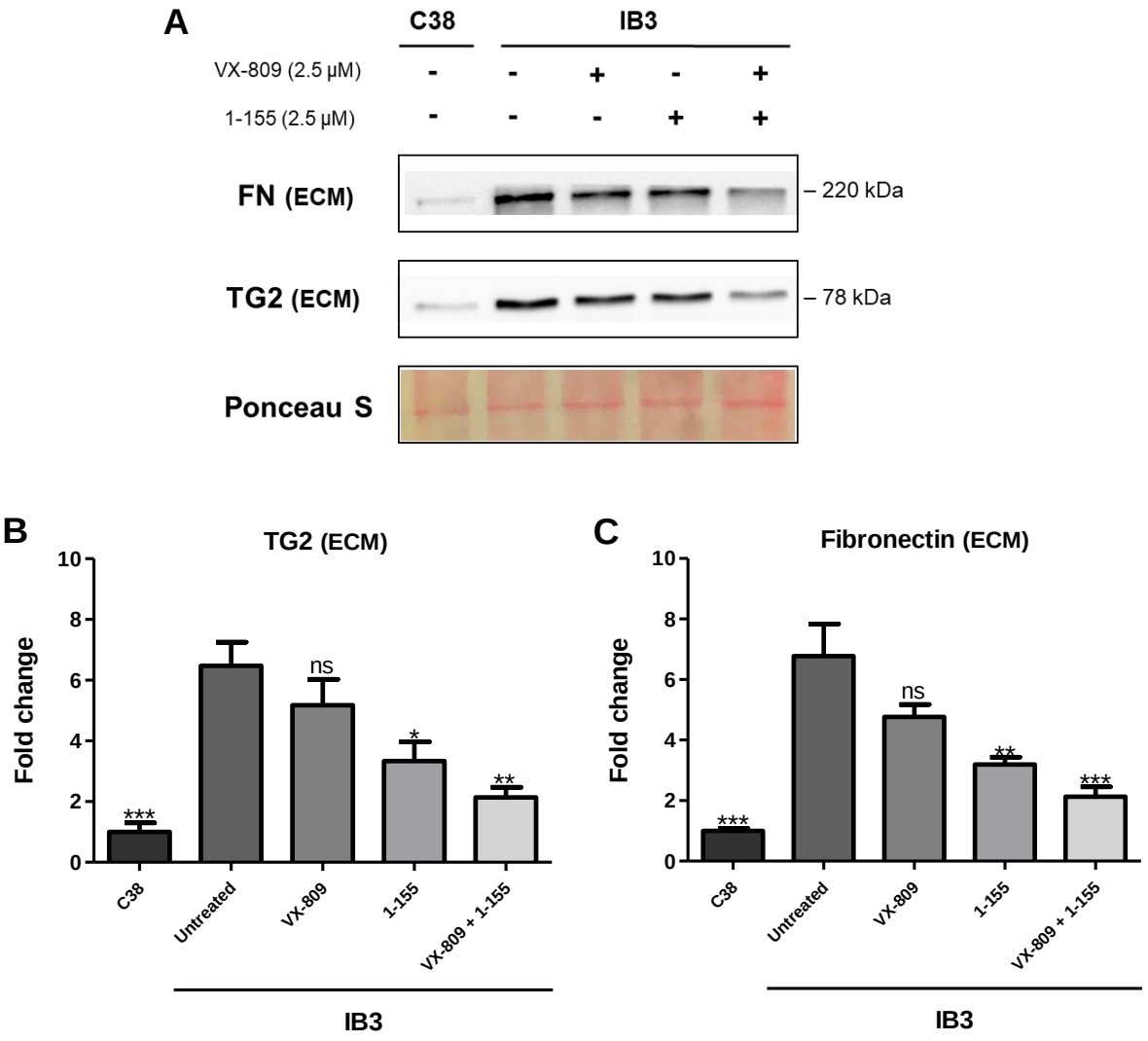

Figure 5.1. Measurement of TG2 and fibronectin protein expression in the ECM of IB3 cells following treatment with VX-809 and 1-155 alone or in combination. IB3 cells were treated with VX-809 (2.5 μM), 1-155 (2.5 μM) or VX-809 (2.5 μM) and 1-155 (2.5 μM) for 72 h, with treatments changed every 24 h. C38 cells were used as a CFTR corrected control. Cells were detached using 2mM EDTA and ECM fractions collected, before proteins were separated using SDS-PAGE. Following protein transfer, western blot analysis was performed for the detection of TG2 and fibronectin in the ECM. Ponceau S staining was used as a loading control. **(A)** Representative western blots of TG2 and fibronectin protein expression in the ECM. Densitometry of **(B)** TG2 (ECM) and **(C)** fibronectin (ECM) protein levels, measured using ImageJ software. Data normalised to Ponceau S staining and expressed as the mean fold change ± SEM, in comparison to untreated IB3 cells. Statistical analysis of three independent experiments (N=3) using a one-way ANOVA, with a post-hoc Tukey test; ns, not significant, **P*<0.05, ***P*<0.01, ****P*<0.001.

5.3.2 The combined effect of a CFTR corrector and cell-impermeable TG2 inhibitor on matrix deposition of TG2, fibronectin and TGFβ1

As shown in Figure 5.1, matrix protein levels of TG2 and fibronectin were decreased, following IB3 cell treatment with VX-809 and 1-155 in combination. Subsequently, 1-155 was replaced with the cell-impermeable compound R281, to determine whether an equivalent response would be observed through inhibition of extracellular TG2. In addition, it is known that TG2 mediated deposition of fibronectin leads to a stiffened ECM, which enhances the mechanical activation of matrix bound TGFβ1 (Klingberg et al., 2014). Therefore, matrix protein levels of TGFβ1 were also measured, to examine the effect of R281 on this downstream pro-fibrotic cytokine.

IB3 cells were treated with either VX-809 (2.5 µM), R281 (500 µM) or VX-809 (2.5 µM) and R281 (500 µM) for 72 h, before cells were detached and the ECM collected. Samples were analysed using western blot analysis. A C38 control was used for comparison of normal ECM protein expression. As illustrated in Figure 5.2, matrix protein levels of TG2, fibronectin and TGFβ1 were reduced across all treatment conditions, compared to untreated IB3 cells. However, decreases in the expression of all three proteins only reached statistical significance for IB3 cells treated with both VX-809 and R281. Further to this, the matrix protein levels of fibronectin and TGFβ1 were found to be largely comparable between C38 cells and IB3 cells treated with VX-809 and R281.

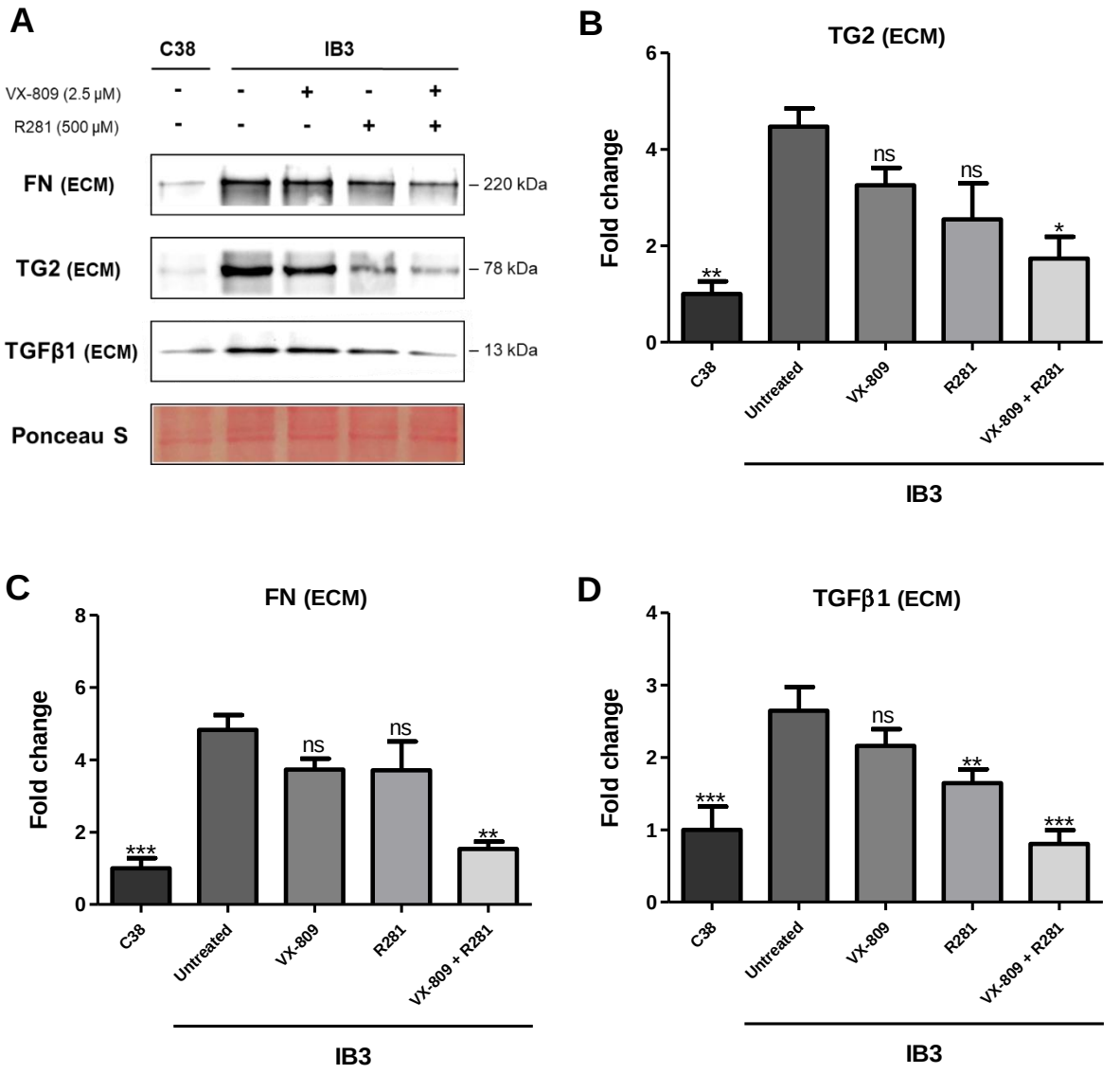

Figure 5.2. Measurement of TG2, fibronectin and TGFβ1 protein expression in the ECM of IB3 cells following treatment with VX-809 and R281 alone or in combination. IB3 cells were treated with VX-809 (2.5 μM), R281 (500 μM) or VX-809 (2.5 μM) and R281 (500 μM) for 72 h, with treatments changed every 24 h. C38 cells were used as a CFTR corrected control. Cells were detached using 2mM EDTA and ECM fractions collected, before proteins were separated using SDS-PAGE. Following protein transfer, western blot analysis was performed for the detection of TG2, fibronectin and TGFβ1 in the ECM. Ponceau S staining was used as a loading control. **(A)** Representative western blots of TG2, fibronectin and TGFβ1 protein expression in the ECM. Densitometry of **(B)** TG2 (ECM), **(C)** fibronectin (ECM) and **(D)** TGFβ1 (ECM) protein levels, measured using ImageJ software. Data normalised to Ponceau S staining and expressed as the mean fold change ± SEM, in comparison to untreated IB3 cells. Statistical analysis of three independent experiments (N=3) using a one-way ANOVA, with a post-hoc Tukey test; ns, not significant, **P*<0.05, ***P*<0.01, ****P*<0.001.

5.3.3 A comparison of C38 cell migration levels when cultured in the secretome of untreated and treated IB3 cells

As demonstrated in Figures 5.1 and 5.2, TG2 overexpression in the ECM was abrogated via combined treatment of IB3 cells with a CFTR corrector and TG2 inhibitor. This suggests that combination treatment in some way restricts the externalisation of TG2. As such, an investigation of the CF airway epithelial cell secretome was conducted, to identify changes in the release of paracrine soluble factors following treatment. Cell migration levels were used as a measure of EMT, to highlight differences between the pro-fibrotic capacity of cell secretomes.

An *in vitro* scratch assay was performed to quantify cell migration levels over 16 h. Immediately after wounding, C38 cells were cultured in the cell secretomes of untreated C38 cells, untreated IB3 cells or IB3 cells which were treated with VX-809 (2.5 µM) and 1-155 (2.5 µM) alone or in combination. All secretomes were collected after 72 h of cell growth. As shown in Figure 5.3, the secretomes of treated IB3 cells caused significantly reduced percentage wound closure, in comparison to the secretome of untreated IB3 cells (4 h and 16h). In addition, a significant decrease in percentage wound closure was observed for C38 cells cultured in the secretome of VX-809 and 1-155 treated IB3 cells, compared to the secretomes of IB3 cells treated with VX-809 or 1-155 alone (4 h and 16h). Notably, the secretomes of both untreated C38 cells and IB3 cells treated with VX-809 and 1-155 were found to generate comparable levels of wound closure, at 4 h and 16 h time points.

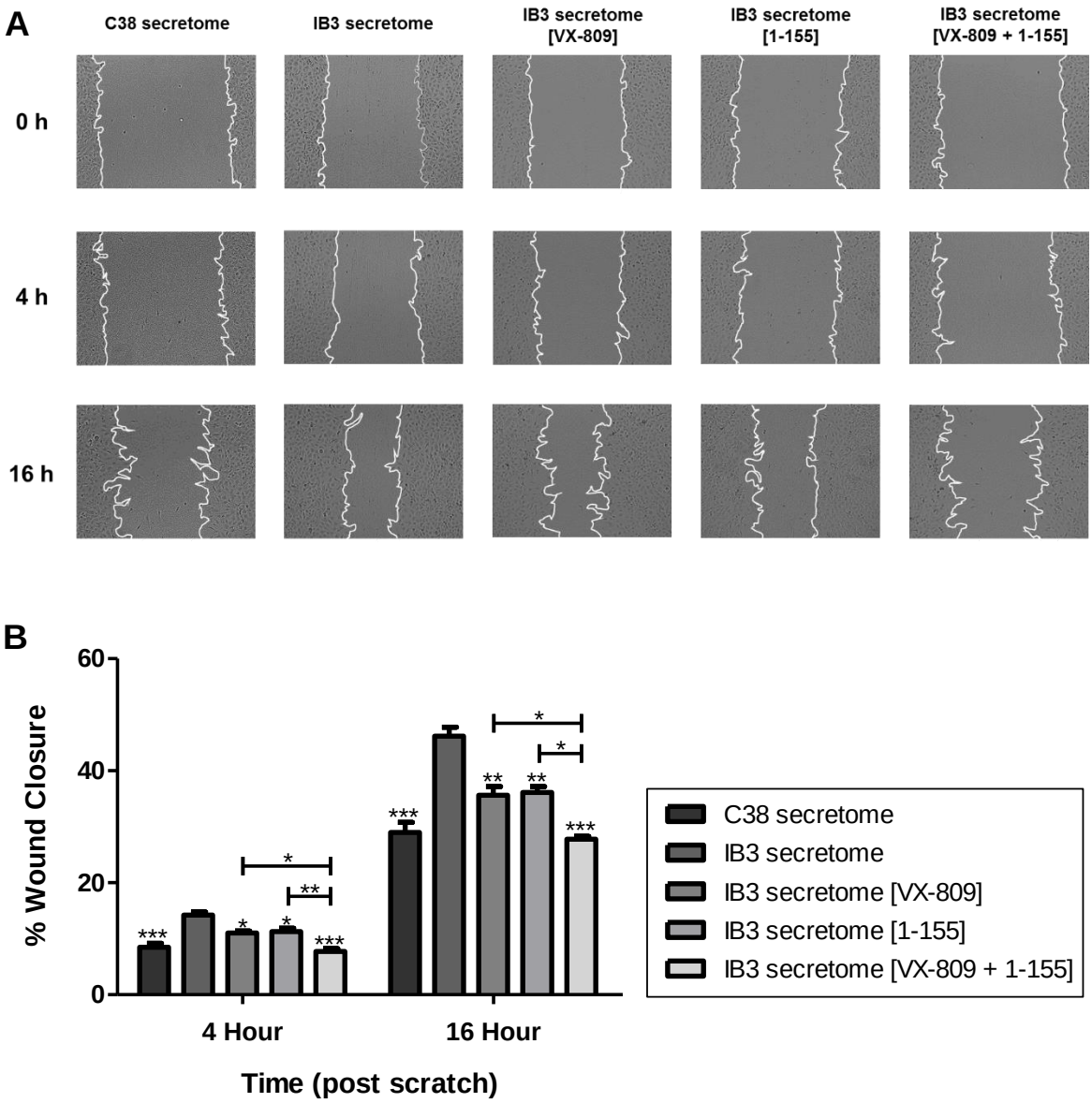

Figure 5.3. Measurement of percentage wound closure for C38 cells when cultured in the secretome released from IB3 cells treated with VX-809 or 1-155 alone or in combination. C38 cells were seeded in a 24 well plate and grown until confluent, before a scratch was made in each cell monolayer. The secretomes of untreated C38 cells, untreated IB3 cells or IB3 cells treated with VX-809 (2.5 µM), 1-155 (2.5 µM) or VX-809 (2.5 µM) and 1-155 (2.5 µM) were added to the wells post-wounding. Cell secretomes were collected after 72 h, in which treatments were changed every 24 h. Images were acquired in triplicate at 0, 4 and 16 h post-wounding. **(A)** Representative images of each scratch, captured at the specified time points. Images were analysed using ImageJ software and **(B)** cell migration calculated as the percentage wound closure, relative to the original area of the wound at 0 h. Data expressed as the mean ± SEM of three independent experiments (N=3), in comparison to C38 cells treated with the secretome of untreated IB3 cells. Statistical analysis performed using a one-way ANOVA, with a post-hoc Tukey test; **P*<0.05, ***P*<0.01, ****P*<0.001.

5.3.4 An experimental approach to examine the role of EVs in TG2 secretion from CF airway epithelial cells

Data shown throughout this study emphasises the importance of TG2 activity in the extracellular environment, with regard to the development of fibrosis in CF airways. Treatment of IB3 cells with the TG2 inhibitor 1-155 either alone or in combination with VX-809, was found to significantly reduce levels of TG2 in the ECM (Figure 5.1) and decrease the pro-fibrotic capacity of the IB3 cell secretome (Figure 5.3). This has led to the formation of a hypothesis, which proposes that the cellular export of TG2 is diminished in response to these treatments. However, the mechanism of TG2 secretion remains poorly understood and has never been investigated in CF. Even beyond CF, only a limited number of studies have attempted to examine the TG2 secretory pathway, with all research indicating that EVs are likely involved in the trafficking of TG2 (Diaz-Hidalgo et al., 2016; Furini et al., 2018; Shinde et al., 2020).

Therefore, an experimental plan was created to research the mechanism of TG2 secretion in CF and the define the role of EVs in this process. A multi-faceted approach was designed involving the optimisation and application of SEC, TRPS, protein concentration assay, transglutaminase activity assay and western blotting, for use with EVs and extracellular soluble protein specifically. A schematic outlining the overall workflow strategy of this novel investigation is shown in Figure 5.4.

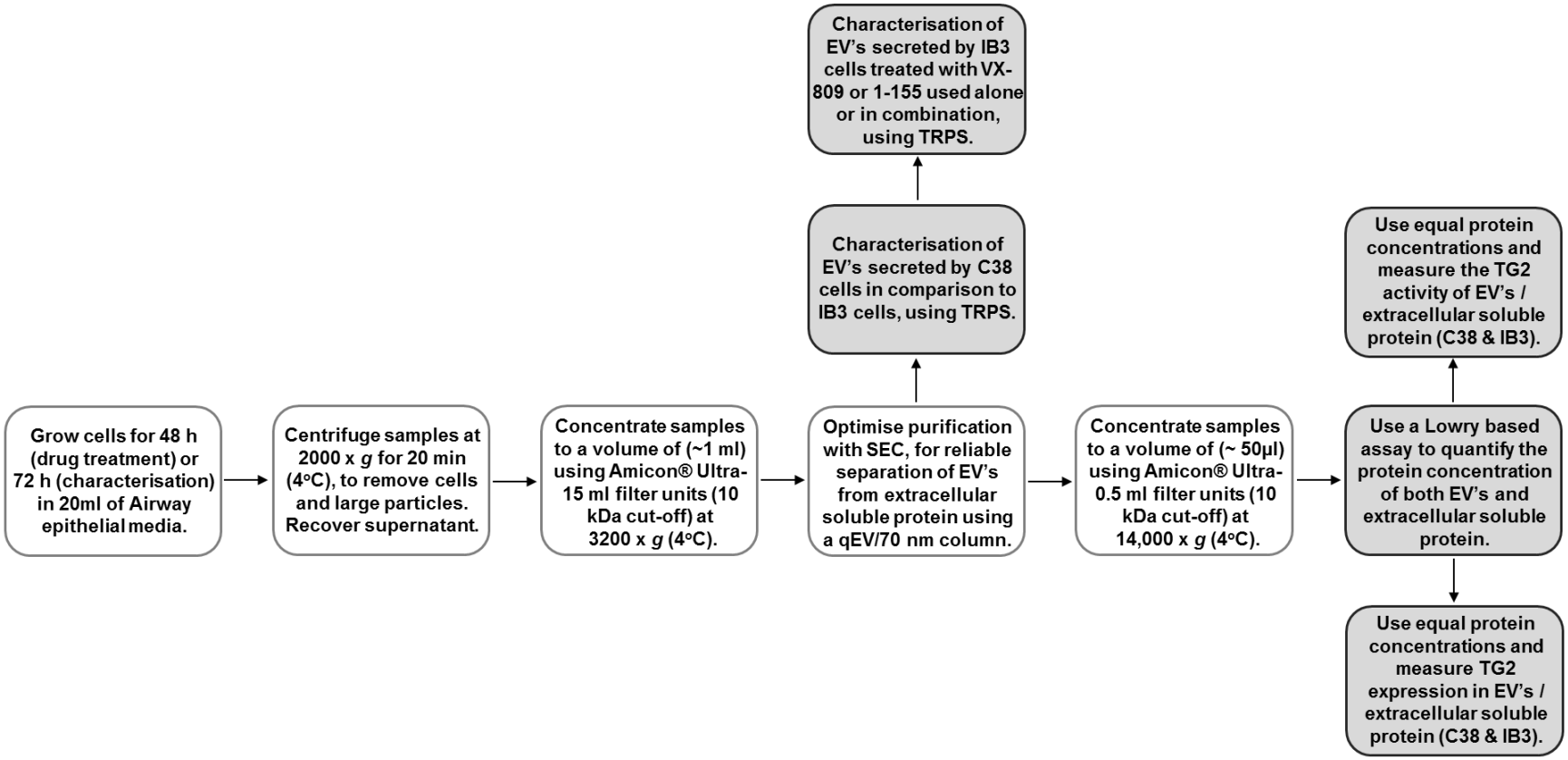

Figure 5.4. Workflow strategy for investigating the mechanism of TG2 secretion in IB3 cells. As of yet, the process by which TG2 is released from CF airway epithelial cells into the ECM has not been determined. The schematic above provides an overview of the experimental workflow strategy, designed to research the TG2 secretory pathway in CF. Following optimisation, EVs and extracellular soluble protein will be purified and separated from the cell secretome using SEC. EVs isolated from C38 and IB3 cells will then be characterised using TRPS, to identify differences in the biophysical properties of EV populations. EVs and extracellular soluble protein samples will be further concentrated in volume before biochemical analysis. A Lowry based assay will be used for comparison of protein concentrations between samples. Protein concentration measurements will also be used to ensure equal levels of EVs or extracellular soluble protein are compared during analysis. Western blotting will be used to quantify TG2 protein expression and a transglutaminase activity assay used to measure TG2 function, within EV and extracellular soluble protein samples. In the final investigation, IB3 cells will be left untreated or treated with compounds and changes between EV populations characterised using TRPS.

5.3.5 Optimisation of SEC for reliable isolation and recovery of EVs and extracellular soluble protein

To determine whether EVs are involved in IB3 cell secretion of TG2, a reliable method was required for isolation of vesicles. Several purification techniques have been widely used in the literature including: ultracentrifugation, density gradient centrifugation, chemical precipitation and SEC (Brennan et al., 2020). The selection of SEC was based on the end goal of preserving EV biofunctionality, while limiting protein contaminants. With drawbacks of extreme centrifugal force and inclusion of additional chemicals, the other techniques were not deemed suitable for this particular investigation.

SEC optimisation was carried out to ensure accurate isolation and separation of EVs from extracellular soluble protein. With downstream analyses dependant on the quality of purification, optimisation was performed as an essential preliminary step. After culturing C38 and IB3 cells for 72 h, cell secretomes were collected and ran through a qEVoriginal/70 nm SEC column. EV concentration was quantified using TRPS and protein concentration measured using a DC^{TM} Protein Assay kit. As shown in Figures 5.5 A and B, the SEC elution zones of EVs and extracellular soluble protein were identical for both C38 and IB3 cell secretomes. Using this data, a SEC protocol was devised to maximise the recovery of EVs and extracellular soluble protein, whilst retaining high levels of purity for each isolate (Figure 5.5 C). This protocol was implemented for use in all other experiments requiring the application of SEC. Upon further comparison of SEC elution profiles, it was found that the IB3 cell secretome contained higher levels of EVs and extracellular soluble protein, over the C38 cell secretome. Intriguingly, a higher protein level was also observed in the EV elution zone of the IB3 cell secretome, compared to the C38 cell secretome.

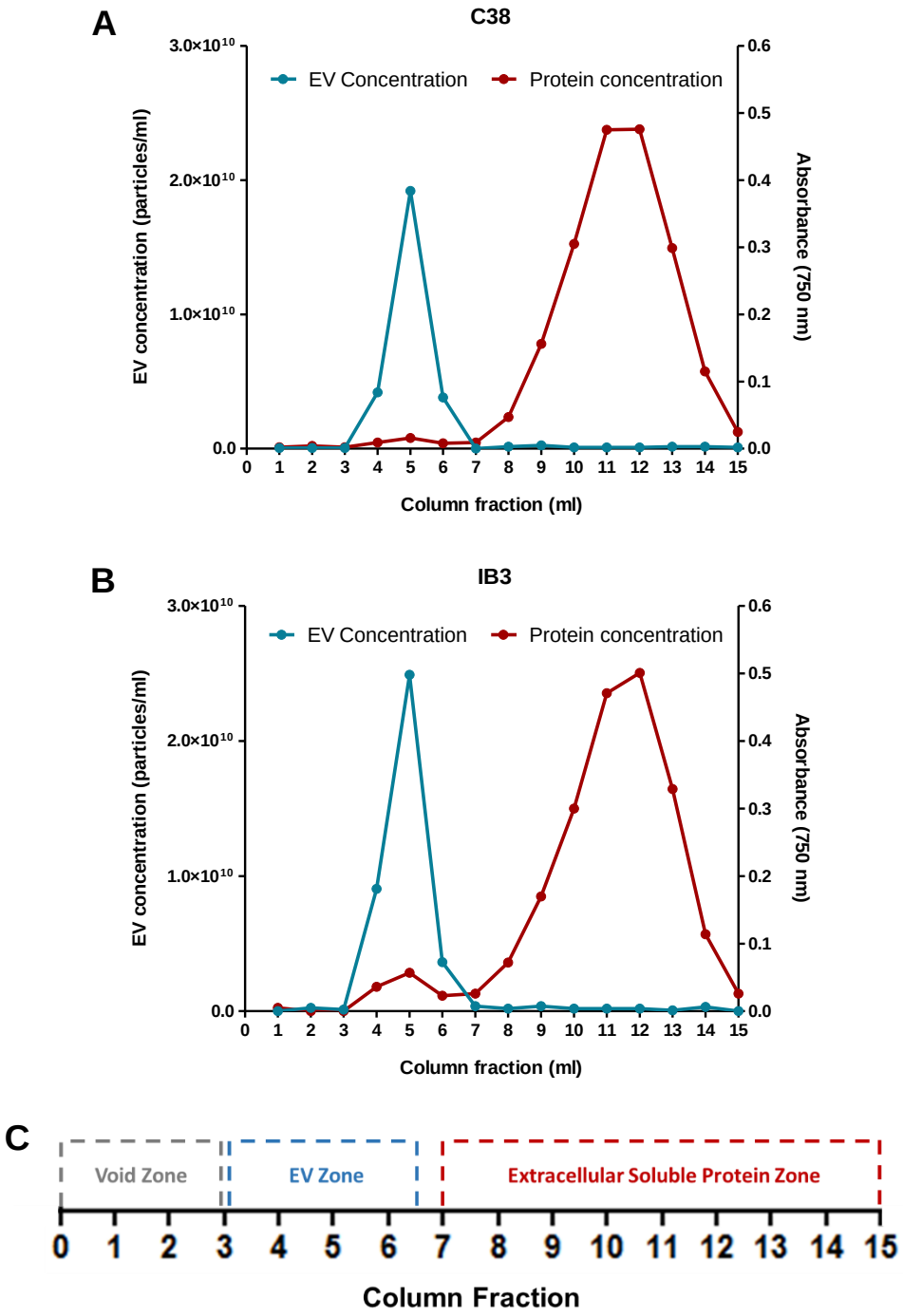

Figure 5.5. Elution profiles of EVs and extracellular soluble protein following SEC of C38 and IB3 cell secretomes. C38 and IB3 cells were grown for 72 h and the cell secretomes collected. Cell secretomes were pre-processed via centrifugation, with recovered supernatants loaded separately on to a qEVoriginal/70 nm SEC column. Samples eluted from the column were collected in 1 ml aliquots, up to a total elution volume of 15 ml. EV and extracellular soluble protein concentration of individual aliquots were measured using TRPS (NP150) and a DC™ Protein Assay kit, respectively. Data analysis of EV concentration was performed using the IZON control suite software. Elution profiles of the **(A)** C38 and **(B)** IB3 cell secretomes following SEC. **(C)** Schematic representation of SEC elution zones**,** determined to be optimal for the recovery of purified EVs and extracellular soluble protein. Elution profiles generated using data from a single experiment (N=1).

5.3.6 Characterisation of EVs secreted by C38 and IB3 cells

A comparison of SEC elution profiles revealed that IB3 cells release more EVs than C38 cells (Figures 5.5 A and B). Furthermore, the IB3 cell secretome was seen to exhibit a large peak in protein concentration within the EV elution zone, in comparison to the C38 cell secretome. This could reflect the higher concentration of EVs or possibly indicate a higher level of EV associated proteins, or a combination of both. However, a more in-depth analysis is required to determine differences between C38 and IB3 cell derived EV populations, as the inferences above are based upon a single optimisation experiment. As such, a biophysical characterisation of the EVs secreted by C38 and IB3 cells was performed.

C38 and IB3 cells were cultured for 72 h, before the cell secretomes were collected and ran through a qEVoriginal/70 nm SEC column. Purified EVs were recovered and analysed using TRPS. A NP150 (EV detectable size range of ~70 - 420 nm) was used to analyse EVs, due to its applicability for measurement of both exosomal and microvesicle size ranges. As shown in Figure 5.6 A, IB3 cells were found to secrete significantly more EVs than C38 cells, with an observed increase of 56% ($p<0.001$). In addition, the concentration of EVs secreted by C38 ($p<0.001$) and IB3 cells ($p<0.001$) were significantly greater, than the level of constituent EVs in the AEM. Intriguingly, the mean size of IB3 cell derived EVs was significantly smaller by approximately 30 nm ($p<0.05$), compared to the mean size of C38 derived EVs (Figure 5.6 B).

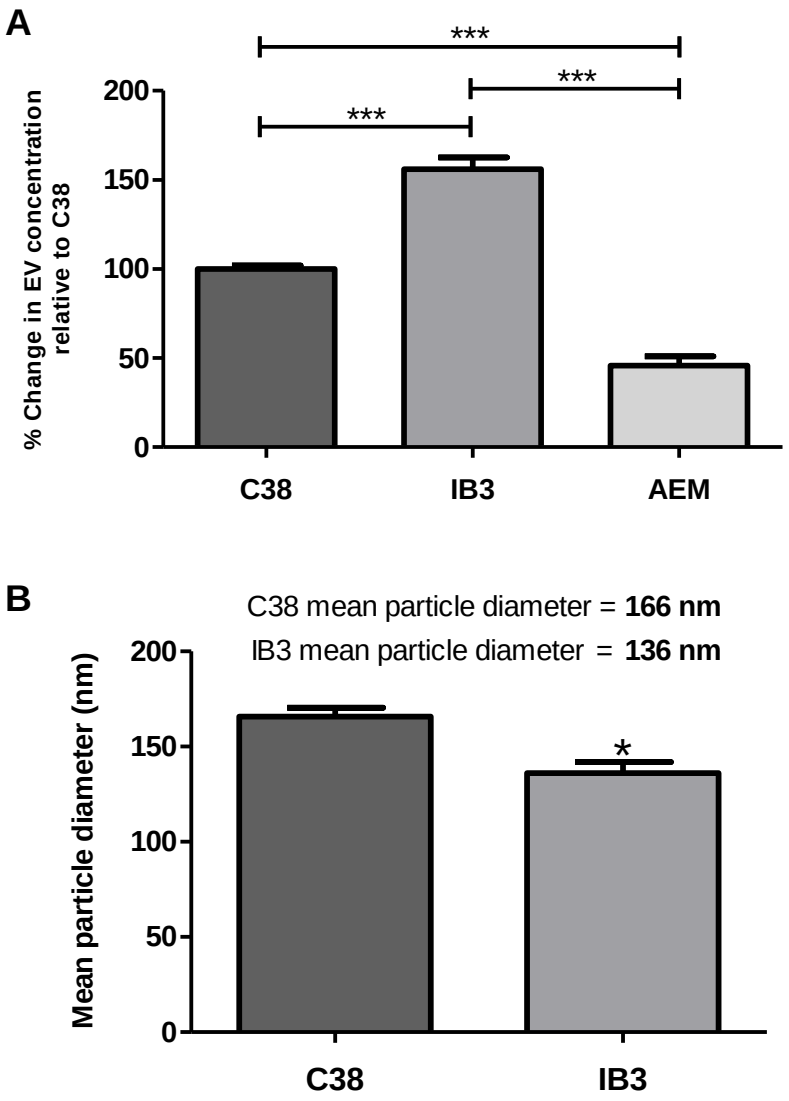

Figure 5.6. Quantification of the concentration and mean particle diameter of C38 and IB3 cell derived EV populations using TRPS. C38 and IB3 cells were grown for 72 h and the cell secretomes collected. AEM was examined to determine the background level of EVs in the cell culture medium. Cell secretomes and AEM were pre-processed via centrifugation, with recovered supernatants loaded separately on to a qEVoriginal/70 nm SEC column. Samples were eluted from the column and EV fractions collected. The **(A)** concentration and **(B)** mean particle diameter of purified EV populations were measured using TRPS (NP150). Data analysis was performed using the IZON control suite software. Data expressed as the mean ± SEM of three independent experiments (N=3), in comparison to C38 cells. Statistical analysis performed using **(A)** a one-way ANOVA, with a post-hoc Tukey test; ***P<0.001 or **(B)** an unpaired, two-tailed t-test; *P<0.05.

5.3.7 Measuring the concentration and size distribution of C38 and IB3 cell derived EV populations when normalised to cell number

As demonstrated in Figures 5.6, IB3 cells secrete more EVs than C38 cells, yet the average diameter of EV generated is approximately 30 nm smaller. These novel data highlight a disparity in the biophysical properties of EV populations produced by C38 and IB3 cells. To further understand the cause of such variance, an investigation into the size distribution of EVs within each EV population was conducted. Furthermore, to give a more accurate assessment of changes in EV concentration, cells were counted immediately after the collection of cell secretomes. This was undertaken to ensure that comparisons between C38 and IB3 cells were relative, by normalising EV concentrations against cell number.

C38 and IB3 cells were cultured for 72 h, before the cell secretomes were collected and viable cells were counted using a Trypan Blue exclusion assay. The cell secretomes were ran through a qEVoriginal/70 nm SEC column and purified EVs recovered. EVs were analysed using TRPS, via an NP150. After 72 h of cell culture, IB3 cells ($p<0.01$) were seen to have a significantly higher growth rate (+19%), in comparison to that of C38 cells (Figure 5.7 A). Subsequently, this data was used to normalise EV concentrations, with IB3 cells ($p<0.05$) continuing to show significantly increased levels of secreted EVs (+30%), compared to C38 cells (Figure 5.7 B). Ultimately, the size distribution of C38 and IB3 cell derived EV populations were determined and normalised against cell number. It was found that the increased production of IB3 cell derived EVs was focused in the exosomal size range, in comparison to C38 cell derived EVs (Figure 5.7 C). A significant rise in EV concentration was measured from 100 – 139 nm in particle diameter.

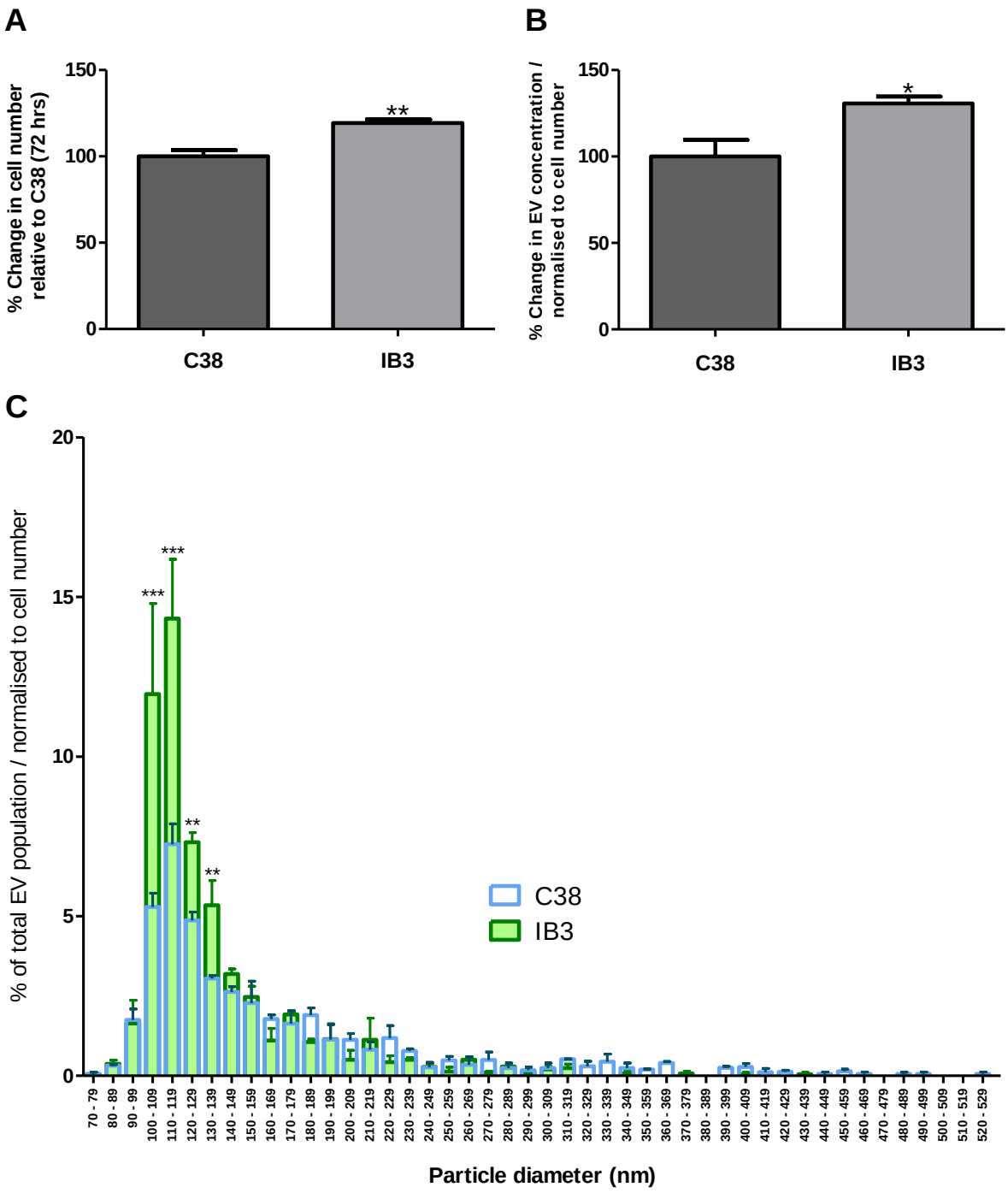

Figure 5.7. The concentration and size distribution of C38 and IB3 cell derived EV populations after normalisation to cell number. C38 and IB3 cells were grown for 72 h and the cell secretomes collected. **(A)** Viable C38 and IB3 cells were counted using a Trypan Blue exclusion assay. Cell secretomes were pre-processed via centrifugation, with recovered supernatants loaded separately on to a qEVoriginal/70 nm SEC column. Samples were eluted from the column and isolated EV fractions collected. The **(B)** concentration and **(C)** size distribution of purified EV populations were measured using TRPS (NP150) and normalised to cell number. Data analysis was performed using the IZON control suite software. Data expressed as the mean ± SEM of three independent experiments (N=3), in comparison to C38 cells. Statistical analysis performed using **(A, B)** an unpaired, two-tailed t-test; *P<0.05, **P<0.01 or **(C)** a two-way ANOVA, with a post-hoc Bonferroni multiple comparison test; **P<0.01, ***P<0.001.

5.3.8 Evaluating the level of cellular resources used in the production of C38 and IB3 cell derived EV populations

IB3 cells are found to secrete a significantly higher concentration of EVs compared to C38 cells (Figure 5.7 B), by producing increased levels of exosomes (Figure 5.7 C). Yet upon further analysis, it was discerned that C38 cells generate more microvesicle sized EVs than IB3 cells (Figure 5.7 C). Thus, it remains unclear whether IB3 cells utilise additional cellular resources to yield more EVs, or instead compensate for enhanced exosome production by diverting EV components away from the synthesis of microvesicles. As such, the total surface area of C38 and IB3 cell derived EV populations was quantified. This was used as a basic method of analysis, for comparing the levels of cellular resources (e.g. membrane area) invested into the production of EVs.

After culturing C38 and IB3 cells for 72 h, cell secretomes were collected and viable cells counted using a Trypan Blue exclusion assay. The cell secretomes were ran through a qEVoriginal/70 nm SEC column, before purified EVs were recovered and analysed using TRPS, via an NP150. Based on the assumption of sphericity, the total surface area of separate EV populations was estimated using the equation ($4\pi r^2$), with values adjusted for EV concentration and cell number. It was found that no significant difference existed between the total surface area of the IB3 cell derived EV population, compared to the EV population secreted by C38 cells (Figure 5.8).

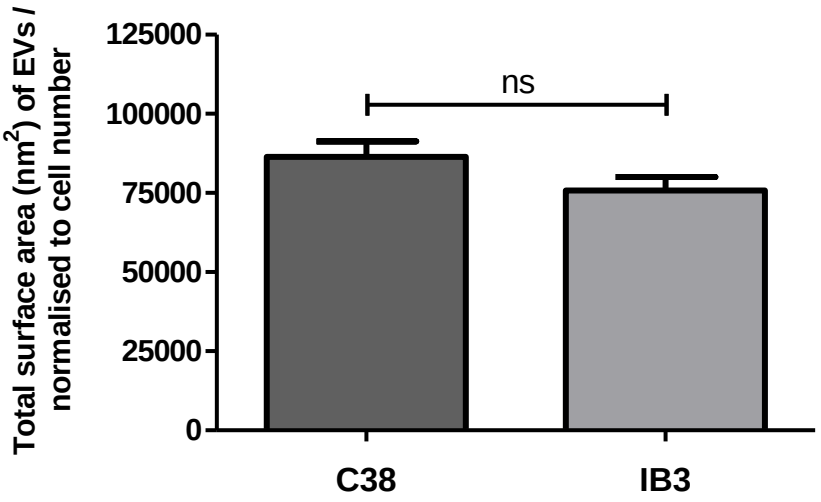

Figure 5.8. Total surface area of C38 and IB3 cell derived EV populations after normalisation to cell number. C38 and IB3 cells were grown for 72 h and the cell secretomes collected. Viable C38 and IB3 cells were counted using a Trypan Blue exclusion assay. Cell secretomes were pre-processed via centrifugation, with recovered supernatants loaded separately on to a qEVoriginal/70 nm SEC column. Samples were eluted from the column and isolated EV fractions collected. The concentration and mean particle diameter of purified EV populations were measured using TRPS (NP150). Data analysis was performed using the IZON control suite software. **(A)** Total surface area of EV populations was calculated using the equation ($4\pi r^2$), with values adjusted for EV concentration and normalised against cell number. Data expressed as the mean ± SEM of three independent experiments (N=3), in comparison to C38 cells. Statistical analysis performed using an unpaired, two-tailed t-test; ns, not significant.

5.3.9 Measuring the protein concentration of EVs and extracellular soluble protein secreted by C38 and IB3 cells

Data shown in Figures 5.7 and 5.8, indicate a shift in the ratio of EV sizes released by CF airway epithelial cells. IB3 cells are seen to use similar levels of cellular resources as C38 cells, but merely redistribute these resources away from the production of microvesicle sized EVs and towards the synthesis of exosomal sized EVs. However, as evidenced in Figure 5.5, a sizable protein peak was observed exclusively in the EV elution zone of the IB3 cell secretome. Taken together, this could suggest that IB3 cell derived exosomes are potentially enriched in protein. Therefore, the protein concentration of C38 and IB3 cell derived EV populations were measured comparatively. Furthermore, the primary role of EVs is to selectively transport cargo (e.g. proteins) for delivery to distant targets outside of the cell (Margolis and Sadovsky, 2019). As such, the concentration of extracellular soluble protein in the secretomes of C38 and IB3 cells was also measured.

After culturing C38 and IB3 cells for 72 h, cell secretomes were collected and ran through a qEVoriginal/70 nm SEC column. Purified EVs and extracellular soluble protein fractions were recovered and concentrated using Amicon® ultra-0.5 ml centrifugal filter units, before the protein concentration of both fractions was measured using a DC™ Protein Assay kit. The protein concentration of the IB3 cell derived EV population was found to be significantly higher than that of the C38 cell derived EV population, with an observed increase of 46% ($p<0.01$) (Figure 5.9 A). Furthermore, both C38 and IB3 cell derived EV populations demonstrated increased levels of protein concentration, compared to constituent EVs of the AEM. In contrast, IB3 cells exhibited only a modest increase in extracellular soluble protein concentration compared to C38 cells, without reaching statistical significance (Figure 5.9 B). In addition, both C38 and IB3 cells were seen to produce higher concentrations of extracellular soluble protein, in comparison to the constituent soluble protein of the AEM.

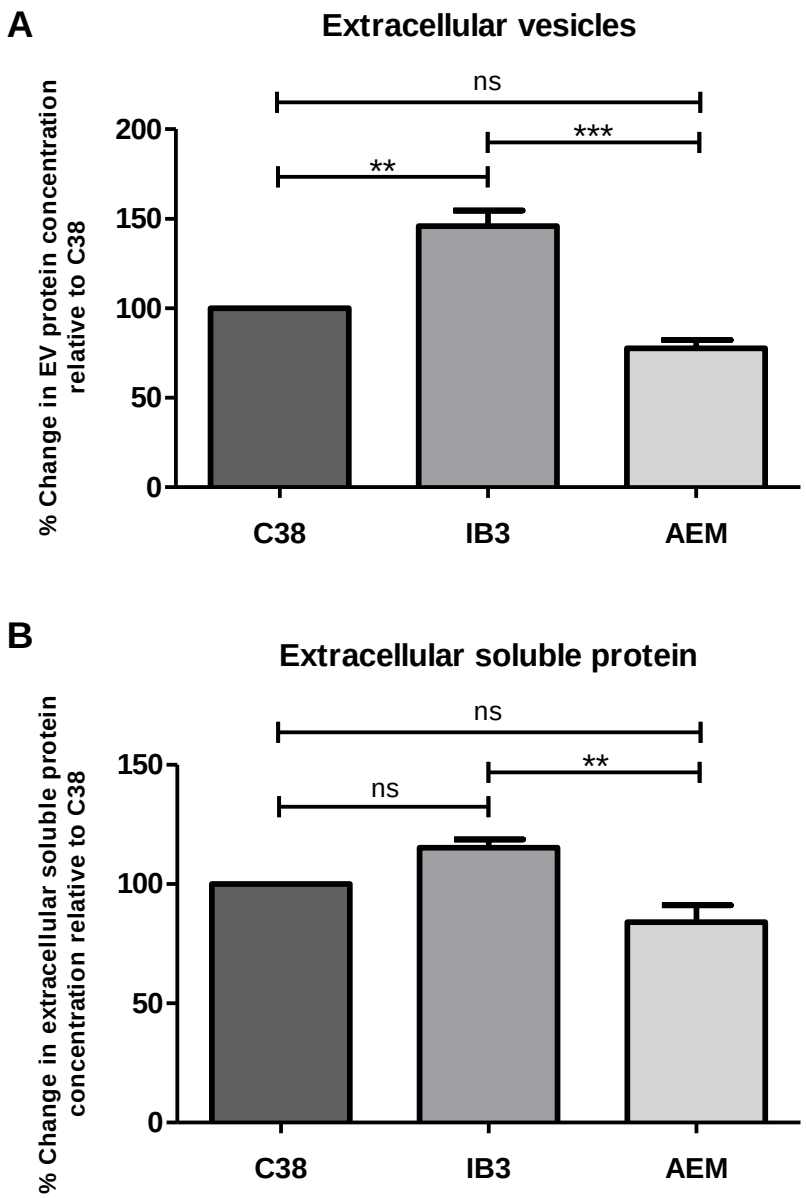

Figure 5.9. Measurement of protein concentration for C38 and IB3 cell derived EVs and extracellular soluble protein using a DC™ protein assay kit. C38 and IB3 cells were grown for 72 h and the cell secretomes collected. AEM was examined to determine the protein concentration of EVs and extracellular soluble protein, within the cell culture medium. Cell secretomes were pre-processed via centrifugation, with recovered supernatants loaded separately on to a qEVoriginal/70 nm SEC column. Samples were eluted from the column and isolated EV and extracellular soluble protein fractions collected. Fractions were concentrated in volume using Amicon® ultra-0.5 ml centrifugal filter units, before the protein concentration of **(A)** EVs and **(B)** extracellular soluble protein was measured using a DC™ Protein Assay kit. Data expressed as the mean ± SEM of three independent experiments (N=3), in comparison to C38 cells. Statistical analysis performed using a one-way ANOVA, with a post-hoc Tukey test; ns, not significant, ***P*<0.01, ****P*<0.001.

5.3.10 The protein expression of TG2 in C38 and IB3 cell derived EVs

Throughout this study the data have shown that externalisation of TG2 into the ECM, is critical to the development of fibrosis in CF airways. However, the route of TG2 secretion has yet to be investigated in CF. A recent study examining the mechanism of TG2 export in chronic kidney disease identified links to an unconventional secretory pathway, specifically involving exosomes (Furini et al., 2018). Novel data from Figures 5.6, 5.7 and 5.9 A, has demonstrated that IB3 cells release high levels of exosomes, which are likely enriched in protein. Considering the parallels, it is quite possible that TG2 is also exported via exosomes in CF airway epithelial cells. To test this hypothesis, an attempt was made to detect the expression of TG2 in purified EVs isolated from the secretome of IB3 cells. The protein TSG101 (a component of the ESCRT sorting machinery) was used as an EV and exosomal marker (Willms et al., 2016).

C38 and IB3 cells were cultured for 72 h, before the cell secretomes were collected and ran through a qEVoriginal/70 nm SEC column. Purified EVs were recovered and concentrated using Amicon® ultra-0.5 ml centrifugal filter units. EVs were then analysed using western blotting, for the detection of TG2 protein expression. Remarkably, the presence of TG2 was identified in EVs secreted by IB3 cells ($p<0.001$) and to a significantly greater level (>4-fold) than C38 cell derived EVs (Figure 5.10). As expected, constituent EVs of the AEM were found to lack the presence of TG2.

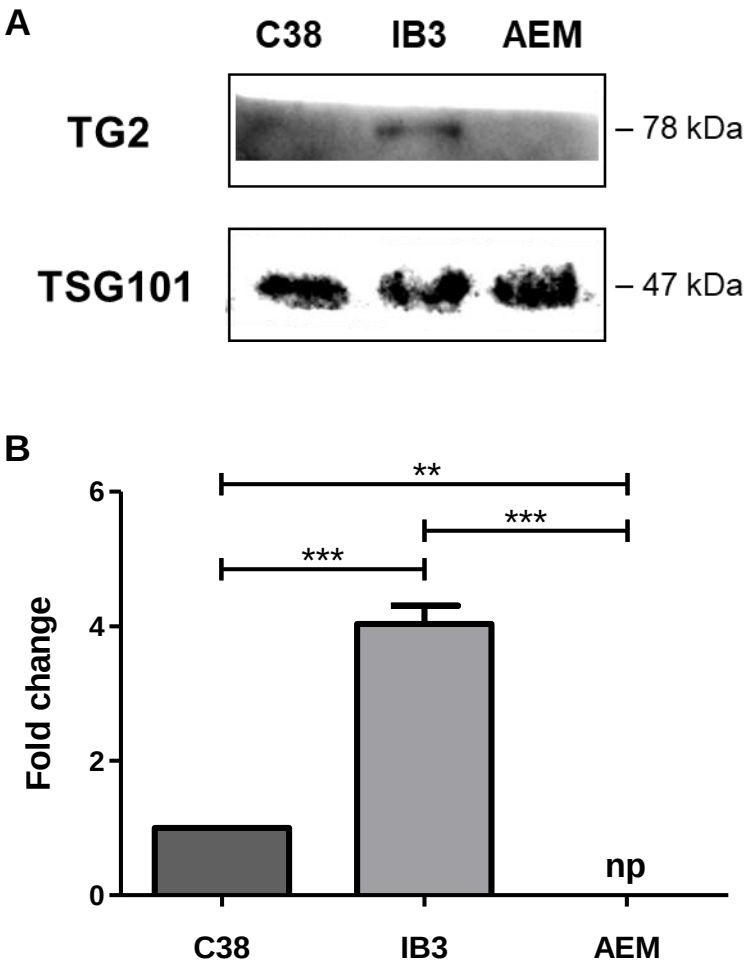

Figure 5.10. Measurement of TG2 protein expression in C38 and IB3 cell derived EVs. C38 and IB3 cells were grown for 72 h and the cell secretomes collected. AEM was examined to determine the background level of TG2 protein expression for EVs, within the cell culture medium. Cell secretomes were pre-processed via centrifugation, with recovered supernatants loaded separately on to a qEVoriginal/70 nm SEC column. Samples were eluted from the column and isolated EV fractions collected. Purified EVs were concentrated in volume using Amicon® ultra-0.5 ml centrifugal filter units, before the protein concentration of EVs was measured using a DC™ Protein Assay kit. Samples were loaded on to a gel at equal protein concentrations and SDS-PAGE used to separate proteins. Following protein transfer, western blot analysis was performed for detection of TG2. The membrane was stripped and reprobed for TSG101. **(A)** Representative western blot of TG2 protein expression. **(B)** Densitometry of TG2 protein levels, measured using ImageJ software; np, not present. Data expressed as the mean fold change ± SEM in comparison to C38 cells. Statistical analysis of three independent experiments (N=3) using a one-way ANOVA, with a post-hoc Tukey test; ***P*<0.01, ****P*<0.001.

5.3.11 The protein expression of free soluble TG2 in C38 and IB3 cell derived secretomes

As revealed in Figure 5.10, EVs secreted by IB3 cells are enriched in TG2, compared to EVs secreted by CFTR corrected C38 cells. However, it is unknown whether TG2 remains internalised / bound to EVs following secretion or is in fact liberated from EVs once externalised into the extracellular environment. Consequently, the soluble protein fraction of C38 and IB3 cell derived secretomes was purified and analysed for detection of TG2 protein expression.

C38 and IB3 cells were cultured for 72 h, before the cell secretomes were collected and ran through a qEVoriginal/70 nm SEC column. The purified soluble protein fraction of each sample was recovered and concentrated using Amicon® ultra-0.5 ml centrifugal filter units. The soluble protein isolates were then analysed using western blotting, for detection of TG2 protein expression. The data shows that TG2 protein levels were significantly increased by >5-fold ($p<0.05$) in the extracellular soluble protein isolate of IB3 cells, in comparison to the extracellular soluble protein isolate of C38 cells (Figure 5.11). An absence of TG2 expression was observed in the constituent soluble protein of the AEM.

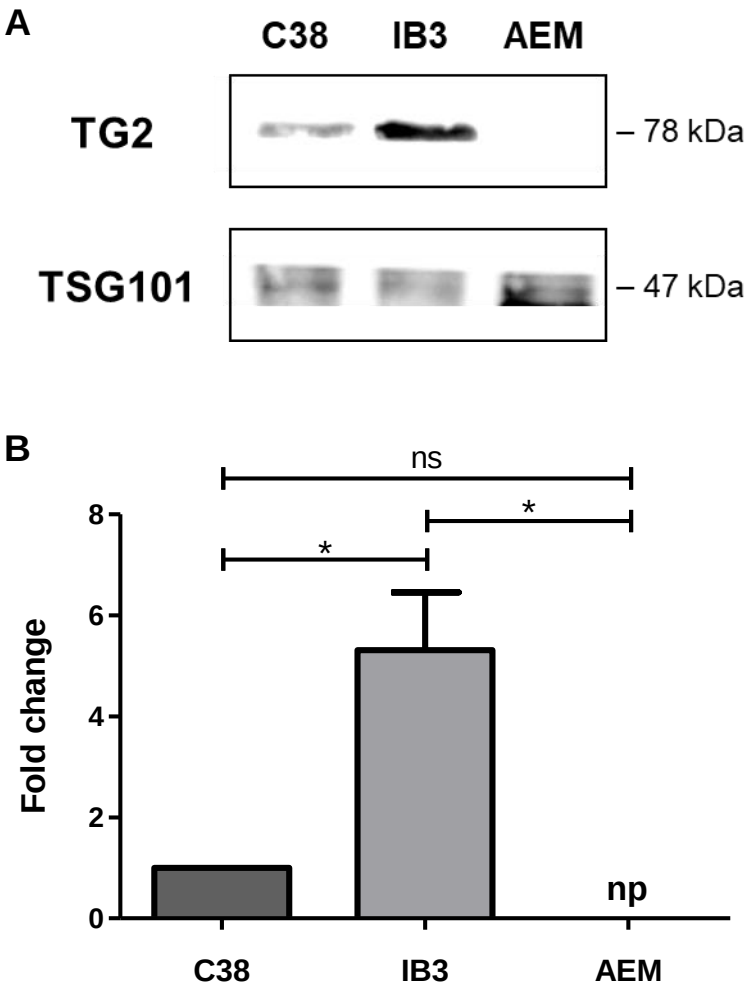

Figure 5.11. Measurement of TG2 protein expression in C38 and IB3 cell derived extracellular soluble protein isolates. C38 and IB3 cells were grown for 72 h and the cell secretomes collected. AEM was examined to determine the background level of TG2 protein expression for soluble protein, within the cell culture medium. Cell secretomes were pre-processed via centrifugation, with recovered supernatants loaded separately on to a qEVoriginal/70 nm SEC column. Samples were eluted from the column and isolated soluble protein fractions collected. Purified soluble protein isolates were concentrated in volume using Amicon® ultra-0.5 ml centrifugal filter units, before the protein concentration of soluble protein isolates was measured using a DC™ Protein Assay kit. Samples were loaded on to a gel at equal protein concentrations and SDS-PAGE used to separate proteins. Following protein transfer, western blot analysis was performed for detection of TG2. The membrane was stripped and reprobed for TSG101. **(A)** Representative western blot of TG2 protein expression. **(B)** Densitometry of TG2 protein levels, measured using ImageJ software; np, not present. Data expressed as the mean fold change ± SEM in comparison to C38 cells. Statistical analysis of two independent experiments (N=2) using a one-way ANOVA, with a post-hoc Tukey test; ns, not significant, *P<0.05.

5.3.12 Measuring the TG2 activity of C38 and IB3 cell derived EV populations

The involvement of EVs in the export of TG2 from IB3 cells has been evidenced in Figure 5.10. Accordingly, TG2 activity was measured to establish whether the enzyme remains catalytically active when in association with EVs. Moreover, during the experimental process of TG2 activity analysis, EVs presumably remain largely intact. As such, TG2 activity levels are likely representative of enzymatic function on the surface of EVs.

C38 and IB3 cells were cultured for 72 h, before the cell secretomes were collected and ran through a qEVoriginal/70 nm SEC column. Purified EVs were recovered and concentrated using Amicon® ultra-0.5 ml centrifugal filter units. The TG2 activity of EVs was then quantified using a transglutaminase activity assay. A negative control of recombinant human TG2 in the absence of Ca^{2+} and presence of EDTA, was used as a reference of null transglutaminase activity. As demonstrated in Figure 5.12, EVs secreted by C38 cells showed little to no TG2 activity, while in comparison a significant level of TG2 activity was found with IB3 cell derived EVs ($p<0.001$).

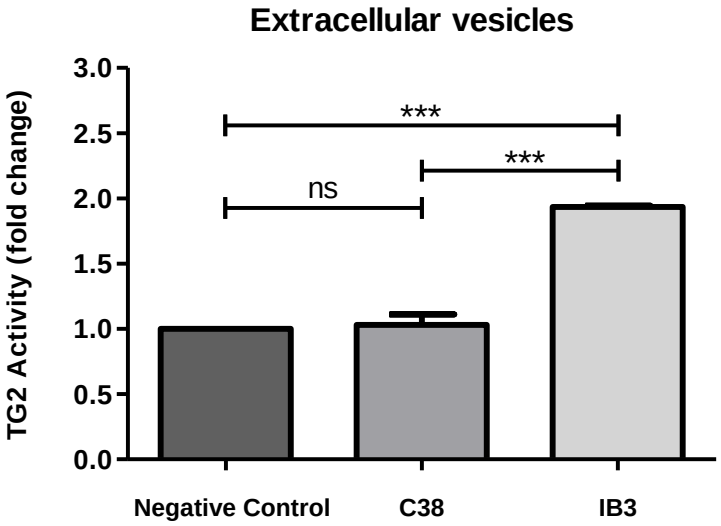

Figure 5.12. Quantification of TG2 activity for C38 and IB3 cell derived EVs using a transglutaminase activity assay. C38 and IB3 cells were grown for 72 h and the cell secretomes collected. Cell secretomes were pre-processed via centrifugation, with recovered supernatants loaded separately on to a qEVoriginal/70 nm SEC column. Samples were eluted from the column and isolated EV fractions collected. Purified EVs were concentrated in volume using Amicon® ultra-0.5 ml centrifugal filter units, before the protein concentration of EVs was measured using a DC™ Protein Assay kit. Biotin-cadaverine incorporation into N,N-dimethylcasein was used as a quantitative measure of TG2 activity, with EV populations tested at equal protein concentrations. A negative control of recombinant human TG2 (400 ng) with the addition of EDTA (10 mM) and in the absence of Ca^{2+} was used. Data expressed as the mean fold change ± SEM in comparison to the negative control. Statistical analysis of three independent experiments (N=3) using a one-way ANOVA, with a post-hoc Tukey test; ns, not significant, ***P<0.001.

5.3.13 Measuring the TG2 activity of extracellular soluble protein isolated from the secretomes of C38 and IB3 cells

As established in Figure 5.11, TG2 exists in its free form within the extracellular environment of IB3 cells. Furthermore, TG2 has also been found to be exported from IB3 cells, via its interaction with EVs (Figure 5.10). This suggests that EVs function to traffic TG2 to the surface of CF airway epithelial cells and upon externalisation TG2 dissociates into the ECM. Thus, an examination of TG2 activity was needed to confirm that TG2 retains its functionality once separated from EVs. Consequently, extracellular soluble protein was isolated from the secretomes of C38 and IB3 cells and TG2 activity measured using a transglutaminase activity assay.

C38 and IB3 cells were cultured for 72 h, before the cell secretomes were collected and ran through a qEVoriginal/70 nm SEC column. The purified soluble protein fraction of each sample was recovered and concentrated using Amicon® ultra-0.5 ml centrifugal filter units. The TG2 activity of soluble protein isolates was then quantified using a transglutaminase activity assay. A negative control of recombinant human TG2 in the absence of Ca^{2+} and presence of EDTA, was used as a reference of null transglutaminase activity. The level of TG2 activity in the extracellular soluble protein isolate of the C38 cell secretome was found to be negligible (Figure 5.13). Conversely, a significant level of TG2 activity ($p<0.01$) was detected in the extracellular soluble protein isolate of the IB3 cell secretome.

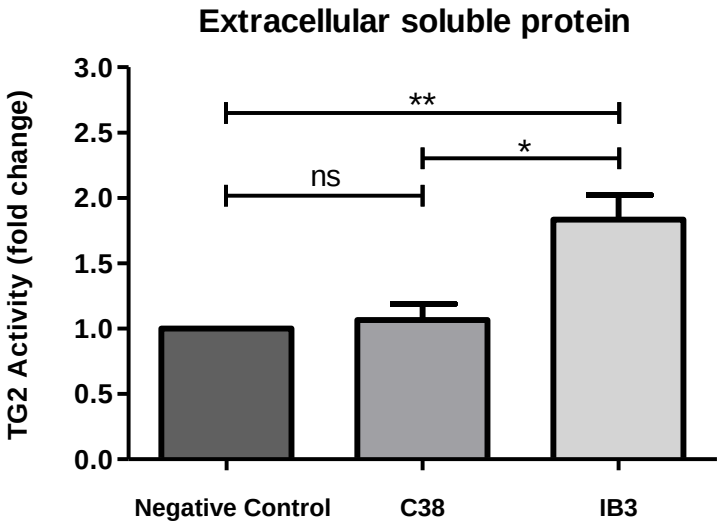

Figure 5.13. Quantification of TG2 activity for C38 and IB3 cell derived extracellular soluble protein isolates using a transglutaminase activity assay. C38 and IB3 cells were grown for 72 h and the cell secretomes collected. Cell secretomes were pre-processed via centrifugation, with recovered supernatants loaded separately on to a qEVoriginal/70 nm SEC column. Samples were eluted from the column and isolated soluble protein fractions collected. Purified soluble protein isolates were concentrated in volume using Amicon® ultra-0.5 ml centrifugal filter units, before the protein concentration of soluble protein isolates was measured using a DC™ Protein Assay kit. Biotin-cadaverine incorporation into N,N-dimethylcasein was used as a quantitative measure of TG2 activity, with soluble protein isolates tested at equal protein concentrations. A negative control of recombinant human TG2 (400 ng) with the addition of EDTA (10 mM) and in the absence of Ca^{2+} was used. Data expressed as the mean fold change ± SEM in comparison to the negative control. Statistical analysis of three independent experiments (N=3) using a one-way ANOVA, with a post-hoc Tukey test; ns, not significant, *P<0.05, **P<0.01.

5.3.14 Characterisation of IB3 cell derived EVs after CFTR corrector and TG2 inhibitor treatment

A disparity exists between the biophysical properties of C38 and IB3 cell derived EV populations. As evidenced in Figure 5.6, IB3 cells secrete a significantly higher concertation of EVs, which are on average 30 nm smaller in particle diameter, compared to C38 cell derived EVs. This variation was found to be a consequence of IB3 cells producing increased levels of exosomes (Figure 5.7 C). For this reason, EV production was measured in response to IB3 cell treatment. An NP100 (EV detectable size range of ~50 - 330 nm) was used to examine EVs, principally in the exosomal size range. The concentration, mean particle diameter and total surface area of EV populations were all analysed to give a comprehensive overview of biophysical variances.

IB3 cells were treated with either VX-809 (2.5 µM), 1-155 (2.5 µM) or VX-809 (2.5 µM) and 1-155 (2.5 µM) for 72 h, before the cell secretomes were collected and ran through a qEVoriginal/70 nm SEC column. Purified EVs were recovered and analysed using TRPS, via an NP100. As shown in Figure 5.14 A, EV concentration was reduced across all treatment conditions, in comparison to untreated IB3 cells. Yet, the decrease was only seen to be significant for IB3 cells treated with VX-809 and 1-155 ($p<0.05$). Moreover, an increase was observed in the mean particle diameter of EVs secreted by IB3 cells treated with 1-155 or VX-809 and 1-155, compared to untreated IB3 cells (Figure 5.14 B). However, changes failed to reach statistical significance. Further to this, the total surface area of EV populations derived from IB3 cells treated with VX-809 ($p<0.05$) or VX-809 and 1-155 ($p<0.05$) was significantly decreased, in comparison to untreated IB3 cells (Figure 5.14C).

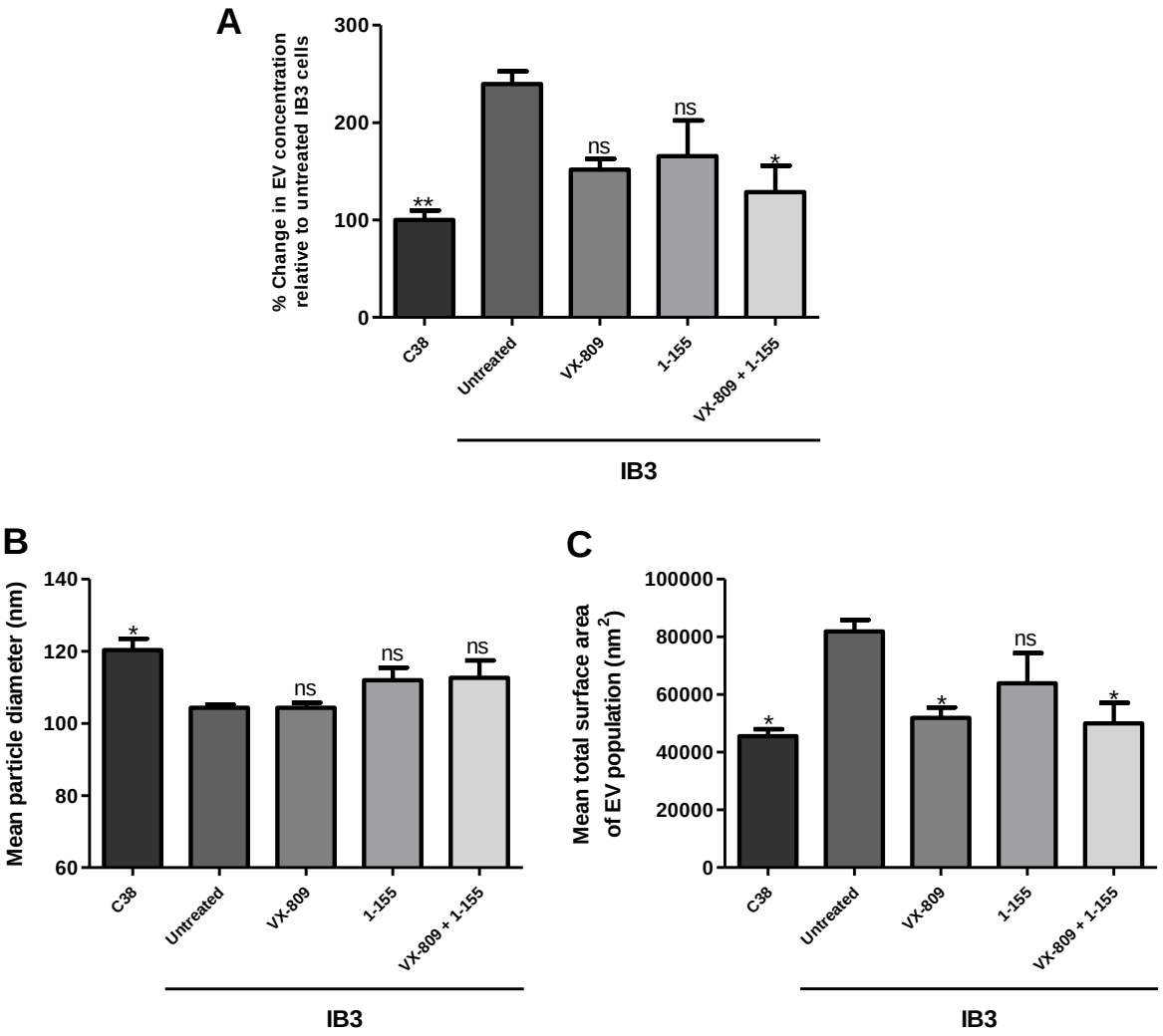

Figure 5.14. Quantification of the concentration, mean particle diameter and total surface area of IB3 cell derived EV populations following treatment with VX-809 and 1-155 alone or in combination. IB3 cells were treated with VX-809 (2.5 µM), 1-155 (2.5 µM) or VX-809 (2.5 µM) and 1-155 (2.5 µM) for 72 h, with treatments changed every 24 h. Cell secretomes were collected and pre-processed via centrifugation, with recovered supernatants loaded separately on to a qEVoriginal/70 nm SEC column. Samples were eluted from the column and EV fractions collected. The **(A)** concentration and **(B)** mean particle diameter of purified EV populations were measured using TRPS (NP100). Data analysis was performed using the IZON control suite software. **(C)** Total surface area of EV populations was calculated using the equation ($4\pi r^2$), with values adjusted for EV concentration. Data expressed as the mean ± SEM of three independent experiments (N=3), in comparison to untreated IB3 cells. Statistical analysis performed using a one-way ANOVA, with a post-hoc Tukey test; ns, not significant, **P*<0.05, ***P*<0.01.

5.3.15 Evaluating the size distribution profiles of EV populations in response to CFTR corrector and TG2 inhibitor treatment

As determined in Figure 5.10, IB3 cells secrete EVs highly enriched in TG2. Furthermore, IB3 cells produce greater levels of exosomes, in comparison to C38 cells (Figure 5.7 C). Taken together, this data indicates that an unconventional exosomal pathway may be used by IB3 cells, for increased export of TG2 into the extracellular environment. As previously demonstrated in Figure 5.14 A, combined treatment of IB3 cells with VX-809 and 1-155 caused a significant decrease in EV secretion. As such, the size distribution of EV populations was investigated, to assess whether combination treatment impacts the secretion of exosomes specifically.

IB3 cells were treated with either VX-809 (2.5 µM), 1-155 (2.5 µM) or VX-809 (2.5 µM) and 1-155 (2.5 µM) for 72 h, before the cell secretomes were collected and ran through a qEVoriginal/70 nm SEC column. Purified EVs were recovered and analysed using TRPS, via an NP100. Significant decreases in EV concentration were measured across all treatment conditions ($p<0.001$) between the particle size range of 60–119 nm, in comparison to untreated IB3 cells (Figure 5.15). Further to this, IB3 cells treated with VX-809 and 1-155 ($p<0.001$) exhibited a significant reduction in EV concentration between the particle size range of 80–99 nm, compared to IB3 cells treated with either VX-809 or 1-155 alone.

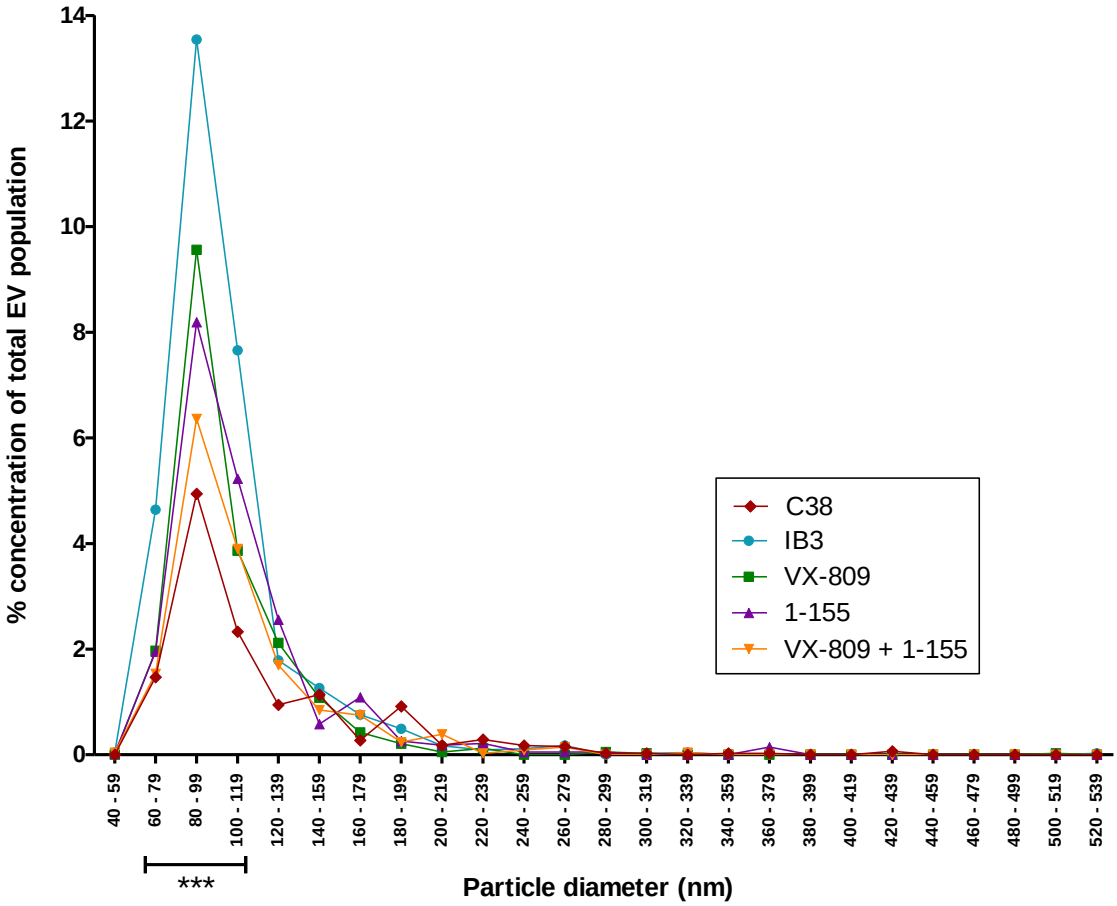

Figure 5.15. Quantification of the size distribution of IB3 cell derived EV populations following treatment with VX-809 and 1-155 alone or in combination. IB3 cells were treated with VX-809 (2.5 µM), 1-155 (2.5 µM) or VX-809 (2.5 µM) and 1-155 (2.5 µM) for 72 h, with treatments changed every 24 h. Cell secretomes were collected and pre-processed via centrifugation, with recovered supernatants loaded separately on to a qEVoriginal/70 nm SEC column. Samples were eluted from the column and EV fractions collected. The size distribution of purified EV populations was measured using TRPS (NP100). Data analysis was performed using the IZON control suite software. Data expressed as the mean of three independent experiments (N=3). Statistical analysis performed using a two-way ANOVA, with a post-hoc Bonferroni multiple comparison test; ***P<0.001.

5.4 Discussion

For several years, EVs were not considered to be of biological importance and were deemed nothing more than a cellular waste removal system (Cocucci et al., 2009). Yet, over the last decade EVs have become recognised as a crucial mechanism of intercellular communication, functioning as carriers of biologically active cargo (Margolis and Sadovsky, 2019). Consequently, research in the field of EVs has expanded dramatically and the tools used for both isolation and measurement of EVs has greatly improved. This has led to the classification of EVs into three distinct subtypes, comprising exosomes, microvesicles and apoptotic bodies. It is in fact the smaller, endosomal derived exosomes which have now been linked to the externalisation of TG2 in a kidney fibrosis model (Furini et al., 2018). Although an exciting discovery, the research is novel and requires further validation in other fibrotic systems. Thus, this chapter aims to investigate the role of EVs in the cellular export of TG2, from CF bronchial epithelial cells.

Data within chapter 4 has demonstrated that IB3 cells overexpress TG2 and fibronectin, which can be reversed via combination treatment with VX-809 and 1-155. However, the pathogenesis of fibrosis mainly centres around the increased externalisation of TG2 and its associated fibrotic remodelling of the ECM. In this chapter, it was revealed that VX-809 and 1-155 can also reduce the deposition of TG2 and fibronectin, specifically in the extracellular environment of IB3 cells. These findings suggest that combination treatment has the capacity to attenuate fibrotic alterations of the ECM in CF airways. Moreover, the use of VX-809 with a cell impermeable TG2 inhibitor (R281) was found to have a comparable effect, as seen with 1-155. This again reaffirms the significance of extracellular TG2 activity in CF and its role in promoting fibrosis. In addition, the treatment of IB3 cells with R281 was found to decrease the protein expression of TGFβ1 in the ECM. The impact of extracellular TG2 inhibition on matrix TGFβ1 levels, further validates the existence of a positive feedback loop between the two proteins in CF airway epithelial cells.

As discussed, the use of VX-809 and R281 attenuates TG2 and TGFβ1 protein levels, in the matrix of IB3 cells. Thus, it may be plausible that combination treatment acts by restricting the vicious self-reinforcing loop of: TG2-mediated activation of TGFβ1 in the ECM, TGFβ1 signal transduction and the increased synthesis / export of TG2. As such, the overall pro-fibrotic capacity of the cell secretome would be expected to be diminished, following the treatment of IB3 cells with VX-809 and 1-155. Indeed, C38 cells cultured in the cell secretome of treated IB3 cells showed reduced cell migration levels, in comparison to C38 cells cultured in the secretome of untreated IB3 cells (4 h and 16h). This is the first study to demonstrate that use of either VX-809 or 1-155, can impact the release of pro-fibrotic paracrine soluble factors, from CF airway epithelial cells. However, it cannot be ruled out that a residual presence of the compounds remained in the cell secretome after its transfer to C38 cells. Yet, it would be unlikely for 1-155 to elicit such a response, as TG2 inhibition has previously been shown to have no effect on the cell migration levels of C38 cells (Nyabam et al., 2016).

With a prominent role discerned for extracellular TG2 activity in CF, a workflow strategy was designed to investigate the mechanism of its externalisation. The first step was to optimise a reliable method for isolating and recovering EVs with preserved biofunctionality. This was crucial as TG2 is potentially associated with the cell surface of EVs (Furini et al., 2018). Multiple isolation techniques exist, yet SEC was chosen as the most suitable method. In fact, a recent review comparing six different exosomal isolation methods found SEC to be the optimal choice, with SEC yielding a high recovery rate of pure and functionally intact exosomes (Sidhom et al., 2020). Preliminary optimisation of SEC demonstrated that EVs could be accurately isolated from extracellular soluble protein. Intriguingly, the IB3 cell secretome was seen to exhibit a large peak in protein concentration within the EV elution zone, compared to C38 cell secretome. This is often indicative of a higher level of EV associated proteins (e.g. TG2), although the increased concentration of EVs cannot be excluded as a possible factor.

With SEC optimisation complete, differences in the biophysical characteristics of C38 and IB3 cell derived EV populations were analysed using TRPS. It was shown that a shift in the production of EV subtype occurs, with IB3 cells releasing significantly higher concentrations of exosomes, compared to C38 cells which release more microvesicles. This fits with the hypothesis that exosome release is involved in the export of TG2 from CF epithelial cells. However, it must also be acknowledged that TRPS measures particles and not EVs exclusively. Lipoprotein particles are lipid-enriched, non-vesicular structures which predominantly exist around the smaller size range of EVs (Mathieu et al., 2019). Thus, it is only assumed that these data reflect changes in EV concentration and not lipoprotein particle concentration. Nevertheless, SEC has been proven to perform relatively well in separating EVs from contaminating lipoprotein particles in a recent investigation (Brennan et al., 2020). Furthermore, the use of 70 nm cut-off SEC columns in this study, likely excludes most of the smaller sized lipoprotein particles (e.g. LDL and HDL), albeit larger lipoprotein particles (e.g. VLDL and chylomicrons) may still remain.

C38 and IB3 cell derived secretomes were subsequently analysed, to test for variances in the protein content of EV populations and extracellular soluble protein. It was shown that IB3 cell derived EVs are significantly enriched in protein, compared to C38 cell derived EVs. A slight increase in extracellular soluble protein concentration was also measured in the IB3 cell secretome compared to C38 cell secretome. Importantly, the protein concentration of both EVs and extracellular soluble protein was found to be considerably lower in AEM, thereby confirming that observed differences were dependent upon cellular activity. Therefore, these findings could potentially indicate that IB3 cells produce EVs loaded with protein cargo, which is then released into the extracellular environment.

To determine whether increased TG2 export might be partially responsible for these differences in protein concentration, both EVs and extracellular soluble protein were measured for TG2 protein levels. Remarkably, TG2 protein expression was found to be upregulated in both IB3 cell derived EVs and extracellular soluble protein fractions.

Moreover, the quantification of TG2 activity in both fractions, served to further validate these findings. These data support the current literature which links the mechanism of TG2 secretion to EV transport (Furini et al., 2018; Shinde et al., 2020) and is the first study to show this in the context of CF. In addition, these results indicate that even in association with EVs, TG2 retains its enzymatic activity when stimulated under the appropriate conditions. As regards the transglutaminase activity assay, EVs are predicted to remain largely intact throughout the experimental process, which suggests that TG2 is present on the surface of EVs. This would support previous observations by Furini et al. (2018). As expected, no TG2 expression or activity was detected in the EV-free AEM.

Although, TG2 expression was not measured in separate EV subtypes, exosomes were previously found to be significantly increased in the secretome of IB3 cells. Indeed, data from the literature also reports the involvement of exosomes in cellular TG2 export (Diaz-Hidalgo et al., 2016; Furini et al., 2018; Shinde et al., 2020). As such, it is highly likely that TG2 is externalised by exosomes in CF bronchial epithelial cells. Therefore, it would be anticipated that combination treatment acts to either reduce the loading of TG2 into exosomes or limit the release of exosomes themselves. To test the latter, IB3 cells were treated with VX-809 and 1-155 alone or in combination and their respective EV populations characterised using TRPS. An NP100 (EV detectable size range of ~50 - 330 nm) was used for analysis, to focus primarily on exosomal changes. It was determined that all treatments could reduce the concentration of IB3 cell derived EVs, although only with VX-809 and 1-155 combined, was the change found to be significant. Moreover, both the use of 1-155 and combination treatment increased the mean particle diameter of EVs, albeit without reaching statistical significance. Interestingly, the mean particle diameter of IB3 cell derived EVs did not vary with the use of VX-809. This possibly suggests that VX-809 causes less exosomes to be released, while 1-155 induces a switch towards microvesicle production, with combination treatment operating through a dual effect. This is an intriguing dynamic and may explain why an additive therapeutic effect is seen when using VX-809 and 1-155 in

combination. Indeed, it could be expected that combination treatment utilises both routes to fully abrogate exosomal associated export of TG2 from IB3 cells. In support of this hypothesis, a significant decrease in exosomal sized EVs ranging from (60 - 119 nm) was seen in response to all treatments. Notably, both VX-809 and 1-155 were shown to reduce the concentration of these exosomes to similar levels, while combination treatment was demonstrated to have a more substantial effect. These novel findings are very fascinating and clearly warrants further investigation.

In conclusion, this chapter has shown that the externalisation and activity of extracellular TG2, is integral to increased deposition of fibronectin and TGFβ1 in the ECM of CF bronchial epithelial cells. Furthermore, the cell secretome of IB3 cells was found to express pro-fibrotic paracrine soluble factors, which could increase cell migration levels of C38 cells. Strikingly, the pro-fibrotic capacity of the IB3 cell secretome was found to be diminished, after the treatment of IB3 cells with VX-809 and 1-155. Characterisation of C38 and IB3 cell derived EVs highlighted disparities between EV populations, with IB3 cells releasing more exosomes and C38 cells releasing increased levels of microvesicles. Furthermore, IB3 cells were seen to generate EVs with a higher protein content, compared to C38 cells. This may be explained by the fact that IB3 cells were found to secrete EVs enriched in TG2. Similarly, enhanced levels of TG2 were also detected in the extracellular soluble protein isolates of IB3 cells. These findings were further supported by the measurement of increased TG2 activity, within both EV and extracellular soluble protein fractions of the IB3 cell secretome. Ultimately, the treatment of IB3 cells with VX-809 or 1-155 was shown to partially reduce increases in exosome secretion, with combination treatment seen to largely reverse these changes entirely.

Chapter 6

Discussion and Future work

CHAPTER 6: DISCUSSION AND FUTURE WORK

6.1 Discussion

Over the past decade, the landscape of CF treatment has changed dramatically with the development of CFTR modulators. The first major breakthrough came in 2011, with a successful phase III trial of Ivacaftor (VX-770) (Ramsey et al., 2011). This pharmacological potentiator had been shown to increase the activity of a defective CFTR and improve the clinical outcome for CF patients carrying at least one G551D mutation. Since then, the development of CFTR modulators has advanced rapidly. First came the introduction of Lumacaftor (VX-809), a CFTR corrector designed to traffic ΔF508 CFTR to the cell surface (Clancy et al., 2012). This subsequently led to the creation of next-generation CFTR correctors and the concept of triple combination therapy (e.g. Kaftrio) (Taylor-Cousar et al., 2019). Undoubtedly, this switch from symptomatic management to CFTR directed precision medicine has helped revolutionise CF treatment, yet it may only be part of the answer.

Continued research of the most common *CFTR* mutation, ΔF508, has led to a better understanding of the key cellular mechanisms disrupted as a consequence of this CFTR defect. It is now recognised that the proteostasis network within CF airway epithelial cells, is severely perturbed (Bodas and Vij, 2019). This suggests that the absence of functional CFTR at the plasma membrane has a wider impact, than the mere loss of its chloride transport. Thus, currently approved CF drugs may be restricted in their effectiveness, as these compounds all target CFTR exclusively. Alternatively, compounds which correct the proteostasis network may provide a complementary therapeutic strategy and one which can be conveniently combined with approved CFTR modulators.

It has previously been revealed that TG2 is integral to changes in the proteostasis network of CF airway epithelial cells (Maiuri et al., 2008; Luciani et al., 2009, 2011). Indeed, TG2 overexpression was recently linked to increases in TGFβ1 levels and EMT induction in CF IB3 cells (Nyabam et al., 2016). This study has attempted to expand upon the initial findings

of that research by further examining the role of TG2 in CF progression, specifically the significance of its extracellular activity. In addition, TG2 was evaluated as a potential therapeutic target in CF, which was assessed using a potent and selective inhibitor of TG2 (1-155). Finally, this study aimed to unravel the mechanism of TG2 externalisation from CF bronchial epithelial cells.

The data presented in chapter 3 are in agreement with the findings by Nyabam et al. (2016), which links increased TG2 protein levels to EMT progression in CF airway epithelial cells. However, the additional characterisation of IB3 cells conducted in this study, has revealed that EMT induction may actually reflect the process of EMT-derived myofibroblast transdifferentiation. Along with the increased protein expression of fibronectin and N-cadherin (mesenchymal markers), IB3 cells were also shown to exhibit high levels of the myofibroblast marker, α-SMA. However, from these data alone it cannot be determined what percentage of epithelial cells undergo EMT or indeed the proportion of those EMT derived cells which transdifferentiate into myofibroblasts. Furthermore, the existence of EMT-derived myofibroblast transdifferentiation in fibrosis is still hotly debated. Several studies have provided conflicting evidence of its absence or presence in fibrotic model systems (Willis et al., 2006; Wu et al., 2007; Humphreys et al., 2010; Rock et al., 2011). It has even been suggested that EMT instead promotes a pro-fibrotic microenvironment for fibroblast-myofibroblast differentiation, while not directly contributing towards the myofibroblast population itself (Hill et al., 2019). Thus, it cannot be ruled out that the EMT-derived myofibroblast transdifferentiation observed in this study, is possibly a feature of *in vitro* cell culture and / or the use of immortalised CF epithelial cells.

It was also shown that TG2 and fibronectin protein levels were elevated in a co-localised manner, within the ECM of IB3 cells. Although this has been well documented in other fibrotic diseases, this is the first study to show this in the context of CF. This may indicate that the increased cellular export of TG2, leads to the enhanced matrix deposition of fibronectin. It has been demonstrated before that this can occur via TG2-mediated

crosslinking of fibronectin (Philp et al., 2018) or through a non-enzymatic binding interaction between the two proteins (S. S. Akimov and Belkin, 2001). Further investigation would be needed to discern the mechanism(s) by which this takes place in CF. In relation to these changes, myofibroblasts are also found to secrete ECM components (e.g. fibronectin) in fibrosis (Klingberg et al., 2013). Taken together, these findings suggest that both the increased externalisation of TG2 and EMT-derived myofibroblast transdifferentiation of airway epithelial cells, leads to fibrotic remodelling of the ECM in CF (Figure 6.1).

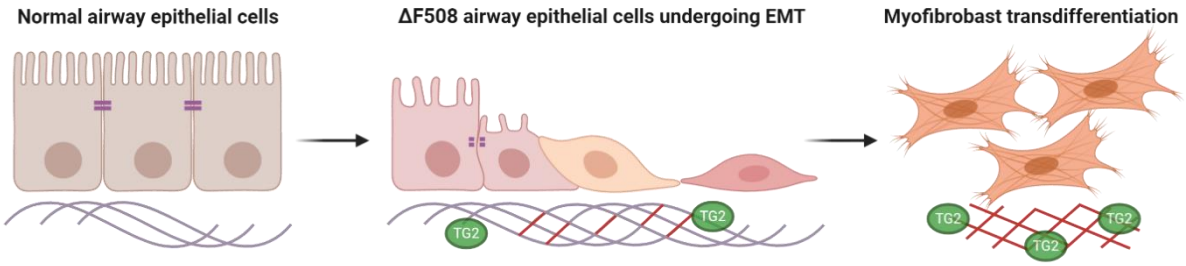

Figure 6.1. The pathogenic processes associated with fibrotic remodelling of the ECM in CF. Normal airway epithelial cells form a structured barrier and maintain a well-organised ECM. By contrast, ΔF508 airway epithelial cells undergo EMT-derived myofibroblast transdifferentiation and externalise high levels of TG2. Both processes can contribute to the increased deposition of ECM components (e.g. fibronectin), which leads to a stiffened and fibrotic matrix in CF airways.

One of the strengths of this study is the use of CF primary HBECs, which provided a more physiologically relevant model system for investigation. In support of IB3 cell studies, the co-localised overexpression of TG2 and fibronectin was also detected in the ECM of CF primary HBECs. Furthermore, CF primary HBECs were demonstrated to exhibit varying levels of EMT progression. Interestingly, this may reflect the existence of partial EMT in CF. This would seem logical, as EMT is recognised as an extremely dynamic process (Fintha et al., 2019). These data may also suggest that the level of EMT progression is linked to the extent of tissue fibrosis. Indeed, 032 cells showed both the highest level of EMT and the greatest matrix deposition of TG2 and fibronectin. Further research would be needed to confirm this, although the same observation has previously been made in another study, which identified EMT intensity as a predictive marker of renal allograft fibrosis levels (Hertig et al., 2008). Overall, it is becoming increasingly evident that EMT participates in tissue

fibrosis. Yet, a major consideration of *in vitro* experiments, is the degree to which tissue culture plasticware influences EMT progression in cells.

Proof of concept experiments examining the effectiveness of two-directional combination treatment (CFTR corrector with a selective TG2 inhibitor), demonstrated a roughly additive therapeutic response. This was evidenced by the combined decrease in TG2 protein levels / increase in TEER values, following the treatment of CF primary HBECs with VX-809 and 1-155 together. A more detailed investigation of two-directional pharmacotherapy using IB3 cells, further substantiated these findings. Interestingly, the exclusive inhibition of extracellular TG2 activity with R281, generated a comparable response as seen with 1-155. Given both the additive nature of combination treatment and the pathogenic significance of extracellular TG2 activity, it is quite possible that VX-809 and 1-155 reduce fibrosis via two alternative pathways.

Data within this study has also highlighted the functional relationship between extracellular TG2 and TGFβ1 in CF airway epithelial cells. Indeed, these results may help to explain the mechanism by which TG2 inhibition attenuates fibrotic changes in CF. It was revealed that a positive feedback loop exists between TG2 and TGFβ1 in IB3 cells, with TGFβ signal transduction operating via canonical and potentially non-canonical pathways. Thus, It is highly probable that the inhibition of extracellular TG2 activity restricts the matrix activation of TGFβ1 and its downstream signalling, which is a known promoter of TG2 transcription (Ritter and Davies, 1998). Subsequently, this would prevent the unabating cycle of TG2-TGFβ1 self-amplification and diminish the pro-fibrotic effects of extracellular TG2. Additional research would be required to assess the involvement of other non-canonical TGFβ pathways besides ERK (e.g. JNK pathway).

On the other hand, it is likely that VX-809 effectuates its response via an intracellular mechanism. It has previously been reported in the literature that the subsistence of ΔF508 CFTR, induces oxidative stress within CF airway epithelial cells (Luciani et al., 2009). This increased generation of ROS results in the SUMOylation of TG2, which prevents its

ubiquitination and therefore its proteasomal degradation (Esposito et al., 2016). Ultimately, this leads to the accumulation of cytosolic TG2. As a result, the treatment of CF airway epithelial cells with VX-809 may circumvent this process, by correcting ΔF508 CFTR and alleviating oxidative stress. Thus, it is plausible that both VX-809 and 1-155 collectively suppress TG2 overexpression in CF, via two separate routes of intracellular and extracellular origin, respectively. However, further investigation would be needed to confirm this hypothesis.

Although these findings are promising, some important questions remain as regards the feasibility of combination treatment. As previously mentioned, the concept of TG2 inhibition has already been tested in CF, with the use of a non-robust pan transglutaminase inhibitor, cysteamine (Tosco et al., 2016). Yet, an open-label trial assessing the tolerability of cysteamine in CF patients, reported adverse reactions for 70% of the participants (Devereux et al., 2016). This may have been due to non-specific off-target effects by cysteamine, or was potentially an outcome of TG2 inhibition. Hence, it is important that the safety and efficacy of 1-155 is evaluated in a clinical setting, along with the impact of intersubject variability. Furthermore, since the start of this study, the development of CFTR modulators has advanced considerably. As a consequence, next-generation CFTR correctors like Elexacaftor, have now become available. As such, it would be pertinent to examine the use of 1-155 in combination with more recent CFTR correctors, to determine whether any additional benefits may be observed. Moreover, investigating the effect of a CFTR potentiator in combination with a CFTR corrector(s) and selective TG2 inhibitor, would also be of relevance. Finally, an important end-point measurement of CF treatment, is an improvement in the level of CFTR expression at the apical membrane and increased chloride transport. Interestingly, it has previously been established that 1-155 can increase the mature form of CFTR at the plasma membrane (Nyabam et al., 2016). Nevertheless, the effect of combination treatment (VX-809 and 1-155) on CFTR has not been addressed in this study and is therefore a crucial point of consideration for future studies.

The mechanism of cellular TG2 export has not previously been investigated in CF. Emerging evidence from the literature suggests that the cell surface trafficking of TG2 is mediated by EVs, specifically exosomes (Diaz-Hidalgo et al., 2016; Furini et al., 2018; Shinde et al., 2020). Data within chapter 5 supports these findings, identifying EV secretion as a key pathway for the externalisation of fibrogenic TG2 in CF. It was shown that IB3 cells secrete EVs with high levels of TG2 protein expression and activity, in comparison to C38 cells. However, a limiting factor of this study and other research is the current methods of EV isolation. Although SEC is typically considered the best available option, contamination from lipoprotein particles still remains an issue. Recently developed techniques, may now improve the purity of EV isolates. For example, a new approach known as dual-mode chromatography, integrates SEC and cation exchange (Van Deun et al., 2020). Cation exchange is incorporated alongside SEC to segregate positively charged lipoprotein particles, from negatively charged EVs. Hence, this technique could be used in future research, to enhance the accuracy of EV analytical studies.

The biophysical characterisation of C38 and IB3 cell derived EV populations, has elucidated the pathogenic importance of exosome synthesis in CF. It was demonstrated that IB3 cells release higher concentrations of exosomal sized EVs, compared to C38 cells which release more microvesicle sized EVs. Considering that TG2 was found to be only associated with IB3 cell derived EVs, it is not unreasonable to assume that exosomes are involved in the export of TG2 from CF airway epithelial cells. In support of this hypothesis, the treatment of IB3 cells with VX-809 and 1-155 combined, was found to completely reverse this increase in exosome secretion. Correspondingly, combination treatment also attenuates TG2 overexpression in the ECM of IB3 cells, which suggests that TG2 externalisation is linked to the release of exosomes. Interestingly, VX-809 and 1-155 seemed to influence exosomal secretion via two separate mechanisms. This observation reinforces the notion that both compounds act independently to reduce cellular TG2 export and may actually reflect their differing mechanisms of action, as discussed previously. Finally, these data are in

agreement with the findings by Furini et al. (2018), which identified exosome-mediated transport of TG2 in a kidney fibrosis model. As a result, this may suggest that TG2 exosomal secretion is a conserved pathway in the pathogenesis of tissue fibrosis.

Despite the novel outcomes of this research, there a few considerations which need to be addressed. As alluded to in the introduction, EVs are a heterogenous population of cell-derived membranous particles, in which different EV subtypes exhibit similar compositions and overlapping sizes (Van Niel et al., 2018). Thus, the quantification of size only functions as a crude marker of EV subtype and cannot be used to definitively characterise changes. However, in this study size was used to provide a general insight into EV population shifts, with regard to the proportion of exosomal and microvesicle sized EVs. At present, common definitions of EV subtypes still rely on size and this will undoubtedly evolve with the development of the EV field (Margolis and Sadovsky, 2019). Furthermore, the cellular export of TG2 has often been found to be dependent upon its interaction with syndecan-4 (Verderio et al., 2009; Scarpellini et al., 2014; Furini et al., 2018). In future studies, it would be interesting to knockout syndecan-4 in CF airway epithelial cells and investigate subsequent changes in exosome secretion and TG2 externalisation.

In conclusion, this study has established a better understanding of the molecular mechanisms underlying TG2-mediated fibrotic changes, in CF airway epithelial cells. It has been demonstrated that these pathogenic alterations depend exclusively on the cellular export of TG2 to the extracellular environment, which likely occurs via the unconventional pathway of exosome secretion. Following the externalisation of TG2, an excessive deposition of fibronectin was measured in the matrix, alongside the increased activation of TGFβ1. It was revealed that TGFβ signal transduction occurs via canonical (Smad) and potentially non-canonical (ERK) pathways in CF. This upregulation in TGFβ signalling was shown to result in the formation of a vicious self-reinforcing feedback loop between TG2 and TGFβ1, which functions as a major driver of EMT-derived myofibroblast transdifferentiation. Ultimately, the inherent persistence of this deleterious cycle, leads to

accumulation of fibrous ECM components and the development of fibrosis in CF airways. Whether this is a common pathogenic feature of all *CFTR* mutations, will still need to be determined. Furthermore, this study has identified a novel therapeutic strategy of two-directional pharmacotherapy, for the treatment of CF. These data reveal for the first time the potential of using a TG2 specific inhibitor in combination with a CFTR corrector, to neutralise the pro-fibrotic sequence of events described above (Figure 6.2).

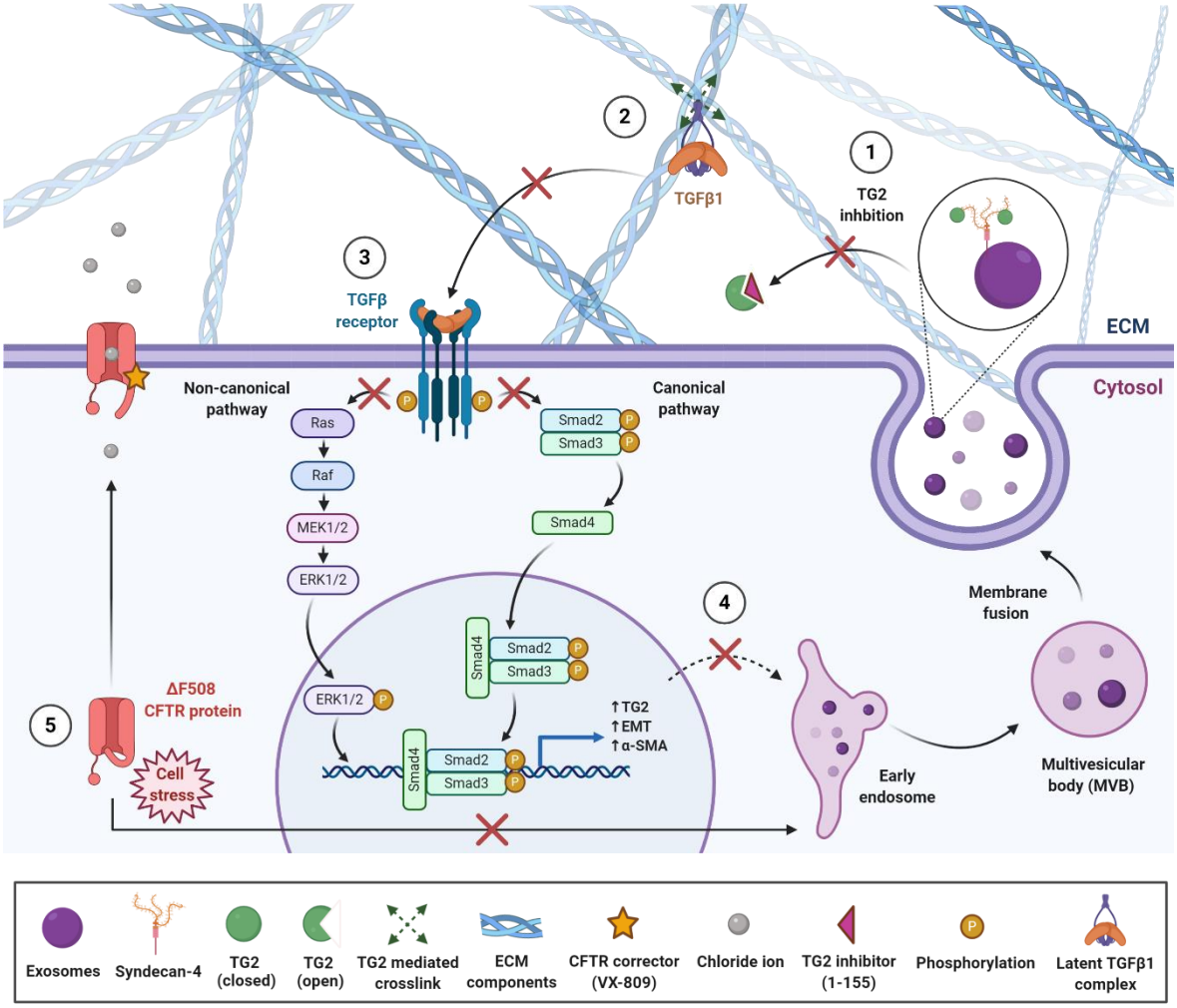

Figure 6.2. The proposed mechanism of two-directional pharmacotherapy in (ΔF508) CF bronchial epithelial cells. The application of an approved CFTR corrector (VX-809) in combination with a TG2 specific inhibitor (1-155), has been proven to negate TG2-mediated fibrotic changes in (ΔF508) CF bronchial epithelial cells. ① TG2 is exported from the cell via an unconventional pathway involving exosomes. Once in the ECM, TG2 adopts an open/active conformation, whereby its active site is impeded by the use of a TG2 inhibitor, 1-155. ② This subsequently prevents TG2-mediated crosslinking of the latent TGFβ1 complex into the ECM. ③ As a result, TGFβ1 is not released and intracellular signal transduction of the downstream canonical (Smad) and non-canonical (ERK) pathways, does not take place. ④ This precludes an upregulation in the expression of TG2, α-SMA and EMT associated proteins. ⑤ In parallel, VX-809 traffics ΔF508 CFTR to the plasma membrane, which alleviates oxidative stress and reduces the accumulation of cytosolic TG2.

6.2 Future work

To further expand upon the findings of this study, future research could focus on the following areas of investigation:

- Examine CF bronchial epithelial cells with *CFTR* mutations besides ΔF508, to determine whether TG2-mediated fibrotic alterations are common feature of all *CFTR* variants or potentially linked to a particular functional class(es) of CFTR defect.

- Continue with the evaluation of two-directional pharmacotherapy by testing the efficacy and safety of combination treatment (VX-809 and 1-155) in a CF animal model. This will be used to assess the viability of progressing combination treatment towards human clinical trials.

- Investigate the underlying molecular mechanisms controlling the attenuation of TG2 externalisation from IB3 cells, following treatment with VX-809. To then evaluate the impact of other approved CFTR modulators, in combination with VX-809 and 1-155.

- To determine the effect of combination treatment (VX-809 and 1-155) on the apical expression of CFTR at the plasma membrane and the level of chloride transport, in CF primary HBECs.

- To perform cryo-electron microscopy on secretome samples after SEC, to assess the purity of EV isolates.

- Isolate exosomes and microvesicles separately from IB3 cell derived EV populations. To then comparatively analyse the level of involvement of both EV subtypes, as regards the externalisation of TG2 from CF airway epithelial cells.

- To knockout syndecan-4 from CF primary HBECs using syndecan-4 targeting siRNA and then examine the effect on TG2 expression in exosomes and microvesicles, which have been isolated from the cell secretome.

References

Ablin, R.J., Owen, S., Jiang, W.G., 2017. Prostate transglutaminase (TGase-4) induces epithelialto-mesenchymal transition in prostate cancer cells. Anticancer Res. 37, 481–488.

Aeschlimann, D., Mosher, D., Paulsson, M., 1996. Tissue transglutaminase and factor XIII in cartilage and bone remodeling. Semin Thromb Hemost. 22, 437–443.

Aeschlimann, D., Thomazy, V., 2000. Protein crosslinking in assembly and remodelling of extracellular matrices: The role of transglutaminases. Connect Tissue Res. 41, 1–27.

Ahvazi, B., Kim, H.C., Kee, S.H., Nemes, Z., Steinert, P.M., 2002. Three-dimensional structure of the human transglutaminase 3 enzyme: Binding of calcium ions changes structure for activation. EMBO J. 21, 2055–2067.

Ai, L., Skehan, R.R., Saydi, J., Lin, T., Brown, K.D., 2012. Ataxia-telangiectasia, mutated (ATM)/nuclear factor κ light chain enhancer of activated B cells (NFκB) signaling controls basal and DNA damage-induced transglutaminase 2 expression. J. Biol Chem. 287, 18330–18341.

Akhurst, R.J., Hata, A., 2012. Targeting the TGFβ signalling pathway in disease. Nat Rev Drug Discov. 11, 790–811.

Akimov, Sergey S., Belkin, A.M., 2001. Cell surface tissue transglutaminase is involved in adhesion and migration of monocytic cells on fibronectin. Blood. 98, 1567–1576.

Akimov, S. S., Belkin, A.M., 2001. Cell-surface transglutaminase promotes fibronectin assembly via interaction with the gelatin-binding domain of fibronectin: A role in TGF-β-dependent matrix deposition. J. Cell Sci. 114, 2989–3000.

Akimov, S.S., Krylov, D., Fleischmana, L.F., Belkin, A.M., 2000. Tissue transglutaminase is an integrin-binding adhesion coreceptor for fibronectin. J. Cell Biol. 148, 825–838.

Alton, E.W.F.W., Boyd, A.C., Davies, J.C., Gill, D.R., Griesenbach, U., Harrison, P.T., Henig, N., Higgins, T., Hyde, S.C., Innes, J.A., Korman, M.S.D., 2016. Genetic medicines for CF: Hype versus reality. Pediatr Pulmonol. 51, S5–S17.

Amaral, M.D., 2015. Novel personalized therapies for cystic fibrosis: Treating the basic defect in all patients. J. Intern Med. 277, 155–166.

Amaral, M.D., Quaresma, M.C., Pankonien, I., 2020. What role does cftr play in development, differentiation, regeneration and cancer? Int J. Mol Sci. 21, 3133.

Ameen, N.A., Marino, C., Salas, P.J.I., 2003. cAMP-dependent exocytosis and vesicle traffic regulate CFTR and fluid transport in rat jejunum in vivo. Am J. Physiol. 284, 429–438.

Antonyak, M.A., Li, B., Boroughs, L.K., Johnson, J.L., Druso, J.E., Bryant, K.L., Holowka, D.A., Cerione, R.A., 2011. Cancer cell-derived microvesicles induce transformation by transferring tissue transglutaminase and fibronectin to recipient cells. Proc Natl Acad Sci USA. 108, 4852–4857.

Arenaccio, C., Chiozzini, C., Columba-Cabezas, S., Manfredi, F., Affabris, E., Baur, A., Federico, M., 2014. Exosomes from Human Immunodeficiency Virus Type 1 (HIV-1)-

Infected Cells License Quiescent CD4 + T Lymphocytes To Replicate HIV-1 through a Nef- and ADAM17-Dependent Mechanism. J. Virol. 88, 11529–11539.

Awatade, N.T., Ramalho, S., Silva, I.A.L., Felício, V., Botelho, H.M., de Poel, E., Vonk, A., Beekman, J.M., Farinha, C.M., Amaral, M.D., 2019. R560S: A class II CFTR mutation that is not rescued by current modulators. J. Cyst Fibros. 18, 182–189.

Awatade, N.T., Uliyakina, I., Farinha, C.M., Clarke, L.A., Mendes, K., Solé, A., Pastor, J., Ramos, M.M., Amaral, M.D., 2015. Measurements of Functional Responses in Human Primary Lung Cells as a Basis for Personalized Therapy for Cystic Fibrosis. EBioMedicine. 2, 147–153.

Awatade, N.T., Wong, S.L., Hewson, C.K., Fawcett, L.K., Kicic, A., Jaffe, A., Waters, S.A., 2018. Human Primary Epithelial Cell Models: Promising Tools in the Era of Cystic Fibrosis Personalized Medicine. Front Pharmacol. 9, 1429.

Badarau, E., Wang, Z., Rathbone, D.L., Costanzi, A., Thibault, T., Murdoch, C.E., El Alaoui, S., Bartkeviciute, M., Griffin, M., 2015. Development of potent and selective tissue transglutaminase inhibitors: Their effect on TG2 function and application in pathological conditions. Chem Biol. 22, 1347–1361.

Baietti, M.F., Zhang, Z., Mortier, E., Melchior, A., Degeest, G., Geeraerts, A., Ivarsson, Y., Depoortere, F., Coomans, C., Vermeiren, E., Zimmermann, P., David, G., 2012. Syndecan-syntenin-ALIX regulates the biogenesis of exosomes. Nat Cell Biol. 14, 677–685.

Bartoszewski, R., Rab, A., Jurkuvenaite, A., Mazur, M., Wakefield, J., Collawn, J.F., Bebok, Z., 2008. Activation of the unfolded protein response by ΔF508 CFTR. Am J. Respir Cell Mol Biol. 39, 448–457.

Bear, C.E., Li, C., Kartner, N., Bridges, R.J., Jensen, T.J., Ramjeesingh, M., Riordan, J.R., 1992. Purification and functional reconstitution of the cystic fibrosis transmembrane conductance regulator (CFTR). Cell. 68, 809–818.

Benn, M.C., Weber, W., Klotzsch, E., Vogel, V., Pot, S.A., 2019. Tissue transglutaminase in fibrosis — more than an extracellular matrix cross-linker. Curr Opin Biomed Eng. 10, 156–164.

Biernacka, A., Dobaczewski, M., Frangogiannis, N.G., 2011. TGF-β signaling in fibrosis. Growth Factors. 29, 196–202.

Bochaton-Piallat, M.L., Gabbiani, G., Hinz, B., 2016. The myofibroblast in wound healing and fibrosis: Answered and unanswered questions. F1000Res. 5, 752.

Bodas, M., Vij, N., 2017. Augmenting autophagy for prognosis based intervention of COPD-pathophysiology. Respir Res. 18, 83.

Bodas, M., Vij, N., 2019. Adapting proteostasis and autophagy for controlling the pathogenesis of cystic fibrosis lung disease. Front Pharmacol. 10, 20.

Boyle, M.P., Bell, S.C., Konstan, M.W., McColley, S.A., Rowe, S.M., Rietschel, E., Huang, X., Waltz, D., Patel, N.R., Rodman, D., 2014. A CFTR corrector (lumacaftor) and a CFTR potentiator (ivacaftor) for treatment of patients with cystic fibrosis who have a phe508del CFTR mutation: A phase 2 randomised controlled trial. Lancet Respir Med. 2, 527–538.

Bozoky, Z., Krzeminski, M., Muhandiram, R., Birtley, J.R., Al-Zahrani, A., Thomas, P.J., Frizzell, R.A., Ford, R.C., Forman-Kay, J.D., 2013. Regulatory R region of the CFTR chloride channel is a dynamic integrator of phospho-dependent intra- and intermolecular interactions. Proc Natl Acad Sci USA. 110, 4427–4436.

Brennan, K., Martin, K., FitzGerald, S.P., O'Sullivan, J., Wu, Y., Blanco, A., Richardson, C., Mc Gee, M.M., 2020. A comparison of methods for the isolation and separation of extracellular vesicles from protein and lipid particles in human serum. Sci Rep. 10, 1039.

Brune, K., Frank, J., Schwingshackl, A., Finigan, J., Sidhaye, V.K., 2015. Pulmonary epithelial barrier function: Some new players and mechanisms. Am J. Physiol. 308, 731–745.

Burhan, I., Furini, G., Lortat-Jacob, H., Atobatele, A.G., Scarpellini, A., Schroeder, N., Atkinson, J., Maamra, M., Nutter, F.H., Watson, P., Vinciguerra, M., Johnson, T.S., Verderio, E.A.M., 2016. Interplay between transglutaminases and heparan sulphate in progressive renal scarring. Sci Rep. 6, 31343.

Buschmann, T., Fuchs, S.Y., Lee, C.G., Pan, Z.Q., Ronai, Z., 2000. SUMO-1 modification of Mdm2 prevents its self-ubiquitination and increases Mdm2 ability to ubiquitinate p53. Cell. 101, 753–762.

Buschow, S.I., Nolte-'t Hoen, E.N.M., van Niel, G., Pols, M.S., ten Broeke, T., Lauwen, M., Ossendorp, F., Melief, C.J.M., Raposo, G., Wubbolts, R., Wauben, M.H.M., Stoorvogel, W., 2009. MHC II In dendritic cells is targeted to lysosomes or t cell-induced exosomes via distinct multivesicular body pathways. Traffic. 10, 1528–1542.

Button, B., Cai, L.H., Ehre, C., Kesimer, M., Hill, D.B., Sheehan, J.K., Boucher, R.C., Rubinstein, M., 2012. A periciliary brush promotes the lung health by separating the mucus layer from airway epithelia. Science. 337, 937–941.

Callebaut, I., Hoffmann, B., Lehn, P., Mornon, J.P., 2017. Molecular modelling and molecular dynamics of CFTR. Cell Mol Life Sci. 74, 3–22.

Cao, L., Shao, M., Schilder, J., Guise, T., Mohammad, K.S., Matei, D., 2012. Tissue transglutaminase links TGF-B, epithelial to mesenchymal transition and a stem cell phenotype in ovarian cancer. Oncogene. 31, 2521–2534.

Carbone, A., Castellani, S., Favia, M., Diana, A., Paracchini, V., Di Gioia, S., Seia, M., Casavola, V., Colombo, C., Conese, M., 2014. Correction of defective CFTR/ENaC function and tightness of cystic fibrosis airway epithelium by amniotic mesenchymal stromal (stem) cells. J. Cell Mol Med. 18, 1631–1643.

Cardoso, I., Stamnaes, J., Andersen, J.T., Melino, G., Iversen, R., Sollid, L.M., 2015. Transglutaminase 2 interactions with extracellular matrix proteins as probed with celiac disease autoantibodies. FEBS J. 282, 2063–2075.

Castellani, S., Guerra, L., Favia, M., Di Gioia, S., Casavola, V., Conese, M., 2012. NHERF1 and CFTR restore tight junction organisation and function in cystic fibrosis airway epithelial cells: Role of ezrin and the RhoA/ROCK pathway. Lab Investig. 92, 1527–1540.

Chadli, L., Sotthewes, B., Li, K., Andersen, S.N., Cahir-McFarland, E., Cheung, M., Cullen, P., Dorjée, A., de Vries-Bouwstra, J.K., Huizinga, T.W.J., Fischer, D.F., DeGroot, J.,

Viney, J.L., Zheng, T.S., Aarbiou, J., Gardet, A., 2019. Identification of regulators of the myofibroblast phenotype of primary dermal fibroblasts from early diffuse systemic sclerosis patients. Sci Rep. 9, 4521.

Chang, F.C., Chou, Y.H., Chen, Y.T., Lin, S.L., 2012. Novel insights into pericyte-myofibroblast transition and therapeutic targets in renal fibrosis. J. Formos Med Assoc. 111, 589-598.

Chang, X.B., Mengos, A., Hou, Y.X., Cui, L., Jensen, T.J., Aleksandrov, A., Riordan, J.R., Gentzsch, M., 2008. Role of N-linked oligosaccharides in the biosynthetic processing of the cystic fibrosis membrane conductance regulator. J. Cell Sci. 121, 2814–2823.

Chappe, V., Hinkson, D.A., Howell, L.D., Evagelidis, A., Liao, J., Chang, X.B., Riordan, J.R., Hanrahan, J.W., 2004. Stimulatory and inhibitory protein kinase C consensus sequences regulate the cystic fibrosis transmembrane conductance regulator. Proc Natl Acad Sci USA. 101, 390–395.

Charras, G.T., Yarrow, J.C., Horton, M.A., Mahadevan, L., Mitchison, T.J., 2005. Non-equilibration of hydrostatic pressure in blebbing cells. Nature. 435, 365–369.

Chen, J.H., Shipston, M., 2020. Protein kinase A phosphorylation potentiates cystic fibrosis transmembrane conductance regulator gating by relieving autoinhibition on the stimulatory C terminus of the regulatory domain. J. Biol Chem. 295, 4577–4590.

Cheng, S.H., Gregory, R.J., Marshall, J., Paul, S., Souza, D.W., White, G.A., O'Riordan, C.R., Smith, A.E., 1990. Defective intracellular transport and processing of CFTR is the molecular basis of most cystic fibrosis. Cell. 63, 827–834.

Cheng, X., Gao, W., Dang, Y., Liu, X., Li, Y., Peng, X., Ye, X., 2013. Both ERK/MAPK and TGF-Beta/Smad signaling pathways play a role in the kidney fibrosis of diabetic mice accelerated by blood glucose fluctuation. J. Diabetes Res. 2013, 463740.

Cholon, D.M., Quinney, N.L., Fulcher, M.L., Esther, C.R., Das, J., Dokholyan, N. V., Randell, S.H., Boucher, R.C., Gentzsch, M., 2014. Cystic fibrosis: Potentiator ivacaftor abrogates pharmacological correction of ΔF508 CFTR in cystic fibrosis. Sci Transl Med. 6, 246ra96.

Chou, C.Y., Streets, A.J., Watson, P.F., Huang, L., Verderio, E.A.M., Johnson, T.S., 2011. A crucial sequence for transglutaminase type 2 extracellular trafficking in renal tubular epithelial cells lies in its N-terminal β-sandwich domain. J. Biol Chem. 286, 27825–27835.

Clancy, J.P., Cotton, C.U., Donaldson, S.H., Solomon, G.M., VanDevanter, D.R., Boyle, M.P., Gentzsch, M., Nick, J.A., Illek, B., Wallenburg, J.C., Sorscher, E.J., Amaral, M.D., Beekman, J.M., Naren, A.P., Bridges, R.J., Thomas, P.J., Cutting, G., Rowe, S., Durmowicz, A.G., Mense, M., Boeck, K.D., Skach, W., Penland, C., Joseloff, E., Bihler, H., Mahoney, J., Borowitz, D., Tuggle, K.L., 2019. CFTR modulator theratyping: Current status, gaps and future directions. J. Cyst Fibros. 18, 22–34.

Clancy, J.P., Rowe, S.M., Accurso, F.J., Aitken, M.L., Amin, R.S., Ashlock, M.A., Ballmann, M., Boyle, M.P., Bronsveld, I., Campbell, P.W., De Boeck, K., Donaldson, S.H., Dorkin, H.L., Dunitz, J.M., Durie, P.R., Jain, M., Leonard, A., McCoy, K.S., Moss, R.B., Pilewski, J.M., Rosenbluth, D.B., Rubenstein, R.C., Schechter, M.S., Botfield, M., Ordoñez, C.L., Spencer-Green, G.T., Vernillet, L., Wisseh, S., Yen, K., Konstan, M.W., 2012. Results of a phase IIa study of VX-809, an investigational CFTR corrector

compound, in subjects with cystic fibrosis homozygous for the F508del-CFTR mutation. Thorax. 67, 12–18.

Clapham, D.E., 1995. Calcium signaling. Cell. 80, 259–268.

Clarke, L.A., Botelho, H.M., Sousa, L., Falcao, A.O., Amaral, M.D., 2015. Transcriptome meta-analysis reveals common differential and global gene expression profiles in cystic fibrosis and other respiratory disorders and identifies CFTR regulators. Genomics. 106, 268–277.

Clarke, L.L., Grubb, B.R., Yankaskas, J.R., Cotton, C.U., McKenzie, A., Boucher, R.C., 1994. Relationship of a non-cystic fibrosis transmembrane conductance regulator-mediated chloride conductance to organ-level disease in Cftr(-/-) mice. Proc Natl Acad Sci USA. 91, 479–483.

Cocucci, E., Racchetti, G., Meldolesi, J., 2009. Shedding microvesicles: artefacts no more. Trends Cell Biol. 19, 43–51.

Cohen-Cymberknoh, M., Shoseyov, D., Breuer, O., Shamali, M., Wilschanski, M., Kerem, E., 2016. Treatment of cystic fibrosis in low-income countries. Lancet Respir Med. 4, 91–92.

Collighan, R.J., Griffin, M., 2009. Transglutaminase 2 cross-linking of matrix proteins: Biological significance and medical applications. Amino Acids. 36, 659–670.

Csanády, L., Vergani, P., Gadsby, D.C., 2019. Structure, gating, and regulation of the CFTR anion channel. Physiol Rev. 99, 707–738.

Cuevas-Ocaña, S., Laselva, O., Avolio, J., Nenna, R., 2020. Landmark papers in respiratory medicine: The era of cftr modulators: Improvements made and remaining challenges. Breathe. 16, 1–5.

Cutting, G.R., 2010. Modifier genes in Mendelian disorders: The example of cystic fibrosis. Ann NY Acad Sci. 1214, 57–69.

Cuyx, S., De Boeck, K., 2019. Treating the Underlying Cystic Fibrosis Transmembrane Conductance Regulator Defect in Patients with Cystic Fibrosis. Semin Respir Crit Care Med. 40, 762–774.

Cystic Fibrosis Genetic Analysis Consortium, 2020. Cystic Fibrosis Mutation Database: Statistics. Available at: http://www.genet.sickkids.on.ca/StatisticsPage.html (Accessed: 17 March 2020).

Davies, J.C., Alton, E.W.F.W., Bush, A., 2007. Cystic fibrosis. BMJ. 335, 1255–1259.

De Boeck, K., 2020. Cystic fibrosis in the year 2020: A disease with a new face. Acta Paediatr. 109, 893–899.

De Boeck, K., Amaral, M.D., 2016. Progress in therapies for cystic fibrosis. Lancet Respir Med. 4, 662–674.

De Boeck, K., Zolin, A., Cuppens, H., Olesen, H. V., Viviani, L., 2014. The relative frequency of CFTR mutation classes in European patients with cystic fibrosis. J. Cyst Fibros. 13, 403–409.

De Boer, R.A., Pokharel, S., Flesch, M., Van Kampen, D.A., Suurmeijer, A.J.H., Boomsma,

F., Van Gilst, W.H., Van Veldhuisen, D.J., Pinto, Y.M., 2004. Extracellular signal regulated kinase and SMAD signaling both mediate the angiotensin II driven progression towards overt heart failure in homozygous TGR(mRen2)27. J. Mol Med. 82, 678–687.

de Jong, O.G., Verhaar, M.C., Chen, Y., Vader, P., Gremmels, H., Posthuma, G., Schiffelers, R.M., Gucek, M., van Balkom, B.W.M., 2012. Cellular stress conditions are reflected in the protein and RNA content of endothelial cell-derived exosomes. J. Extracell Vesicles. 1, 18396.

de Jong, P.M., van Sterkenburg, M.A.J.A., Kempenaar, J.A., Dijkman, J.H., Ponec, M., 1993. Serial culturing of human bronchial epithelial cells derived from biopsies. In Vitro Cell Dev Biol Anim. 29, 379–387.

De Laurenzi, V., Melino, G., 2001. Gene Disruption of Tissue Transglutaminase. Mol Cell Biol. 21, 148–155.

De Stefano, D., Villella, V.R., Esposito, S., Tosco, A., Sepe, A., De Gregorio, F., Salvadori, L., Grassia, R., Leone, C.A., De Rosa, G., Maiuri, M.C., Pettoello-Mantovani, M., Guido, S., Bossi, A., Zolin, A., Venerando, A., Pinna, L.A., Mehta, A., Bona, G., Kroemer, G., Maiuri, L., Raia, V., 2014. Restoration of CFTR function in patients with cystic fibrosis carrying the F508del-CFTR mutation. Autophagy. 10, 2053–2074.

Desmouliere, A., Redard, M., Darby, I., Gabbiani, G., 1995. Apoptosis mediates the decrease in cellularity during the transition between granulation tissue and scar. Am J. Pathol. 146, 56–66.

Desterro, J.M.P., Rodriguez, M.S., Hay, R.T., 1998. SUMO-1 modification of IκBα inhibits NF-κB activation. Mol Cell. 2, 233–239.

Devereux, G., Steele, S., Griffiths, K., Devlin, E., Fraser-Pitt, D., Cotton, S., Norrie, J., Chrystyn, H., O'Neil, D., 2016. An Open-Label Investigation of the Pharmacokinetics and Tolerability of Oral Cysteamine in Adults with Cystic Fibrosis. Clin Drug Investig. 36, 605–612.

Dewulf, J., Vermeulen, F., Wanyama, S., Thomas, M., Proesmans, M., Dupont, L., De Boeck, K., 2015. Treatment burden in patients with at least one class IV or V CFTR mutation. Pediatr Pulmonol. 50, 1230–1236.

Diaz-Hidalgo, L., Altuntas, S., Rossin, F., D'Eletto, M., Marsella, C., Farrace, M.G., Falasca, L., Antonioli, M., Fimia, G.M., Piacentini, M., 2016. Transglutaminase type 2-dependent selective recruitment of proteins into exosomes under stressful cellular conditions. Biochim Biophys Acta. 1863, 2084–2092.

Dodge, J.A., Lewis, P.A., Stanton, M., Wilsher, J., 2007. Cystic fibrosis mortality and survival in the UK: 1947-2003. Eur Respir J. 29, 522–526.

Dorin, J.R., Dickinson, P., Alton, E.W.F.W., Smith, S.N., Geddes, D.M., Stevenson, B.J., Kimber, W.L., Fleming, S., Clarke, A.R., Hooper, M.L., Anderson, L., Beddington, R.S.P., Porteous, D.J., 1992. Cystic fibrosis in the mouse by targeted insertional mutagenesis. Nature. 359, 211–215.

Dousmanis, A.G., Nairn, A.C., Gadsby, D.C., 2002. Distinct Mg2+-dependent steps rate limit opening and closing of a single CFTR Cl- channel. J. Gen Physiol. 119, 545–559.

Doyle, L., Wang, M., 2019. Overview of Extracellular Vesicles, Their Origin, Composition,

Purpose, and Methods for Exosome Isolation and Analysis. Cells. 8, 727.

Duarte, L., Matte, C.R., Bizarro, C.V., Ayub, M.A.Z., 2020. Transglutaminases: part I-origins, sources, and biotechnological characteristics. World J. Microbiol Biotechnol. 36, 15.

Durie, P.R., Kent, G., Phillips, M.J., Ackerley, C.A., 2004. Characteristic Multiorgan Pathology of Cystic Fibrosis in a Long-Living Cystic Fibrosis Transmembrane Regulator Knockout Murine Model. Am J. Pathol. 164, 1481–1493.

Eckert, R.L., Kaartinen, M.T., Nurminskaya, M., Belkin, A.M., Colak, G., Johnson, G.V.W., Mehta, K., 2014. Transglutaminase regulation of cell function. Physiol Rev. 94, 383–417.

Ehre, C., Ridley, C., Thornton, D.J., 2014. Cystic fibrosis: An inherited disease affecting mucin-producing organs. Int J. Biochem Cell Biol. 52, 136–145.

El Hiani, Y., Linsdell, P., 2015. Functional architecture of the cytoplasmic entrance to the cystic fibrosis transmembrane conductance regulator chloride channel pore. J. Biol Chem. 290, 15855–15865.

Espitia Pinzón, N., Brevé, J.J.P., Bol, J.G.J.M., Drukarch, B., Baron, W., van Dam, A.M., 2017. Tissue transglutaminase in astrocytes is enhanced by inflammatory mediators and is involved in the formation of fibronectin fibril-like structures. J. Neuroinflammation. 14, 260.

Esposito, S., Tosco, A., Villella, V.R., Raia, V., Kroemer, G., Maiuri, L., 2016. Manipulating proteostasis to repair the F508del-CFTR defect in cystic fibrosis. Mol Cell Pediatr. 3, 13.

Farinha, C.M., Canato, S., 2017. From the endoplasmic reticulum to the plasma membrane: mechanisms of CFTR folding and trafficking. Cell Mol Life Sci. 74, 39–55.

Fay, J.F., Aleksandrov, L.A., Jensen, T.J., Cui, L.L., Kousouros, J.N., He, L., Aleksandrov, A.A., Gingerich, D.S., Riordan, J.R., Chen, J.Z., 2018. Cryo-EM Visualization of an Active High Open Probability CFTR Anion Channel. Biochemistry. 57, 6234–6246.

Feng, L.B., Grosse, S.D., Green, R.F., Fink, A.K., Sawicki, G.S., 2018. Precision medicine in action: The impact of Ivacaftor on cystic fibrosis-related hospitalizations. Health Aff. 37, 773–779.

Feriotto, G., Calza, R., Bergamini, C.M., Griffin, M., Wang, Z., Beninati, S., Ferretti, V., Marzola, E., Guerrini, R., Pagnoni, A., Cavazzini, A., Casciano, F., Mischiati, C., 2017. Involvement of cell surface TG2 in the aggregation of K562 cells triggered by gluten. Amino Acids. 49, 551–565.

Fesus, L., Piacentini, M., 2002. Transglutaminase 2: An enigmatic enzyme with diverse functions. Trends Biochem Sci. 27, 534–539.

Finnson, K.W., Almadani, Y., Philip, A., 2020. Non-canonical (non-SMAD2/3) TGF-β signaling in fibrosis: Mechanisms and targets. Semin Cell Dev Biol. 101, 115–122.

Fintha, A., Gasparics, Á., Rosivall, L., Sebe, A., 2019. Therapeutic targeting of fibrotic epithelial-mesenchymal transition–an outstanding challenge. Front Pharmacol. 10, 388.

Flotte, T.R., Afione, S.A., Solow, R., Drumm, M.L., Markakis, D., Guggino, W.B., Zeitlin, P.L., Carter, B.J., 1993. Expression of the cystic fibrosis transmembrane conductance regulator from a novel adeno-associated virus promoter. J. Biol Chem. 268, 3781–3790.

Flume, P.A., Liou, T.G., Borowitz, D.S., Li, H., Yen, K., Ordoñez, C.L., Geller, D.E., 2012. Ivacaftor in subjects with cystic fibrosis who are homozygous for the F508del-CFTR mutation. Chest. 142, 718–724.

Foglia, B., Cannito, S., Bocca, C., Parola, M., Novo, E., 2019. ERK pathway in activated, myofibroblast-like, hepatic stellate cells: A critical signaling crossroad sustaining liver fibrosis. Int J. Mol Sci. 20, 2700.

Fox, B.A., Yee, V.C., Pedersen, L.C., Le Trong, I., Bishop, P.D., Stenkamp, R.E., Teller, D.C., 1999. Identification of the calcium binding site and a novel ytterbium site in blood coagulation factor XIII by x-ray crystallography. J. Biol Chem. 274, 4917–4923.

Frost, F.J., Nazareth, D.S., Charman, S.C., Winstanley, C., Walshaw, M.J., 2019. Ivacaftor Is Associated with Reduced Lung Infection by Key Cystic Fibrosis Pathogens A Cohort Study Using National Registry Data. Ann Am Thorac Soc. 16, 1375–1382.

Fujimoto, M., Kanzaki, H., Nakayama, H., Higuchi, T., Hatayama, H., Iwai, M., Kaneko, Y., Mori, T., Fujita, J., 1996. Requirement for transglutaminase in progesterone-induced decidualization of human endometrial stromal cells. Endocrinology. 137, 1096–1101.

Furini, G., Burhan, I., Huang, L., Savoca, M.P., Atobatele, A., Johnson, T., Verderio, E.A.M., 2020. Insights into the heparan sulphate-dependent externalisation of transglutaminase-2 (TG2) in glucose-stimulated proximal-like tubular epithelial cells. Anal Biochem. 603, 113628.

Furini, G., Schroeder, N., Huang, L., Boocock, D., Scarpellini, A., Coveney, C., Tonoli, E., Ramaswamy, R., Ball, G., Verderio, C., Johnson, T.S., Verderio, E.A.M., 2018. Proteomic profiling reveals the transglutaminase-2 externalization pathway in kidneys after unilateral ureteric obstruction. J. Am Soc Nephrol. 29, 880–905.

Furini, G., Verderio, E.A.M., 2019. Spotlight on the Transglutaminase 2-Heparan Sulfate Interaction. Med Sci. 7, 5.

Garbuzenko, O.B., Kbah, N., Kuzmov, A., Pogrebnyak, N., Pozharov, V., Minko, T., 2019. Inhalation treatment of cystic fibrosis with lumacaftor and ivacaftor co-delivered by nanostructured lipid carriers. J. Control Release. 296, 225–231.

Glozman, R., Okiyoneda, T., Mulvihill, C.M., Rini, J.M., Barriere, H., Lukacs, G.L., 2009. N-glycans are direct determinants of CFTR folding and stability in secretory and endocytic membrane traffic. J. Cell Biol. 184, 847–862.

Granados, A., Chan, C.L., Ode, K.L., Moheet, A., Moran, A., Holl, R., 2019. Cystic fibrosis related diabetes: Pathophysiology, screening and diagnosis. J. Cyst Fibros. 18, S3–S9.

Grant, L.R., Milic, I., Devitt, A., 2019. Apoptotic cell-derived extracellular vesicles: Structure–function relationships. Biochem Soc Trans. 47, 509–516.

Gregory, R.J., Cheng, S.H., Rich, D.P., Marshall, J., Paul, S., Hehir, K., Ostedgaard, L., Klinger, K.W., Welsh, M.J., Smith, A.E., 1990. Expression and characterization of the cystic fibrosis transmembrane conductance regulator. Nature. 347, 382–386.

Grenard, P., Bates, M.K., Aeschlimann, D., 2001. Evolution of transglutaminase genes: Identification of a transglutaminase gene cluster on human chromosome 15q15: Structure of the gene encoding transglutaminase X and a novel gene family member, transglutaminase Z. J. Biol Chem. 276, 33066–33078.

Griese, M., Costa, S., Linnemann, R.W., Mall, M.A., McKone, E.F., Polineni, D., Quon, B.S., Ringshausen, F.C., Taylor-Cousar, J.L., Withers, N.J., Moskowitz, S.M., Daines, C.L., 2021. Safety and efficacy of elexacaftor/tezacaftor/ivacaftor for 24 weeks or longer in people with cystic fibrosis and one or more F508del alleles: Interim results of an open-label phase 3 clinical trial. Am J. Respir Crit Care Med. 203, 381–385.

Griffin, M., Casadio, R., Bergamini, C.M., 2002. Transglutaminases: Nature's biological glues. Biochem J. 368, 377–396.

Griffin, M., Mongeot, A., Collighan, R., Saint, R.E., Jones, R.A., Coutts, I.G.C., Rathbone, D.L., 2008. Synthesis of potent water-soluble tissue transglutaminase inhibitors. Bioorg Med Chem Lett. 18, 5559–5562.

Gross, S.R., Balklava, Z., Griffin, M., 2003. Importance of tissue transglutaminase in repair of extracellular matrices and cell death of dermal fibroblasts after exposure to a solarium ultraviolet a source. J. Invest Dermatol. 121, 412–423.

Gruenert, D.C., Willems, M., Cassiman, J.J., Frizzell, R.A., 2004. Established cell lines used in cystic fibrosis research. J. Cyst Fibros. 3, 191–196.

Guilbault, C., Saeed, Z., Downey, G.P., Radzioch, D., 2007. Cystic fibrosis mouse models. Am J. Respir Cell Mol Biol. 36, 1–7.

Gundemir, S., Colak, G., Tucholski, J., Johnson, G.V.W., 2012. Transglutaminase 2: A molecular Swiss army knife. Biochim Biophys Acta. 1823, 406–419.

Gunderson, K.L., Kopito, R.R., 1995. Conformational states of CFTR associated with channel gating: The role of ATP binding and hydrolysis. Cell. 82, 231–239.

Han, B.G., Cho, J.W., Cho, Y.D., Jeong, K.C., Kim, S.Y., Lee, B. Il, 2010. Crystal structure of human transglutaminase 2 in complex with adenosine triphosphate. Int J. Biol Macromol. 47, 190–195.

Han, S.T., Rab, A., Pellicore, M.J., Davis, E.F., McCague, A.F., Evans, T.A., Joynt, A.T., Lu, Z., Cai, Z., Raraigh, K.S., Hong, J.S., Sheppard, D.N., Sorscher, E.J., Cutting, G.R., 2018. Residual function of cystic fibrosis mutants predicts response to small molecule CFTR modulators. JCI insight. 3, e121159.

Haroon, Z.A., Hettasch, J.M., Lai, T., Dewhirst, M.W., Greenberg, C.S., 1999. Tissue transglutaminase is expressed, active, and directly involved in rat dermal wound healing and angiogenesis. FASEB J. 13, 1787–1795.

Hegedus, T., Aleksandrov, A., Mengos, A., Cui, L., Jensen, T.J., Riordan, J.R., 2009. Role of individual R domain phosphorylation sites in CFTR regulation by protein kinase A. Biochim Biophys Acta. 1788, 1341–1349.

Heijerman, H.G.M., McKone, E.F., Downey, D.G., Van Braeckel, E., Rowe, S.M., Tullis, E., Mall, M.A., Welter, J.J., Ramsey, B.W., McKee, C.M., Marigowda, G., Moskowitz, S.M., Waltz, D., Sosnay, P.R., Simard, C., Ahluwalia, N., Xuan, F., Zhang, Y., Taylor-Cousar, J.L., McCoy, K.S., McCoy, K., Donaldson, S., Walker, S., Chmiel, J., Rubenstein, R., Froh, D.K., Neuringer, I., Jain, M., Moffett, K., Taylor-Cousar, J.L., Barnett, B., Mueller,

G., Flume, P., Livingston, F., Mehdi, N., Teneback, C., Welter, J., Jain, R., Kissner, D., Patel, K., Calimano, F.J., Johannes, J., Daines, C., Keens, T., Scher, H., Chittivelu, S., Reddivalam, S., Klingsberg, R.C., Johnson, L.G., Verhulst, S., Macedo, P., Downey, D., Connett, G., Nash, E., Withers, N., Lee, T., Bakker, M., Heijerman, H., Vermeulen, F., Knoop, C., De Wachter, E., van der Meer, R., Merkus, P., Majoor, C., 2019. Efficacy and safety of the elexacaftor plus tezacaftor plus ivacaftor combination regimen in people with cystic fibrosis homozygous for the F508del mutation: a double-blind, randomised, phase 3 trial. Lancet. 394, 1940–1948.

Heijink, I.H., Noordhoek, J.A., Timens, W., Van Oosterhout, A.J.M., Postma, D.S., 2014. Abnormalities in airway epithelial junction formation in chronic obstructive pulmonary disease. Am J. Respir Crit Care Med. 189, 1439–1442.

Hertig, A., Anglicheau, D., Verine, J., Pallet, N., Touzot, M., Ancel, P.Y., Mesnard, L., Brousse, N., Baugey, E., Glotz, D., Legendre, C., Rondeau, E., Xu-Dubois, Y.C., 2008. Early epithelial phenotypic changes predict graft fibrosis. J. Am Soc Nephrol. 19, 1584–1591.

Hill, C., Jones, M., Davies, D., Wang, Y., 2019. Epithelial-Mesenchymal Transition Contributes to Pulmonary Fibrosis via Aberrant Epithelial/Fibroblastic Cross-Talk. J. Lung Heal Dis. 3, 31–35.

Hinz, B., Phan, S.H., Thannickal, V.J., Galli, A., Bochaton-Piallat, M.L., Gabbiani, G., 2007. The myofibroblast: One function, multiple origins. Am J. Pathol. 170, 1807–1816.

Hinz, B., Phan, S.H., Thannickal, V.J., Prunotto, M., Desmoulire, A., Varga, J., De Wever, O., Mareel, M., Gabbiani, G., 2012. Recent developments in myofibroblast biology: Paradigms for connective tissue remodeling. Am J. Pathol. 180, 1340–1355.

Hitomi, K., Horio, Y., Ikura, K., Yamanishi, K., Maki, M., 2001. Analysis of epidermal-type transglutaminase (TGase 3) expression in mouse tissues and cell lines. Int J. Biochem Cell Biol. 33, 491–498.

Hoshino, A., Costa-Silva, B., Shen, T.L., Rodrigues, G., Hashimoto, A., Tesic Mark, M., Molina, H., Kohsaka, S., Di Giannatale, A., Ceder, S., Singh, S., Williams, C., Soplop, N., Uryu, K., Pharmer, L., King, T., Bojmar, L., Davies, A.E., Ararso, Y., Zhang, T., Zhang, H., Hernandez, J., Weiss, J.M., Dumont-Cole, V.D., Kramer, K., Wexler, L.H., Narendran, A., Schwartz, G.K., Healey, J.H., Sandstrom, P., Jørgen Labori, K., Kure, E.H., Grandgenett, P.M., Hollingsworth, M.A., De Sousa, M., Kaur, S., Jain, M., Mallya, K., Batra, S.K., Jarnagin, W.R., Brady, M.S., Fodstad, O., Muller, V., Pantel, K., Minn, A.J., Bissell, M.J., Garcia, B.A., Kang, Y., Rajasekhar, V.K., Ghajar, C.M., Matei, I., Peinado, H., Bromberg, J., Lyden, D., 2015. Tumour exosome integrins determine organotropic metastasis. Nature. 527, 329–335.

Huber, M., Rettler, I., Bernasconi, K., Frenk, E., Lavrijsen, S.P.M., Ponec, M., Bon, A., Lautenschlager, S., Schorderet, D.F., Hohl, D., 1995. Mutations of keratinocyte transglutaminase in lamellar ichthyosis. Science. 267, 525–528.

Hudson, R.P., Dawson, J.E., Chong, P.A., Yang, Z., Millen, L., Thomas, P.J., Brouillette, C.G., Forman-Kay, J.D., 2017. Direct binding of the Corrector VX-809 to Human CFTR NBD1: Evidence of an Allosteric coupling between the Binding site and the NBD1:CL4 Interface. Mol Pharmacol. 92, 124–135.

Humphreys, B.D., Lin, S.L., Kobayashi, A., Hudson, T.E., Nowlin, B.T., Bonventre, J. V., Valerius, M.T., McMahon, A.P., Duffield, J.S., 2010. Fate tracing reveals the pericyte

and not epithelial origin of myofibroblasts in kidney fibrosis. Am J. Pathol. 176, 85–97.

Hunt, J.F., Wang, C., Ford, R.C., 2013. Cystic fibrosis transmembrane conductance regulator (ABCC7) structure. Cold Spring Harb Perspect Med. 3, a009514.

Hwang, T.C., Yeh, J.T., Zhang, J., Yu, Y.C., Yeh, H.I., Destefano, S., 2018. Structural mechanisms of CFTR function and dysfunction. J. Gen Physiol. 150, 539–570.

Ientile, R., Caccamo, D., Griffin, M., 2007. Tissue transglutaminase and the stress response. Amino Acids. 33, 385–394.

Iwano, M., Plieth, D., Danoff, T.M., Xue, C., Okada, H., Neilson, E.G., 2002. Evidence that fibroblasts derive from epithelium during tissue fibrosis. J. Clin Invest. 110, 341–350.

Jang, T.H., Lee, D.S., Choi, K., Jeong, E.M., Kim, I.G., Kim, Y.W., Chun, J.N., Jeon, J.H., Park, H.H., 2014. Crystal structure of transglutaminase 2 with GTP complex and amino acid sequence evidence of evolution of GTP binding site. PLoS One. 9, e107005.

Jeon, J.H., Lee, H.J., Jang, G.Y., Kim, C.W., Shin, D.M., Cho, S.Y., Yeo, E.J., Park, S.C., Kim, I.G., 2004. Different inhibition characteristics of intracellular transglutaminase activity by cystamine and cysteamine. Exp Mol Med. 36, 576–581.

Jeong, E.M., Lee, K.B., Kim, G.E., Kim, C.M., Lee, J.H., Kim, H.J., Shin, J.W., Kwon, M.A., Park, H.H., Kim, I.G., 2020. Competitive binding of magnesium to calcium binding sites reciprocally regulates transamidase and GTP hydrolysis activity of transglutaminase 2. Int J. Mol Sci. 21, 791.

Jiang, W.G., Ablin, R.J., 2011. Prostate transglutaminase: A unique transglutaminase and its role in prostate cancer. Biomark Med. 5, 285–291.

Jih, K.Y., Li, M., Hwang, T.C., Bompadre, S.G., 2011. The most common cystic fibrosis-associated mutation destabilizes the dimeric state of the nucleotide-binding domains of CFTR. J. Physiol. 589, 2719–2731.

Jin, X., Stamnaes, J., Klöck, C., DiRaimondo, T.R., Sollid, L.M., Khosla, C., 2011. Activation of extracellular transglutaminase 2 by thioredoxin. J. Biol Chem. 286, 37866–37873.

Johnson, J.R., Nishioka, M., Chakir, J., Risse, P.A., Almaghlouth, I., Bazarbashi, A.N., Plante, S., Martin, J.G., Eidelman, D., Hamid, Q., 2013. IL-22 contributes to TGF-β1-mediated epithelial-mesenchymal transition in asthmatic bronchial epithelial cells. Respir Res. 14, 118.

Johnson, T.S., El-Koraie, A.F., Skill, N.J., Baddour, N.M., El Nahas, A.M., Njloma, M., Adam, A.G., Griffin, M., 2003. Tissue transglutaminase and the progression of human renal scarring. J. Am Soc Nephrol. 14, 2052–2062.

Johnson, T.S., Fisher, M., Haylor, J.L., Hau, Z., Skill, N.J., Jones, R., Saint, R., Coutts, I., Vickers, M.E., El Nahas, A.M., Griffin, M., 2007. Transglutaminase inhibition reduces fibrosis and preserves function in experimental chronic kidney disease. J. Am Soc Nephrol. 18, 3078–3088.

Jonsdottir, H.R., Arason, A.J., Palsson, R., Franzdottir, S.R., Gudbjartsson, T., Isaksson, H.J., Gudmundsson, G., Gudjonsson, T., Magnusson, M.K., 2015. Basal cells of the human airways acquire mesenchymal traits in idiopathic pulmonary fibrosis and in culture. Lab Investig. 95, 1418–1428.

Jouret, F., Devuyst, O., 2009. CFTR and defective endocytosis: New insights in the renal phenotype of cystic fibrosis. Pflugers Arch. 457, 1227–1236.

Kang, J.H., Lee, J.S., Hong, D., Lee, S.H., Kim, N., Lee, W.K., Sung, T.W., Gong, Y.D., Kim, S.Y., 2016. Renal cell carcinoma escapes death by p53 depletion through transglutaminase 2-chaperoned autophagy. Cell Death Dis. 7, e2163.

Keating, D., Marigowda, G., Burr, L., Daines, C., Mall, M.A., McKone, E.F., Ramsey, B.W., Rowe, S.M., Sass, L.A., Tullis, E., McKee, C.M., Moskowitz, S.M., Robertson, S., Savage, J., Simard, C., Van Goor, F., Waltz, D., Xuan, F., Young, T., Taylor-Cousar, J.L., 2018. VX-445–Tezacaftor–Ivacaftor in Patients with Cystic Fibrosis and One or Two Phe508del Alleles. N Engl J. Med. 379, 1612–1620.

Keillor, J.W., Apperley, K.Y.P., 2016. Transglutaminase inhibitors: A patent review. Expert Opin Ther Pat. 26, 49–63.

Keillor, J.W., Apperley, K.Y.P., Akbar, A., 2015. Inhibitors of tissue transglutaminase. Trends Pharmacol Sci. 36, 32–40.

Kelly, J., 2017. Environmental scan of cystic fibrosis research worldwide. J. Cyst Fibros. 16, 367–370.

Keogh, R.H., Szczesniak, R., Taylor-Robinson, D., Bilton, D., 2018. Up-to-date and projected estimates of survival for people with cystic fibrosis using baseline characteristics: A longitudinal study using UK patient registry data. J. Cyst Fibros. 17, 218–227.

Kim, K.K., Kugler, M.C., Wolters, P.J., Robillard, L., Galvez, M.G., Brumwell, A.M., Sheppard, D., Chapman, H.A., 2006. Alveolar epithelial cell mesenchymal transition develops in vivo during pulmonary fibrosis and is regulated by the extracellular matrix. Proc Natl Acad Sci USA. 103, 13180–13185.

Kim, N., Kang, J.H., Lee, W.K., Kim, S.G., Lee, J.S., Lee, S.H., Park, J.B., Kim, K.H., Gong, Y.D., Hwang, K.Y., Kim, S.Y., 2018. Allosteric inhibition site of transglutaminase 2 is unveiled in the N terminus. Amino Acids. 50, 1583–1594.

Király, R., Cssz, É., Kurtán, T., Antus, S., Szigeti, K., Simon-Vecsei, Z., Korponay-Szabó, I.R., Keresztessy, Z., Fésüs, L., 2009. Functional significance of five noncanonical Ca2+-binding sites of human transglutaminase 2 characterized by site-directed mutagenesis. FEBS J. 276, 7083–7096.

Klingberg, F., Chau, G., Walraven, M., Boo, S., Koehler, A., Chow, M.L., Olsen, A.L., Im, M., Lodyga, M., Wells, R.G., White, E.S., Hinz, B., 2018. The fibronectin ED-A domain enhances recruitment of latent TGF-β-binding protein-1 to the fibroblast matrix. J. Cell Sci. 131, jcs201293.

Klingberg, F., Chow, M.L., Koehler, A., Boo, S., Buscemi, L., Quinn, T.M., Costell, M., Alman, B.A., Genot, E., Hinz, B., 2014. Prestress in the extracellular matrix sensitizes latent TGF-β1 for activation. J. Cell Biol. 207, 283–297.

Klingberg, F., Hinz, B., White, E.S., 2013. The myofibroblast matrix: Implications for tissue repair and fibrosis. J. Pathol. 229, 298–309.

Klöock, C., Khosla, C., 2012. Regulation of the activities of the mammalian transglutaminase family of enzymes. Protein Sci. 21, 1781–1791.

Kobelska-Dubiel, N., Klincewicz, B., Cichy, W., 2014. Liver disease in cystic fibrosis. Prz Gastroenterol. 9, 136–141.

Kolosova, I., Nethery, D., Kern, J.A., 2011. Role of Smad2/3 and p38 MAP kinase in TGF-β1-induced epithelial-mesenchymal transition of pulmonary epithelial cells. J. Cell Physiol. 226, 1248–1254.

König, I.R., Fuchs, O., Hansen, G., von Mutius, E., Kopp, M. V., 2017. What is precision medicine? Eur Respir J. 50, 1700391.

Konstan, M.W., VanDevanter, D.R., Rowe, S.M., Wilschanski, M., Kerem, E., Sermet-Gaudelus, I., DiMango, E., Melotti, P., McIntosh, J., De Boeck, K., 2020. Efficacy and safety of ataluren in patients with nonsense-mutation cystic fibrosis not receiving chronic inhaled aminoglycosides: The international, randomized, double-blind, placebo-controlled Ataluren Confirmatory Trial in Cystic Fibrosis (ACT CF). J. Cyst Fibros. 19, 595–601.

Kopito, L.E., Kosasky, H.J., Shwachman, H., 1973. Water and electrolytes in cervical mucus from patients with cystic fibrosis. Fertil Steril. 24, 512–516.

Kowal, J., Arras, G., Colombo, M., Jouve, M., Morath, J.P., Primdal-Bengtson, B., Dingli, F., Loew, D., Tkach, M., Théry, C., 2016. Proteomic comparison defines novel markers to characterize heterogeneous populations of extracellular vesicle subtypes. Proc Natl Acad Sci USA. 113, E968–E977.

Kreda, S.M., Davis, C.W., Rose, M.C., 2012. CFTR, mucins, and mucus obstruction in cystic fibrosis. Cold Spring Harb Perspect Med. 2, a009589.

Kuncio, G.S., Tsyganskaya, M., Zhu, J., Liu, S.L., Nagy, L., Thomazy, V., Davies, P.J.A., Zern, M.A., 1998. TNF-α modulates expression of the tissue transglutaminase gene in liver cells. Am J. Physiol. 274, G240–G245.

Kunzelmann, K., Schreiber, R., Hadorn, H.B., 2017. Bicarbonate in cystic fibrosis. J. Cyst Fibros. 16, 653–662.

Lamouille, S., Xu, J., Derynck, R., 2014. Molecular mechanisms of epithelial-mesenchymal transition. Nat Rev Mol Cell Biol. 15, 178–196.

Liu, F., Mih, J.D., Shea, B.S., Kho, A.T., Sharif, A.S., Tager, A.M., Tschumperlin, D.J., 2010. Feedback amplification of fibrosis through matrix stiffening and COX-2 suppression. J. Cell Biol. 190, 693–706.

Liu, F., Zhang, Z., Csanády, L., Gadsby, D.C., Chen, J., 2017. Molecular Structure of the Human CFTR Ion Channel. Cell. 169, 85-95.

Liu, F., Zhang, Z., Levit, A., Levring, J., Touhara, K.K., Shoichet, B.K., Chen, J., 2019. Structural identification of a hotspot on CFTR for potentiation. Science. 364, 1184–1188.

Liu, S., Cerione, R.A., Clardy, J., 2002. Structural basis for the guanine nucleotide-binding activity of tissue transglutaminase and its regulation of transamidation activity. Proc Natl Acad Sci USA. 99, 2743–2747.

Livraghi-Butrico, A., Grubb, B.R., Wilkinson, K.J., Volmer, A.S., Burns, K.A., Evans, C.M., O'Neal, W.K., Boucher, R.C., 2017. Contribution of mucus concentration and secreted mucins Muc5ac and Muc5b to the pathogenesis of muco-obstructive lung disease.

Mucosal Immunol. 10, 829.

Loh, C.Y., Chai, J.Y., Tang, T.F., Wong, W.F., Sethi, G., Shanmugam, M.K., Chong, P.P., Looi, C.Y., 2019. The E-Cadherin and N-Cadherin Switch in Epithelial-to-Mesenchymal Transition: Signaling, Therapeutic Implications, and Challenges. Cells. 8, 1118.

Loo, T.W., Clarke, D.M., 2017. Corrector VX-809 promotes interactions between cytoplasmic loop one and the first nucleotide-binding domain of CFTR. Biochem Pharmacol. 136, 24–31.

Lopes-Pacheco, M., 2020. CFTR Modulators: The Changing Face of Cystic Fibrosis in the Era of Precision Medicine. Front Pharmacol. 10, 1662.

Lortat-Jacob, H., Burhan, I., Scarpellini, A., Thomas, A., Imberty, A., Vivès, R.R., Johnson, T., Gutierrez, A., Verderio, E.A.M., 2012. Transglutaminase-2 interaction with heparin: Identification of a heparin binding site that regulates cell adhesion to fibronectin-transglutaminase-2 matrix. J. Biol Chem. 287, 18005–18017.

Lowry, O.H., Rosebrough, N.J., Farr, A.L., Randall, R.J., 1951. Protein measurement with the Folin phenol reagent. J. Biol Chem. 193, 265–275.

Luciani, A., Villella, V.R., Esposito, S., Brunetti-Pierri, N., Medina, D., Settembre, C., Gavina, M., Pulze, L., Giardino, I., Pettoello-Mantovani, M., D'Apolito, M., Guido, S., Masliah, E., Spencer, B., Quaratino, S., Raia, V., Ballabio, A., Maiuri, L., 2010. Defective CFTR induces aggresome formation and lung inflammation in cystic fibrosis through ROS-mediated autophagy inhibition. Nat Cell Biol. 12, 863–875.

Luciani, A., Villella, V.R., Esposito, S., Brunetti-Pierri, N., Medina, D.L., Settembre, C., Gavina, M., Raia, V., Ballabio, A., Maiuri, L., 2011. Cystic fibrosis: A disorder with defective autophagy. Autophagy. 7, 104–106.

Luciani, A., Villella, V.R., Vasaturo, A., Giardino, I., Raia, V., Pettoello-Mantovani, M., D'Apolito, M., Guido, S., Leal, T., Quaratino, S., Maiuri, L., 2009. SUMOylation of Tissue Transglutaminase as Link between Oxidative Stress and Inflammation. J. Immunol. 183, 2775–2784.

Luengen, A.E., Kniebs, C., Buhl, E.M., Cornelissen, C.G., Schmitz-Rode, T., Jockenhoevel, S., Thiebes, A.L., 2020. Choosing the Right Differentiation Medium to Develop Mucociliary Phenotype of Primary Nasal Epithelial Cells In Vitro. Sci Rep. 10, 6963.

Lukacs, G.L., Mohamed, A., Kartner, N., Chang, X.B., Riordan, J.R., Grinstein, S., 1994. Conformational maturation of CFTR but not its mutant counterpart (ΔF508) occurs in the endoplasmic reticulum and requires ATP. EMBO J. 13, 6076–6086.

Madala, S.K., Schmidt, S., Davidson, C., Ikegami, M., Wert, S., Hardie, W.D., 2012. MEK-ERK pathway modulation ameliorates pulmonary fibrosis associated with epidermal growth factor receptor activation. Am J. Respir Cell Mol Biol. 46, 380–388.

Mahmood, M.Q., Reid, D., Ward, C., Muller, H.K., Knight, D., Sohal, S.S., Walters, E.H., 2017. Transforming growth factor (TGF) β 1 and Smad signalling pathways: A likely key to EMT-associated COPD pathogenesis. Respirology. 22, 133–140.

Maiuri, L., Luciani, A., Giardino, I., Raia, V., Villella, V.R., D'Apolito, M., Pettoello-Mantovani, M., Guido, S., Ciacci, C., Cimmino, M., Cexus, O.N., Londei, M., Quaratino, S., 2008. Tissue Transglutaminase Activation Modulates Inflammation in Cystic Fibrosis via

PPARγ Down-Regulation. J. Immunol. 180, 7697–7705.

Maki, M., Houghton, L.A., Whorwell, P.J., 1997. Tissue transglutaminase as the autoantigen of coeliac disease. Gut. 41, 565–566.

Malorni, W., Farrace, M.G., Matarrese, P., Tinari, A., Ciarlo, L., Mousavi-Shafaei, P., D'Eletto, M., Di Giacomo, G., Melino, G., Palmieri, L., Rodolfo, C., Piacentini, M., 2009. The adenine nucleotide translocator 1 acts as a type 2 transglutaminase substrate: Implications for mitochondrial-dependent apoptosis. Cell Death Differ. 16, 1480–1492.

Margolis, L., Sadovsky, Y., 2019. The biology of extracellular vesicles: The known unknowns. PLoS Biol. 17, e3000363.

Marie, G., Dunning, C.J., Gaspar, R., Grey, C., Brundin, P., Sparr, E., Linse, S., 2015. Acceleration of α-synuclein aggregation by exosomes. J. Biol Chem. 290, 2969–2982.

Marson, F.A.L., Bertuzzo, C.S., Ribeiro, J.D., 2017. Personalized or precision medicine? The example of cystic fibrosis. Front Pharmacol. 8, 390.

Martiniano, S.L., Sagel, S.D., Zemanick, E.T., 2016. Cystic fibrosis: A model system for precision medicine. Curr Opin Pediatr. 28, 312–317.

Mastroberardino, P.G., Farrace, M.G., Viti, I., Pavone, F., Fimia, G.M., Melino, G., Rodolfo, C., Piacentini, M., 2006. "Tissue" transglutaminase contributes to the formation of disulphide bridges in proteins of mitochondrial respiratory complexes. Biochim Biophys Acta. 1757, 1357–1365.

Masur, S.K., Dewal, H.S., Dinh, T.T., Erenburg, I., Petridou, S., 1996. Myofibroblasts differentiate from fibroblasts when plated at low density. Proc Natl Acad Sci USA. 93, 4219–4223.

Mathieu, M., Martin-Jaular, L., Lavieu, G., Théry, C., 2019. Specificities of secretion and uptake of exosomes and other extracellular vesicles for cell-to-cell communication. Nat Cell Biol. 21, 9–17.

McKone, E.F., Borowitz, D., Drevinek, P., Griese, M., Konstan, M.W., Wainwright, C., Ratjen, F., Sermet-Gaudelus, I., Plant, B., Munck, A., Jiang, Y., Gilmartin, G., Davies, J.C., 2014. Long-term safety and efficacy of ivacaftor in patients with cystic fibrosis who have the Gly551Asp-CFTR mutation: A phase 3, open-label extension study (PERSIST). Lancet Respir Med. 2, 902–910.

McKone, E.F., Emerson, S.S., Edwards, K.L., Aitken, M.L., 2003. Effect of genotype on phenotype and mortality in cystic fibrosis: A retrospective cohort study. Lancet. 361, 1671–1676.

Mehta, K., Kumar, A., Kim, H.I., 2010. Transglutaminase 2: A multi-tasking protein in the complex circuitry of inflammation and cancer. Biochem Pharmacol. 80, 1921–1929.

Merkert, S., Schubert, M., Olmer, R., Engels, L., Radetzki, S., Veltman, M., Scholte, B.J., Zöllner, J., Pedemonte, N., Galietta, L.J.V., von Kries, J.P., Martin, U., 2019. High-Throughput Screening for Modulators of CFTR Activity Based on Genetically Engineered Cystic Fibrosis Disease-Specific iPSCs. Stem Cell Reports. 12, 1389–1403.

Middleton, P.G., Mall, M.A., Dřevínek, P., Lands, L.C., McKone, E.F., Polineni, D., Ramsey, B.W., Taylor-Cousar, J.L., Tullis, E., Vermeulen, F., Marigowda, G., McKee, C.M.,

Moskowitz, S.M., Nair, N., Savage, J., Simard, C., Tian, S., Waltz, D., Xuan, F., Rowe, S.M., Jain, R., 2019. Elexacaftor–Tezacaftor–Ivacaftor for Cystic Fibrosis with a Single Phe508del Allele. N Engl J. Med. 381, 1809–1819.

Milara, J., Peiró, T., Serrano, A., Cortijo, J., 2013. Epithelial to mesenchymal transition is increased in patients with COPD and induced by cigarette smoke. Thorax. 68, 410–420.

Montoro, D.T., Haber, A.L., Biton, M., Vinarsky, V., Lin, B., Birket, S.E., Yuan, F., Chen, S., Leung, H.M., Villoria, J., Rogel, N., Burgin, G., Tsankov, A.M., Waghray, A., Slyper, M., Waldman, J., Nguyen, L., Dionne, D., Rozenblatt-Rosen, O., Tata, P.R., Mou, H., Shivaraju, M., Bihler, H., Mense, M., Tearney, G.J., Rowe, S.M., Engelhardt, J.F., Regev, A., Rajagopal, J., 2018. A revised airway epithelial hierarchy includes CFTR-expressing ionocytes. Nature. 560, 319–324.

Mou, H., Brazauskas, K., Rajagopal, J., 2015. Personalized medicine for cystic fibrosis: Establishing human model systems. Pediatr Pulmonol. 50, S14–S23.

Moyer, B.D., Demon, J., Karlson, K.H., Reynolds, D., Wang, S., Mickle, J.E., Milewski, M., Cutting, G.R., Guggino, W.B., Li, M., Stanton, B.A., 1999. A PDZ-interacting domain in CFTR is an apical membrane polarization signal. J. Clin Invest. 104, 1353–1361.

Muhlebach, M.S., Zorn, B.T., Esther, C.R., Hatch, J.E., Murray, C.P., Turkovic, L., Ranganathan, S.C., Boucher, R.C., Stick, S.M., Wolfgang, M.C., 2018. Initial acquisition and succession of the cystic fibrosis lung microbiome is associated with disease progression in infants and preschool children. PLoS Pathog. 14, e1006798.

Muma, N.A., 2007. Transglutaminase is linked to neurodegenerative diseases. J. Neuropathol Exp Neurol. 66, 258–263.

Nabhan, J.F., Hu, R., Oh, R.S., Cohen, S.N., Lu, Q., 2012. Formation and release of arrestin domain-containing protein 1-mediated microvesicles (ARMMs) at plasma membrane by recruitment of TSG101 protein. Proc Natl Acad Sci USA. 109, 4146–4151.

Nadella, V., Wang, Z., Johnson, T.S., Griffin, M., Devitt, A., 2015. Transglutaminase 2 interacts with syndecan-4 and CD44 at the surface of human macrophages to promote removal of apoptotic cells. Biochim Biophys Acta. 1853, 201–212.

Nakaoka, H., Perez, D.M., Baek, K.J., Das, T., Husain, A., Misono, K., Im, M.J., Graham, R.M., 1994. Gh: A GTP-Binding protein with transglutaminase activity and receptor signaling function. Science. 264, 1593–1596.

Nanda, N., Iismaa, S.E., Owens, W.A., Husain, A., Mackay, F., Graham, R.M., 2001. Targeted Inactivation of Gh/Tissue Transglutaminase II. J. Biol Chem. 276, 20673–20678.

Nardacci, R., Iacono, O. Lo, Ciccosanti, F., Falasca, L., Addesso, M., Amendola, A., Antonucci, G., Craxi, A., Fimia, G.M., Iadevaia, V., Melino, G., Ruco, L., Tocci, G., Ippolito, G., Piacentini, M., 2003. Transglutaminase type II plays a protective role in hepatic injury. Am J. Pathol. 162, 1293–1303.

Nunes, I., Gleizes, P.E., Metz, C.N., Rifkin, D.B., 1997. Latent transforming growth factor-β binding protein domains involved in activation and transglutaminase-dependent cross-linking of latent transforming growth factor-β. J. Cell Biol. 136, 1151–1163.

Nurminskaya, M. V., Belkin, A.M., 2012. Cellular Functions of Tissue Transglutaminase. Int

Rev Cell Mol Biol. 294, 1–97.

Nyabam, S., Wang, Z., Thibault, T., Oluseyi, A., Basar, R., Marshall, L., Griffin, M., 2016. A novel regulatory role for tissue transglutaminase in epithelial-mesenchymal transition in cystic fibrosis. Biochim Biophys Acta. 1863, 2234–2244.

Nyabam, S.K., 2015. Understanding the link between Transglutaminase and the induction of Fibrosis in Cystic Fibrosis (CF). PhD thesis, Aston University, Birmingham. Available at: https://research.aston.ac.uk/en/studentTheses/understanding-the-link-between-transglutaminase-and-the-induction (Accessed: 05 May 2020).

O'Sullivan, B.P., Freedman, S.D., 2009. Cystic fibrosis. Lancet. 373, 1891–1904.

Ohta, H., Chiba, S., Ebina, M., Furuse, M., Nukiwa, T., 2012. Altered expression of tight junction molecules in alveolar septa in lung injury and fibrosis. Am J. Physiol. 302, 193–205.

Okiyoneda, T., Barrière, H., Bagdány, M., Rabeh, W.M., Du, K., Höhfeld, J., Young, J.C., Lukacs, G.L., 2010. Peripheral protein quality control removes unfolded CFTR from the plasma membrane. Science. 329, 805–810.

Okiyoneda, T., Lukacs, G.L., 2007. Cell surface dynamics of CFTR: The ins and outs. Biochim Biophys Acta. 1773, 476–479.

Olsen, K.C., Epa, A.P., Kulkarni, A.A., Kottmann, R.M., McCarthy, C.E., Johnson, G. V., Thatcher, T.H., Phipps, R.P., Sime, P.J., 2014. Inhibition of transglutaminase 2, a novel target for pulmonary fibrosis, by two small electrophilic molecules. Am J. Respir Cell Mol Biol. 50, 737–747.

Olsen, K.C., Sapinoro, R.E., Kottmann, R.M., Kulkarni, A.A., Iismaa, S.E., Johnson, G.V.W., Thatcher, T.H., Phipps, R.P., Sime, P.J., 2011. Transglutaminase 2 and its role in pulmonary fibrosis. Am J. Respir Crit Care Med. 184, 699–707.

Owji, H., Nezafat, N., Negandaripour, M., Hajiebrahimi, A., and Ghasemi, Y., 2018. A comprehensive review of signal peptides: structure, roles, and applications. Eur J. Cell Biol. 97, 422–441.

Pan, C., Kumar, C., Bohl, S., Klingmueller, U., Mann, M., 2009. Comparative proteomic phenotyping of cell lines and primary cells to assess preservation of cell type-specific functions. Mol Cell Proteomics. 8, 443–450.

Paranjape, S.M., Mogayzel, P.J., 2018. Cystic fibrosis in the era of precision medicine. Paediatr Respir Rev. 25, 64–72.

Paul, B.D., Snyder, S.H., 2019. Therapeutic Applications of Cysteamine and Cystamine in Neurodegenerative and Neuropsychiatric Diseases. Front Neurol. 10, 1315.

Perez, A., Issler, A.C., Cotton, C.U., Kelley, T.J., Verkman, A.S., Davis, P.B., 2007. CFTR inhibition mimics the cystic fibrosis inflammatory profile. Am J. Physiol. 292, L383–L395.

Philp, C.J., Siebeke, I., Clements, D., Miller, S., Habgood, A., John, A.E., Navaratnam, V., Hubbard, R.B., Jenkins, G., Johnson, S.R., 2018. Extracellular matrix cross-linking enhances fibroblast growth and protects against matrix proteolysis in lung fibrosis. Am J. Respir Cell Mol Biol. 58, 594–603.

Piacentini, M., D'Eletto, M., Farrace, M.G., Rodolfo, C., Del Nonno, F., Ippolito, G., Falasca, L., 2014. Characterization of distinct sub-cellular location of transglutaminase type II: changes in intracellular distribution in physiological and pathological states. Cell Tissue Res. 358, 793–805.

Piera-Velazquez, S., Li, Z., Jimenez, S.A., 2011. Role of endothelial-mesenchymal transition (EndoMT) in the pathogenesis of fibrotic disorders. Am J. Pathol. 179, 1074–1080.

Pinkas, D.M., Strop, P., Brunger, A.T., Khosla, C., 2007. Transglutaminase 2 undergoes a large conformational change upon activation. PLoS Biol. 5, 2788–2796.

Plugis, N.M., Palanski, B.A., Weng, C.H., Albertelli, M., Khosla, C., 2017. Thioredoxin-1 selectively activates transglutaminase 2 in the extracellular matrix of the small intestine: Implications for celiac disease. J. Biol Chem. 292, 2000–2008.

Popov, Y., Sverdlov, D.Y., Sharma, A.K., Bhaskar, K.R., Li, S., Freitag, T.L., Lee, J., Dieterich, W., Melino, G., Schuppan, D., 2011. Tissue transglutaminase does not affect fibrotic matrix stability or regression of liver fibrosis in mice. Gastroenterology. 140, 1642–1652.

Pranke, I.M., Hatton, A., Simonin, J., Jais, J.P., Le Pimpec-Barthes, F., Carsin, A., Bonnette, P., Fayon, M., Stremler-Le Bel, N., Grenet, D., Thumerel, M., Mazenq, J., Urbach, V., Mesbahi, M., Girodon-Boulandet, E., Hinzpeter, A., Edelman, A., Sermet-Gaudelus, I., 2017. Correction of CFTR function in nasal epithelial cells from cystic fibrosis patients predicts improvement of respiratory function by CFTR modulators. Sci Rep. 7, 7375.

Prasanna Murthy, S.N., Iismaa, S., Begg, G., Freymann, D.M., Graham, R.M., Lorand, L., 2002. Conserved tryptophan in the core domain of transglutaminase is essential for catalytic activity. Proc Natl Acad Sci USA. 99, 2738–2742.

Protasevich, I., Yang, Z., Wang, C., Atwell, S., Zhao, X., Emtage, S., Wetmore, D., Hunt, J.F., Brouillette, C.G., 2010. Thermal unfolding studies show the disease causing F508del mutation in CFTR thermodynamically destabilizes nucleotide-binding domain 1. Protein Sci. 19, 1917–1931.

Qiu, J.F., Zhang, Z.Q., Chen, W., Wu, Z.Y., 2007. Cystamine ameliorates liver fibrosis induced by carbon tetrachloride via inhibition of tissue transglutaminase. World J. Gastroenterol. 13, 4328–4332.

Quinton, P.M., 1983. Chloride impermeability in cystic fibrosis. Nature. 301, 421–422.

Quinton, P.M., 2008. Cystic fibrosis: impaired bicarbonate secretion and mucoviscidosis. Lancet. 372, 415–417.

Quittner, A.L., Saez-Flores, E., Barton, J.D., 2016. The psychological burden of cystic fibrosis. Curr Opin Pulm Med. 22, 187–191.

Ramsey, B.W., Davies, J., McElvaney, N.G., Tullis, E., Bell, S.C., Dřevínek, P., Griese, M., McKone, E.F., Wainwright, C.E., Konstan, M.W., Moss, R., Ratjen, F., Sermet-Gaudelus, I., Rowe, S.M., Dong, Q., Rodriguez, S., Yen, K., Ordoñez, C., Elborn, J.S., 2011. A CFTR Potentiator in Patients with Cystic Fibrosis and the G551D Mutation. N Engl J. Med. 365, 1663–1672.

Randell, S.H., Fulcher, M.L., O'Neal, W., Olsen, J.C., 2011. Primary epithelial cell models for cystic fibrosis research. Methods Mol Biol. 742, 285–310.

Raposo, G., Nijman, H.W., Stoorvogel, W., Leijendekker, R., Harding, C. V., Melief, C.J.M., Geuze, H.J., 1996. B lymphocytes secrete antigen-presenting vesicles. J. Exp Med. 183, 1161–1172.

Riordan, J.R., Rommens, J.M., Kerem, B., Alon, N., Rozmahel, R., Grzelczak, Z., Zielenski, J., Lok, S., Plavsic, N., Chou, J.L., Drumm, M.L., Iannuzzi, M.C., Collins, F.S., Lap-Chee, T., 1989. Identification of the cystic fibrosis gene: Cloning and characterization of complementary DNA. Science. 245, 1066–1073.

Ritter, S.J., Davies, P.J.A., 1998. Identification of a transforming growth factor-β1/bone morphogenetic protein 4 (TGF-β1/BMP4) response element within the mouse tissue transglutaminase gene promoter. J. Biol Chem. 273, 12798–12806.

Rock, J.R., Barkauskas, C.E., Cronce, M.J., Xue, Y., Harris, J.R., Liang, J., Noble, P.W., Hogan, B.L.M., 2011. Multiple stromal populations contribute to pulmonary fibrosis without evidence for epithelial to mesenchymal transition. Proc Natl Acad Sci USA. 108. E1475–E1483.

Rogers, C.S., Hao, Y., Rokhlina, T., Samuel, M., Stoltz, D.A., Li, Y., Petroff, E., Vermeer, D.W., Kabel, A.C., Yan, Z., Spate, L., Wax, D., Murphy, C.N., Rieke, A., Whitworth, K., Linville, M.L., Korte, S.W., Engelhardt, J.F., Welsh, M.J., Prather, R.S., 2008. Production of CFTR-null and CFTR-ΔF508 heterozygous pigs by adeno-associated virus - Mediated gene targeting and somatic cell nuclear transfer. J. Clin Invest. 118, 1571–1577.

Rosen, B.H., Chanson, M., Gawenis, L.R., Liu, J., Sofoluwe, A., Zoso, A., Engelhardt, J.F., 2018a. Animal and model systems for studying cystic fibrosis. J. Cyst Fibros. 17, S28-S34.

Rosen, B.H., Evans, T.I.A., Moll, S.R., Gray, J.S., Liang, B., Sun, X., Zhang, Y., Jensen-Cody, C.W., Swatek, A.M., Zhou, W., He, N., Rotti, P.G., Tyler, S.R., Keiser, N.W., Anderson, P.J., Brooks, L., Li, Y., Pope, R.M., Rajput, M., Hoffman, E.A., Wang, K., Harris, J.K., Parekh, K.R., Gibson-Corley, K.N., Engelhardt, J.F., 2018b. Infection is not required for mucoinflammatory lung disease in CFTR-Knockout ferrets. Am J. Respir Crit Care Med. 197, 1308–1318.

Rossin, F., Villella, V.R., D'Eletto, M., Farrace, M.G., Esposito, S., Ferrari, E., Monzani, R., Occhigrossi, L., Pagliarini, V., Sette, C., Cozza, G., Barlev, N.A., Falasca, L., Fimia, G.M., Kroemer, G., Raia, V., Maiuri, L., Piacentini, M., 2018. TG2 regulates the heat-shock response by the post-translational modification of HSF1. EMBO Rep. 19, e45067.

Rowe, S.M., Daines, C., Ringshausen, F.C., Kerem, E., Wilson, J., Tullis, E., Nair, N., Simard, C., Han, L., Ingenito, E.P., McKee, C., Lekstrom-Himes, J., Davies, J.C., 2017. Tezacaftor–Ivacaftor in Residual-Function Heterozygotes with Cystic Fibrosis. N Engl J. Med. 377, 2024–2035.

Ruan, Q., Tucholski, J., Gundemir, S., Johnson Voll, G.V.W., 2008. The Differential Effects of R580A Mutation on Transamidation and GTP Binding Activity of Rat and Human Type 2 Transglutaminase. Int J. Clin Exp Med. 1, 248–259.

Ruan, Y.C., Wang, Y., da Silva, N., Kim, B., Diao, R.Y., Hill, E., Brown, D., Chan, H.C., Breton, S., 2014. CFTR interacts with ZO-1 to regulate tight junction assembly and epithelial differentiation through the ZONAB pathway. J. Cell Sci. 127, 4396–4408.

Rygiel, K.A., Robertson, H., Marshall, H.L., Pekalski, M., Zhao, L., Booth, T.A., Jones, D.E.J., Burt, A.D., Kirby, J.A., 2008. Epithelial-mesenchymal transition contributes to portal tract fibrogenesis during human chronic liver disease. Lab Investig. 88, 112–123.

Sabharwal, S., 2016. Gastrointestinal manifestations of cystic fibrosis. Gastroenterol Hepatol. 12, 43–47.

Sachs, N., Papaspyropoulos, A., Zomer-van Ommen, D.D., Heo, I., Böttinger, L., Klay, D., Weeber, F., Huelsz-Prince, G., Iakobachvili, N., Amatngalim, G.D., Ligt, J., Hoeck, A., Proost, N., Viveen, M.C., Lyubimova, A., Teeven, L., Derakhshan, S., Korving, J., Begthel, H., Dekkers, J.F., Kumawat, K., Ramos, E., Oosterhout, M.F., Offerhaus, G.J., Wiener, D.J., Olimpio, E.P., Dijkstra, K.K., Smit, E.F., Linden, M., Jaksani, S., Ven, M., Jonkers, J., Rios, A.C., Voest, E.E., Moorsel, C.H., Ent, C.K., Cuppen, E., Oudenaarden, A., Coenjaerts, F.E., Meyaard, L., Bont, L.J., Peters, P.J., Tans, S.J., Zon, J.S., Boj, S.F., Vries, R.G., Beekman, J.M., Clevers, H., 2019. Long-term expanding human airway organoids for disease modeling. EMBO J. 38, e100300.

Santhanam, L., Berkowitz, D.E., Belkin, A.M., 2011. Nitric oxide regulates non-classical secretion of tissue transglutaminase. Commun Integr Biol. 4, 584–586.

Sarkar, N.K., Clarke, D.D., Waelsch, H., 1957. An enzymically catalyzed incorporation of amines into proteins. Biochim Biophys Acta. 25, 451–452.

Sarrazin, S., Lamanna, W.C., Esko, J.D., 2011. Heparan sulfate proteoglycans. Cold Spring Harb Perspect Biol. 3, 1–33.

Savina, A., Fader, C.M., Damiani, M.T., Colombo, M.I., 2005. Rab11 promotes docking and fusion of multivesicular bodies in a calcium-dependent manner. Traffic. 6, 131–143.

Savoca, M.P., Tonoli, E., Atobatele, A.G., Verderio, E.A.M., 2018. Biocatalysis by transglutaminases: A review of biotechnological applications. Micromachines. 9, 562.

Sawicki, G.S., McKone, E.F., Pasta, D.J., Millar, S.J., Wagener, J.S., Johnson, C.A., Konstan, M.W., 2015. Sustained benefit from ivacaftor demonstrated by combining clinical trial and cystic fibrosis patient registry data. Am J. Respir Crit Care Med. 192, 836–842.

Scarpellini, A., Germack, R., Lortat-Jacob, H., Muramatsu, T., Billett, E., Johnson, T., Verderio, E.A.M., 2009. Heparan sulfate proteoglycans are receptors for the cell-surface trafficking and biological activity of transglutaminase-2. J. Biol Chem. 284, 18411–18423.

Scarpellini, A., Huang, L., Burhan, I., Schroeder, N., Funck, M., Johnson, T.S., Verderio, E.A.M., 2014. Syndecan-4 knockout leads to reduced extracellular transglutaminase-2 and protects against tubulointerstitial fibrosis. J. Am Soc Nephrol. 25, 1013–1027.

Schmidt, O., Teis, D., 2012. The ESCRT machinery. Curr Biol. 22, R116–R120.

Schneider, E.K., 2018. Cytochrome P450 3A4 Induction: Lumacaftor versus Ivacaftor Potentially Resulting in Significantly Reduced Plasma Concentration of Ivacaftor. Drug Metab Lett. 12, 71–74.

Scudiero, D.A., Shoemaker, R.H., Paull, K.D., Monks, A., Tierney, S., Nofziger, T.H., Currens, M.J., Seniff, D., Boyd, M.R., 1988. Evaluation of a Soluble

Tetrazolium/Formazan Assay for Cell Growth and Drug Sensitivity in Culture Using Human and Other Tumor Cell Lines. Cancer Res. 48, 4827–4833.

Sebastian, A., Rishishwar, L., Wang, J., Bernard, K.F., Conley, A.B., McCarty, N.A., Jordan, I.K., 2013. Origin and evolution of the cystic fibrosis transmembrane regulator protein R domain. Gene. 523, 137–146.

Seibert, F.S., Chang, X.B., Aleksandrov, A.A., Clarke, D.M., Hanrahan, J.W., Riordan, J.R., 1999. Influence of phosphorylation by protein kinase A on CFTR at the cell surface and endoplasmic reticulum. Biochim Biophys Acta. 1461, 275–283.

Semaniakou, A., Croll, R.P., Chappe, V., 2019. Animal models in the pathophysiology of cystic fibrosis. Front Pharmacol. 9, 1475.

Serohijos, A.W.R., Hegedus, T., Aleksandrov, A.A., He, L., Cui, L., Dokholyan, N. V., Riordan, J.R., 2008. Phenylalanine-508 mediates a cytoplasmic-membrane domain contact in the CFTR 3D structure crucial to assembly and channel function. Proc Natl Acad Sci USA. 105, 3256–3261.

Shah, V.S., Meyerholz, D.K., Tang, X.X., Reznikov, L., Alaiwa, M.A., Ernst, S.E., Karp, P.H., Wohlford-Lenane, C.L., Heilmann, K.P., Leidinger, M.R., Allen, P.D., Zabner, J., McCray, P.B., Ostedgaard, L.S., Stoltz, D.A., Randak, C.O., Welsh, M.J., 2016. Airway acidification initiates host defense abnormalities in cystic fibrosis mice. Science. 351, 503–507.

Shei, R.J., Peabody, J.E., Kaza, N., Rowe, S.M., 2018. The epithelial sodium channel (ENaC) as a therapeutic target for cystic fibrosis. Curr Opin Pharmacol. 43, 152–165.

Shimada, J., Suzuki, Y., Kim, S.J., Wang, P.C., Matsumura, M., Kojima, S., 2001. Transactivation via RAR/RXR-Sp1 interaction: Characterization of binding between Sp1 and GC box motif. Mol Endocrinol. 15, 1677–1692.

Shinde, A., Paez, J.S., Libring, S., Hopkins, K., Solorio, L., Wendt, M.K., 2020. Transglutaminase-2 facilitates extracellular vesicle-mediated establishment of the metastatic niche. Oncogenesis. 9, 16.

Shinde, A. V., Su, Y., Palanski, B.A., Fujikura, K., Garcia, M.J., Frangogiannis, N.G., 2018. Pharmacologic inhibition of the enzymatic effects of tissue transglutaminase reduces cardiac fibrosis and attenuates cardiomyocyte hypertrophy following pressure overload. J. Mol Cell Cardiol. 117, 36–48.

Shleikin, A.G., Danilov, N.P., 2011. Evolutionary-biological peculiarities of transglutaminase. Structure, physiological functions, application. J. Evol Biochem Physiol. 47, 1–14.

Sidhom, K., Obi, P.O., Saleem, A., 2020. A review of exosomal isolation methods: Is size exclusion chromatography the best option? Int J. Mol Sci. 21, 6466.

Siegel, M., Strnad, P., Watts, R.E., Choi, K., Jabri, B., Omary, M.B., Khosla, C., 2008. Extracellular transglutaminase 2 is catalytically inactive, but is transiently activated upon tissue injury. PLoS One. 3, e1861.

Slaughter, T.F., Achyuthan, K.E., Lai, T.S., Greenberg, C.S., 1992. A microtiter plate transglutaminase assay utilizing 5-(biotinamido)pentylamine as substrate. Anal Biochem. 205, 166–171.

Snodgrass, S.M., Cihil, K.M., Cornuet, P.K., Myerburg, M.M., Swiatecka-Urban, A., 2013. Tgf-β1 Inhibits Cftr Biogenesis and Prevents Functional Rescue of ΔF508-Cftr in Primary Differentiated Human Bronchial Epithelial Cells. PLoS One. 8, e63167.

Snouwaert, J.N., Brigman, K.K., Latour, A.M., Malouf, N.N., Boucher, R.C., Smithies, O., Koller, B.H., 1992. An animal model for cystic fibrosis made by gene targeting. Science. 257, 1083–1088.

Srinivasan, B., Kolli, A.R., Esch, M.B., Abaci, H.E., Shuler, M.L., Hickman, J.J., 2015. TEER Measurement Techniques for In Vitro Barrier Model Systems. J. Lab Autom. 20, 107–126.

Stamnaes, J., Pinkas, D.M., Fleckenstein, B., Khosla, C., Sollid, L.M., 2010. Redox regulation of transglutaminase 2 activity. J. Biol Chem. 285, 25402–25409.

Stern, M., Bertrand, D.P., Bignamini, E., Corey, M., Dembski, B., Goss, C.H., Pressler, T., Rault, G., Viviani, L., Elborn, J.S., Castellani, C., 2014. European cystic fibrosis society standards of care: Quality management in cystic fibrosis. J. Cyst Fibros. 13, S43–S59.

Stevenson, B.R., Siliciano, J.D., Mooseker, M.S., Goodenough, D.A., 1986. Identification of ZO-1: A high molecular weight polypeptide associated with the tight junction (Zonula Occludens) in a variety of epithelia. J. Cell Biol. 103, 755–766.

Stoltz, D.A., Meyerholz, D.K., Pezzulo, A.A., Ramachandran, S., Rogan, M.P., Davis, G.J., Hanfland, R.A., Wohlford-Lenane, C., Dohrn, C.L., Bartlett, J.A., Nelson IV, G.A., Eugene, C., Taft, P.J., Ludwig, P.S., Estin, M., Hornick, E.E., Launspach, J.L., Samuel, M., Rokhlina, T., Karp, P.H., Ostedgaard, L.S., Uc, A., Starner, T.D., Horswill, A.R., Brogden, K.A., Prather, R.S., Richter, S.S., Shilyansky, J., McCray, P.B., Zabner, J., Welsh, M.J., 2010. Cystic fibrosis pigs develop lung disease and exhibit defective bacterial eradication at birth. Sci Transl Med. 2, 29ra31.

Stone, R.C., Pastar, I., Ojeh, N., Chen, V., Liu, S., Garzon, K.I., Tomic-Canic, M., 2016. Epithelial-mesenchymal transition in tissue repair and fibrosis. Cell Tissue Res. 365, 495–506.

Stuffers, S., Sem Wegner, C., Stenmark, H., Brech, A., 2009. Multivesicular endosome biogenesis in the absence of ESCRTs. Traffic. 10, 925–937.

Sueblinvong, V., Whittaker, L.A., 2007. Fertility and Pregnancy: Common Concerns of the Aging Cystic Fibrosis Population. Clin Chest Med. 28, 433–443.

Sun, X., Yan, Z., Yi, Y., Li, Z., Lei, D., Rogers, C.S., Chen, J., Zhang, Y., Welsh, M.J., Leno, G.H., Engelhardt, J.F., 2008. Adeno-associated virus - Targeted disruption of the CFTR gene in cloned ferrets. J. Clin Invest. 118, 1578–1583.

Suto, N., Ikura, K., Sasaki, R., 1993. Expression induced by interleukin-6 of tissue-type transglutaminase in human hepatoblastoma HepG2 cells. J. Biol Chem. 268, 7469–7473.

Szondy, Z., Korponay-Szabó, I., Király, R., Sarang, Z., Tsay, G.J., 2017. Transglutaminase 2 in human diseases. Biomed. 7, 15.

Tahlan, A., Ahluwalia, J., 2014. Factor XIII: Congenital deficiency factor XIII, acquired deficiency, factor XIII A-subunit, and factor XIII B-subunit. Arch Pathol Lab Med. 138, 278–281.

Tatsukawa, H., Tani, Y., Otsu, R., Nakagawa, H., Hitomi, K., 2017. Global identification and analysis of isozyme-specific possible substrates crosslinked by transglutaminases using substrate peptides in mouse liver fibrosis. Sci Rep. 7, 45049.

Taylor-Cousar, J.L., Mall, M.A., Ramsey, B.W., McKone, E.F., Tullis, E., Marigowda, G., McKee, C.M., Waltz, D., Moskowitz, S.M., Savage, J., Xuan, F., Rowe, S.M., 2019. Clinical development of triple-combination CFTR modulators for cystic fibrosis patients with one or two F508del alleles. ERJ Open Res. 5, 00082–02019.

Taylor-Cousar, J.L., Munck, A., McKone, E.F., van der Ent, C.K., Moeller, A., Simard, C., Wang, L.T., Ingenito, E.P., McKee, C., Lu, Y., Lekstrom-Himes, J., Elborn, J.S., 2017. Tezacaftor–Ivacaftor in Patients with Cystic Fibrosis Homozygous for Phe508del. N Engl J. Med. 377, 2013–2023.

Telci, D., Collighan, R.J., Basaga, H., Griffin, M., 2009. Increased TG2 expression can result in induction of transforming growth factor β1, causing increased synthesis and deposition of matrix proteins, which can be regulated by nitric oxide. J. Biol Chem. 284, 29547–29558.

Telci, D., Wang, Z., Li, X., Verderio, E.A.M., Humphries, M.J., Baccarini, M., Basaga, H., Griffin, M., 2008. Fibronectin-tissue transglutaminase matrix rescues RGD-impaired cell adhesion through syndecan-4 and β1 integrin co-signaling. J. Biol Chem. 283, 20937–20947.

Thomas, P.J., Shenbagamurthi, P., Ysern, X., Pedersen, P.L., 1991. Cystic fibrosis transmembrane conductance regulator: Nucleotide binding to a synthetic peptide. Science. 251, 555–557.

Tice, JA., Kuntz, KM., Wherry, K., Chapman, R., Seidner, M., Pearson, SD., Rind, DM., Modulator Treatments for Cystic Fibrosis: Effectiveness and Value; Final Evidence Report and Meeting Summary. Institute for Clinical and Economic Review. Available at: https://icer-review.org/material/cystic-fibrosis-2-evidence-report/ (Accessed: 18 September 2020).

To, W.S., Midwood, K.S., 2011. Plasma and cellular fibronectin: Distinct and independent functions during tissue repair. Fibrogenes Tissue Repair. 4, 21.

Tosco, A., De Gregorio, F., Esposito, S., De Stefano, D., Sana, I., Ferrari, E., Sepe, A., Salvadori, L., Buonpensiero, P., Di Pasqua, A., Grassia, R., Leone, C.A., Guido, S., De Rosa, G., Lusa, S., Bona, G., Stoll, G., Maiuri, M.C., Mehta, A., Kroemer, G., Maiuri, L., Raia, V., 2016. A novel treatment of cystic fibrosis acting on-target: Cysteamine plus epigallocatechin gallate for the autophagy-dependent rescue of class II-mutated CFTR. Cell Death Differ. 23, 1380–1393.

Trajkovic, K., Hsu, C., Chiantia, S., Rajendran, L., Wenzel, D., Wieland, F., Schwille, P., Brügger, B., Simons, M., 2008. Ceramide triggers budding of exosome vesicles into multivesicular endosomes. Science. 319, 1244–1247.

Troilo, H., Steer, R., Collins, R.F., Kielty, C.M., Baldock, C., 2016. Independent multimerization of Latent TGFβ Binding Protein-1 stabilized by cross-linking and enhanced by heparan sulfate. Sci Rep. 6, 34347.

Tschumperlin, D.J., Liu, F., Tager, A.M., 2013. Biomechanical regulation of mesenchymal cell function. Curr Opin Rheumatol. 25, 92–100.

Upchurch, H.F., Conway, E., Patterson, M.K., Maxwell, M.D., 1991. Localization of cellular transglutaminase on the extracellular matrix after wounding: Characteristics of the matrix bound enzyme. J. Cell Physiol. 149, 375–382.

Valley, H.C., Bukis, K.M., Bell, A., Cheng, Y., Wong, E., Jordan, N.J., Allaire, N.E., Sivachenko, A., Liang, F., Bihler, H., Thomas, P.J., Mahiou, J., Mense, M., 2019. Isogenic cell models of cystic fibrosis-causing variants in natively expressing pulmonary epithelial cells. J. Cyst Fibros. 18, 476–483.

Van De Water, L., Varney, S., Tomasek, J.J., 2013. Mechanoregulation of the Myofibroblast in Wound Contraction, Scarring, and Fibrosis: Opportunities for New Therapeutic Intervention. Adv Wound Care. 2, 122–141.

Van Den Akker, J., Van Weert, A., Afink, G., Bakker, E.N.T.P., Van Der Pol, E., Böing, A.N., Nieuwland, R., VanBavel, E., 2012. Transglutaminase 2 is secreted from smooth muscle cells by transamidation-dependent microparticle formation. Amino Acids. 42, 961–973.

Van Deun, J., Jo, A., Li, H., Lin, H.Y., Weissleder, R., Im, H., Lee, H., 2020. Integrated Dual-Mode Chromatography to Enrich Extracellular Vesicles from Plasma. Adv Biosyst. 4, e1900310.

Van Goor, F., Hadida, S., Grootenhuis, P.D.J., Burton, B., Cao, D., Neuberger, T., Turnbull, A., Singh, A., Joubran, J., Hazlewood, A., Zhou, J., McCartney, J., Arumugam, V., Decker, C., Yang, J., Young, C., Olson, E.R., Wine, J.J., Frizzell, R.A., Ashlock, M., Negulescu, P., 2009. Rescue of CF airway epithelial cell function in vitro by a CFTR potentiator, VX-770. Proc Natl Acad Sci USA. 106, 18825–18830.

Van Goor, F., Hadida, S., Grootenhuis, P.D.J., Burton, B., Stack, J.H., Straley, K.S., Decker, C.J., Miller, M., McCartney, J., Olson, E.R., Wine, J.J., Frizzell, R.A., Ashlock, M., Negulescu, P.A., 2011. Correction of the F508del-CFTR protein processing defect in vitro by the investigational drug VX-809. Proc Natl Acad Sci USA. 108, 18843–18848.

van Niel, G., Charrin, S., Simoes, S., Romao, M., Rochin, L., Saftig, P., Marks, M.S., Rubinstein, E., Raposo, G., 2011. The Tetraspanin CD63 Regulates ESCRT-Independent and -Dependent Endosomal Sorting during Melanogenesis. Dev Cell. 21, 708–721.

Van Niel, G., D'Angelo, G., Raposo, G., 2018. Shedding light on the cell biology of extracellular vesicles. Nat Rev Mol Cell Biol. 19, 213–228.

Ventura, M.A.E., Sajko, K., Hils, M., Pasternack, R., Greinwald, R., Tewes, B., Schuppan, D., 2018. Su1161 - The Oral Transglutaminase 2 (TG2) Inhibitor Zed1227 Blocks TG2 Activity in a Mouse Model of Intestinal Inflammation. Gastroenterology. 154, S490.

Verderio, E.A.M., Johnson, T., Griffin, M., 2004. Tissue transglutaminase in normal and abnormal wound healing: Review article. Amino Acids. 26, 387–404.

Verderio, E.A.M., Scarpellini, A., Johnson, T.S., 2009. Novel interactions of TG2 with heparan sulfate proteoglycans: Reflection on physiological implications. Amino Acids. 36, 671–677.

Verderio, E.A.M., Telci, D., Okoye, A., Melino, G., Griffin, M., 2003. A Novel RGD-independent Cell Adhesion Pathway Mediated by Fibronectin-bound Tissue Transglutaminase Rescues Cells from Anoikis. J. Biol Chem. 278, 42604–42614.

Verhaeghe, C., Remouchamps, C., Hennuy, B., Vanderplasschen, A., Chariot, A., Tabruyn, S.P., Oury, C., Bours, V., 2007. Role of IKK and ERK pathways in intrinsic inflammation of cystic fibrosis airways. Biochem Pharmacol. 73, 1982–1994.

Villarroya-Beltri, C., Baixauli, F., Mittelbrunn, M., Fernández-Delgado, I., Torralba, D., Moreno-Gonzalo, O., Baldanta, S., Enrich, C., Guerra, S., Sánchez-Madrid, F., 2016. ISGylation controls exosome secretion by promoting lysosomal degradation of MVB proteins. Nat Commun. 7, 13588.

Wainwright, C.E., Elborn, J.S., Ramsey, B.W., Marigowda, G., Huang, X., Cipolli, M., Colombo, C., Davies, J.C., De Boeck, K., Flume, P.A., Konstan, M.W., McColley, S.A., McCoy, K., McKone, E.F., Munck, A., Ratjen, F., Rowe, S.M., Waltz, D., Boyle, M.P., 2015. Lumacaftor–Ivacaftor in Patients with Cystic Fibrosis Homozygous for Phe508del CFTR . N Engl J. Med. 373, 220–231.

Wang, F., Zeltwanger, S., Hu, S., Hwang, T.C., 2000. Deletion of phenylalanine 508 causes attenuated phosphorylation-dependent activation of CFTR chloride channels. J. Physiol. 524, 637–648.

Wang, Z., Collighan, R.J., Pytel, K., Rathbone, D.L., Li, X., Griffin, M., 2012. Characterization of heparin-binding site of tissue transglutaminase: Its importance in cell surface targeting, matrix deposition, and cell signaling. J. Biol Chem. 287, 13063–13083.

Wang, Z., Stuckey, D.J., Murdoch, C.E., Camelliti, P., Lip, G.Y.H., Griffin, M., 2018. Cardiac fibrosis can be attenuated by blocking the activity of transglutaminase 2 using a selective small-molecule inhibitor. Cell Death Dis. 9, 613.

Ward, C.L., Omura, S., Kopito, R.R., 1995. Degradation of CFTR by the ubiquitin-proteasome pathway. Cell. 83, 121–127.

Wei, Y., Wang, D., Jin, F., Bian, Z., Li, L., Liang, H., Li, M., Shi, L., Pan, C., Zhu, D., Chen, X., Hu, G., Liu, Y., Zhang, C.Y., Zen, K., 2017. Pyruvate kinase type M2 promotes tumour cell exosome release via phosphorylating synaptosome-associated protein 23. Nat Commun. 8, 14041.

Weiler, C.A., Drumm, M.L., 2013. Genetic influences on cystic fibrosis lung disease severity. Front Pharmacol. 4, 40.

Weiser, N., Molenda, N., Urbanova, K., Bähler, M., Pieper, U., Oberleithner, H., Schillers, H., 2011. Paracellular permeability of bronchial epithelium is controlled by CFTR. Cell Physiol Biochem. 28, 289–296.

Whitcutt, M.J., Adler, K.B., Wu, R., 1988. A biphasic chamber system for maintaining polarity of differentiation of culture respiratory tract epithelial cells. In Vitro Cell Dev Biol. 24, 420–428.

World Health Organization, 2004. The molecular genetic epidemiology of cystic fibrosis. Available at: https://apps.who.int/iris/handle/10665/68702 (Accessed: 20 March 2020).

Wilke, M., Buijs-Offerman, R.M., Aarbiou, J., Colledge, W.H., Sheppard, D.N., Touqui, L., Bot, A., Jorna, H., De Jonge, H.R., Scholte, B.J., 2011. Mouse models of cystic fibrosis: Phenotypic analysis and research applications. J. Cyst Fibros. 10, S152–S171.

William P. Katt, Marc A. Antonyak, Richard A. Cerione, 2018. Opening up about Tissue Transglutaminase: When Conformation Matters More than Enzymatic Activity. Med

One. 3, e180011.

Williams, M.T.S., de Courcey, F., Comer, D., Elborn, J.S., Ennis, M., 2016. Bronchial epithelial cell lines and primary nasal epithelial cells from cystic fibrosis respond differently to cigarette smoke exposure. J. Cyst Fibros. 15, 467–472.

Willis, B.C., DuBois, R.M., Borok, Z., 2006. Epithelial origin of myofibroblasts during fibrosis in the lung. Proc Am Thorac Soc. 3, 377–382.

Willms, E., Johansson, H.J., Mäger, I., Lee, Y., Blomberg, K.E.M., Sadik, M., Alaarg, A., Smith, C.I.E., Lehtiö, J., El Andaloussi, S., Wood, M.J.A., Vader, P., 2016. Cells release subpopulations of exosomes with distinct molecular and biological properties. Sci Rep. 6, 22519.

Wipff, P.J., Rifkin, D.B., Meister, J.J., Hinz, B., 2007. Myofibroblast contraction activates latent TGF-β1 from the extracellular matrix. J. Cell Biol. 179, 1311–1323.

Wnuk, D., Paw, M., Ryczek, K., Bochenek, G., Sładek, K., Madeja, Z., Michalik, M., 2020. Enhanced asthma-related fibroblast to myofibroblast transition is the result of profibrotic TGF-β/Smad2/3 pathway intensification and antifibrotic TGF-β/Smad1/5/(8)9 pathway impairment. Sci Rep. 10, 16492.

Wu, Z., Yang, L., Cai, L., Zhang, M., Cheng, X., Yang, X., Xu, J., 2007. Detection of epithelial to mesenchymal transition in airways of a bleomycin induced pulmonary fibrosis model derived from an α-smooth muscle actin-Cre transgenic mouse. Respir Res. 8, 1.

Wynn, T.A., 2007. Common and unique mechanisms regulate fibrosis in various fibroproliferative diseases. J. Clin Invest. 117, 524–529.

Xiao, C., Puddicombe, S.M., Field, S., Haywood, J., Broughton-Head, V., Puxeddu, I., Haitchi, H.M., Vernon-Wilson, E., Sammut, D., Bedke, N., Cremin, C., Sones, J., Djukanović, R., Howarth, P.H., Collins, J.E., Holgate, S.T., Monk, P., Davies, D.E., 2011. Defective epithelial barrier function in asthma. J. Allergy Clin Immunol. 128, 549-556.

Yoon, J.C., Casella, J.L., Litvin, M., Dobs, A.S., 2019. Male reproductive health in cystic fibrosis. J. Cyst Fibros. 18, S105–S110.

Yu, X., Deng, L., Wang, D., Li, N., Chen, X., Cheng, X., Yuan, J., Gao, X., Liao, M., Wang, M., Liao, Y., 2012. Mechanism of TNF-α autocrine effects in hypoxic cardiomyocytes: Initiated by hypoxia inducible factor 1α, presented by exosomes. J. Mol Cell Cardiol. 53, 848–857.

Zeitlin, P.L., Lu, L., Rhim, J., Cutting, G., Stetten, G., Kieffer, K.A., Craig, R., Guggino, W.B., 1991. A cystic fibrosis bronchial epithelial cell line: immortalization by adeno-12-SV40 infection. Am J. Respir Cell Mol Biol. 4, 313–319.

Zemanick, E.T., Polineni, D., 2019. Unraveling the CFTR function–phenotype connection for precision treatment in cystic fibrosis. Am J. Respir Crit Care Med. 199, 1053–1054.

Zemskov, E.A., Mikhailenko, I., Hsia, R.C., Zaritskaya, L., Belkin, A.M., 2011. Unconventional secretion of tissue transglutaminase involves phospholipid-dependent delivery into recycling endosomes. PLoS One. 6, e19414.

Zhang, Z., Chen, J., 2016. Atomic Structure of the Cystic Fibrosis Transmembrane

Conductance Regulator. Cell. 167, 1586-1597.

Zhang, Z., Liu, F., Chen, J., 2017. Conformational Changes of CFTR upon Phosphorylation and ATP Binding. Cell. 170, 483-491.

Zhang, Z., Liu, F., Chen, J., 2018. Molecular structure of the ATP-bound, phosphorylated human CFTR. Proc Natl Acad Sci USA. 115, 12757–12762.

Zhou, B., von Gise, A., Ma, Q., Hu, Y.W., Pu, W.T., 2010. Genetic fate mapping demonstrates contribution of epicardium-derived cells to the annulus fibrosis of the mammalian heart. Dev Biol. 338, 251–261.

Zolin, A., Orenti, A., Naehrlich, L., Jung, A., van Rens, J., Fox, A., Krasnyk, M., Cosgriff, R., Hatziagorou, E., Mei-Zahav, M., Storms, V., 2020. ECFSPR Annual Report 2018. Available at: https://www.ecfs.eu/projects/ecfs-patient-registry/annual-reports (Accessed: 10 November 2020).

Zonca, S., Pinton, G., Wang, Z., Soluri, M.F., Tavian, D., Griffin, M., Sblattero, D., Moro, L., 2017. Tissue transglutaminase (TG2) enables survival of human malignant pleural mesothelioma cells in hypoxia. Cell Death Dis. 8, e2592.